SILENCING OF SEX CHROMOSOMES

FROM MEIOSIS TO EARLY EMBRYONIC DEVELOPMENT

INACTIVATIE VAN GESLACHTSCHROMOSOMEN

VAN MEIOSE TOT DE VROEG EMBRYONALE ONTWIKKELING

"Silence is sometimes the best answer"
(*the Dalai Lama XIV*)

Voor Alice

SILENCING OF SEX CHROMOSOMES

FROM MEIOSIS TO EARLY EMBRYONIC DEVELOPMENT

SILENCING OF SEX CHROMOSOMES

FROM MEIOSIS TO EARLY EMBRYONIC DEVELOPMENT

INACTIVATIE VAN GESLACHTSCHROMOSOMEN
VAN MEIOSE TOT DE VROEG EMBRYONALE ONTWIKKELING

Proefschrift

ter verkrijging van de graad van doctor aan de
Erasmus Universiteit Rotterdam
op gezag van de rector magnificus

Prof. dr. H.G. Smidt

en volgens besluit van het College voor Promoties.

De openbare verdediging zal plaatsvinden op
vrijdag 15 oktober 2010 om 11:30 uur

door

Sam Schoenmakers
geboren te Heerlen

ERASMUS UNIVERSITEIT ROTTERDAM

PROMOTIECOMMISSIE

Promotoren   Prof.dr. J.A. Grootegoed
Prof.dr. J.S.E. Laven

Overige leden   Prof.dr. F. Grosveld
Dr. W. Vermeulen
Dr. P. de Boer

Co-promoter   Dr. W.M. Baarends

Paranimfen   S.T.H. Bontemps
E. Wassenaar
A.P. Nagtegaal
L.A.M. Santegoets

TABLE OF CONTENTS

CHAPTER 1

GENERAL INTRODUCTION
## AIM AND SCOPE

St art stamcel

THE NUCLEUS

In order to fit the whole genome into the cell nucleus, the DNA has to be organized into a condensed structure. The basic structure is the double helix structure of the DNA. The formation of nucleosomes mediates the first level of condensation: 147 base pairs of the double helix of DNA is wrapped around an octamer of two of each of the histones H2A, H2B, H3 and H4 in 1.67 turns [1]. The complex of core histone proteins and the DNA that is folded around it, is the most simple form of chromatin [2, 3]. The nucleosomes are organized into 30 nm chromatin fibers, and the fibers themselves are then again condensed. Nucleosomes and fibres can undergo conformational and spatial changes, making the DNA either accessible or inaccessible for the transcription machinery by a regulatory mechanism that causes post-translational modifications to the N- and C-terminal amino acid tails of histones, such as acetylation, methylation, sumoylation, ubiquitylation and phosphorylation. These modifications can be recognized by specific binding-proteins, included in chromatin, which can lead to a change in nucleosome configuration and thereby regulate the activity inactivity of a gene or gene region (reviewed in [2]).

CELL DIVISION: MITOSIS AND MEIOSIS

The nucleus of virtually all somatic cells in vertebrates contains a complete diploid (2n) genome, which is distributed over 23 chromosome pairs in human [4], 20 pairs in mouse [5], 39 pairs in dog (http://www.ncbi.nlm.nih.gov/sites/entrez?Db=genomeprj&cmd=ShowDetailView&TermToSearch=10726), and respectively 35 and 38 pairs in zebra finch and chicken (http://www.ncbi.nlm.nih.gov/sites/entrez?db=genomeprj). In all species, each chromosome pair consists of one paternally- and one maternally-derived chromosome. The sex chromosome pair is special, and differs between the two sexes. In mammals, females carry two X chromosomes and males are XY. The X chromosome is large and gene-rich, whereas the Y chromosome is small and gene poor. Small regions of the X and Y chromosomes share sequence identity, and these regions are called the pseudoautosomal regions. They reflect the common origin of the sex chromosomes (reviewed in [6]).

Mitosis occurs when cells proliferate, and results in the formation of two new identical diploid (2n) daughter cells, whereas two specialized meiotic divisions are required for the formation of haploid (n) gametes from a diploid (2n) precursor cell (Figure 1).

Before either mitosis or meiosis can occur, replication of the genetic material has to take place. During this synthesis phase (S phase), each chromosome in the nucleus is replicated, forming a chromosome consisting of two identical sister
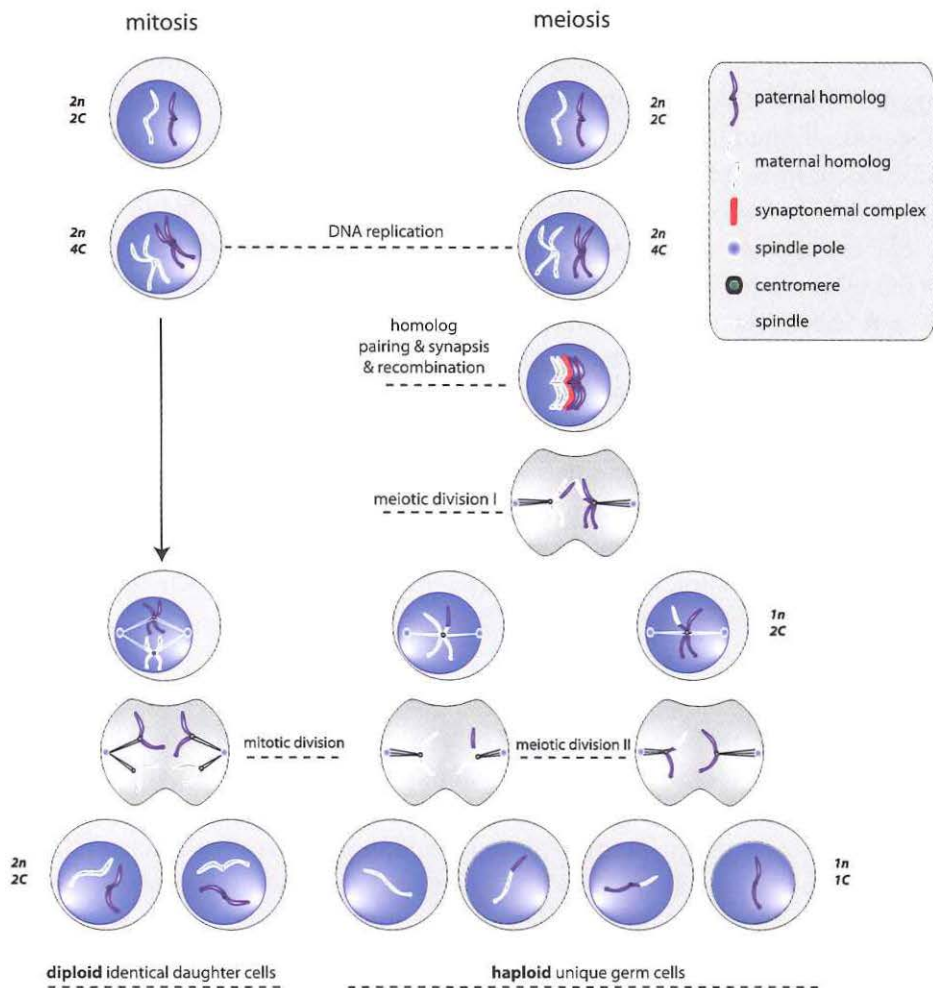
Figure 1. Overview of mitosis and meiosis. Mitosis in diploid cells (2n, 2C) starts with a round of DNA replication generating chromosomes consisting of two sister chromatids, that have doubled the amount of genetic material (2n, 4C). The mitotic division divides the replicated genome over two identical daughter cells (2n, 2C). Meiosis also starts with DNA replication (2n, 4C), which is followed by homologous chromosome pairing and meiotic recombination. The first meiotic division separates the replicated and recombined homologous chromosomes into two new haploid daughter cells (1n, 2C), and the second meiotic division divides the replicated or sister chromatids over the germ cells (1n, 1C).

chromatids, which are held together by a special protein complex of cohesins (reviewed in [7, 8]). In mitosis, this is followed by alignment of all chromosomes at the metaphase plate, the cohesins are removed, and the sister chromatids are separated in a bipolar fashion, leading to the formation of two new identical
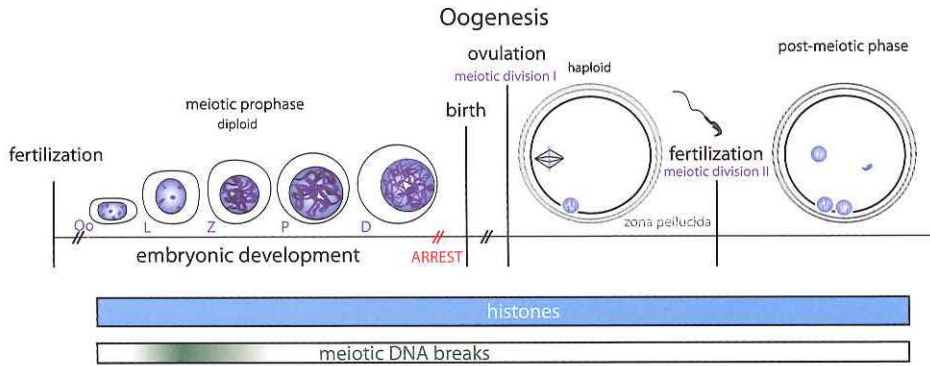
Figure 2. Overview of oogenesis. The process of oogenesis starts a few weeks after fertilization in humans, and approximately 13 days after fertilization in mouse, and all oocytes arrest at the diplotene (D) stage before birth (Oo = oogenia, L = leptoten, Z = zygotene, P = pachytene, D = diplotene/dictyotene) [24]. During the first meiotic prophase, the protein SPO11 induced hundreds of DNA double strand breaks throughout the genome, while the genome continues to be packed around histones. Shortly before ovulation, meiotic prophase continues, and the first meiotic division is completed. This division generated the secondary oocyte and the first polar body. Subsequently, the oocyte arrests again at metaphase II. Only after fertilization, the second meiotic division is completed, and the second polar body is formed. Since all oocytes have reached diplotene/dictyotene before birth, the supply is limited, and when no more oocytes are available, menopause starts.

daughter nuclei (2n). Finally, the cell itself divides and each of its two daughter cells contains one of the newly formed nuclei.

Meiosis encompasses a meiotic S phase and a meiotic prophase, followed by the two meiotic divisions: meiosis I and II (Figure 1). Following S phase (resulting in 2n, 4C cells, where 1C is the amount of DNA in a haploid gamete), homologous chromosome sets align, pair and recombine, after which the homologous chromosomes are separated in opposite directions in the first meiotic division, leading to the formation of haploid daughter cells containing a single set of 23 (human) chromosomes that each still consist of two sister chromatids (1n, 2C). Meiosis I is a so-called reductional division, whereas meiosis II is an equational division, resembling a mitotic division, in which the chromosomes align at the metaphase II plate and sister chromatids are pulled apart from each other. The net result of meiosis I and meiosis II in males is the generation of 4 haploid gametes (1n, 1C) from one primary spermatocyte (2n, 4C), and each haploid nucleus carries one homolog of each chromosome pair, that consists of a single chromatid. In females, the metaphase plate is oriented such that meiosis I and II result in the formation of only one haploid oocyte, containing almost all the cytoplasm, and two polar bodies.

As mentioned above, meiosis leads to the production of haploid gametes, which are needed for sexual reproduction. Missegregation of chromosomes in either one of the meiotic divisions leads to an unequal number of chromatids in the gametes, resulting in an aneuploid embryo, which is mostly lethal to it (see [8]). In order to obtain proper segregation of chromosomes in meiosis, correct alignment, pairing and association of the homologous chromosome pair has to be ensured.

During meiotic prophase, homologous chromosomes need to locate and recognize each other whereafter they can proceed with their alignment, pairing, synapsis, and recombination. Meiotic recombination leads to the formation of chiasmata, which ensure stable physical connections between homologous chromosomes, needed for proper segregation of the homologs. The chiasmata represent sites of crossover, meaning exchange of genetic information between two non-sister chromatids resulting in new allelic combinations that are instrumental to obtain genetic diversity necessary for natural selection in relation to sexual reproduction and environmental factors.

So, the first important step in chromosome pairing is identification of homology. Upon entering the meiotic prophase, all chromosomes undergo the final S phase in the preleptotene stage (reviewed in [9]). At leptotene, meiotic DNA double strand breaks (DSBs) are introduced throughout the genome and homologous chromosomal pairing is initiated. Meiotic DSBs are required for the completion of chromosome pairing [10] and some of these DSBs are converted into crossovers. At zygotene, DSBs are repaired through the homologous recombination repair pathway, while the paired homologs start to become physically connected through the formation of the proteinaceous synaptonemal complex [11]. This process is called synapsis. When synapsis and DSB repair is completed during pachytene, the crossovers between the homologs are formed. During diplotene, the synaptonemal complex is gradually degraded, and homologs remain connected through their chiasmata and sister chromatid cohesion. The chromosomes start to condense in diakinesis I, as the nuclear membrane disappears and the first meiotic spindle is formed. At metaphase I, the homologous chromosomes align along the equatorial plane. Loss of sister chromatid cohesion along chromosome arms allows separation of homologous chromosomes during metaphase I (reviewed in [8, 12]), and meiosis I is completed when each haploid chromosome set arrives at its pole in telophase I. Each daughter cell carries one copy of each chromosome, and each chromosome consists of two sister chromatids (1n, 2C).

Meiosis II follows quickly, and loss of the remaining sister chromatid cohesion at the centromeres (reviewed in[8, 12]) allows separation of the sister chromatids,

and results in the formation of definitive male and female gametes that contain a haploid genome with each chromosome consisting of a single chromatid (1n, 1C).

GERM CELLS

In the mammalian early postimplantation embryo, extra-embryonic cells in proximity to the epiblast start expressing BMP4 [13], which induces primordial germ cell (PGCs) development in a number of adjacent epiblast cells. Next, these cells move to the extra-embryonic mesoderm, from where they then migrate back towards the genital ridges inside the embryonic part to form the germ cell lineage. During this migration, the PGCs continue to proliferate and divide and finally colonize the developing gonadal regions (reviewed in [14]). Upon arrival in the gonads, the PGCs are completely epigenetically reprogrammed and reset by genome-wide DNA demethylation and posttranslational modification of histones [15].

Inductive signals from somatic cells, depending on the sex chromosomal constitution (XY versus XX) of these cells, direct gonadal and ultimately embryonic development into respectively either male or female [16, 17]. Male sex determination is directed through expression of the Y chromosomal *Sry* gene, which causes cellular differentiation of supporting cells into Sertoli cells and formation of testis cords in which the pre-Sertoli cells enclose the PGCs, thereby committing the germ cells to spermatogenesis [18, 19]. In the classical view, it is the lack of *Sry* gene expression or action that will result in ovary development, and the absence of testis cord formation will recruit the germ cells into the oogenic pathway.

Although *Sry* is the dominant male sex determining gene in placental mammals, it has been determined that female sex determination requires the activity of genes such as *Foxl2*, *Rspo1* and *Wnt4* [20-22]. Knockout of *Rspo1* [20] and combined knockout of *Foxl2* and *Wnt4* [21, 22] leads to extensive XX-sex reversal in mice. In addition, in human, loss of RSPO1 function is associated with complete XX sex reversal [23].

OOGENESIS (Figure 2)

The germ cells in the developing ovaries undergo several rounds of mitosis during the colonization process and their differentiation into oogonia. Already at the embryonic stage of development, all oogonia enter meiotic prophase, whereafter they are named primary oocytes. Primary oocytes progress through the first stages of the prophase of meiosis I and arrest in diplotene (reviewed in [24]), now termed dictyotene. At dictyotene, socalled primordial follicles are formed in which the dictyate oocytes are enclosed by one layer of pre-granulosa cells. Only
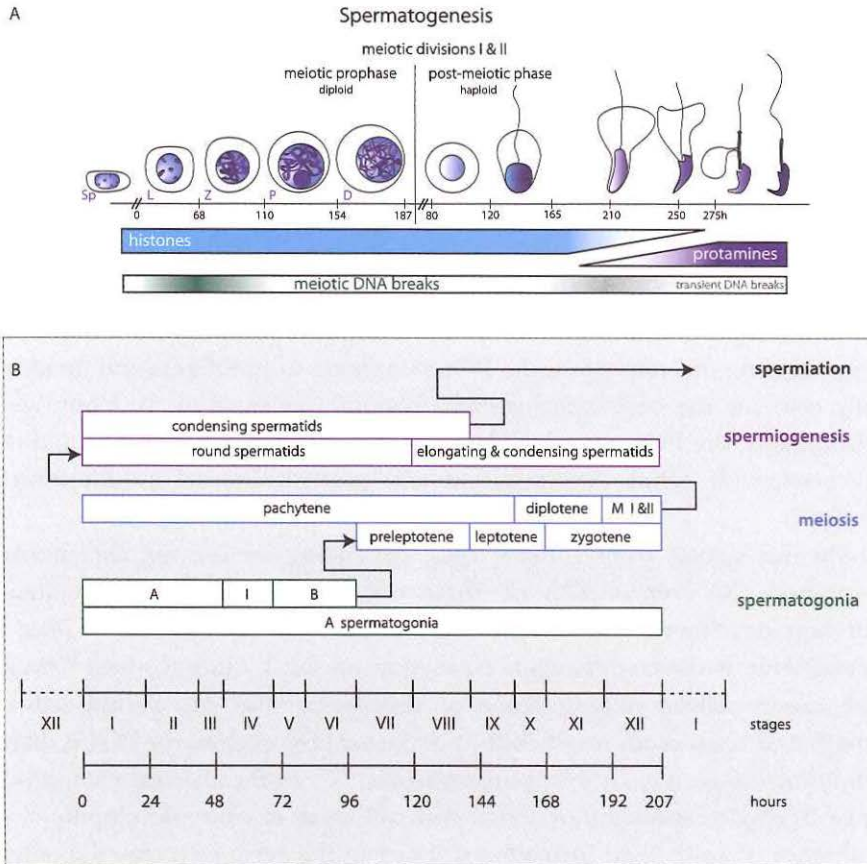
Figure 3. Overview of spermatogenesis. (a) The process of spermatogenesis starts with the onset of puberty and continues until death. In the first meiotic prophase, several hundreds of DNA double strand breaks are induced throughout the whole genome by the toposisomerase-like enzyme SPO11, to enable chromosome pairing and meiotic recombination. During the postmeiotic phase, after the two successive meiotic divisions, the whole genome becomes completely reorganized. All histones are removed and replaced by protamines. This histone-to-protamine exchange is accompanied by the introduction of transient DNA double strand breaks to remove supercoils and allow repackaging of the DNA by protamines. The protein-exchange allows compaction of chromatin, necessary for the final DNA condensation in the mature spermatozoa. (b) Spermatogenesis involves cycles of mitotic divisions, proliferation and differentiation of type A spermatogonia (A). Some differentiate through intermediate spermatogonia (I) into type B spermatogonia and finally enter as primary spermatocytes the first meiotic prophase (leptotene, zygotene, pachytene and diplotene). After the two successive meiotic divisions (MI & II), spermatids enter the postmeiotic phase or spermiogenesis. Spermiogenesis is divided into 16 steps in the mouse, based on the progressive formation of the acrosome of the spermatids. Between step 8 and step 13 the round spermatid nucleus undergoes morphological changes resulting in elongation and condensation of the sperm head. Mouse spermatogenesis is divided into 12 different continuous stages of the cycle of the seminiferous epithelium (adapted from [74-77]).
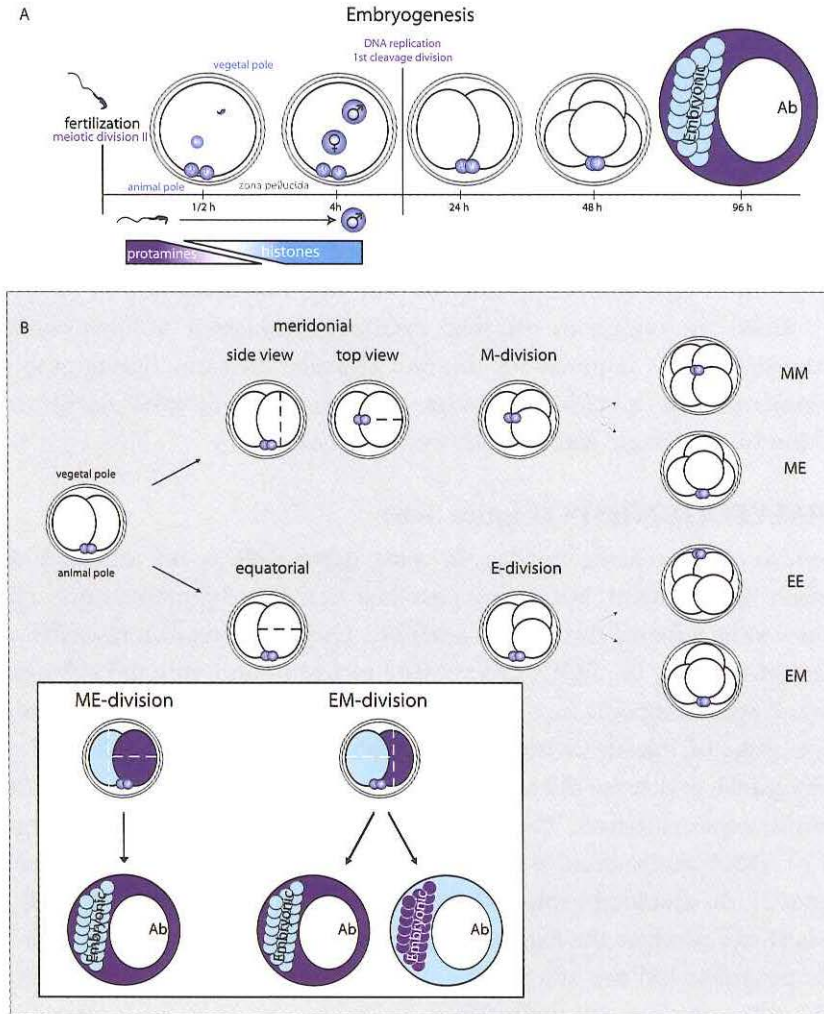
Figure 4. Overview of early embryogenesis. (a) Directly after fertilization, the secondary oocytes completes its second meiotic division and all protamines of the paternal genome are removed and replaced by maternal histones. This protamine-to-histone exchange occurs within 30 minutes, and 4 hours after fertilization both the paternal and maternal pronucleus have formed [34, 35]. Around 24 hours after fertilization, the first cleavage division takes place, and the second cleavages divisions follow approximately 24 hours later, resulting in a 4-cell stage-embryo. (b) 2-cell stage blastomeres can divide either meridional (M) or equatorial (E). The upper row represents embryos, in which the first blastomere undergoes a meridional division, and the second does so equatorial (ME-embryos). MM-embryos originate from two meridional second cleavage divisions. The lower row shows embryos undergoing first an equatorial division, which is followed by either a meridional division (EM-embryos) or another equatorial division (EE-embryos) [38]. Boxed area: In ME-embryos the progeny of the earlier M-divided blastomere contributes to the embryonic part of the blastocyst, whereas in EM-embryos the blastomeres from the first divided E-embryo contribute to either the embryonic part or the abembryonic (Ab) part [38].

during postnatal reproductive life, the resting primordial follicles are recruited for growth. The pre-ovulatory surges of the hormones FSH and LH induce resumption of oocyte meiosis I, and the first meiotic division is completed just prior to ovulation, resulting in the formation of the small first polar body (1n, 2C), and a large secondary oocyte (1n, 2C). This secondary oocyte immediately proceeds with meiosis II, to arrest again at metaphase II. Fertilization triggers the metaphase II to anaphase II transition, and a second polar body is formed, as well as the female haploid pronucleus (1n, 1C). The formation of small polar bodies allows the oocyte to maintain maximal cytoplasmic volume containing the maternal factors required for the first cleavage divisions during embryonic development. This specific regulation of meiosis in females results in the formation of one single gamete and two polar bodies.

SPERMATOGENESIS (Figure 3ab)

In contrast to oogenesis, meiosis in male germ cells is not initiated during embryonic development, but during postnatal testis development at puberty, and continues to be initiated throughout adult life. During the fetal en neonatal period of spermatogenesis, the PGCs differentiate to form gonocytes and subsequently into type A spermatogonia (reviewed in [14]). Around puberty, type A spermatogonia undergo cycles of mitotic divisions to maintain of pool of undifferentiated type A spermatogonia, and some differentiate into type B spermatogonia and ultimately into primary spermatocytes. The diploid primary spermatocytes (2n) undergo one round of DNA duplication (4C) and then commence meiosis I. After finishing metaphase I, the resulting haploid (1n, 2C) secondary spermatocytes quickly enter meioisis II and produce the haploid (1n, 1C) postmeiotic round spermatids. Male meiotic prophase and the two meiotic divisions together take 26 days in human, and 11-12 days in mice (see figure 3b) [25].

Spermatogenesis includes a unique postmeiotic development phase, which does not occur in oogenesis. The postmeiotic haploid male germ cells, called spermatids, differentiate without cell division into spermatozoa during a process named spermiogenesis, Spermiogenesis takes 38 and 21 days in men and mice, respectively [25]. During spermiogenesis, spermatids undergo radical morphological and biochemical alterations, completely remodeling the paternal chromatin to ensure a tightly packed and condensed male nucleus in spermatozoa. In the early postmeiotic elongating spermatids, histones are first replaced with transition proteins TP1 and TP2 [26], which are subsequently replaced by protamines PRM1 and PRM2 in the late postmeiotic condensing spermatids (reviewed in [27]) and this is accompanied by transcriptional inactivation of the complete genome. The histone-to-protamine exchange allows the formation of a highly condensed

chromatin structure. The topoisomerase IIb [27] relieves the tension caused by the supercoiling during the transition phase and introduces controlled and transient DNA breaks [28-32] facilitating the final protamine exchange. Finally, the late condensed spermatids are released from the Sertoli cells into the lumen of the seminiferous tubules, in a process named spermiation, and are transported to the epididymis to undergo maturation to spermatozoa with full motility and fertilizing capacity.

FERTILIZATION AND EARLY EMBRYONIC DEVELOPMENT (Figure 4ab)

When the sperm meets the travelling secondary oocyte up the female reproductive tract, it first has to pass the species-specific zona pellucida, which surrounds the oocyte. Upon binding to the zona the individual sperm undergoes the acrosome reaction, which allows penetration of the zona pellucida. Next, the so-called equatorial segment of the sperm head binds to its receptor on the membrane of the oocyte, the membranes fuse, and this most likely triggers the endogenous release of Ca^{2+} stored in the endoplasmic reticulum (reviewed in [33]). This increase in intracellular Ca^{2+} triggers the completion of the second meiotic division of the female metaphase II genome, and causes exocytosis of granules residing right under the cellmembrane, the cortical granules, which initiates alterations in the zona pellucida preventing access for other sperm (reviewed in [33]).

The fertilized oocyte, now called zygote, contains the haploid female pronucleus and the decondensing male pronucleus, which undergoes a protamine-to-(maternal) histone transition and active DNA demethylation, but leaving some inherited imprints on the paternal genome intact. This is followed by replication of the paternal and maternal genomes. When the zygote goes into M phase, the nuclear membranes of both replicated pronuclei disintegrate, and paternal and maternal chromosomes align on the metaphase plate after which the first cleavage division takes place [34,35] (Figure 4a).

Early mammalian embryonic development has been viewed as a random occurrence of cleavage divisions until formation of the blastocyst stage, where polarity is first witnessed by the asymmetric location of the inner cell mass (ICM), giving rise to the future embryo proper, at the so-called embryonic pole, opposite from the abembryonic pole. This polarization appears to occur at a relatively late stage compared to what is observed for other species such as insects and amphibians, where dorso-ventral polarity is already determined respectively during oogenesis [36,37] or right after fertilization [36]. However, asymmetry in the zygote can be observed already shortly after fertilization, also in mammals (reviewed in [38]): simultaneously with the formation of the paternal pronucleus, the second

polar body (1n, 1C) is expelled from the secondary oocyte, marking the animal pole, and the zygote rapidly changes its shape by cytoskeletal reorganisation. This actin-mediated reorganisation causes the zygote to become flattened, resulting in the formation of a short animal-vegetal axis (AV-axis) with the sperm entry point (SEM) on the vegetal pole [39, 40]. The first cleavage division appears to occur preferentially along this AV-axis [39, 41], and both resulting blastomeres inherit animal and vegetal components of the zygote (Figure 4b).

Recent results indicate that mammalian embryos and cleavage divisions are flexible, since it has been shown that up to a quarter of a 8-cell stage preimplantation human embryo can be removed without disrupting its development [42], and in mouse embryos research showed that embryo biopsy does not lead to reduced birthweight or altered subsequent growth to weaning [43-47]. However, they seem to be biased, since the second cleavage divisions produce 4-cell stage embryos with apparent different developmental potential and capabilities, depending on the orientation and order of divisions [38]. The second cleavage divisions occur asynchronous, and each blastomere can either divide meridionally (M, parallel to the AV-axis), producing 2 blastomeres with again animal and vegetal components, or equatorally (E) with one blastomere inheriting mainly animal parts and one blastomere vegetal parts. Similar to the first cleavage division, these second cleavage divisions are biased; the combination of an M with an E division, irrespective of the order in which the divisions occur (ME or EM), accounts for the greater majority (~80%) of the 4-cell stage embryos [38]. It has been established that in the case of ME-embryos, most of the progeny of the blastomeres that have undergone the first (M) division will contribute to the embryonic part or pluripotent inner cell mass (ICM), and the progeny from the subsequent E-division contribute more to the abembryonic part. In the EM embryos, the earlier E dividing blastomere contributes to either the embryonic or abembryonic part. In contrast, the progeny of the blastomeres in EE and MM embryos contribute randomly to both parts of the ICM [38] (Figure 4b).

The differential developmental potential of blastomeres of ME embryos appears to be associated with an epigenetic asymmetry: blastomeres derived from M divisions along the AV-axis show higher methylation levels of histone H3 on lysine residues 17 and 26 compared to the progeny of the E-dividing blastomere [48] Chimeras from different combinations of either M- or E-division derived blastomeres show that individual blastomeres with differential epigenetic states have different developmental potencies [38, 48, 49].

After the first few cleavage divisions the number of blastomeres increases to approximately 16-32 in the morula. During these early cleavage divisions, passive

global DNA demethylation takes place, which removes methylation from the maternal genome, again leaving genomic imprints intact [50-52].

At the 8-cell stage, blastomeres become polarized along their apical-basal axis as several proteins become asymmetrically localized [41, 53-55], and the 4th and 5th cleavage divisions can be divided in symmetrical divisions, generating only outer daughter cells, and asymmetrical divisions, leading to inner (basal regions) and outer (apical region) daughter cells (reviewed in [56]). Subsequently, tight junctions are formed between the outer cells separating the apical (outer cells) and basal (inner cells) regions [57]. The outer cells will give rise to the trophectoderm, whereas the inner cells will shape the ICM or the embryo proper. The ICM will retain pluripotency and is able to form all cell types, while the trophectoderm will give rise to the extra-embryonic tissue. Before implantation in the uterine wall, a cavity within the developing embryo forms. At this stage, the so-called blastocyste stage, the ICM (now subdivided in epiblast and hypoblast) lies in the blastocyst cavity, and is surrounded by the trophoblast. The epiblast is what ultimately gives rise to the three different germ layers: the ectoderm, mesoderm and endoderm, which together will form the future embryo, whilst the hypo- and trophoblast form the extraembryonic tissue.

In mammals, the XX females and XY males have to compensate for the dosage difference in X-linked genes between them [58]. This gene dosage compensation is achieved through inactivation of one of the X chromosomes during early female embryonic development (reviewed in [59]). During early mouse embryonic development, two separate phases of X chromosome inactivation (XCI) occur. First, the paternal X chromosome is specifically inactivated by unknown imprinting between the 4- and 8-cell stage.

Following implantation, the pluripotent epiblast cells in the female mouse embryo, start to differentiate into somatic cell lineages and undergo a second wave of XCI: the inactivated paternal X chromosome becomes reactivated, followed by random X chromosome inactivation [60-62]. Imprinted paternal X inactivation, however, is maintained in the extra-embryonic tissue [63, 64]. In humans, early female preimplantation embryos, X chromosome inactivation also takes place, from the 8-cell stage onwards [65]. However, it is still not certain if this early human XCI concerns either the maternal or paternal X chromosome and occurs through an imprinted pathway.

AIM AND SCOPE OF THIS THESIS

Correct pairing of homologous chromosomes in meiotic prophase requires the formation and repair of endogenously induced DNA double strand breaks. When chromosomes lack a homologous pairing partner or are not able to pair

correctly (e.g. due to translocations), the unpaired regions show persistent presence of DNA repair proteins and are subjected to meiotic transcriptional inactivation. This process is named meiotic silencing of unsynapsed chromatin (MSUC) [66, 67]. If these inactivated chromosomes contain genes that are essential during meiotic prophase, meiosis is arrested, leading to fertility disorders. Mammalian males are always faced with a pairing problem of their heterologous sex chromosomes (X and Y) due to the evolutionary degeneration of the Y chromsome. In meiotic prophase of human and mice, they pair and synapse only in the short pseudoautosomal regions, leaving the rest of the chromosomal arms unpaired. This unpaired or unsynapsed state is detected, and triggers a special form of MSUC, named meiotic sex chromosome inactivation (MSCI) (reviewed in [68]). In contrast with the infertility or reduced fertility that is associated with the occurrence of MSUC, spermatocytes are able to cope with the loss of X chromosome gene transcription, due to evolutionary adaptations which include the testis-specific expression of retroposed autosomal copies of several essential X chromosomal genes [69].

The central topic of this thesis concerns the mechanisms and consequences of MSUC and MSCI. To gain a broader understanding, we manipulated MSCI and MSUC in mammals, but we also studied meiotic chromosome pairing in birds, which have a female heterogametic sex chromosome system. In addition, we analysed chromatin reorganization and sex chromosome behaviour during spermatid differentiation and in early embryos. Successively in this thesis, the emphasis shifts from meiotic prophase (Chapters 2, 3, 4, 5 and 6) to postmeiotic development (Chapters 7 and 8) and early embryonic development (Chapters 8 and 9).

Chapter 2 provides a more detailed introduction of specific aspects related to the aims of this thesis. The first aim of this work was to gain insight in the mechanisms that initiate both MSUC and MSCI. Since homologous chromosome pairing and MSUC / MSCI share components of the DNA repair machinery, we first studied if there is a link between the presence of DNA double strand breaks and the repair of these breaks, homology recognition, and MSUC (Chapter 3). MSCI and MSUC have been described in a diversity of species, indicating an evolutionary advantage for these mechanisms. We analysed if MSCI also occurs in birds, a vertebrate species with ZW female heterogamety, which shows complete heterologous synapsis of the Z and W sex chromosomes (Chapter 4). In addition, we analysed the process of MSUC in male zebra finches, which carry a single and therefore continuous unpaired chromosome, the so-called germ cell restricted or GCR chromosome, to compare meiotic events for the GRC with this of the avian sex chromosomes (Chapter 5). Finally, we analysed the behaviour of X and Y chromosomes during the meiotic prophase in a different clade of vertebrate

species, the male dog, to establish how representative the XY pair of the male mouse during meiosis is for mammals in general (Chapter 6).

Recent observations have revealed that MSCI does not end after completion of the meiotic prophase. Rather, inactivation of sex chromosomes in male mammals is continued during postmeiotic spermatid development (PMSC, postmeiotic sex chromatin). In Chapters 7 and 8, we address the second aim of this thesis, to study the role of the ubiquitin-conjugating enzyme HR6B/UBE2B in meiotic and postmeiotic chromatin structure regulation. This study evolved from previous observations that *Hr6b/Ube2b* knockout male mice have low sperm counts and aberrant morphology of sperm heads, resulting in male infertility. This is associated with specific aberrations of chromatin structure, in particular of the X and Y chromosome [70]. In humans, sub- and infertility can often be overcome through the use of assisted reproduction techniques (ART) such as in vitro fertilization (IVF) and intracytoplasmic sperm injection (ICSI). By using these techniques, fertilization is facilitated by bringing the sperm and the oocyte in close contact (IVF) or through introduction of the sperm (ICSI) or spermatid (ROSI, round spermatid injection) into the oocyte by injection. We suggested that our *Hr6b/Ube2b* knockout mouse infertility model could provide valuable information about the relation between dysregulation of chromatin structure in spermatogenesis and its consequences for early embryonic development. Hence, we have studied the role of HR6B/UBE2B in maintaining genome integrity in spermatogenesis and early embryonic development, by using ICSI and ROSI in the mouse (Chapter 8).

During early female embryo development in the mouse, the paternal X chromosome is subjected to imprinted inactivation. It has been suggested that this imprinting is functionally linked to the meiotic inactivation of X and Y in the male germline [58, 71], although this is debated in view of the observation that the paternal X chromosome shows expression from zygotic gene activation until the 4-cell stage in female mouse embryos [72, 73]. Imprinted paternal X inactivation is initiated around the 4-cell stage but it does not occur simultaneously in all blastomeres within one embryo. This observation led to the third aim of this thesis, described in Chapter 9, where we studied the possible link between the timing of paternal X chromosome inactivation in individual blastomeres and the order and orientation of the cleavage divisions during early embryonic development.

The General Discussion (Chapter 10) summarizes the findings of this thesis, and possible future prospects are discussed.

REFERENCES

1. Luger K, Mader AW, Richmond RK, Sargent DF, Richmond TJ. Crystal structure of the nucleosome core particle at 2.8 A resolution. *Nature.* Sep 18 1997;389(6648):251-260.
2. Campos EI, Reinberg D. Histones: annotating chromatin. *Annu Rev Genet.* 2009;43:559-599.
3. Luger K, Hansen JC. Nucleosome and chromatin fiber dynamics. *Curr Opin Struct Biol.* Apr 2005;15(2):188-196.
4. De Grouchy J. Chromosome phylogenies of man, great apes, and Old World monkeys. *Genetica.* Aug 31 1987;73(1-2):37-52.
5. Painter TS. A Comparison of the Chromosomes of the Rat and Mouse with Reference to the Question of Chromosome Homology in Mammals. *Genetics.* Mar 1928;13(2):180-189.
6. Graves JA. Sex chromosome specialization and degeneration in mammals. *Cell.* Mar 10 2006;124(5):901-914.
7. Belmont AS. Mitotic chromosome structure and condensation. *Curr Opin Cell Biol.* Dec 2006;18(6):632-638.
8. Nasmyth K. Segregating sister genomes: the molecular biology of chromosome separation. *Science.* Jul 26 2002;297(5581):559-565.
9. Bhalla N, Dernburg AF. Prelude to a division. *Annu Rev Cell Dev Biol.* 2008;24:397-424.
10. Mahadevaiah SK, Turner JM, Baudat F, et al. Recombinational DNA double-strand breaks in mice precede synapsis. *Nat Genet.* Mar 2001;27(3):271-276.
11. de Boer E, Heyting C. The diverse roles of transverse filaments of synaptonemal complexes in meiosis. *Chromosoma.* Jun 2006;115(3):220-234.
12. Suja JA, Barbero JL. Cohesin complexes and sister chromatid cohesion in mammalian meiosis. *Genome Dyn.* 2009;5:94-116.
13. Lawson KA, Dunn NR, Roelen BA, et al. Bmp4 is required for the generation of primordial germ cells in the mouse embryo. *Genes Dev.* Feb 15 1999;13(4):424-436.
14. Culty M. Gonocytes, the forgotten cells of the germ cell lineage. *Birth Defects Res C Embryo Today.* Mar 2009;87(1):1-26.
15. Hayashi K, Surani MA. Resetting the epigenome beyond pluripotency in the germline. *Cell Stem Cell.* Jun 5 2009;4(6):493-498.
16. Adams IR, McLaren A. Sexually dimorphic development of mouse primordial germ cells: switching from oogenesis to spermatogenesis. *Development.* Mar 2002;129(5):1155-1164.
17. McLaren A, Southee D. Entry of mouse embryonic germ cells into meiosis. *Dev Biol.* Jul 1 1997;187(1):107-113.
18. Brennan J, Capel B. One tissue, two fates: molecular genetic events that underlie testis versus ovary development. *Nat Rev Genet.* Jul 2004;5(7):509-521.
19. Wilhelm D, Koopman P. The makings of maleness: towards an integrated view of male sexual development. *Nat Rev Genet.* Aug 2006;7(8):620-631.
20. Chassot AA, Ranc F, Gregoire EP, et al. Activation of beta-catenin signaling by Rspo1 controls differentiation of the mammalian ovary. *Hum Mol Genet.* May 1 2008;17(9):1264-1277.
21. Garcia-Ortiz JE, Pelosi E, Omari S, et al. Foxl2 functions in sex determination and histogenesis throughout mouse ovary development. *BMC Dev Biol.* 2009;9:36.
22. Ottolenghi C, Pelosi E, Tran J, et al. Loss of Wnt4 and Foxl2 leads to female-to-male sex reversal extending to germ cells. *Hum Mol Genet.* Dec 1 2007;16(23):2795-2804.
23. Parma P, Radi O, Vidal V, et al. R-spondin1 is essential in sex determination, skin differentiation and malignancy. *Nat Genet.* Nov 2006;38(11):1304-1309.

24. Pepling ME. From primordial germ cell to primordial follicle: mammalian female germ cell development. *Genesis*. Dec 2006;44(12):622-632.

25. Marchetti F, Wyrobek AJ. Mechanisms and consequences of paternally-transmitted chromosomal abnormalities. *Birth Defects Res C Embryo Today*. Jun 2005;75(2):112-129.

26. Wouters-Tyrou D, Martinage A, Chevaillier P, Sautiere P. Nuclear basic proteins in spermiogenesis. *Biochimie*. Feb 1998;80(2):117-128.

27. Leduc F, Nkoma GB, Boissonneault G. Spermiogenesis and DNA repair: a possible etiology of human infertility and genetic disorders. *Syst Biol Reprod Med*. Jan-Feb 2008;54(1):3-10.

28. Laberge RM, Boissonneault G. Chromatin remodeling in spermatids: a sensitive step for the genetic integrity of the male gamete. *Arch Androl*. Mar-Apr 2005;51(2):125-133.

29. Laberge RM, Boissonneault G. On the nature and origin of DNA strand breaks in elongating spermatids. *Biol Reprod*. Aug 2005;73(2):289-296.

30. McPherson S, Longo FJ. Chromatin structure-function alterations during mammalian spermatogenesis: DNA nicking and repair in elongating spermatids. *Eur J Histochem*. 1993;37(2):109-128.

31. McPherson SM, Longo FJ. Nicking of rat spermatid and spermatozoa DNA: possible involvement of DNA topoisomerase II. *Dev Biol*. Jul 1993;158(1):122-130.

32. Risley MS, Einheber S, Bumcrot DA. Changes in DNA topology during spermatogenesis. *Chromosoma*. 1986;94(3):217-227.

33. Malcuit C, Kurokawa M, Fissore RA. Calcium oscillations and mammalian egg activation. *J Cell Physiol*. Mar 2006;206(3):565-573.

34. Sutovsky P, Schatten G. Paternal contributions to the mammalian zygote: fertilization after sperm-egg fusion. *Int Rev Cytol*. 2000;195:1-65.

35. Wright SJ. Sperm nuclear activation during fertilization. *Curr Top Dev Biol*. 1999;46:133-178.

36. Gurdon JB. The generation of diversity and pattern in animal development. *Cell*. Jan 24 1992;68(2):185-199.

37. St Johnston D, Nusslein-Volhard C. The origin of pattern and polarity in the Drosophila embryo. *Cell*. Jan 24 1992;68(2):201-219.

38. Piotrowska-Nitsche K, Perea-Gomez A, Haraguchi S, Zernicka-Goetz M. Four-cell stage mouse blastomeres have different developmental properties. *Development*. Feb 2005;132(3):479-490.

39. Gray D, Plusa B, Piotrowska K, et al. First cleavage of the mouse embryo responds to change in egg shape at fertilization. *Curr Biol*. Mar 9 2004;14(5):397-405.

40. Piotrowska K, Zernicka-Goetz M. Early patterning of the mouse embryo--contributions of sperm and egg. *Development*. Dec 2002;129(24):5803-5813.

41. Plusa B, Frankenberg S, Chalmers A, et al. Downregulation of Par3 and aPKC function directs cells towards the ICM in the preimplantation mouse embryo. *J Cell Sci*. Feb 1 2005;118(Pt 3):505-515.

42. Hardy K, Martin KL, Leese HJ, Winston RM, Handyside AH. Human preimplantation development in vitro is not adversely affected by biopsy at the 8-cell stage. *Hum Reprod*. Aug 1990;5(6):708-714.

43. Gentry WL, Critser ES. Growth of mouse pups derived from biopsied blastocysts. *Obstet Gynecol*. Jun 1995;85(6):1003-1006.

44. Gentry WL, Critser ES. Developmental potential of microbiopsied murine blastocysts. *Obstet Gynecol*. Jan 1995;85(1):57-59.

45. Tarkowski AK. Experiments on the development of isolated blastomers of mouse eggs. *Nature*. Oct 24 1959;184:1286-1287.

46. Tarkowski AK. Studies on mouse chimeras developed from eggs fused in vitro. *Natl Cancer Inst Monogr.* Mar 1963;11:51-71.

47. Tsunoda Y, McLaren A. Effect of various procedures on the viability of mouse embryos containing half the normal number of blastomeres. *J Reprod Fertil.* Sep 1983;69(1):315-322.

48. Torres-Padilla ME, Parfitt DE, Kouzarides T, Zernicka-Goetz M. Histone arginine methylation regulates pluripotency in the early mouse embryo. *Nature.* Jan 11 2007;445(7124):214-218.

49. Piotrowska-Nitsche K, Zernicka-Goetz M. Spatial arrangement of individual 4-cell stage blastomeres and the order in which they are generated correlate with blastocyst pattern in the mouse embryo. *Mech Dev.* Apr 2005;122(4):487-500.

50. Kouzarides T. Chromatin modifications and their function. *Cell.* Feb 23 2007;128(4):693-705.

51. van der Heijden GW, Derijck AA, Ramos L, Giele M, van der Vlag J, de Boer P. Transmission of modified nucleosomes from the mouse male germline to the zygote and subsequent remodeling of paternal chromatin. *Dev Biol.* Oct 15 2006;298(2):458-469.

52. van der Heijden GW, Dieker JW, Derijck AA, et al. Asymmetry in histone H3 variants and lysine methylation between paternal and maternal chromatin of the early mouse zygote. *Mech Dev.* Sep 2005;122(9):1008-1022.

53. Jedrusik A, Parfitt DE, Guo G, et al. Role of Cdx2 and cell polarity in cell allocation and specification of trophectoderm and inner cell mass in the mouse embryo. *Genes Dev.* Oct 1 2008;22(19):2692-2706.

54. Thomas FC, Sheth B, Eckert JJ, Bazzoni G, Dejana E, Fleming TP. Contribution of JAM-1 to epithelial differentiation and tight-junction biogenesis in the mouse preimplantation embryo. *J Cell Sci.* Nov 1 2004;117(Pt 23):5599-5608.

55. Vinot S, Le T, Ohno S, Pawson T, Maro B, Louvet-Vallee S. Asymmetric distribution of PAR proteins in the mouse embryo begins at the 8-cell stage during compaction. *Dev Biol.* Jun 15 2005;282(2):307-319.

56. Wu Q, Bruce AW, Jedrusik A, et al. CARM1 is required in embryonic stem cells to maintain pluripotency and resist differentiation. *Stem Cells.* Nov 2009;27(11):2637-2645.

57. Fleming TP, Sheth B, Fesenko I. Cell adhesion in the preimplantation mammalian embryo and its role in trophectoderm differentiation and blastocyst morphogenesis. *Front Biosci.* Aug 1 2001;6:D1000-1007.

58. Huynh KD, Lee JT. Inheritance of a pre-inactivated paternal X chromosome in early mouse embryos. *Nature.* Dec 18 2003;426(6968):857-862.

59. Payer B, Lee JT. X chromosome dosage compensation: how mammals keep the balance. *Annu Rev Genet.* 2008;42:733-772.

60. Mak W, Nesterova TB, de Napoles M, et al. Reactivation of the paternal X chromosome in early mouse embryos. *Science.* Jan 30 2004;303(5658):666-669.

61. Okamoto I, Heard E. The dynamics of imprinted X inactivation during preimplantation development in mice. *Cytogenet Genome Res.* 2006;113(1-4):318-324.

62. Rastan S. Timing of X-chromosome inactivation in postimplantation mouse embryos. *J Embryol Exp Morphol.* Oct 1982;71:11-24.

63. Takagi N, Sasaki M. Preferential inactivation of the paternally derived X chromosome in the extraembryonic membranes of the mouse. *Nature.* Aug 21 1975;256(5519):640-642.

64. West JD, Frels WI, Chapman VM, Papaioannou VE. Preferential expression of the maternally derived X chromosome in the mouse yolk sac. *Cell.* Dec 1977;12(4):873-882.

65. van den Berg IM, Laven JS, Stevens M, et al. X chromosome inactivation is initiated in human preimplantation embryos. *Am J Hum Genet.* Jun 2009;84(6):771-779.
66. Turner JM, Mahadevaiah SK, Fernandez-Capetillo O, et al. Silencing of unsynapsed meiotic chromosomes in the mouse. *Nat Genet.* Jan 2005;37(1):41-47.
67. van der Laan R, Uringa EJ, Wassenaar E, et al. Ubiquitin ligase Rad18Sc localizes to the XY body and to other chromosomal regions that are unpaired and transcriptionally silenced during male meiotic prophase. *J Cell Sci.* Oct 1 2004;117(Pt 21):5023-5033.
68. Turner JM. Meiotic sex chromosome inactivation. *Development.* May 2007;134(10):1823-1831.
69. Wang PJ. X chromosomes, retrogenes and their role in male reproduction. *Trends Endocrinol Metab.* Mar 2004;15(2):79-83.
70. Baarends WM, Wassenaar E, Hoogerbrugge JW, et al. Loss of HR6B ubiquitin-conjugating activity results in damaged synaptonemal complex structure and increased crossing-over frequency during the male meiotic prophase. *Mol Cell Biol.* Feb 2003;23(4):1151-1162.
71. Kalantry S, Purushothaman S, Bowen RB, Starmer J, Magnuson T. Evidence of Xist RNA-independent initiation of mouse imprinted X-chromosome inactivation. *Nature.* Jul 30 2009;460(7255):647-651.
72. Okamoto I, Arnaud D, Le Baccon P, et al. Evidence for de novo imprinted X-chromosome inactivation independent of meiotic inactivation in mice. *Nature.* Nov 17 2005;438(7066):369-373.
73. Patrat C, Okamoto I, Diabangouaya P, et al. Dynamic changes in paternal X-chromosome activity during imprinted X-chromosome inactivation in mice. *Proc Natl Acad Sci U S A.* Mar 31 2009;106(13):5198-5203.
74. Oakberg EF. Duration of spermatogenesis in the mouse and timing of stages of the cycle of the seminiferous epithelium. *Am J Anat.* Nov 1956;99(3):507-516.
75. Oakberg EF. A description of spermiogenesis in the mouse and its use in analysis of the cycle of the seminiferous epithelium and germ cell renewal. *Am J Anat.* Nov 1956;99(3):391-413.
76. Oud JL, de Jong JH, de Rooij DG. A sequential analysis of meiosis in the male mouse using a restricted spermatocyte population obtained by a hydroxyurea/triaziquone treatment. *Chromosoma.* Feb 21 1979;71(2):237-248.
77. Russell LD, Ettlin R.A., Hikim A.P.S. and Clegg E.D. Histological and histopathological evaluation of the testis. 1990.

CHAPTER 2

MEIOTIC PAIRING OF HOMOLOGOUS CHROMOSOMES AND SILENCING OF HETEROLOGOUS REGIONS
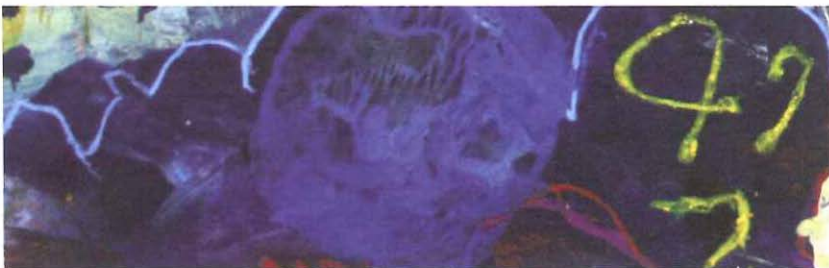
ABSTRACT

In meiotic prophase, homologous chromosomes pair and recombine, which ensures correct segregation of the homologs at the metaphase to anaphase transition of the first meiotic division. As a first step, early in meiotic prophase, DNA double-strand breaks (DSBs) are introduced by SPO11 at hundreds of sites throughout the genome. In mammals, formation and repair of these breaks is essential for the pairing process. The sex chromosomes, X and Y, are largely heterologous and pair only in the small pseudoautosomal homologous regions. The large heterologous regions show delayed repair of DSBs and asynapsis, which triggers meiotic sex chromosome inactivation (MSCI) leading to formation of the transcriptionally silenced XY body. Initiation of XY body formation is known to require phosphorylation of H2AX, which is also associated with damage-induced DSB repair in somatic cells.

MSCI is considered as a specialized form of a general meiotic silencing mechanism that also silences autosomal unsynapsed chromatin during male and female meiotic prophase: meiotic silencing of unsynapsed chromatin (MSUC). Whereas the XY pair remains always largely unsynapsed and inactivated, autosomal nonhomologous regions frequently show heterologous synapsis and escape from inactivation. Hence, MSUC is less efficient than MSCI. However, if MSUC occurs, MSCI is incomplete, indicating that the two mechanisms are functionally interacting.

Herein, we briefly review how X and Y evolved from a pair of autosomes, in relation to X-chromosomal dosage compensation in females and MSCI in males. Next we describe current ideas about initiation and maintenance of MSCI and MSUC. Insight in the mechanism of meiotic silencing is highly relevant for our understanding of male infertility associated with translocations, in particular when these occur between an autosome and the X. Furthermore, we anticipate that dysregulation of MSCI may impact on early embryonic development.

1. INTRODUCTION

The presence of the largely nonhomologous, or heterologous, X and Y chromosomes in the genome of mammalian males during meiosis is associated with specific problems. The Y chromosome is much smaller than the X chromosome and carries very few genes. The human X chromosome harbors at least 1000 genes. The X and Y share homology in the short pseudo-autosomal regions (PARs) that contain approximately 28 genes in humans (reviewed in [1]). Despite the current differences in length and gene content, X and Y have evolved from a pair of homologous autosomes (reviewed in [2]). DNA sequence analyses have revealed ancestral homology between genes on X and Y, and have confirmed the evolutionary relationship between X and Y [3,4]. Below, we will address how X and Y have become so divergent and how this has complicated regulation of X and Y pairing, their recombination and gene expression during meiosis.

A remarkable achievement of meiosis is the separation of homologous chromosomes. This process requires that homologous chromosomes can find each other, align over their full length, and stick together until the metaphase to anaphase transition of the first meiotic division. Moreover, in order to ensure that complete genome sets are separated during the metaphase-to-anaphase I transition, pairing between nonhomologous chromosomes needs to be prevented. One important aspect of the meiotic prophase is meiotic recombination. This involves the induction and repair of DNA double-strand breaks (DSBs), which leads to exchange of genetic information between homologous chromosomes. It is evident that correct repair of these DSBs is essential for the maintenance of genome integrity. This is important for cells undergoing mitosis, but it is even more important for germ cells. Errors in the separation mechanism lead to an unequal number of chromosomes (aneuploidy) in the resulting gametes, which is mostly incompatible with survival of the developing embryo, but can be viable when it concerns a small chromosome (trisomy 21) or the sex chromosomes. Therefore, it appears counterintuitive for a cell to generate DSBs on purpose upon entrance into meiosis.

With this review, we aim to highlight known and putative links between meiotic DSBs repair, homology recognition, synapsis, and detection and silencing of nonhomologous or heterologous regions such as the largely heterologous X and Y chromosomes or regions resulting from chromosomal aberrations such as translocations. Basic insight in these processes will contribute to our understanding of causes of male infertility, and may help to estimate the possible risks for the offspring, resulting from the application of assisted reproduction techniques using sperm from males with fertility problems resulting from impaired MSCI or activated MSUC.

2. EVOLUTION OF SEX CHROMOSOMES

Several events and mechanisms have contributed to the present heteromorphic length and gene content of the now largely heterologous sex chromosomes. Since there is no situation in the life cycle of mammals in which two Y chromosomes are present in the same nucleus, it also never recombines with another Y chromosome. In contrast, an X chromosome can pair and recombine with another X chromosome during meiotic prophase in XX oocytes. The Y does recombine with the X chromosome in spermatocytes, but solely in the short homologous PARs.

In an early mammalian ancestor, the initiation of the progressive differentiation of X and Y most likely started with the evolution of the dominant male sex-determining gene *SRY* on one member of a pair of autosomes [5], leading to the formation of a sex chromosome pair [6]. Meiotic recombination within the region containing the *SRY* gene became repressed, consolidating the new XX/XY sex-determining system, with a proto-X and proto-Y. How this is initially achieved is not known, but several mechanisms have been suggested (reviewed in [7]). For example, if *SRY* was located in a small reversed region of the genome, this could have contributed to the repression of meiotic recombination in that region. In addition, or alternatively, other male beneficial genes incorporated next to *SRY* might allow selection to act on this male-specific region as a whole, and this would be favoured by suppression of recombination in this whole region between the proto-Y and proto-X, to keep *SRY* in one functional unit with other male beneficial genes. With time, the region of suppressed recombination has expanded, and now encompasses the whole male-specific region of the Y (MSY), which is most of the Y chromosome.

The complete lack of meiotic recombination for the MSY has resulted in the gradual loss of the majority of functional genes that were present on the original proto-Y chromosome through various selection mechanisms that act during evolution (reviewed in [8]). In addition, accumulation of repetitive sequences on Y has led to the formation of large heterochromatic regions [9]. Complete degeneration of the human Y chromosome has been predicted to occur in approximately 14 million years (MY) [2]. However, recent sequence analyses of multiple single-copy Y chromosomal genes in more than 100 men of diverse genetic background has shown that there is very little variation in the protein coding regions of these genes; implying that natural selection effectively operates to preserve Y chromosome functionality in man [10]. In addition, human Y-linked genes have been surprisingly well conserved as compared to chimpanzee Y-linked genes. Comparative sequencing showed that no gene loss from Y has occurred in human during the 6 MY that separate the two species [10, 11]. Hence,

the widely suggested rate of Y chromosomal decline, with 4-5 single-copy genes disappearing every one million years, does not seem applicable for the human Y chromosome. Total degeneration of the Y chromosome may also be prevented, or at least delayed, via intra-Y-homolog recombination between palindromic regions [12], containing multi-copy genes, particular involved in spermatogenesis, although this is a vulnerable system, described as an Achilles' heel [13].

Stepwise fusion of the X chromosome with autosomal chromosomes, the so-called different evolutionary strata, and a series of Y-inversion events have also added to the current heteromorphic state of the sex chromosomes [2, 3]. Finally, acquirement of individual genes by autosome-to-Y and autosome-to-X transpositions also contributed to XY differentiation. Since most of these transposed genes and the remaining functional genes on Y have a testis-specific expression, the Y chromosome seems to have masculinized, and its functional regions exist mainly out of male-beneficial genes [14].

Mammalian XY differentiation began approximately 200 MY ago and the last major rearrangement on the human X chromosome occurred 30-50 MY ago [3]. The oldest part of the Y chromosome contains the sex determining gene *SRY* (distal tip of Yp) and the PARs, where X and Y can still recombine. Where the Y chromosome has evolved into a male beneficial gene enriched chromosome, the X chromosome has become enriched for genes benefical for reproduction and brain development [15]. The evolutionairy changes that occurred on X and Y, generating huge differences, complicate the pairing and recombination process during male meiotic prophase. Still, the heterologous X and Y need to associate, to ensure correct separation of X and Y during the first metaphase-to-anaphase transition.

3. HOMOLOGOUS CHROMOSOME PAIRING IN MEIOTIC PROPHASE

In meiotic prophase, all homologous chromosomes need to recognize each other before they can proceed with alignment, pairing, synapsis and recombination. Alignment and initiation of pairing occurs following the final S phase, in leptotene, pairing progresses during zygotene and is followed by synapsis, which is completed in pachytene nuclei. Synapsis is achieved by the formation of the synaptonemal complex (SC) between the chromosomal axes of the paired homologous chromosomes. X and Y also need to recognize each other, but at the same time, pairing of the heterologous regions needs to be avoided to prevent incorrect recombination. The exact mechanism by which homologous chromosomes recognize each other and prevent association between nonhomologous or heterologous chromosomes in meiotic prophase in mammals

is still enigmatic, although two important processes are known to be essential for chromosome pairing: bouquet formation and the generation and repair of meiotic DSBs.

3.1 Bouquet formation

After DNA replication in preleptotene, the telomeric repeats of all chromosomes associate with the nuclear envelope in leptotene, while the chromosomal arms loop towards the center of the nucleus. This is followed by aggregation and clustering near the centrosome, forming the transient meiotic bouquet (reviewed in [16, 17]). Specific components of the inner and outer nuclear membrane have been shown be essential for bouquet formation and (homologous) chromosome pairing in mouse [17]. Telomeric movements along the nuclear membrane enable the occurrence of transient interactions between the chromosomes [18], possibly contributing to homology recognition and pairing. Also, specific unique (DNA) sequences or chromatin components such as yet unknown pairing centers and centromeres may contribute to the initial homologous interactions (reviewed in [16]).

3.2 Meiotic DNA double strand break formation

Simultaneously with formation of the bouquet configuration of chromosomes at leptotene, several hundreds of meiotic DNA double strand breaks (DSBs) are induced by the topoisomerase-like enzyme SPO11 throughout the genome [19]. The presence of DSBs leads to activation of the checkpoint kinase ATM, which phosphorylates histone H2AX (forming γH2AX) in the regions surrounding the breaks [20-22]. In somatic cells, γH2AX marks damage-induced DSBs [22]. Formation and repair of meiotic SPO11 induced-DSBs is essential to achieve complete and correct chromosome pairing [23, 24].

3.3 Synaptonemal complex formation

During formation and repair of meiotic DSBs, a proteinaceous structure is assembled between the homologs. This structure, named the synaptonemal complex (SC), physically connects the homologous chromosomes, facilitates and stabilizes synapsis, and enables meiotic recombination (reviewed in [25]).

The assembly of the SC starts with the formation of the axial elements (AE) at leptotene, when SYCP2 and SYCP3 proteins form filaments along the chromosomal axes of the connected sister chromatids (reviewed in [26]). During this phase, specific sites on the chromosomes, such as "sticky" centromeric and pericentric heterochromatic regions in respectively budding yeast and *Drosophila* (reviewed in [16]), and pairing initiating regions in *Caenorhabditis elegans* [27], could establish transient interactions and stabilize the aligning chromosomes (reviewed in [16]). The sites of meiotic DSB repair (see below) seem to form the first physical

connections between homologous chromosomes, and could function as initiation sites of synapsis, at least in budding yeast (reviewed in [16]). However, the clustered and paired telomeres at the bouquet stage could also function as starting points of synapsis. This is suggested by the observation that synapsis during meiosis in humans appears to initiate from both ends of the SC, proceeding to the middle of the aligned chromosomal axes [28].

Apart from SYCP2 and SYCP3, the chromosomal axes also contain cohesins, in a protein complex that holds sister chromatids together. The meiosis-specific cohesin proteins REC8 and SMC1β colocalize with the AE component SYCP3 [29]. Analysis of mice deficient for genes encoding meiosis-specific components of the cohesin complex have shown that they are not only required to keep the sister chromatids connected during the first metaphase-to-anaphase transition, but cohesins also regulate the length of the SC and synapsis [30, 31].

Upon homologous chromosome alignment, the transverse element (TE) protein SYPC1, in cooperation with the central element (CE) components SYCE1, SYCE2 and TEX12, connects the homologous AEs (reviewed in [26]). The appearance of SYCP1 defines the moment of synapsis and the AEs are now termed lateral elements (LEs) in the completed SC. Knockout of each of these genes leads to very similar synaptic defects: meiotic chromosome pairs in spermatocytes from $Sycp1^{-/-}$, $Syce1^{-/-}$, $Syce2^{-/-}$, and $Tex12^{-/-}$ mice show normal alignment, but do not synapse and fail to complete repair of meiotic DSBs. In addition, the X and Y chromosomes do not pair in these mutants [32-35]. Also, in SYCP2 and SYCP3 deficient mice, chromosome pairing is also severely affected [36, 37]. It is important to note that the severity of the meiotic phenotype that is observed upon mutation of genes involved in meiotic recombination or synaptonemal complex formation is frequently different between males and females [38, 39]. For example, In $Sycp3$ knockout females, meiosis proceeds up to the diplotene stage, but many oocytes are lost during the first week of postnatal development [40]. Some oocytes even survive until adulthood, and embryos obtained from such oocytes are frequently aneuploid [40]. This and other sex-differences observed for the functions of genes involved in meiosis are thought to be due at least in part to a sex-differential regulation of checkpoints [41] (see also 3.5).

3.4 Meiotic DNA double strand break repair

In mitotic cells, DSBs can be repaired via nonhomologous end-joining (NHEJ) or via homologous recombination (HR) pathways. For the latter process, an intact homologous template is required, for which, after S phase, the sister chromatid is usually available.

In meiotic prophase, expression of proteins involved in NHEJ is repressed [43] and all meiotic DSBs thus need to be repaired by the more accurate HR

pathway. The meiotic DSB repair process is quite different from homologous recombination repair of damage-induced DSBs in somatic cells. First, meiotic breaks are not induced by damage or stalled replication forks, but generated by SPO11, an enzyme that remains covalently attached to the cleavage site [44]. SPO11 is an enzyme conserved from yeast to worm, flies and mammals. The DSBs are formed after the final S-phase and depend on several accessory factors that may help to localize and activate SPO11 (reviewed in [45]). Meiotic DSBs are not distributed at random in the genome but concentrate in so-called hotspots. Recent evidence indicates that histone modifications such as H3K4 trimethylation are involved in creating the chromatin environment that forms a hotspot [46]. SPO11 functions as a dimer, where one molecule remains covalently attached to each DSB end upon generation of the break (reviewed in [45].)

To allow DNA repair through HR, endonucleolytic cleavage of these protein-linked DSBs is necessary to remove the attached SPO11 together with some oligonucleotides [44]. In fission yeast, subunits of the MRN complex (MRE11, RAD50 and NSB1) in combination with the endonuclease Ctp1 are required for meiotic DSB processing, including cleavage and subsequent resection of the ends [47, 48] yielding 3'ended single-stranded DNA (ssDNA) overhangs [49] on each end of the break. The MRN complex is also involved in sensing the presence of (meiotic) DSBs, and aids in the localization of the kinase ATM to damage sites (reviewed in [50]).

Apart from the different origin and initial processing of SPO11-induced breaks compared to damage-induced DSBs in somatic cells, the homologous recombination mechanism itself has also been adapted for meiosis. The most important meiotic specialization of this repair pathway involves the inhibition of the use of the sister chromatid as a template for repair, thereby stimulating the search for the homologous chromosome. Several meiosis-specific DNA repair proteins and the synaptonemal complex contribute to the so-called interhomolog bias of the meiotic DSB-repair machinery. After the 3' ssDNA overhangs on each end of the DSB have been formed, the strand exchange protein RAD51, essential for strand invasion of the homologous DNA, forms filaments on these overhangs in mitotic cells [51]. Using immunocytology, the formation of RAD51 filaments can be observed as foci. In meiotic cells, not only RAD51, but also its meiosis-specific paralogue DMC1 assembles on the processed ssDNA ends [52] and these RAD51/DMC1 filaments initiate the search for homology ([53], reviewed in [54]). From these two repair proteins, DMC1 is believed to be the one that promotes repair via the homolog [55, 56]. When the ssDNA filament invades the dsDNA of the homolog, this brings them in close proximity to each other. The search for homology is most likely facilitated by the bouquet configuration and

the active movements of the chromosomes. This whole process of searching, occurring on several sites of DSB repair on each chromosome pair, most likely mediates correct alignment and pairing of homologous chromosomes.

Once homology has been detected, the ssDNA with the RAD51/DMC1 filaments invades the homologous template and a brief phase of DNA synthesis occurs (reviewed in [54]). Subsequently, crossovers (actual exchange of chromatids arms) and noncrossovers (gene conversion events) are formed through separate pathways that are strictly regulated; the number of crossovers is rather constant per species and sex, and highly outnumbered by the number of noncrossovers. Special mechanisms reduce the likelihood of two crossovers occurring in close proximity of each other, but ensure that each chromosome pair, including X and Y, contains at least one —obligate— crossover. In addition, Kleckner et al.[57] reported that the number of crossover sites correlates to the length of the SC. This indicates that there is a complex functional interplay between the formation and processing of meiotic DSBs and the structure of the chromosomes. It is not clear what the molecular basis of crossover interference is in mammals.

The importance of the generation and in particular the repair of meiotic DSBs for chromosome pairing is illustrated also by the infertility phenotypes of respectively *Spo11* and *Dmc1* knockout mice [23, 24, 58, 59]. In the absence of meiotic DSBs, in *Spo11* knockout mice, nonhomologous synapsis is observed, in addition to asynapsis [23, 24]. Thus, ongoing meiotic DSB repair, or repair-associated signaling, may inhibit nonhomologous synapsis. Still, when DSB repair is stalled in certain mutant mouse models, nonhomologous synapsis also occurs, indicating that these incompletely repaired DSBs cannot completely prevent heterologous synapsis [34, 59-61].

3.5 Meiotic checkpoint regulation during male meiotic prophase

To maintain genomic integrity, the repair process and the associated pairing of homologous chromosomes need to be tightly controlled. In budding yeast, two main meiotic cell cycle checkpoints have been identified: the replication or double-strand-break checkpoint, coupling the completion of premeiotic DNA replication to the introduction of SPO11-induced meiotic DSBs, and the pachytene checkpoint, monitoring correct (homologous) DSB repair, meiotic recombination, and synapsis (reviewed in [62]).

Careful analysis of many meiotic mutants in mouse has revealed that incomplete meiotic DSB repair and synapsis trigger apoptosis around midpachytene, corresponding to Stage IV of the cycle of the seminiferous epithelium in mouse (Figure 3b, Chapter 1) [42, 63], indicating that a checkpoint operates at this stage. It has been proposed that this checkpoint is triggered by failure to inactivate the X and Y chromosome (meiotic sex chromosome inactivation, see below), and this

idea (reviewed in [64, 65]) would provide at least one attractive possible reason for the sex-difference in meiotic phenotypes of many mutants.

The two related kinases ATM and ATR perform pivotal functions in the activation of cell cycle checkpoints in somatic cells. The SPO11 mediated induction of meiotic DSBs activates ATM, which enables the first meiotic wave of phosphorylation of H2AX [20]. ATR is expressed somewhat later, and is required for γH2AX formation on XY body chromatin (see below) [20, 66]. $Atm^{-/-}$ spermatocytes show a failure in meiotic DSB repair and chromosome synapsis, and apoptosis is induced at the mid-pachytene checkpoint, indicating that ATM is not required for this checkpoint [67]. $Spo11$ heterozygosity allows progression of the meiotic prophase of $Atm^{-/-}$ spermatocytes until the first metaphase, when increased spermatogenetic apoptosis is still observed, indicating that metaphase I also functions as a checkpoint moment [67, 68]. In these $Spo^{+/-}Atm^{-/-}$ mice, reduced or delayed formation of meiotic DSBs may help ATR to compensate for the loss of ATM [67, 68].

In many organisms, cell cycle checkpoint proteins (such as ATR and ATM) not only function as surveillance proteins, but are also indispensable for completion of DSB repair and meiotic recombination. Phosphorylation of the yeast meiosis-specific HORMA-domain protein HOP1 by ATR and ATM homologs (MEC1 and TEL1) is required for meiotic prophase checkpoint activation as well as for interhomolog-directed repair [69]. Recently, two mammalian homologs of the yeast Hop1 protein, named HORMAD1 and HORMAD2, have been identified [33]. Early in meiotic prophase, HORMAD1 and 2 accumulate on unsynapsed chromosomal axes. They are removed when the SC forms between homologous chromosomes [33]. As expected, HORMAD1 and 2 both remain present on the unsynapsed parts of X and Y [33, 70].

4. SEX CHROMOSOMAL BEHAVIOUR DURING MAMMALIAN SPERMATOGENESIS

4.1 Pairing of X and Y in meiotic prophase

As mentioned above in section 2, the X and Y chromosomes are largely heterologous as a consequence of the evolutionary degeneration of Y and reorganisation of X. During zygotene, synapsis between X and Y is initiated in the pseudoautosomal regions (PARs) and appears to continue along most (90%) of the length of the Y chromosome at early pachytene in mouse (Figure 1AB and [71]), including nonhomologous regions. Apparently this heterologous synapsis is a transient state since hereafter X and Y desynapse gradually until they only remain connected at their homologous tips in late pachytene and diplotene [71]. This observation indicates that progression of synapsis is dynamic, allowing desynapsis
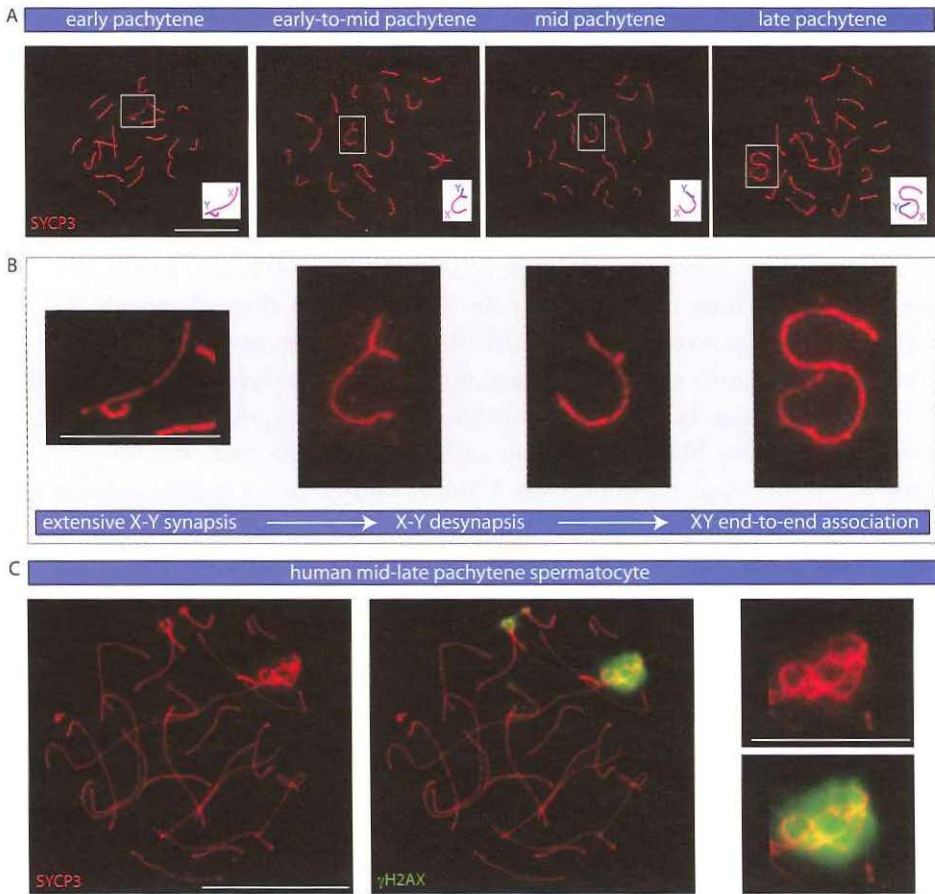
Figure 1. Extensive (heterologous) synapsis between X and Y at early pachytene is followed by desynapsis and subsequent end-to-end association. (a) Overview of the different XY associations during pachytene in mouse spermatocytes. Spermatocyte spread nuclei immunostained for SYCP3 (red). The position of the XY pair is indicated by a box and the appearance of the SC is schematically depicted in the lower right corner of each image. Bar represents 10 μm. (b) Enlargement of the XY pair from the panel, and the bar represents 5 μm. (c) Human spermatocyte in pachytene stained for SYCP3 (red) and γH2AX (green). Bar represents 10 μm. Higher magnifications of XY pair are shown on the right. Bar represents 5 μm.

when an unknown control mechanism detects absence of homology. For the XY pair, this mechanism appears to be efficient, since persistent heterologous synapsis between X and Y is not observed.

Throughout pachytene and diplotene, X and Y reside in a specific chromatin region adjacent to the nuclear membrane, named the XY body. In human spermatocytes, the morphology of the X and Y chromosomal axes is more

complicated in pachytene nuclei as compared to mouse, although extensive synapsis has also been described [72]. Partial synapsis is visible in immunofluorescent analyses of early pachytene nuclei, but the XY chromatin condenses rapidly thereafter, and the SC structure has a disorganized appearance (Figure 1c and [71 73]), forming the XY body.

4.2 Meiotic DSB repair at X and Y

Chromosomes or chromosomal regions without a homologous pairing partner can only repair their meiotic DSBs (in these regions) through recombination with the sister chromatid or via NHEJ. Since both these pathways appear to be repressed during early meiotic prophase, meiotic DSBs in such regions may remain unrepaired. During the zygotene-to-pachytene transition, the XY pair becomes easily recognizable because it is the only chromosome pair with incomplete synapsis. At this stage, the number of RAD51/DMC1 foci in spermatocyte nuclei has already decreased dramatically compared to leptotene/zygotene [75]. Few foci still persist on the autosomes in early pachytene, but the unsynapsed part of the X chromosome is always marked by several persistent RAD51/DMC1 foci [75, 76]. Concomitant with the gradual decrease in the number of RAD51/DMC1 foci, the overall level of γH2AX also decreases. However, a second wave of γH2AX formation occurs specifically on the XY body and this phosphorylation is mediated by ATR [20, 66]. ATR first localizes the unsynapsed parts of the XY pair, after which it also spreads to the synapsed part [77-79]. The unsynapsed part of the X chromosome is also marked by increased levels of persistent foci of DSB repair and checkpoint proteins (Table I) until late pachytene/early diplotene, indicating that repair of DSBs along the X chromosome is severely delayed.

Surprisingly, RAD51 foci are only rarely observed along the unsynapsed part of the Y in mice [76]. It is not known whether SPO11 does not induce breaks on this part of Y. RNA-FISH analyses have provided indications that the Y chromosome is already partially inactive in mouse spermatogonia and a heterochromatic chromatin structure encompassing most of the Y chromosome may interfere with access of SPO11 to the DNA [80]. Also, these breaks might somehow be more rapidly repaired on Y compared to the X chromosome. In human, due to the repetitive nature of the Y chromosome, such repair might occur via intra-chromosomal recombination during zygotene, simultaneously with homologous recombination repair on autosomes [13, 14].

In addition to several DSB repair and checkpoint proteins (Table 1), the postreplication DNA repair pathway proteins HR6A, HR6B and RAD18 also accumulate on the X and Y chromosomes during pachytene [81]. HR6A and HR6B encode two very similar mammalian homologs of the ubiquitin-conjugating enzyme RAD6 in yeast [82] and form a complex with the ubiquitin ligase RAD18

Table 1. Proteins involved in DNA repair and checkpoint activation enriched on the XY body

Protein	Function	Pattern on XY	Reference
ATR	Protein kinase involved in DNA replication, DNA damage response and checkpoint activation	Axial elements and chromatin	[78]
BLM	Member of the RecQ helicase family, functions in DSB repair	XY body chromatin	[138]
BRCA1	Functions in homologous recombination repair of DSBs. Ubiquitin ligase activity. Checkpoint mediator protein	Axial elements	[139]
BRCA2	Functions in homologous recombination repair of DSBs, stimulates RAD51 filament formation	Axial elements	[140]
DMC1	Meiosis-specific paralogue of RAD51	Focal (X) along axial elements	[52]
γH2AX	γH2AX phosporylated at S129, mediated by ATR at the XY body	XY body chromatin	[20, 21, 52]
H2AK119ub1	H2A mono-ubiquitylated at K119, silences chromatin and recruits DSB repair proteins	XY body chromatin	[98]
HORMAD1/2	Meiosis-specific HORMA domain containing proteins involved in DSB repair, interhomolog bias and checkpoint activation	Axial elements	[33, 141]
HR6B	Functions in DSB and postreplication repair and is required for H2B ubiquitylation. Ubiquitin-conjugating enzyme activity	XY body chromatin	[81]
Ku70	Involved in nonhomologous end-joining pathway	XY body chromatin	[43]
MDC1	Early responder to DSBs, facilitates ATM and MRE11 complex recruitment	XY body chromatin	[142]
MRE11	Component of the MRE11 complex, involved in sensing and repair of DSBs and checkpoint signalling. Endonuclease activity	XY body chromatin	[43]
RAD1	Component of the 9-1-1 complex, involved in cell cycle checkpoint activation	Axial elements	[143]
RAD18	Functions in DSB and postreplication repair pathways. Ubiquitin ligase activity. Ubiquitylates PCNA	XY body chromatin	[81]

Table 1. Continuation

Protein	Function	Pattern on XY	Reference
RAD51	Catalyzes homologous recombination reaction using ATP-dependent DNA binding activity and a DNA-dependent ATPase	Focal (X) along axial elements	76
TOPBP1	Functions in DNA replication and DNA damage response, activates ATR	Axial elements and chromatin	144, 145
53BP1	Role in the recruitment of proteins to double stranded breaks in DNA. Checkpoint mediator protein	XY body chromatin	142

[83]. In yeast, the RAD6-RAD18 complex is required for the ubiquitylation of the sliding clamp protein PCNA [84], which forms a trimeric ring around the DNA and is indispensable for DNA replication. HR6A and HR6B are also involved in the ubiquitylation of the histone H2B in yeast and mammalian cells [85, 86]. Although HR6A and HR6B perform redundant essential functions in somatic cells [87], HR6B is specifically required during meiotic and postmeiotic male germ cell development [88].

Around mid-diplotene, the DNA repair proteins and γH2AX have disappeared from the XY body, indicating that the breaks have been repaired. At this stage, repair via the sister-chromatid may no longer be blocked. Alternatively, or in addition, NHEJ may have been reactivated at this stage and participate in repair of the persistent meiotic DSBs [89].

In contrast to delayed DSB repair on the unsynapsed parts of X and Y, repair of DSBs that localize to the pseudoautosomal region of the XY pair appears to occur with normal, or perhaps even accelerated timing [90]. RAD51 foci do not persist in this region of X and Y, and the single obligate crossover appears to be formed slightly ahead of the crossovers on the autosomes [90],

4.3 Meiotic sex chromosome inactivation (MSCI)

During the consecutive stages of spermatogenesis, X- and Y-linked genes show three different expression profiles. In mitotically dividing spermatogonia, genes from the X and Y chromosomes are actively transcribed, and male germ-cell specific genes have been found to be overrepresented on the X chromosome in these cell types [91]. However, as mentioned above, Namekawa et al. [80] reported that in type A and B spermatogonia, the Y chromosome appears to be at least partially inactive, based on results from RNA FISH analyses.

Upon entrance into meiotic prophase, transcription of genes located on the X chromosome starts to decrease [15]. Concomitant with completion of synapsis between all autosomes around the zygotene-to-pachytene transition, meiotic sex chromosome inactivation (MSCI) is initiated and the largely unsynapsed X and Y form the inactivated XY body (or sex body) in the periphery of the nucleus [92]. The XY body is a specialized chromatin domain, not a membrane enclosed vesicle, which remains visible as a more or less separate DAPI domain until the end of meiotic prophase. Immunocytochemical analyses have shown that the XY body is visibly depleted for RNA polymerase II from midpachytene onwards [80, 93]. In addition, microarray analyses of isolated cell types have shown that the average RNA expression level of X chromosomal genes is very low in spermatocytes as compared to spermatogonia fractions [80]. However, many X-linked miRNA genes escape MSCI since they remain actively transcribed by RNA polymerase II throughout meiosis [94]. How the transcription of miRNAs is achieved in the XY body is unclear; perhaps specific factors that bind to miRNA gene promoters allow RNA polymerase to transcribe these genes. The amount of RNA polymerase II that is actually involved in this miRNA-related process may be low, explaining why the whole XY body appears to be devoid of RNA polymerase II.

The X chromosome contains many genes that perform functions that are essential for cell viability. For several of these genes, retroposed intronless copies have emerged on autosomes during the course of evolution, which can compensate for the loss of transcription from the X-encoded variant because of MSCI, and these autosomal retroposed genes mostly show testis-specific expression [95].

The ATR-mediated phosphorylation of H2AX is the earliest known histone modification on the XY body and this modification has been shown to be required for the initiation of MSCI [96]. In addition, unknown chromatin components become sumoylated around late zygotene [97] followed by ubiquitylation of H2A on the XY [98] and deposition of histone macroH2A1.2 ([96] around early pachytene. In pachytene, the X and Y chromosomes also undergo a series of histone modifications, such as deacetylation of H3 and H4 [99], most likely contributing to transcriptional silencing of the XY body. In addition, a global nucleosome replacement occurs around midpachytene [100]. The exact functions of these modifications and proteins are not known, but they could play a role in the maintenance of MSCI.

So far, a few knockout mouse models have been described in which initiation of MSCI is perturbed. In the complete absence of formation of meiotic DSBs, as occurs in *Spo11*^{-/-} mice, chromosome pairing in spermatocytes is severely affected;

X and Y hardly ever associate in these cells and are not silenced. This indicates that DSB formation could be essential for "true" XY body formation. However, one or two subnuclear regions containing part of the asynapsed chromatin but mostly not overlapping with X and Y still show enhanced accumulation of ATR and γH2AX in the *Spo11*^{-/-} mice [20], apparently independent of the presence of meiotic DSBs. These so-called pseudo-XY body regions are also transcriptionally silenced [101], similar to the silencing of the XY body in wild types. Thus, it seems that in the absence of meiotic DSBs, there is still some unknown activity on (part of the) asynapsed axes that nucleates the formation of a silenced chromatin area; the pseudo-XY body.

When meiotic DSB repair is blocked, such as in *Dmc1* knockout mice, the XY body or a pseudo-XY body are not formed [58, 59], and in such nuclei, RAD51 and γH2AX persist at many sites in the nucleus. This indicates that components of the DSB-repair machinery and the XY silencing machinery may be shared and limiting in amount. In addition, such nuclei also show impaired homologous chromosome pairing. Based upon the fact that in *Spo11* mutants, the pseudo-XY body forms on only a small part of the asynapsed axes, it appears that the presence of asynapsed axes by itself is not sufficient to trigger meiotic silencing. However, the pseudo-XY body formation in the *Spo11* knockout also argues against meiotic DSBs being the sole factor in the initiation of MSCI. The presence of DSB-repair associated proteins on the XY body and the inhibition of XY body formation and MSCI when DSB-repair is blocked, point towards a link between the DSB-repair machinery and the XY silencing machinery.

Apart from proteins encoded by the *Spo11* and meiotic-DSB repair genes, the poly(ADP-ribose) polymerase 2 (PARP2) enzyme also appears to be involved in MSCI. *Parp2*^{-/-} spermatocytes show a general decrease in crossover frequency, defective SC formation between X and Y chromosomes and also an impairment in MSCI. PARP2 controls chromatin structure and genomic integrity in response to DNA damage, again providing a link between DNA damage response pathways and MSCI [102].

Taken together, it appears likely that the detection of heterologous regions is tightly coupled to the process of homology recognition. Both processes appear to have DSB-dependent and DSB-independent aspects. In addition, checkpoint proteins, such as ATR and perhaps also the newly identified HORMAD proteins, play essential roles in marking unsynapsed regions (often containing persistent meiotic DSBs) for meiotic silencing.

4.4 Meiotic silencing of unsynapsed chromatin (MSUC)

MSCI appears to be a specialized form of a general meiotic silencing mechanism that silences unsynapsed (autosomal) heterologous chromatin in spermatocytes and oocytes [103, 104], termed meiotic silencing of unsynapsed chromatin, MSUC [105].

This mechanism is activated for example when translocations or inversions interfere with normal chromosome pairing, and on the single X chromosome in oocytes of XO mice [103,104]. In these unsynapsed, silenced, heterologous chromatin regions, persistence of meiotic DSB repair proteins is also observed, similar to what has been reported for the unsynapsed part of the X chromosome in the XY body. The X and Y chromosomes in spermatocytes are always subjected to meiotic silencing, but autosomal chromosomes with nonhomologous regions or the single X chromosomes in XO oocytes can sometimes evade MSUC by achieving heterologous synapsis.

Variable heterologous synapsis is detected when specific translocations cause a pairing problem. For example, in mice carrying two similar but not identical translocations between chromosome 1 and chromosome 13, a heterologous region of approximately 40 Mb is present on both the small 1^{13} bivalent and the large 13^1 bivalent. The small translocation bivalent shows heterologous synapsis in only 40% of the nuclei, whereas the larger bivalent with a heterologous region with the same size succeeds to complete heterologous synapsis in more then 95% of the nuclei [106]. Such heterologous synapsis is thought to occur via an adaptive process, called synaptic adjustment. The axial/lateral elements of the SC can be considered as a basal axis that connects the loops of chromatin. The length of these loops determines axis length, and during synaptic adjustment, chromatin loop length is adjusted to equalize the axis length of the two chromosomal regions that are heterologous [107]. It is evident that heterologous synapsis should be generally avoided, because it interferes with homologous chromosome pairing. However, heterologous synapsis of small regions may help the cell to escape from a possible synapsis checkpoint or may prevent silencing of essential meiotic genes by MSUC, allowing spermatocytes with a minor pairing problem to survive and continue with their meiotic progression.

Certain heterologous regions remain unsynapsed in a fraction of pachytene nuclei, whereas they synapse heterologously in the rest of the nuclei [81, 107]. When heterologous regions remain unsynapsed, they accumulate the DNA repair- and MSCI-linked proteins DMC1/RAD51, BRCA1, ATR, HR6B and RAD18, and the phosphorylated form of H2AX, in human and mouse spermatocytes and oocytes [103, 104, 108], and this is then always associated with transcriptional silencing of these unsynapsed regions. Conversely, when heterologous synapsis occurs, DNA repair proteins are not observed in these synapsed regions, and the chromatin is
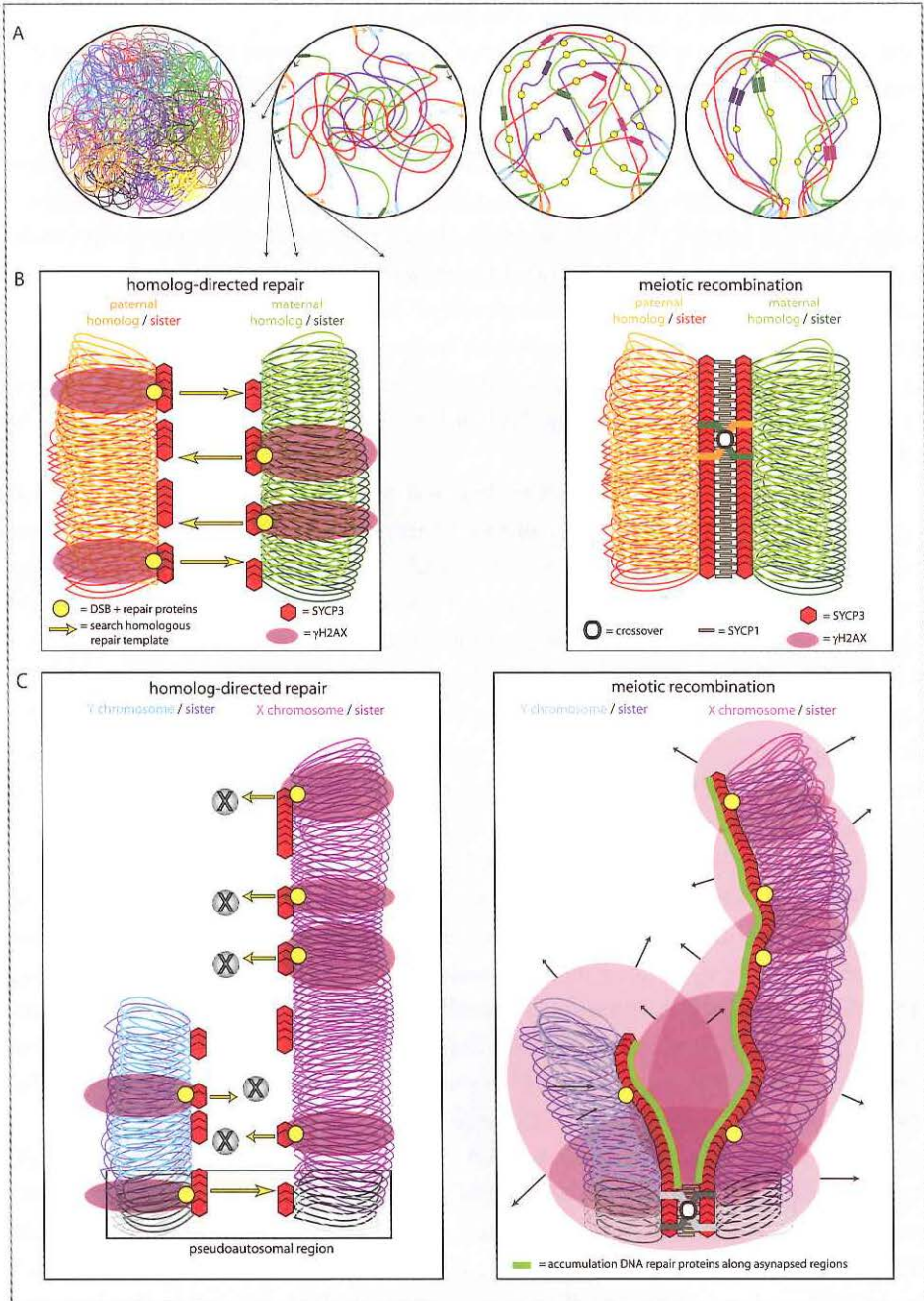
Figure 2. Model for the process of homology recognition, linked to meiotic DSB repair and MSCI. (a) In early leptotene, all telomeres become attached to the nuclear membrane, and cytoskeletal fibres originating in the cytoplasm pull the telomeres along on the membrane. Simultaneously, hundreds of meiotic DSBs are induced (yellow dots) ▷

not silenced. Thus, there is a tight coupling between the prolonged presence of DNA repair proteins, hence the persistence of DSBs and unsynapsed silenced chromatin.

In spermatocytes in which MSUC has been activated, MSCI seems to be impaired [109]. This appears somewhat similar to what is observed in *Spo11*^{-/-}, *Atm*^{-/-} and *Dmc1*^{-/-} mouse mutants with impaired meiotic DSB repair as mentioned in sections 3.5 and 4.3. In such mutants, persistent DSB sites also interfere with MSCI [20, 42, 58, 59, 63, 67, 68, 96, 101]. These findings indicate that functional components of the DNA repair machinery and the MSCI/MSUC machinery are shared and limiting in their amount; for example, the amount of ATM/ATR that has to phosphorylate H2AX may be limiting. Unsynapsed and silenced autosomal chromosomes often localize adjacent to the silenced X and Y chromosomes; formation of such a single silenced chromatin region may help to concentrate the shared factors that mediate MSCI and MSUC within the same region of the spermatocyte nucleus.

▷ throughout the genome, and a search for a homologous repair-template is initiated. The chromosomal movements facilitate numerous transient interchromosomal interactions, allowing an efficient homology scan by the DSB repair machinery. If homology is confirmed, stable interactions can be formed, and strand invasions associated with DNA repair follow. Pairing regions and "sticky heterochromatic" regions (colored rectangled block) may also contribute to homology recognition and aid in the stabilisation of homologous pairing. (b) Each individual autosomal homologous chromosome pair acquires many DSBs and simultaneously assembles the lateral element, SYCP3, of the synaptonemal complex. The homology-directed meiotic DSB repair occurs in association with the assembly of the SC, and the intimate contacts that occur during strand invasion allow SYCP1 and other central elements of the SC to assemble between the SYCP3 proteins on both homologs. Some of the DSBs (at least one per chromosome pair) are converted to crossovers, and these are required for proper segregation during the first metaphase to anaphase transition. Following completion of the DNA repair process, H2AX becomes dephosphorylated. (c) The X and Y chromosomes undergo the same processes as the autosomes: induction of DSBs and assembly of SYCP3. However, apart from the pseudoautosomal region in which the obligatory crossover will be formed, no regions of homology are present. This interferes with the homologous recombination repair process of meiotic DSBs on the X chromosome, due to the absence of a homologous repair-template. SYCP1 deposition and SC formation initiates from the pseudoautosomal region, but does not proceed, or is unstable, in the heterologous regions. The delayed repair of DSBs could cause continuous accumulation of DNA repair proteins, and above a certain threshold ATR may be recruited. Alternatively, or in addition, accumulation of (DNA repair) proteins that specifically associate with the unsynapsed chromosomal axes may recruit ATR. This leads to spreading of ATR and other (DNA repair) proteins along the XY chromosomal axes. Subsequently, phosphorylation of H2AX spreads into the surrounding chromatin, mediating recruitment of downstream factors, including the factors that mediate transcriptional silencing in the XY body.

4.5 Postmeiotic silencing of sex chromosomes (PMSC)

Inactivation of the majority of X- and Y- chromosomal genes continues beyond meiotic prophase, in spermatids, and persists until the end of spermatogenesis, when the whole genome is shut down [80, 93]. Around late pachytene, the inactivated XY pair acquires di- and trimethylated H3K9, that is associated with transcriptional repression [99]. H3K9me3 mediates the recruitment of the Chromobox protein 1 (CBX1), a well known heterochromatin marker, to the XY chromatin [110]. The histone methylation marks and CBX1 remain present on X and Y until the histone-to-protamine transition in late spermiogenesis [80, 93], indicating continued repression of X and Y. Recently, it has been shown that the multi-copy Y-chromosomal gene *Sly* plays a pivotal role in X- and Y-chromosome silencing in mouse spermatids [111]. Through inhibition of *Sly* expression with small RNAs expressed from a transgene, it was shown that *Sly* is involved in the maintenance of CBX1 and H3K9me3 on X and Y in postmeiotic nuclei [111]. In addition, deficiency for SLY leads to a global postmeiotic de-repression of X and Y genes, resulting in sperm defects [111, 112].

How can expression of a Y chromosomal gene function in the maintenance of repression of Y chromosomal gene transcription, if it is repressed by MSCI itself? This can be explained by the fact that, although most X- and Y-encoded genes remain repressed in postmeiotic cells, [80, 93] the majority of X- and Y-linked multi-copy genes —including *Sly*— show postmeiotic re-expression [113]. In addition, a small number of single-copy genes are re-expressed [113, 114].

5. SILENCING OF X AND Y DURING SPERMATOGENESIS AND X CHROMOSOME INACTIVATION IN FEMALE SOMATIC CELLS ARE INDEPENDENT MECHANISMS

It can be imagined that MSCI and postmeiotic repression of X and Y would leave some epigenetic mark that could affect the regulation of gene expression from the sex chromosomes in early embryos. This idea is relevant in the context of the fact that species with heterologous sex chromosomes not only have to deal with pairing problems in meiotic prophase of the heterogametic sex, they also have to compensate for the dosage difference in X-linked genes between males and females [115]. Female mammals achieve dosage compensation through inactivation of one of their X chromosomes during early development (reviewed in [116]). The active X shows a twofold upregulation in somatic tissues in both male and females, to equalize the average X chromosomal gene expression level to that of autosomes [117, 118].

From the 2-cell stage onwards in mouse embryos, the paternal X chromosome is specifically inactivated in female mouse embryos. This imprinted form of XCI persists in the extraembryonic tissues but is reversed and replaced by random X-inactivation in the embryo proper. The process of mammalian X chromosome inactivation is thought to have spread gradually over those regions of the X that had lost homology with Y (reviewed [2]), most likely paralleling the occurrence of the different strata. The fact that most of the human X-linked genes without a Y homolog that still escape XCI are located on the younger strata [119] supports this idea, and indicates that XCI may still be expanding.

In order for XCI to occur, the presence of the X inactivation center (Xic) is necessary [120, 121]. Several non-coding RNA genes are located in the Xic, including the *Xist* en *Tsix* genes. [122-124]. *Xist* is specifically expressed from the inactivated X chromosome (Xi), and is required for XCI to occur in *cis*. The spreading of *Xist* RNA over the X chromosome from which it is transcribed induces its heterochromatinization [125, 126]. *Tsix* is transcribed antisense to *Xist,* and both genes overlap in mice. *Tsix* negatively regulates expression of *Xist.* Recently, it was described that human female preimplantation embryos also show progressive *Xist* RNA accumulation on one of the two X chromosomes [127]. It is not known whether this early XCI occurs at random or only on the paternal X, as in mouse.

Althought *Xist* and *Tsix* genes are not required for MSCI and PMSC [123, 128], it has been suggested that the two mechanisms (MSCI and XCI) might be functionally connected. As described above, the inactivation of X and Y during meiosis may leave an epigenetic imprint on the X chromosome, and this might play a role in the imprinted paternal X chromosome inactivation (XCI) in the early female mouse embryo from the two-cell stage onward. To test the hypothesis that MSCI facilitates paternal X-inactivation in the early mouse embryo, Okamoto et al. [129], analysed expression of an autosomally localized transgenic copy of *Xist* in germ cells and early embryos. They found that the transgene was not silenced by MSUC during meiotic prophase, and that the transgenic *Xist* gene still showed expression only when present on the paternal copy in the zygote. In addition, they showed that the paternal X chromosome is active in two-cell embryos, excluding the inheritance of the X in a "pre-inactive state" [129]. The *Xist* gene is absent from the marsupial genome and imprinted inactivation of the paternal X in this species occurs in all cells by an unknown mechanism. MSCI does occur in the male germline of marsupials, but —similar to mouse and man— the paternal X is active in early embryos [111], again arguing against a link between MSCI and imprinted X-inactivation, even in the absence of *Xist* [111]. In contrast to the theory that proposes a pre-inactive paternal X, it has also been suggested that the protamine-to-histone transition occurring directly after fertilization in
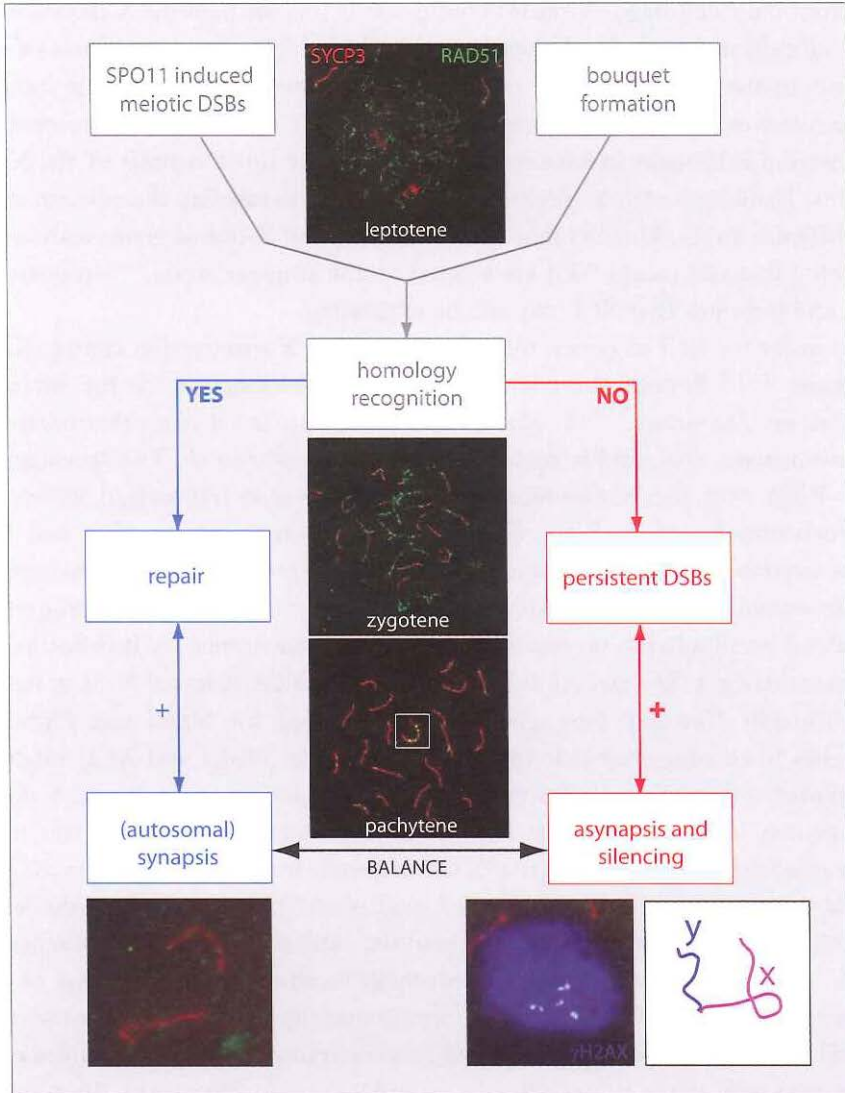
Figure 3. Persistent meiotic DSBs homology recognition and transcriptional silencing of heterologous regions. SPO11-induced DSBs and the bouquet configuration of the chromosomes both contribute to the homology recognition process. Numerous RAD51 foci in leptotene nuclei mark the intitiation of the homology search. If homology recognition occurs, DSB repair proceeds and this is coupled to stimulation of progression of SC formation in zygotene nuclei (and SC formation may also help to complete the DSB repair process), leading to the complete SC with few remaining RAD51 foci in diplotene. If homology recognition does not occur, the DSB persists, additional DSB repair proteins accumulate, and spread along the chromatin, and progression of SC formation is inhibited (and lack of SC formation also inhibits invasion of the homologous template). This is associated with the recruitment of ATR to asynapsed regions, which ▷

the male pronucleus of the zygote may facilitate rapid activation of the paternal X chromosome, thereby enhancing the chance of *Xist* transcription from the paternal X [130]. This hypothesis has not yet been tested.

6. MEIOTIC SILENCING OF SEX CHROMOSOMES IN A SPECIES WITH FEMALE HETEROGAMETY

In contrast to the XY/XX male/female sex chromosome system in mammals, birds have a ZW female and ZZ male sex chromosome constitution. Recently, it was discovered that sex in birds is determined by the dosage of the Z-linked *DMRT1* gene. The higher *DMRT1* dose in ZZ chickens drives the bipotential gonads to become testes [47]. Similar to the mammalian male Y chromosome, the avian female W chromosome carries few genes; so far only 4 genes have been identified [131]. In addition, the gene content of the Z chromosome appears to have masculinized, showing an overrepresentation of male-biased genes [131]. This is comparable to the over-representation of female-biased genes on the mammalian X chromosome [132].

The heterologous mammalian X and Y chromosomes remain largely unsynapsed during the male meiotic prophase. However, despite the fact that the avian Z and W are also largely nonhomologous, they synapse completely during the female meiotic prophase in chicken oocytes. MSCI and MSUC in mammals are always associated with asynapsis, and it has been suggested that the heterologous synapsis of Z and W in bird oocytes needs to occur to escape from such a silencing mechanism, since the presence of a silenced Z chromosome would be incompatible with oocyte development during the lengthy (arrested) meiotic prophase in females [133].

The complete heterologous synapsis of Z and W is difficult to understand; how does the cell allow heterologous synapsis between Z and W and simultaneously prevent synapsis between nonhomologous autosomal chromosomal pairs?

It is apparent that during homologous chromosome pairing, in zygotene, the Z and W are the last pair to synapse. RAD51 foci indicative of the presence of (unrepaired) DSBs, persist on the asynapsed axes, but disappear where heterologous synapsis has taken place. The obligatory crossover in the pseudoautosomal region of Z and W is formed with normal timing, as a single

▷ induces a second wave of γH2AX formation and transcriptional silencing. The balance between progression and inhibition of synapsis and DNA repair (black horizontal arrow) determines the final outcome in pachytene. The XY body in the pachytene nucleus is encircled. Spread mouse spermatocyte nuclei were stained with antibodies against RAD51 (green) and SYCP3 (red). The DNA was stained with DAPI (blue), with exception of the lower left and right images of synapsed autosomal chromosomes (left) and the XY body (right). Here, localization of γH2AX is shown in blue, and the DNA is not stained.

MLH1 focus can be observed on the ZW of most pachytene oocytes. This crossover is essential to ensure correct separation of Z and W during the first meiotic division. Recently, we have shown that Z and W are temporarily silenced, during the stage of complete synapsis, in chicken pachytene oocytes (Chapter 4, [134]). This mechanism, which is independent from the final achievement of synapsis, may use mechanisms different MSUC/MSCI in mammals.

7. WHAT DRIVES MEIOTIC SILENCING IN MOUSE AND MAN?

The chromosomal pairing dance of X and Y leading to the bouquet stage starts with telomere attachment to the nuclear envelope, followed by active movements along the membrane, aided by cytoskeletal fibers, until they meet and cluster together. The sex chromosomal telomeres most likely still share homology, and the largely nonhomologous regions outside of the telomeric regions may remain undetected during these early stages of chromosome pairing. At the end of the dynamic bouquet stage, when homologous telomeres have paired and clustered, the chromosomes keep moving around and most likely scan and assess homology during transient states of interaction. Around this time, when the chromosomes are already actively being pulled around, SC assembly starts with de deposition of SYCP3 along the axes, SPO11 introduces DSBs throughout the genome and ATM mediates the first wave of γH2AX formation in regions surrounding the meiotic DSBs. The movement of chromosomes gives the ssDNA strands coated with RAD51/DMC1 the opportunity to invade homologous dsDNA and temporary recombination intermediates are formed. If homology is not established, recombination intermediates are destabilized and the search continues. If a homologous template is encountered, the repair process can continue and is completed to form crossovers and noncrossovers while γH2AX and RAD51 foci disappear concomitant with the formation of the complete SC.

The X and Y chromosomes initiate synapsis from the PARs, but by the end of zygotene, the X chromosomal arm is still left with numerous RAD51/DMC1 foci. A second wave of γH2AX formation is then induced and covers the complete X and Y chromosomes, marking the formation of the XY body and initiation of MSCI.

The persistence of DNA repair proteins on meiotic DSBs may be used as an indicator for the absence of a homologous partner. Alternatively, or in addition, persistence of DSB repair proteins may inhibit progression of synapsis.
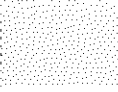
For the initiation of MSCI in mammals, two mechanisms appear to come together: The mechanism that regulates progression of synapsis along aligned and paired chromosomes and the mechanism of meiotic-DSB repair (Figure 3). These two mechanisms are tightly coupled; in DSB-repair mutants synapsis

cannot proceed, in mutants that lack components of the SC, DSB repair is impaired and in both cases true XY body formation does not take place. The formation of the pseudo-XY body in *Spo11* knockout mice supports the hypothesis that formation of a silenced asynapsed region is independent of meiotic DSBs. However, the lack of silencing associated with the majority of unsynapsed axes in these mutants, and the presence of many DNA repair related molecules in the pseudo-XY body, indicate that asynapsis alone does not do the job, and implicate functions of DSB-repair proteins in forming the final inactive chromosome structure.

The recruitment of ATR, to replace ATM at such sites, appears to be the crucial event in the initiation of meiotic silencing and could be the rate-limiting factor in MSUC/MSCI. It remains to be established if this recruitment is normally initially triggered by the presence of persistent DSBs, or by the presence of some component that specifically associates with asynapsed axes, or depends on both features associated with nonhomologous chromatin. If ATR is initially recruited by the persistent DSBs, it may subsequently spread along the chromosomal axes and into the chromosome loops until the end of the chromosomes is reached. This then results in the massive phosphorylation of H2AX, and incorporation of macroH2A, chromatin sumoylation, H2A ubiquitylation and other histone modifications occur downstream. Together, this results in the formation of the silenced XY body. This putative sequence of events is schematically summarized in Figure 2.

8. CLINICAL RELEVANCE OF MEIOTIC SILENCING

Interference with MSCI appears to be incompatible with fertility in mouse and man [59, 96, 102, 135]. Inappropriate expression of X and Y-linked genes during meiotic prophase may trigger apoptosis of pachytene spermatocytes due to the toxic effects of the expression of one or more of these genes [64, 65]. In addition, activation of MSUC due to the presence of chromosomal aberrations that interfere with normal chromosome pairing may also trigger germ cell death due to inappropriate inactivation of genes essential for meiosis. For example, X-autosome translocations are frequently associated with male infertility [122, 136, 137], which is most likely due to spreading of the meiotic silencing signal from the X to the (asynapsed) autosomal part of the translocation chromosome [104]. In addition, autosome-to-autosome translocations can trigger MSUC and are associated with (sub)fertility in mouse [106] and man [135]. It cannot be excluded that inappropriate regulation of chromosome regions during spermatogenesis due to defective MSCI and/or activation of MSUC affects regulation of gene expression in the early embryo via transmission of epigenetic marks.

Therefore, in the context of the field of assisted human reproduction techniques (MESA, TESA, IVF and ICSI), it is of utmost importance to understand the basics of the meiotic silencing mechanisms, in order to estimate the possible risks of producing zygotes from gametes in which MSCI was incomplete, and/or MSUC was activated.

REFERENCES

1. Helena Mangs A, Morris BJ. The Human Pseudoautosomal Region (PAR): Origin, Function and Future. *Curr Genomics.* Apr 2007;8(2):129-136.
2. Graves JA. Sex chromosome specialization and degeneration in mammals. *Cell.* Mar 10 2006;124(5):901-914.
3. Lahn BT, Page DC. Four evolutionary strata on the human X chromosome. *Science.* Oct 29 1999;286(5441):964-967.
4. Handley LJ, Ceplitis H, Ellegren H. Evolutionary strata on the chicken Z chromosome: implications for sex chromosome evolution. *Genetics.* May 2004;167(1):367-376.
5. Koopman P, Gubbay J, Vivian N, Goodfellow P, Lovell-Badge R. Male development of chromosomally female mice transgenic for Sry. *Nature.* May 9 1991;351(6322):117-121.
6. Ohno S. *Sex chromosomes and sex-linked genes.* Berlin: Springer; 1967.
7. Bergero R, Charlesworth D. The evolution of restricted recombination in sex chromosomes. *Trends Ecol Evol.* Feb 2009;24(2):94-102.
8. Bachtrog D. A dynamic view of sex chromosome evolution. *Curr Opin Genet Dev.* Dec 2006;16(6):578-585.
9. Lippman Z, Gendrel AV, Black M, et al. Role of transposable elements in heterochromatin and epigenetic control. *Nature.* Jul 22 2004;430(6998):471-476.
10. Hughes JF, Skaletsky H, Pyntikova T, et al. Chimpanzee and human Y chromosomes are remarkably divergent in structure and gene content. *Nature.* Jan 13.
11. Hughes JF, Skaletsky H, Pyntikova T, et al. Conservation of Y-linked genes during human evolution revealed by comparative sequencing in chimpanzee. *Nature.* Sep 1 2005;437(7055):100-103.
12. Rozen S, Skaletsky H, Marszalek JD, et al. Abundant gene conversion between arms of palindromes in human and ape Y chromosomes. *Nature.* Jun 19 2003;423(6942):873-876.
13. Lange J, Skaletsky H, van Daalen SK, et al. Isodicentric Y chromosomes and sex disorders as byproducts of homologous recombination that maintains palindromes. *Cell.* Sep 4 2009;138(5):855-869.
14. Skaletsky H, Kuroda-Kawaguchi T, Minx PJ, et al. The male-specific region of the human Y chromosome is a mosaic of discrete sequence classes. *Nature.* Jun 19 2003;423(6942):825-837.
15. Khil PP, Smirnova NA, Romanienko PJ, Camerini-Otero RD. The mouse X chromosome is enriched for sex-biased genes not subject to selection by meiotic sex chromosome inactivation. *Nat Genet.* Jun 2004;36(6):642-646.
16. Bhalla N, Dernburg AF. Prelude to a division. *Annu Rev Cell Dev Biol.* 2008;24:397-424.
17. Ding X, Xu R, Yu J, Xu T, Zhuang Y, Han M. SUN1 is required for telomere attachment to nuclear envelope and gametogenesis in mice. *Dev Cell.* Jun 2007;12(6):863-872.
18. Ding DQ, Yamamoto A, Haraguchi T, Hiraoka Y. Dynamics of homologous chromosome pairing during meiotic prophase in fission yeast. *Dev Cell.* Mar 2004;6(3):329-341.
19. Keeney S, Giroux CN, Kleckner N. Meiosis-specific DNA double-strand breaks are catalyzed by Spo11, a member of a widely conserved protein family. *Cell.* Feb 7 1997;88(3):375-384.
20. Bellani MA, Romanienko PJ, Cairatti DA, Camerini-Otero RD. SPO11 is required for sex-body formation, and Spo11 heterozygosity rescues the prophase arrest of Atm-/- spermatocytes. *J Cell Sci.* Aug 1 2005;118(Pt 15):3233-3245.
21. Mahadevaiah SK, Turner JM, Baudat F, et al. Recombinational DNA double-strand breaks in mice precede synapsis. *Nat Genet.* Mar 2001;27(3):271-276.
22. Rogakou EP, Boon C, Redon C, Bonner WM. Megabase chromatin domains involved in DNA double-strand breaks in vivo. *J Cell Biol.* Sep 6 1999;146(5):905-916.

23. Baudat F, Manova K, Yuen JP, Jasin M, Keeney S. Chromosome synapsis defects and sexually dimorphic meiotic progression in mice lacking Spo11. *Mol Cell.* Nov 2000;6(5):989-998.
24. Romanienko PJ, Camerini-Otero RD. The mouse Spo11 gene is required for meiotic chromosome synapsis. *Mol Cell.* Nov 2000;6(5):975-987.
25. Heyting C. Synaptonemal complexes: structure and function. *Curr. Opin. Cell. Biol.* 1996;8:389-396.
26. Costa Y, Cooke HJ. Dissecting the mammalian synaptonemal complex using targeted mutations. *Chromosome Res.* 2007;15(5):579-589.
27. MacQueen AJ, Phillips CM, Bhalla N, Weiser P, Villeneuve AM, Dernburg AF. Chromosome sites play dual roles to establish homologous synapsis during meiosis in C. elegans. *Cell.* Dec 16 2005;123(6):1037-1050.
28. Brown PW, Judis L, Chan ER, et al. Meiotic synapsis proceeds from a limited number of subtelomeric sites in the human male. *Am J Hum Genet.* Oct 2005;77(4):556-566.
29. Eijpe M, Offenberg H, Jessberger R, Revenkova E, Heyting C. Meiotic cohesin REC8 marks the axial elements of rat synaptonemal complexes before cohesins SMC1beta and SMC3. *J Cell Biol.* Mar 3 2003;160(5):657-670.
30. Revenkova E, Eijpe M, Heyting C, et al. Cohesin SMC1 beta is required for meiotic chromosome dynamics, sister chromatid cohesion and DNA recombination. *Nat Cell Biol.* Jun 2004;6(6):555-562.
31. Xu H, Beasley MD, Warren WD, van der Horst GT, McKay MJ. Absence of mouse REC8 cohesin promotes synapsis of sister chromatids in meiosis. *Dev Cell.* Jun 2005;8(6):949-961.
32. Bolcun-Filas E, Costa Y, Speed R, et al. SYCE2 is required for synaptonemal complex assembly, double strand break repair, and homologous recombination. *J Cell Biol.* Mar 12 2007;176(6):741-747.
33. Wojtasz L, Daniel K, Roig I, et al. Mouse HORMAD1 and HORMAD2, two conserved meiotic chromosomal proteins, are depleted from synapsed chromosome axes with the help of TRIP13 AAA-ATPase. *PLoS Genet.* Oct 2009;5(10):e1000702.
34. de Vries FA, de Boer E, van den Bosch M, et al. Mouse Sycp1 functions in synaptonemal complex assembly, meiotic recombination, and XY body formation. *Genes Dev.* Jun 1 2005;19(11):1376-1389.
35. Hamer G, Novak I, Kouznetsova A, Hoog C. Disruption of pairing and synapsis of chromosomes causes stage-specific apoptosis of male meiotic cells. *Theriogenology.* Feb 2008;69(3):333-339.
36. Yang F, De La Fuente R, Leu NA, Baumann C, McLaughlin KJ, Wang PJ. Mouse SYCP2 is required for synaptonemal complex assembly and chromosomal synapsis during male meiosis. *J Cell Biol.* May 22 2006;173(4):497-507.
37. Yuan L, Liu JG, Zhao J, Brundell E, Daneholt B, Hoog C. The murine SCP3 gene is required for synaptonemal complex assembly, chromosome synapsis, and male fertility. *Mol Cell.* Jan 2000;5(1):73-83.
38. Hunt PA, Hassold TJ. Sex matters in meiosis. *Science.* Jun 21 2002;296(5576):2181-2183.
39. Morelli MA, Cohen PE. Not all germ cells are created equal: aspects of sexual dimorphism in mammalian meiosis. *Reproduction (Cambridge, England).* Dec 2005;130(6):761-781.
40. Yuan L, Liu JG, Hoja MR, Wilbertz J, Nordqvist K, Hoog C. Female germ cell aneuploidy and embryo death in mice lacking the meiosis-specific protein SCP3. *Science.* May 10 2002;296(5570):1115-1118.
41. Wang H, Hoog C. Structural damage to meiotic chromosomes impairs DNA recombination and checkpoint control in mammalian oocytes. *J Cell Biol.* May 22 2006;173(4):485-495.

42. Ashley T, Gaeth AP, Creemers LB, Hack AM, de Rooij DG. Correlation of meiotic events in testis sections and microspreads of mouse spermatocytes relative to the mid-pachytene checkpoint. *Chromosoma*. Sep 2004;113(3):126-136.

43. Goedecke W, Eijpe M, Offenberg HH, van Aalderen M, Heyting C. Mre11 and Ku70 interact in somatic cells, but are differentially expressed in early meiosis. *Nat Genet*. Oct 1999;23(2):194-198.

44. Neale MJ, Pan J, Keeney S. Endonucleolytic processing of covalent protein-linked DNA double-strand breaks. *Nature*. Aug 18 2005;436(7053):1053-1057.

45. Keeney S, Neale MJ. Initiation of meiotic recombination by formation of DNA double-strand breaks: mechanism and regulation. *Biochem Soc Trans*. Aug 2006;34(Pt 4):523-525.

46. Borde V, Robine N, Lin W, Bonfils S, Geli V, Nicolas A. Histone H3 lysine 4 trimethylation marks meiotic recombination initiation sites. *Embo J*. Jan 21 2009;28(2):99-111.

47. Milman N, Higuchi E, Smith GR. Meiotic DNA double-strand break repair requires two nucleases, MRN and Ctp1, to produce a single size class of Rec12 (Spo11)-oligonucleotide complexes. *Mol Cell Biol*. Nov 2009;29(22):5998-6005.

48. Williams RS, Dodson GE, Limbo O, et al. Nbs1 flexibly tethers Ctp1 and Mre11-Rad50 to coordinate DNA double-strand break processing and repair. *Cell*. Oct 2 2009;139(1):87-99.

49. Acharya SN, Many AM, Schroeder AP, et al. Coprinus cinereus rad50 mutants reveal an essential structural role for Rad50 in axial element and synaptonemal complex formation, homolog pairing and meiotic recombination. *Genetics*. Dec 2008;180(4):1889-1907.

50. Borde V, Cobb J. Double functions for the Mre11 complex during DNA double-strand break repair and replication. *Int J Biochem Cell Biol*. Jun 2009;41(6):1249-1253.

51. Haaf T, Golub EI, Reddy G, Radding CM, Ward DC. Nuclear foci of mammalian Rad51 recombination protein in somatic cells after DNA damage and its localization in synaptonemal complexes. *Proc Natl Acad Sci U S A*. Mar 14 1995;92(6):2298-2302.

52. Tarsounas M, Morita T, Pearlman RE, Moens PB. RAD51 and DMC1 form mixed complexes associated with mouse meiotic chromosome cores and synaptonemal complexes. *J. Cell. Biol*. 1999;147(2):207-220.

53. Kinebuchi T, Kagawa W, Enomoto R, et al. Structural basis for octameric ring formation and DNA interaction of the human homologous-pairing protein Dmc1. *Mol Cell*. May 7 2004;14(3):363-374.

54. Neale MJ, Keeney S. Clarifying the mechanics of DNA strand exchange in meiotic recombination. *Nature*. Jul 13 2006;442(7099):153-158.

55. Bishop DK, Park D, Xu L, Kleckner N. DMC1: a meiosis-specific yeast homolog of E. coli recA required for recombination, synaptonemal complex formation, and cell cycle progression. *Cell*. May 1 1992;69(3):439-456.

56. Schwacha A, Kleckner N. Identification of joint molecules that form frequently between homologs but rarely between sister chromatids during yeast meiosis. *Cell*. Jan 14 1994;76(1):51-63.

57. Kleckner N, Storlazzi A, Zickler D. Coordinate variation in meiotic pachytene SC length and total crossover/chiasma frequency under conditions of constant DNA length. *Trends Genet*. Nov 2003;19(11):623-628.

58. Pittman DL, Cobb J, Schimenti KJ, et al. Meiotic prophase arrest with failure of chromosome synapsis in mice deficient for Dmc1, a germline-specific RecA homolog. *Mol Cell*. Apr 1998;1(5):697-705.

59. Yoshida K, Kondoh G, Matsuda Y, Habu T, Nishimune Y, Morita T. The mouse RecA-like gene Dmc1 is required for homologous chromosome synapsis during meiosis. *Mol Cell.* Apr 1998;1(5):707-718.

60. Edelmann W, Cohen PE, Kneitz B, et al. Mammalian MutS homologue 5 is required for chromosome pairing in meiosis. *Nat Genet.* Jan 1999;21(1):123-127.

61. Kneitz B, Cohen PE, Avdievich E, et al. MutS homolog 4 localization to meiotic chromosomes is required for chromosome pairing during meiosis in male and female mice. *Genes Dev.* May 1 2000;14(9):1085-1097.

62. Hochwagen A, Amon A. Checking your breaks: surveillance mechanisms of meiotic recombination. *Curr Biol.* Mar 21 2006;16(6):R217-228.

63. Ashley T, Westphal C, Plug-de Maggio A, de Rooij DG. The mammalian mid-pachytene checkpoint: meiotic arrest in spermatocytes with a mutation in Atm alone or in combination with a Trp53 (p53) or Cdkn1a (p21/cip1) mutation. *Cytogenet Genome Res.* 2004;107(3-4):256-262.

64. Burgoyne PS, Mahadevaiah SK, Turner JM. The management of DNA double-strand breaks in mitotic G2, and in mammalian meiosis viewed from a mitotic G2 perspective. *Bioessays.* Oct 2007;29(10):974-986.

65. Burgoyne PS, Mahadevaiah SK, Turner JM. The consequences of asynapsis for mammalian meiosis. *Nat Rev Genet.* Mar 2009;10(3):207-216.

66. Turner JM, Aprelikova O, Xu X, et al. BRCA1, histone H2AX phosphorylation, and male meiotic sex chromosome inactivation. *Curr Biol.* Dec 14 2004;14(23):2135-2142.

67. Barchi M, Mahadevaiah S, Di Giacomo M, et al. Surveillance of different recombination defects in mouse spermatocytes yields distinct responses despite elimination at an identical developmental stage. *Mol Cell Biol.* Aug 2005;25(16):7203-7215.

68. Di Giacomo M, Barchi M, Baudat F, Edelmann W, Keeney S, Jasin M. Distinct DNA-damage-dependent and -independent responses drive the loss of oocytes in recombination-defective mouse mutants. *Proc Natl Acad Sci U S A.* Jan 18 2005;102(3):737-742.

69. Carballo JA, Johnson AL, Sedgwick SG, Cha RS. Phosphorylation of the axial element protein Hop1 by Mec1/Tel1 ensures meiotic interhomolog recombination. *Cell.* Mar 7 2008;132(5):758-770.

70. Fukuda T, Daniel K, Wojtasz L, Toth A, Hoog C. A novel mammalian HORMA domain-containing protein, HORMAD1, preferentially associates with unsynapsed meiotic chromosomes. *Exp Cell Res.* Jan 15;316(2):158-171.

71. Tres LL. Extensive pairing of the XY bivalent in mouse spermatocytes as visualized by whole-mount electron microscopy. *J Cell Sci.* Jun 1977;25:1-15.

72. Chandley AC, Goetz P, Hargreave TB, Joseph AM, Speed RM. On the nature and extent of XY pairing at meiotic prophase in man. *Cytogenetics and cell genetics.* 1984;38(4):241-247.

73. de Boer P, Giele M, Lock MT, et al. Kinetics of meiosis in azoospermic males: a joint histological and cytological approach. *Cytogenetic and genome research.* 2004;105(1):36-46.

74. Metzler-Guillemain C, Usson Y, Mignon C, et al. Organization of the X and Y chromosomes in human, chimpanzee and mouse pachytene nuclei using molecular cytogenetics and three-dimensional confocal analyses. *Chromosome Res.* 2000;8(7):571-584.

75. Moens PB, Kolas NK, Tarsounas M, Marcon E, Cohen PE, Spyropoulos B. The time course and chromosomal localization of recombination-related proteins at meiosis in the mouse are compatible with models that can resolve the early DNA-DNA interactions without reciprocal recombination. *J Cell Sci.* Apr 15 2002;115(Pt 8):1611-1622.

76. Moens PB, Chen DJ, Shen Z, et al. Rad51 immunocytology in rat and mouse spermatocytes and oocytes. *Chromosoma.* Sep 1997;106(4):207-215.

77. Baart EB, de Rooij DG, Keegan KS, de Boer P. Distribution of Atr protein in primary spermatocytes of a mouse chromosomal mutant: a comparison of preparation techniques. *Chromosoma*. 2000;109(1-2):139-147.

78. Keegan KS, Holtzman DA, Plug AW, et al. The Atr and Atm protein kinases associate with different sites along meiotically pairing chromosomes. *Genes Dev*. Oct 1 1996;10(19):2423-2437.

79. Moens PB, Tarsounas M, Morita T, et al. The association of ATR protein with mouse meiotic chromosome cores. *Chromosoma*. May 1999;108(2):95-102.

80. Namekawa SH, Park PJ, Zhang LF, et al. Postmeiotic sex chromatin in the male germline of mice. *Curr Biol*. Apr 4 2006;16(7):660-667.

81. van der Laan R, Uringa EJ, Wassenaar E, et al. Ubiquitin ligase Rad18Sc localizes to the XY body and to other chromosomal regions that are unpaired and transcriptionally silenced during male meiotic prophase. *J Cell Sci*. Oct 1 2004;117(Pt 21):5023-5033.

82. Koken MH, Reynolds P, Jaspers-Dekker I, et al. Structural and functional conservation of two human homologs of the yeast DNA repair gene RAD6. *Proc Natl Acad Sci U S A*. Oct 15 1991;88(20):8865-8869.

83. Xin H, Lin W, Sumanasekera W, Zhang Y, Wu X, Wang Z. The human RAD18 gene product interacts with HHR6A and HHR6B. *Nucleic Acids Res*. Jul 15 2000;28(14):2847-2854.

84. Hoege C, Pfander B, Moldovan GL, Pyrowolakis G, Jentsch S. RAD6-dependent DNA repair is linked to modification of PCNA by ubiquitin and SUMO. *Nature*. Sep 12 2002;419(6903):135-141.

85. Kim J, Guermah M, McGinty RK, et al. RAD6-Mediated transcription-coupled H2B ubiquitylation directly stimulates H3K4 methylation in human cells. *Cell*. May 1 2009;137(3):459-471.

86. Sung P, Prakash S, Prakash L. The RAD6 protein of Saccharomyces cerevisiae polyubiquitinates histones, and its acidic domain mediates this activity. *Genes Dev*. Nov 1988;2(11):1476-1485.

87. Roest HP, Baarends WM, de Wit J, et al. The ubiquitin-conjugating DNA repair enzyme HR6A is a maternal factor essential for early embryonic development in mice. *Mol Cell Biol*. Jun 2004;24(12):5485-5495.

88. Roest HP, van Klaveren J, de Wit J, et al. Inactivation of the HR6B ubiquitin-conjugating DNA repair enzyme in mice causes male sterility associated with chromatin modification. *Cell*. Sep 6 1996;86(5):799-810.

89. Ahmed EA, Philippens ME, Kal HB, de Rooij DG, de Boer P. Genetic probing of homologous recombination and non-homologous end joining during meiotic prophase in irradiated mouse spermatocytes. *Mutat Res*. Jun 1 2010;688(1-2):12-18.

90. Anderson LK, Reeves A, Webb LM, Ashley T. Distribution of crossing over on mouse synaptonemal complexes using immunofluorescent localization of MLH1 protein. *Genetics*. Apr 1999;151(4):1569-1579.

91. Wang PJ, McCarrey JR, Yang F, Page DC. An abundance of X-linked genes expressed in spermatogonia. *Nat Genet*. Apr 2001;27(4):422-426.

92. Solari AJ. The behavior of the XY pair in mammals. *Int Rev Cytol*. 1974;38(0):273-317.

93. Turner JM, Mahadevaiah SK, Ellis PJ, Mitchell MJ, Burgoyne PS. Pachytene asynapsis drives meiotic sex chromosome inactivation and leads to substantial postmeiotic repression in spermatids. *Dev Cell*. Apr 2006;10(4):521-529.

94. Song R, Ro S, Michaels JD, Park C, McCarrey JR, Yan W. Many X-linked microRNAs escape meiotic sex chromosome inactivation. *Nat Genet*. Apr 2009;41(4):488-493.

95. Wang PJ. X chromosomes, retrogenes and their role in male reproduction. *Trends Endocrinol Metab*. Mar 2004;15(2):79-83.

96. Fernandez-Capetillo O, Mahadevaiah SK, Celeste A, et al. H2AX is required for chromatin remodeling and inactivation of sex chromosomes in male mouse meiosis. *Dev Cell.* Apr 2003;4(4):497-508.

97. Vigodner M, Morris PL. Testicular expression of small ubiquitin-related modifier-1 (SUMO-1) supports multiple roles in spermatogenesis: silencing of sex chromosomes in spermatocytes, spermatid microtubule nucleation, and nuclear reshaping. *Dev Biol.* Jun 15 2005;282(2):480-492.

98. Baarends WM, Hoogerbrugge JW, Roest HP, et al. Histone ubiquitination and chromatin remodeling in mouse spermatogenesis. *Dev Biol.* Mar 15 1999;207(2):322-333.

99. Khalil AM, Driscoll DJ. Histone H3 lysine 4 dimethylation is enriched on the inactive sex chromosomes in male meiosis but absent on the inactive X in female somatic cells. *Cytogenet Genome Res.* 2006;112(1-2):11-15.

100. van der Heijden GW, Derijck AA, Posfai E, et al. Chromosome-wide nucleosome replacement and H3.3 incorporation during mammalian meiotic sex chromosome inactivation. *Nat Genet.* Feb 2007;39(2):251-258.

101. Mahadevaiah SK, Bourc'his D, de Rooij DG, Bestor TH, Turner JM, Burgoyne PS. Extensive meiotic asynapsis in mice antagonises meiotic silencing of unsynapsed chromatin and consequently disrupts meiotic sex chromosome inactivation. *J Cell Biol.* Jul 28 2008;182(2):263-276.

102. Dantzer F, Mark M, Quenet D, et al. Poly(ADP-ribose) polymerase-2 contributes to the fidelity of male meiosis I and spermiogenesis. *Proc Natl Acad Sci U S A.* Oct 3 2006;103(40):14854-14859.

103. Baarends WM, Wassenaar E, van der Laan R, et al. Silencing of unpaired chromatin and histone H2A ubiquitination in mammalian meiosis. *Mol Cell Biol.* Feb 2005;25(3):1041-1053.

104. Turner JM, Mahadevaiah SK, Fernandez-Capetillo O, et al. Silencing of unsynapsed meiotic chromosomes in the mouse. *Nat Genet.* Jan 2005;37(1):41-47.

105. Schimenti J. Synapsis or silence. *Nat Genet.* Jan 2005;37(1):11-13.

106. Peters AH, Plug AW, de Boer P. Meiosis in carriers of heteromorphic bivalents: sex differences and implications for male fertility. *Chromosome Res.* Aug 1997;5(5):313-324.

107. Moses MJ, Poorman PA. Synaptosomal complex analysis of mouse chromosomal rearrangements. II. Synaptic adjustment in a tandem duplication. *Chromosoma.* 1981;81(4):519-535.

108. Garcia-Cruz R, Roig I, Robles P, Scherthan H, Garcia Caldes M. ATR, BRCA1 and gammaH2AX localize to unsynapsed chromosomes at the pachytene stage in human oocytes. *Reprod Biomed Online.* Jan 2009;18(1):37-44.

109. Homolka D, Ivanek R, Capkova J, Jansa P, Forejt J. Chromosomal rearrangement interferes with meiotic X chromosome inactivation. *Genome Res.* Oct 2007;17(10):1431-1437.

110. Lachner M, O'Carroll D, Rea S, Mechtler K, Jenuwein T. Methylation of histone H3 lysine 9 creates a binding site for HP1 proteins. *Nature.* Mar 1 2001;410(6824):116-120.

111. Cocquet J, Ellis PJ, Yamauchi Y, et al. The multicopy gene Sly represses the sex chromosomes in the male mouse germline after meiosis. *PLoS Biol.* Nov 2009;7(11):e1000244.

112. Ellis PJ, Clemente EJ, Ball P, et al. Deletions on mouse Yq lead to upregulation of multiple X- and Y-linked transcripts in spermatids. *Hum Mol Genet.* Sep 15 2005;14(18):2705-2715.

113. Mueller JL, Mahadevaiah SK, Park PJ, Warburton PE, Page DC, Turner JM. The mouse X chromosome is enriched for multicopy testis genes showing postmeiotic expression. *Nat Genet.* Jun 2008;40(6):794-799.

114. Hendriksen PJ, Hoogerbrugge JW, Themmen AP, et al. Postmeiotic transcription of X and Y chromosomal genes during spermatogenesis in the mouse. *Dev Biol*. Aug 1995;170(2):730-733.

115. Huynh KD, Lee JT. Inheritance of a pre-inactivated paternal X chromosome in early mouse embryos. *Nature*. Dec 18 2003;426(6968):857-862.

116. Payer B, Lee JT. X chromosome dosage compensation: how mammals keep the balance. *Annu Rev Genet*. 2008;42:733-772.

117. Nguyen DK, Disteche CM. Dosage compensation of the active X chromosome in mammals. *Nat Genet*. Jan 2006;38(1):47-53.

118. Lin H, Gupta V, Vermilyea MD, et al. Dosage compensation in the mouse balances up-regulation and silencing of X-linked genes. *PLoS Biol*. Dec 2007;5(12):e326.

119. Carrel L, Willard HF. X-inactivation profile reveals extensive variability in X-linked gene expression in females. *Nature*. Mar 17 2005;434(7031):400-404.

120. Brown CJ, Ballabio A, Rupert JL, et al. A gene from the region of the human X inactivation centre is expressed exclusively from the inactive X chromosome. *Nature*. Jan 3 1991;349(6304):38-44.

121. Rastan S. Non-random X-chromosome inactivation in mouse X-autosome translocation embryos--location of the inactivation centre. *J Embryol Exp Morphol*. Dec 1983;78:1-22.

122. Kalz-Fuller B, Sleegers E, Schwanitz G, Schubert R. Characterisation, phenotypic manifestations and X-inactivation pattern in 14 patients with X-autosome translocations. *Clin Genet*. May 1999;55(5):362-366.

123. Marahrens Y, Panning B, Dausman J, Strauss W, Jaenisch R. Xist-deficient mice are defective in dosage compensation but not spermatogenesis. *Genes Dev*. Jan 15 1997;11(2):156-166.

124. Penny GD, Kay GF, Sheardown SA, Rastan S, Brockdorff N. Requirement for Xist in X chromosome inactivation. *Nature*. Jan 11 1996;379(6561):131-137.

125. Plath K, Fang J, Mlynarczyk-Evans SK, et al. Role of histone H3 lysine 27 methylation in X inactivation. *Science*. Apr 4 2003;300(5616):131-135.

126. Silva J, Mak W, Zvetkova I, et al. Establishment of histone h3 methylation on the inactive X chromosome requires transient recruitment of Eed-Enx1 polycomb group complexes. *Dev Cell*. Apr 2003;4(4):481-495.

127. van den Berg IM, Laven JS, Stevens M, et al. X chromosome inactivation is initiated in human preimplantation embryos. *Am J Hum Genet*. Jun 2009;84(6):771-779.

128. Turner JM, Mahadevaiah SK, Elliott DJ, et al. Meiotic sex chromosome inactivation in male mice with targeted disruptions of Xist. *J Cell Sci*. Nov 1 2002;115(Pt 21):4097-4105.

129. Okamoto I, Arnaud D, Le Baccon P, et al. Evidence for de novo imprinted X-chromosome inactivation independent of meiotic inactivation in mice. *Nature*. Nov 17 2005;438(7066):369-373.

130. Heard E, Chaumeil J, Masui O, Okamoto I. Mammalian X-chromosome inactivation: an epigenetics paradigm. *Cold Spring Harb Symp Quant Biol*. 2004;69:89-102.

131. Sequence and comparative analysis of the chicken genome provide unique perspectives on vertebrate evolution. *Nature*. Dec 9 2004;432(7018):695-716.

132. Khil PP, Oliver B, Camerini-Otero RD. X for intersection: retrotransposition both on and off the X chromosome is more frequent. *Trends Genet*. Jan 2005;21(1):3-7.

133. Jablonka E, Lamb MJ. Meiotic pairing constraints and the activity of sex chromosomes. *J Theor Biol*. Jul 8 1988;133(1):23-36.

134. Schoenmakers S, Wassenaar E, Hoogerbrugge JW, Laven JS, Grootegoed JA, Baarends WM. Female meiotic sex chromosome inactivation in chicken. *PLoS Genet*. May 2009;5(5):e1000466.
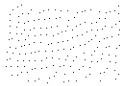
135. Leng M, Li G, Zhong L, Hou H, Yu D, Shi Q. Abnormal synapses and recombination in an azoospermic male carrier of a reciprocal translocation t(1;21). *Fertil Steril.* Apr 2009;91(4):1293 e1217-1222.

136. Ma S, Yuen BH, Penaherrera M, Koehn D, Ness L, Robinson W. ICSI and the transmission of X-autosomal translocation: a three-generation evaluation of X;20 translocation: case report. *Hum Reprod.* Jul 2003;18(7):1377-1382.

137. Madan K. Balanced structural changes involving the human X: effect on sexual phenotype. *Hum Genet.* 1983;63(3):216-221.

138. Walpita D, Plug AW, Neff NF, German J, Ashley T. Bloom's syndrome protein, BLM, colocalizes with replication protein A in meiotic prophase nuclei of mammalian spermatocytes. *Proc Natl Acad Sci U S A.* May 11 1999;96(10):5622-5627.

139. Scully R, Chen J, Plug A, et al. Association of BRCA1 with Rad51 in mitotic and meiotic cells. *Cell.* Jan 24 1997;88(2):265-275.

140. Chen J, Silver DP, Walpita D, et al. Stable interaction between the products of the BRCA1 and BRCA2 tumor suppressor genes in mitotic and meiotic cells. *Mol Cell.* Sep 1998;2(3):317-328.

141. Fukuda T, Daniel K, Wojtasz L, Toth A, Hoog C. A novel mammalian HORMA domain-containing protein, HORMAD1, preferentially associates with unsynapsed meiotic chromosomes. *Exp Cell Res.* Aug 15 2009.

142. Ahmed EA, van der Vaart A, Barten A, et al. Differences in DNA double strand breaks repair in male germ cell types: lessons learned from a differential expression of Mdc1 and 53BP1. *DNA Repair (Amst).* Sep 1 2007;6(9):1243-1254.

143. Freire R, Murguia JR, Tarsounas M, Lowndes NF, Moens PB, Jackson SP. Human and mouse homologs of Schizosaccharomyces pombe rad1(+) and Saccharomyces cerevisiae RAD17: linkage to checkpoint control and mammalian meiosis. *Genes Dev.* 1998;12(16):2560-2573.

144. Perera D, Perez-Hidalgo L, Moens PB, et al. TopBP1 and ATR colocalization at meiotic chromosomes: role of TopBP1/Cut5 in the meiotic recombination checkpoint. *Mol Biol Cell.* Apr 2004;15(4):1568-1579.

145. Reini K, Uitto L, Perera D, Moens PB, Freire R, Syvaoja JE. TopBP1 localises to centrosomes in mitosis and to chromosome cores in meiosis. *Chromosoma.* May 2004;112(7):323-330.

CHAPTER 3

INCREASED FREQUENCY OF ASYNAPSIS
AND ASSOCIATED MEIOTIC SILENCING OF
HETEROLOGOUS CHROMATIN IN THE PRESENCE
OF IRRADIATION-INDUCED EXTRA
DNA DOUBLE STRAND BREAKS

ABSTRACT

In meiotic prophase of male placental mammals, the heterologous X and Y chromosomes remain largely unsynapsed, which activates meiotic sex chromosome inactivation (MSCI), leading to formation of the transcriptionally silenced XY body. MSCI is most likely related to meiotic silencing of unsynapsed chromatin (MSUC), a mechanism that can silence autosomal unsynapsed chromatin. However, heterologous synapsis and escape from silencing also occur. In mammalian species, formation of DNA double strand breaks (DSBs) during leptotene precedes meiotic chromosome pairing. These DSBs are essential to achieve full synapsis of homologous chromosomes. We generated 25% extra meiotic DSBs by whole body irradiation of mice. This leads to a significant increase in meiotic recombination frequency. In mice carrying translocation chromosomes with synaptic problems, we observed an approximately 35% increase in asynapsis and MSUC of the nonhomologous region in the smallest chromosome pair following irradiation. However, the same nonhomologous region in the largest chromosome pair, shows complete synapsis and escape from MSUC in almost 100% of the nuclei, irrespective of exposure to irradiation. We propose that prevention of synapsis and associated activation of MSUC is linked to the presence of unrepaired meiotic DSBs in the nonhomologous region. Also, spreading of synaptonemal complex formation from regions of homology may act as an opposing force, and drive heterologous synapsis.

INTRODUCTION

In meiotic prophase, homologous chromosomes align and synapse. This is accompanied by formation of a tripartite, proteinaceous structure, the synaptonemal complex (SC), which physically connects the homologous chromosomes along their axes (reviewed by [1]). In *Saccharomyces cerevisiae* and mouse, chromosome pairing is preceded by induction of DNA double strand breaks (DSBs) by the topoisomerase-like protein SPO11 [2, 3]. The DSB sites are marked by phosphorylation of serine 139 of histone H2AX, resulting in formation of γH2AX [3]. During processing of the DSBs, RAD51 and DMC1 form filaments on single-stranded DNA ends, that are visible as discrete foci following immunocytochemical detection (reviewed in [4]). The presence of RAD51 foci indicates the initiation of the meiotic recombination repair process. Subsequently, different mechanisms are thought to be responsible for formation of crossover and non-crossover products via homologous recombination. During male mammalian meiotic prophase, the number of RAD51 foci decreases to almost zero on the synapsed SC of autosomes around mid-pachytene, while RAD51 foci persist on the single unsynapsed X chromosome until late pachytene [5].

Analyses of *spo11* mutants have shown that chromosome pairing is severely impaired in the absence of meiotic DSBs in yeast, plant, and mouse species [6-9]. However, in yeast *spo11* mutants, a small fraction of the nuclei is still capable of showing complete and correct synapsis of homologous chromosomes [10, 11]. In *Caenorhabditis elegans* and *Drosophila melanogaster*, meiotic DSBs are induced after the assembly of the SC, and chromosome pairing occurs independent of SPO11 (reviewed by [1]). In yeast and mammalian species, telomere dynamics during leptotene, leading to bouquet formation, is thought to facilitate homology recognition, and this appears to be coupled to the regulation of meiotic DSB repair (reviewed by [1]). These data indicate that DSB dependent and DSB independent homologous chromosome pairing mechanisms exist. In male placental mammals, the pairing mechanisms are challenged by the presence of the largely heterologous X and Y chromosomes. These chromosomes pair only in the short pseudoautosomal regions (PARs), and form the transcriptionally silent XY body that localizes in the periphery of the nucleus during pachytene and diplotene stages of meiotic prophase [12]. This process is called meiotic sex chromosome inactivation (MSCI). Following the meiotic divisions, the sex chromosomes remain transcriptionally repressed, with exception of a few genes [13-15]. Recent data have shown that inactivation of X and Y during male meiotic prophase (MSCI) is related to a more general mechanism named meiotic silencing of unsynapsed chromatin (MSUC) [16-18]. Recruitment of DNA repair proteins, such as checkpoint kinase ATR by the BRCA1 protein and subsequent
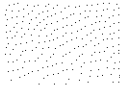
phosphorylation of serine 139 of H2AX have been shown to be essential for MSUC/MSCI [19]. MSUC also detects and silences autosomal nonhomologous chromatin regions, in male and female meiosis [16, 18]. However, heterologous synapsis and escape from silencing also occur [16, 18, 20]. For example, in oocytes from XO females, heterologous (self)synapsis of the X and associated escape from MSUC occurs in approximately 50% of the nuclei [16]. It is unknown whether the process of heterologous synapsis precludes MSUC activation, or whether the lack of MSUC activation allows heterologous synapsis. In the fungus *Neurospora crassa*, a mechanism named meiotic silencing by unpaired DNA (MSUD) occurs at the single gene level, and requires components of the RNAi machinery [21, 22]. For MSUC, a link with RNA-mediated silencing has also been suggested [23], providing support for a possible functional relation between MSUC and MSUD, although MSUD appears to be far more efficient than MSUC.

In mouse *Spo11* mutants, meiotic DSBs are not formed, there is no homologous chromosome pairing, and the XY body does not develop [7, 8, 24]. Instead, H2AX phosphorylation occurs in one or more restricted areas, forming a so-called pseudo sex body [24, 25].

In mammals, pairing of homologous chromosomes and subsequent establishment of the SC depend on the induction and repair of meiotic DSBs (reviewed by [1]). In regions that lack, or do not find a homologous partner, unrepaired DSBs often appear to persist, followed by asynapsis and MSUC [18, 26]. It could be envisioned that DSBs and associated repair proteins in the nonhomologous region impede the progression of (heterologous) synapsis, which could result in asynapsis and lead to activation of MSUC. Alternatively, the choice between heterologous synapsis and asynapsis may be independent from the presence of unrepaired DSBs. To try to obtain more insight in the role of DSBs in the detection of nonhomologous chromatin, we aimed to induce extra meiotic DSBs to test if this would increase the frequency of asynapsis and associated MSUC.

For yeast, fungi and flies, it has been shown that irradiation-induced DSBs can replace SPO11-generated DSBs, and partially rescue *spo11* deficient phenotypes [27-29]. Therefore, we used irradiation to induce extra DSBs during early meiotic prophase in the mouse. As a model, we used mice that are double heterozygote for the T(1;13)70H and T(1;13)1Wa translocations (referred to as T/T' in Figure 1a). During meiotic prophase in T/T' mice, two heteromorphic bivalents, 1^{13} and 13^1, are formed. The larger 13^1 bivalent shows complete synapsis in almost all nuclei (Figure 1b). However, the small 1^{13} bivalent displays varying degrees of asynapsis throughout meiotic prophase [30] (Figure 1b). For these mice, we analysed the effects of irradiation on the frequency of meiotic recombination, and the occurrence of MSUC.
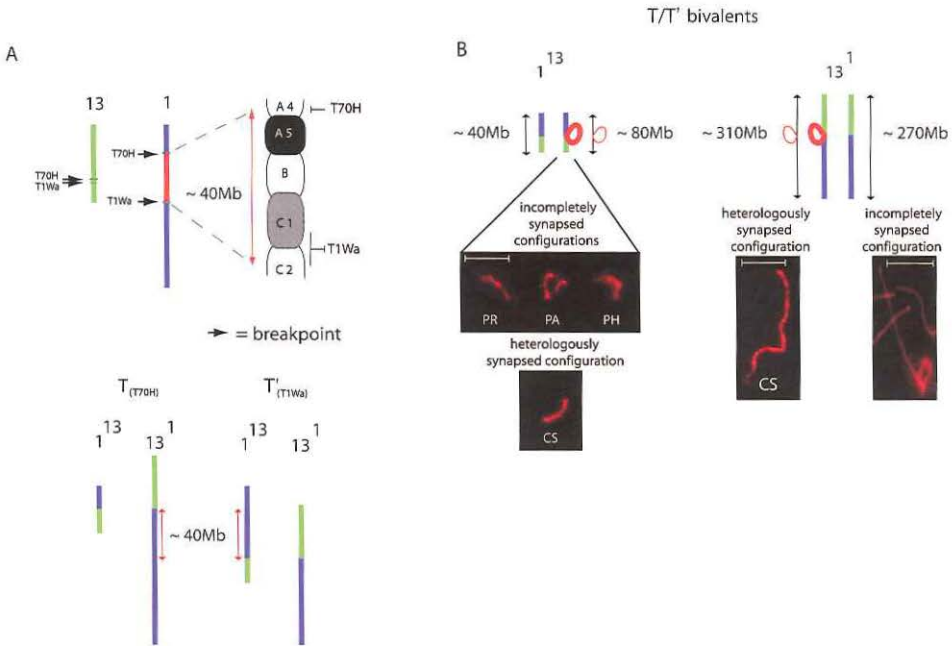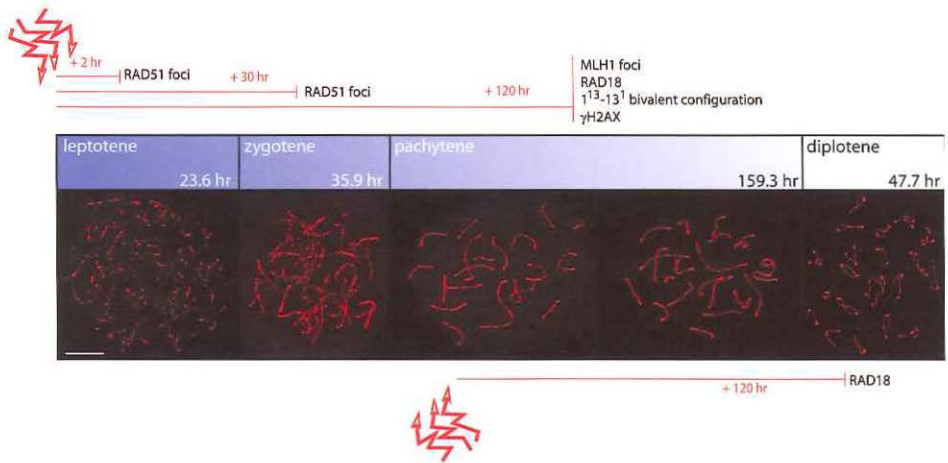
Figure 1. Schematic presentation of the T/T' mouse model. (a) The T/T' mice are generated by cross-breeding T and T' mice with two different translocations involving chromosomes 1 and 13. The breakpoints in chromosome 1 differ between T and T', and the T/T' offspring is double heterozygous for the two different 1^{13} translocations. The breakpoint of T70H has been mapped to the R band in 1A4 [65]. In the NCBI map viewer (www.ensembl.org) band 1A4 is localized between 20.3 and 22.3 Mb from the centromere. The T1Wa breakpoint has been mapped between the 1C1.2 and 1C2 subbands, which corresponds to approximately 55-66 Mb from the centromere. The *Ctla4* gene has been mapped distal from the T1Wa breakpoint and localizes at 61.1 Mb from the centromere [66]. Therefore, we estimate that the region of nonhomology in the 1^{13} and 13^1 bivalents has a size of approximately 35-40Mb. G-light bands (1A4, 1B and 1C2) and G-dark bands (1C1 and 1A5) of the region between the T1Wa and T70H breakpoints on chromosome 1 are indicated. This region corresponds to the regions of nonhomology that are present in the 1^{13} and 13^1 meiotic bivalents in mice which are double heterozygote for the two translocations. (b) Morphology of incompletely or heterologous synapsed 1^{13} and 13^1 bivalents immunostained for SYCP3 in spermatocyte spread nuclei. The incompletely synapsed group of the 1^{13} bivalent consists of: PR (= partially synapsed rest), PA (= partially synapsed A shape), and PH (= partially synapsed horseshoe shape). Heterologously synapsed 1^{13} bivalents: CS (= completely synapsed). IS (=incompletely synapsed). Bar represents 5 µm.

RESULTS AND DISCUSSION

Exposure to irradiation increases the number of RAD51 foci in leptotene and zygotene nuclei

During leptotene, SPO11 is one of the major determinants in the initiation of the meiotic recombination process as it catalyses the formation of DNA DSBs [6, 31]. In Neurospora crassa and Saccharomyces cerevisiae spo11 mutants, exposure to ionising radiation can partially restore the meiotic process, suggesting that the radiation-induced DSBs can replace Spo11 protein generated meiotic DSBs in these species [32, 33]. We first asked if irradiation-induced DSBs, when generated in male mouse leptotene nuclei, could be incorporated in the meiotic recombination process. Substages of the first meiotic prophase were distinguished according to the morphology of the axial elements of the synaptonemal complex (SC) after immunostaining with anti-SYCP3 (Figure 2). To visualize and quantify the number of meiotic DSBs we used an antibody against the homologous recombination repair protein RAD51. This protein forms filaments on 3' end single-strand DNA overhangs of meiotic DSBs shortly after SPO11 has generated the meiotic DSBs [5]. These sites are first marked by phosphorylation of serine 139 of H2AX (γH2AX), but this modification spreads, and discrete foci cannot be counted during leptotene [3].

Figure 2. Experimental setup in relation to the duration of the substages of meiotic prophase in mouse. The upper bar shows a schematic representation of the different meiotic prophase substages in male mice, with corresponding time lengths (hours) in the lower right corners [46]. The lower panel shows the different substages according to the morphology of the lateral element of the synaptonemal complex, immunostained for SYCP3 (red). Timing of irradiation and immunofluorescent analyses (RAD51, MLH1, RAD18, γH2AX, 1^{13} and 13^{1} bivalent configuration) are indicated. Bar represents 10 μm.

In mouse spermatocytes, around 400 RAD51 foci are detected at the leptotene stage [34], 250 foci are still present at the leptotene-to-zygotene transition, and 200 around mid-zygotene, followed by a decrease to almost zero when pachytene progresses [35]. On the XY body, RAD51 foci persist until the end of pachytene [5]. After removal of RAD51, other repair, or repair related, proteins such as RPA and MSH4 accumulate and form similar foci [35]. We irradiated mice with a dose of 4Gy of whole body irradiation, to find out if the irradiation could induce extra meiotic DSBs. This dose will kill most of the spermatogonia and preleptotene spermatocytes, but more than half of the spermatocytes at later stages will survive [36]. Two hours after irradiation, we found an increase of approximately 25% in the total number of RAD51 foci in wild type leptotene nuclei (Figure 3ab).

Subsequently, we investigated the effect of these irradiation-induced extra DSBs during the consecutive stages of meiotic prophase. First, testicular cells were isolated 30 h after irradiation. During this time period, irradiated leptotene cells will have progressed to the zygotene stage (Figure 2). At the mid-zygotene stage, we found an increase of 12% in the total number of RAD51 foci (Figure 3cd). This indicates that almost 80% of the extra irradiation-induced RAD51 foci have disappeared within thirty hours, as compared to 55% of SPO11-induced DSBs (Figure 3b,d). Based on these findings it appears that irradiation-induced DSBs are processed slightly faster than SPO11-induced DSBs. This repair of induced DSBs in leptotene/zygotene nuclei appears to be slower than repair of the majority of irradiation-induced foci during pachytene, as recently reported [37, 38]. This difference may be explained by the fact that repair of DSBs in leptotene/zygotene of meiotic prophase appears to be carried out exclusively by the HR pathway, in the absence of the nonhomologous end-joining (NHEJ) proteins KU70 [39] and 53BP1 [37]. In addition, HR using the sister chromatid as repair template is suppressed [40]. From mid-pachytene onwards, NHEJ can be carried out [37, 39]. Based on these features and our findings, it appears that repair of irradiation-induced DSBs during leptotene/zygotene is slower than during pachytene. Still, our irradiation-induced DSBs appear to be processed somewhat faster than the programmed meiotic DSBs.

In vitro experiments using mammalian cell lines have shown that approximately 35 DSBs per Gy can be generated in mitotic G1 stage (2C amount of DNA) cells [41, 42]. *In vivo*, an average of 19 DSBs per Gy was measured in mouse neonatal metaphase germ cells (4C amount of DNA) [43]. A reduced sensitivity of testicular cells to ionizing radiation may be explained by the relatively low oxygen level in the testis, which could protect the tissue against double strand break induction [44, 45]. Based on these data, we would expect an average of around 100 extra DSBs following 4Gy of irradiation, and this is in line with our observations, although
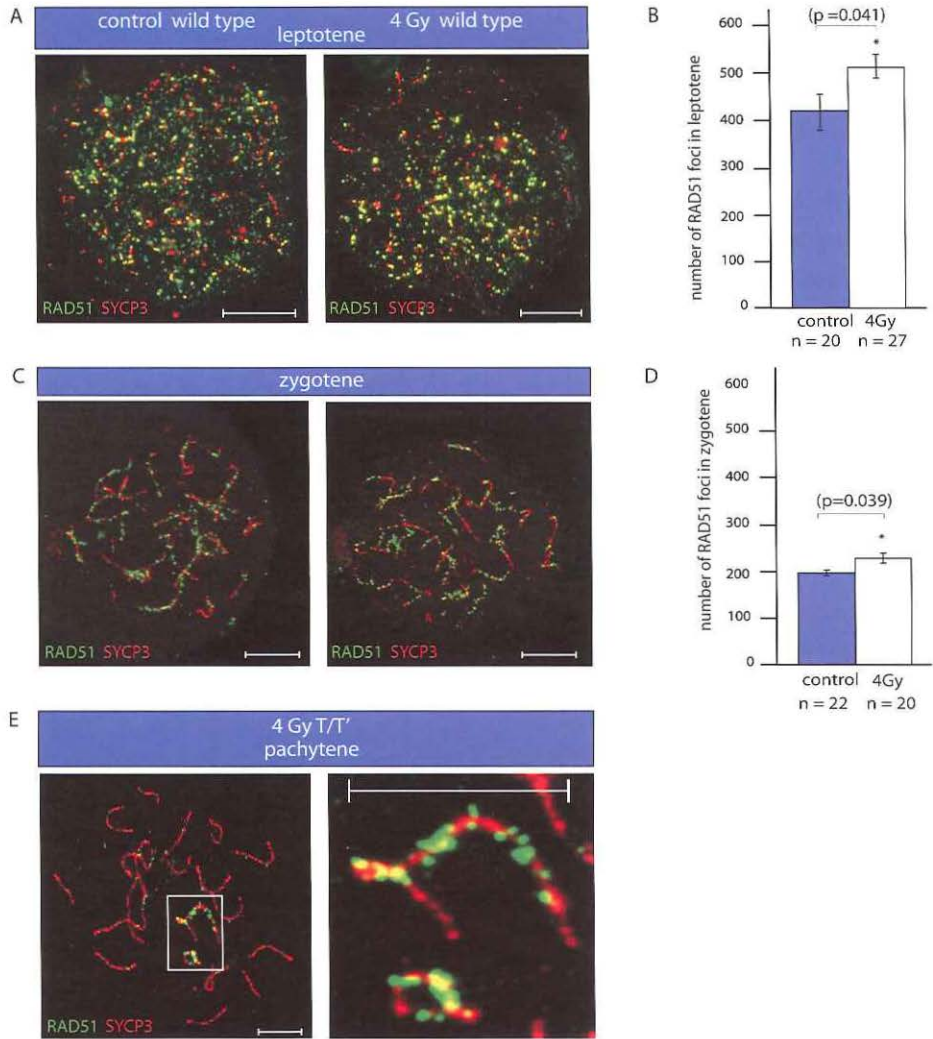
Figure 3. Radiation induces extra RAD51 foci in spermatocytes. (a) Control (left) and 2 hours post 4Gy irradiation (right) leptotene spermatocyte nuclei from wild type mice, immunostained for SYCP3 (red) and RAD51 (green). Bar represents 10 μm. (b) Graphical representation of the average number of RAD51 foci in leptotene nuclei in control (n=20 nuclei / 2 wild type mice) and irradiated nuclei (n=27/ 2 wild type mice). Error bars represent the standard error of the mean. * Indicates a significant difference (p<0.05) as compared to control. (c) Control (left) and 30 hours post 4Gy irradiation (right) zygotene spermatocyte nuclei from wild type mice, immunostained for SYCP3 (red) and RAD51 (green). Bar represents 10 μm. (d) Graphical representation of the average number of RAD51 foci in zygotene nuclei in control (n=22 nuclei / 2 wild type mice) and irradiated nuclei (n=20/ 2 wild type mice). Error bars represent the standard error of the mean. * Indicates a significant difference (p<0.05) as compared to control. (e) Irradiated T/T' pachytene spermatocyte nucleus immunostained for SYCP3 (red) ▷

we do not exclude that multiple DSBs may sometimes cluster together into a single RAD51 focus, which would lead to an underestimate of the total.

Together, our observations on the behavior of RAD51 foci indicate that the irradiation-induced extra DBSs may at least partially be incorporated in the meiotic recombination process.

Irradiation-induced extra DSBs can be converted into crossovers

Next, we exposed 5 adult male T/T' mice carrying the 1^{13} and 13^1 translocation bivalents (Figure 1) to 4Gy of ionizing irradiation, and sham irradiated 4 control T/T'mice. Since full synapsis of homologous chromosomes is achieved in pachytene nuclei, we assumed that only breaks that were induced prior to pachytene could be incorporated in the meiotic recombination pathway. This creates a window of maximally 60 hours (Figure 2). We chose to analyse testicular cells five days after irradiation. At this point, spermatocytes that were irradiated at leptotene and zygotene will have progressed to mid and late pachytene, at Stages IV-VII of the cycle of the spermatogenic epithelium [46] (Figure 2). First, we analysed whether the presence of irradiation-induced extra DSBs might increase crossing-over frequency. In general, only a minority of the meiotic DSBs are converted to actual crossovers. Of the initial number of 400 RAD51 foci, only around 25 crossovers are formed. The DSBs that are processed to 'non-crossover' products are thought to participate in the meiotic homology search, alignment and pairing of homologous chromosomes [1]. To analyse the number of crossovers, we used an antibody that detects the mismatch repair protein MLH1. This protein accumulates at sites of crossing-over during pachytene, forming distinct foci [47, 48]. It has been shown [49] that MLH1 foci are present in mouse pachytene nuclei from Stage IV tubules onwards. MLH1 foci disappear at the end of pachytene [47, 48], most likely in Stage VIII-IX tubules [50], corresponding to an estimated time period of around 80 hours.

We performed double immunofluorescent staining for MLH1 and SYCP3 on mid-pachytene nuclei from irradiated and control T/T' males, and counted MLH1 foci on the synaptonemal complexes (SCs) (Figure 4a). After irradiation, we found a small but significant increase in the number of MLH1 foci (Figure 4b). To analyse this further, we grouped SCs in those with zero, 1, 2 and 3 MLH1 foci. We detected a significant increase in the number of SCs with 3 MLH1 foci in irradiated nuclei compared to controls (Figure 4c). Accordingly, the percentage of SCs with 1 focus showed a tendency to decrease and the percentage of SCs

▷ and RAD51 (green). Part of the left picture is enlarged in the right picture, and shows clusters of persistent RAD51 foci on the small 1^{13} translocation bivalent and the X and Y chromosomes. Bar represents 10 μm.
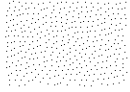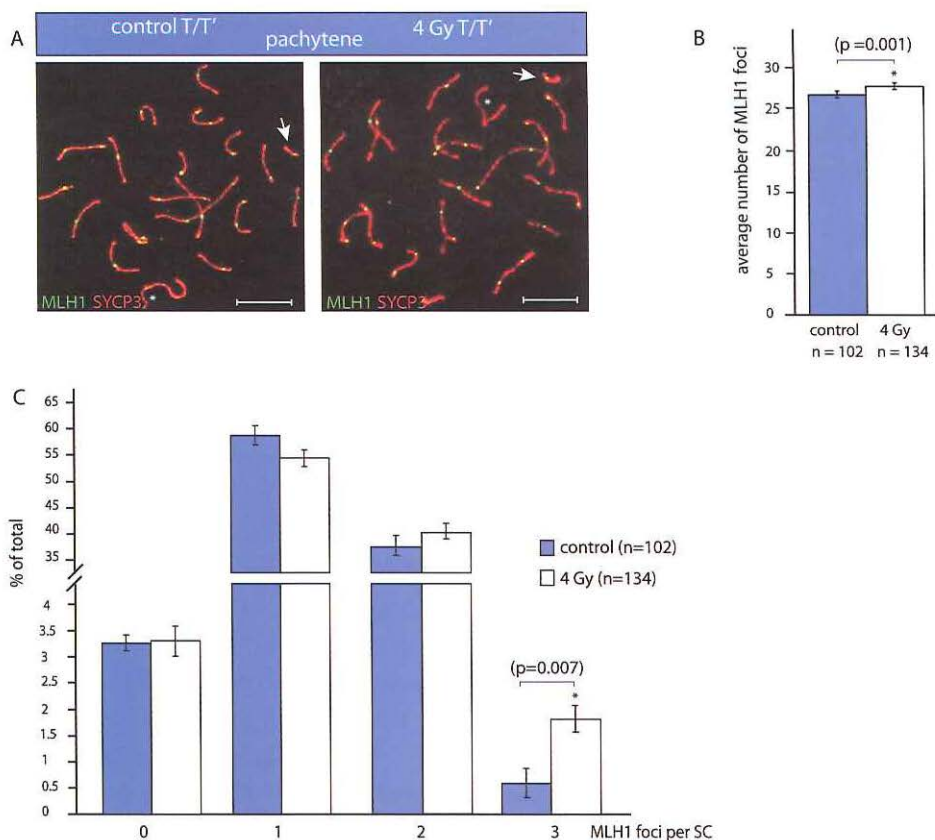
Figure 4. Radiation-induced double strand breaks increase crossing over frequency. (a) Immunostaining of control (left) and irradiated (right) T/T' pachytene spermatocyte nuclei for SYCP3 (red) and MLH1 (green). The number of MLH1 foci in this control nucleus (left) is 26, and 27 in the irradiated nucleus (right). Asterisks indicate the XY pair, arrows indicate the 1^{13} bivalent. Bar represents 10 mm. (b) Graph of the average number of MLH1 foci in pachytene nuclei from control (= 26.5, with n= 102 analysed nuclei / 4 mice) and irradiated (=27.6, with n = 134 analysed nuclei / 5 mice) T/T' mice. Error bars represent the standard error of the mean. * indicates a significant difference (p<0.05) as compared to the control. (c) Graph showing the percentage of SCs with 0, 1, 2 or 3 MLH1 foci per SC in pachytene spermatocytes of control (n = 102 analysed nuclei / 4 mice) and irradiated (n = 134 analysed nuclei / 5 mice) T/T' mice. Error bars represent the standard error of the mean. * indicates a significant difference (p<0.05) as compared to the control.

with 2 foci a tendency to increase. We detected approximately 3% SCs without an MLH1 focus, mostly representing the XY chromosomes (78%) and the 1^{13} bivalent (21%). This finding can be explained by the fact that the MLH1 focus on the synapsed part of the XY pair usually appears and disappears slightly ahead
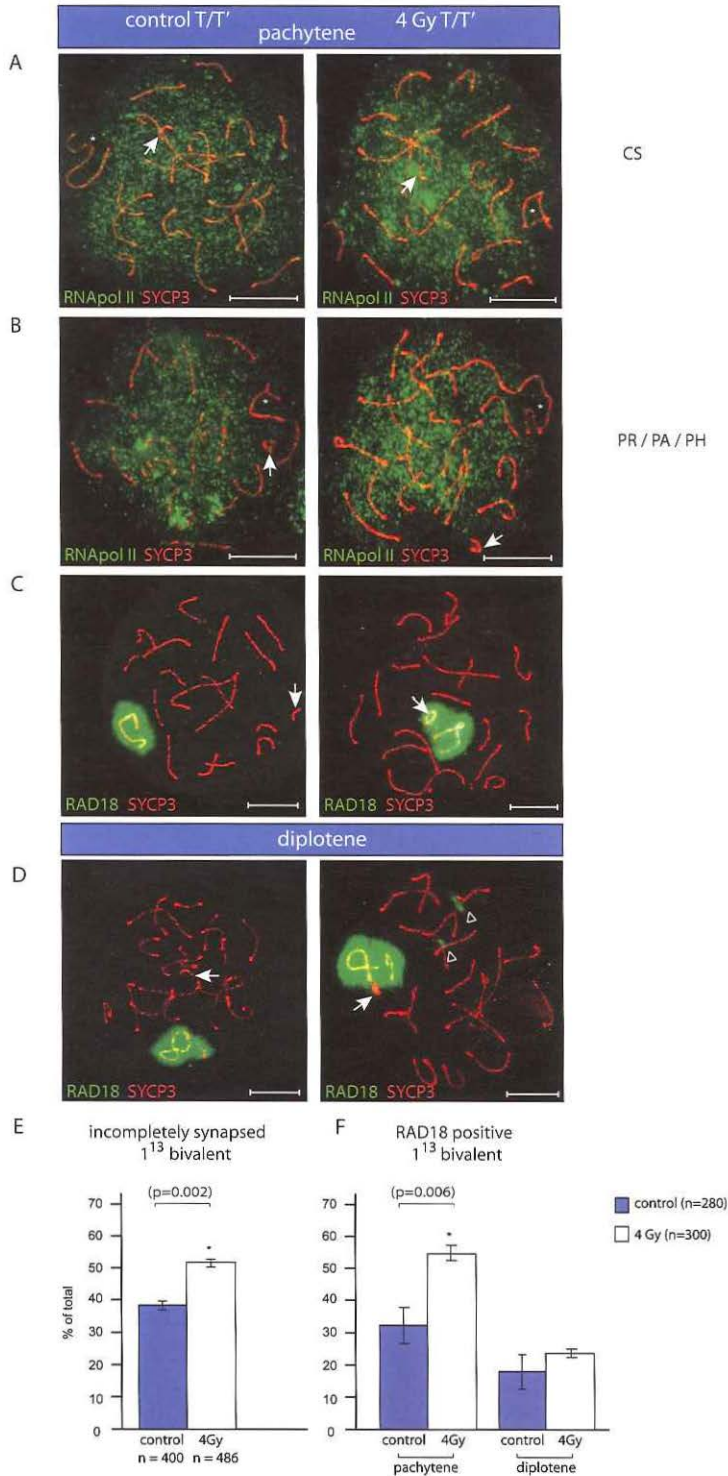
of the autosomal MLH1 foci [48], and therefore may already have disappeared in part of the analysed nuclei. The 1^{13} bivalent is often silenced by MSUC and localizes close to the XY body. From this, it can be suggested that the dynamics of the MLH1 focus on 1^{13} might be similar to that of the MLH1 focus on XY. In addition, the 1^{13} bivalent may actually lack an MLH1 focus in some cases, since it has been reported that approximately 2% of the 1^{13} chromosomes appear as univalents at the diakinesis-metaphase I transition [51].

Our analysis shows that a 25% increase in the number of DSBs caused by irradiation in leptotene, decreases to 10% in zygotene nuclei and ultimately leads to a 4% increase in the number of crossovers in pachytene nuclei. In zygotene nuclei, pairing has already initiated, and irradiation-induced DSBs in these cells may have a reduced chance to become incorporated in the cross-over process, compared to DSBs induced in leptotene cells. In addition, the time window from leptotene to zygotene (60 hours) is slightly shorter than the time window during pachytene that was analysed (80 hours). Together, this may result in an underestimation of the effect of irradiation on the number of meiotic crossovers. Generally, the number of crossovers per nucleus is highly regulated, and the distribution is non-random [52]. A crossover interference mechanism ensures the presence of at least one crossover per bivalent and also reduces the likelihood of two crossovers occurring in close proximity to each other (reviewed by [53]). This mechanism may direct repair of extra DSBs towards non-crossover events. Alternatively, or in addition, SPO11-induced DSBs might be preferred crossover sites, compared to irradiation-induced DSBs.

Radiation-induced DSBs during leptotene increase the frequency of asynapsis and associated MSUC of the 1^{13} bivalent

We hypothesized that the detection of unsynapsed nonhomologous chromatin, and subsequent initiation of MSUC, might be linked to the presence of unrepaired meiotic DSBs in such regions. Persistent meiotic DSBs appear to be present on the XY body, as indicated by the persistence of RAD51 foci on the X axial elements until late pachytene. In the present experiments, the 1^{13} bivalent in the spread nuclei from irradiated and control mice also contains persistent RAD51 foci on the unsynapsed loop (Figure 3e), in accordance with earlier reports [26].

Based upon this observation, and on the fact that XY body formation depends on SPO11 [24], we investigated whether irradiation during leptotene affects the frequency of heterologous synapsis of the 1^{13} and 13^1 bivalents in pachytene nuclei of T/T' mice. The 1^{13} bivalent is easy to identify as it has the shortest SC complex in the spread nuclei. Previously, we have shown that when the 1^{13} bivalent is incompletely synapsed, it becomes transcriptionally silenced and often localizes adjacent to the XY body [16]. In addition, several proteins such as ATR and

control T/T' pachytene 4 Gy T/T'

A

RNApol II SYCP3   RNApol II SYCP3   CS

B

RNApol II SYCP3   RNApol II SYCP3   PR / PA / PH

C

RAD18 SYCP3   RAD18 SYCP3

diplotene

D

RAD18 SYCP3   RAD18 SYCP3

E incompletely synapsed
   1¹³ bivalent

F RAD18 positive
   1¹³ bivalent

control (n=280)
4 Gy (n=300)

ubiquitinylated histone H2AK119ub1, that associate with XY body chromatin, accumulate on the 1^{13} bivalent chromatin when it is incompletely synapsed [16, 54]. In nuclei where the 1^{13} bivalent shows complete (heterologous) synapsis, this bivalent behaves similar to the autosomes and is not silenced. First, we scored the morphology of the 1^{13} bivalent in mid-pachytene nuclei from control and irradiated T/T'mice. Mid-pachytene nuclei were randomly selected based on the MLH1 and SYCP3 staining pattern. We found that nuclei with incompletely synapsed 1^{13} bivalents are significantly more frequent in irradiated T/T' testes compared to non-irradiated controls (Figure 5e). Immunostaining for RNA polymerase II was used to visualize regions of active transcription. Very low to no RNA polymerase II signal was found around the incompletely synapsed 1^{13} bivalents, whereas normal staining was observed when the 1^{13} bivalents synapsed heterologously. The relation between synapsis and silencing of the 1^{13} bivalent was similar in control and irradiated nuclei (Figure 5ab). Hence, in both groups, only completely synapsed 1^{13} bivalents escaped silencing. From this, we conclude that the presence of nonhomologous chromatin of the small 1^{13} bivalent is detected more often in nuclei that are irradiated at early prophase.
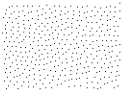
◁ **Figure 5. Exposure to 4 Gy increases the frequency of non-synapsed 1^{13} bivalents in pachytene spermatocytes.** (a) Control and irradiated T/T' pachytene spermatocyte spread nuclei immunostained for SYCP3 (red) and RNA polymerase II (green). RNA pol II staining signal is normal in the region of completely synapsed (CS) 1^{13} translocation bivalent, and very low in the XY body region (*). The arrows point to the T/T' bivalent. Bar represents 10μm. (b) Control and irradiated T/T' pachytene spermatocyte spread nuclei immunostained for SYCP3 (red) and RNApol II (green). RNApol II staining signal is very low in the XY body region (*) and also in the region of the incompletely synapsed 1^{13} bivalent. The arrows point to the T/T' bivalent. Bar represents 10μm. (c) Control (left) and irradiated (right) T/T' pachytene spermatocyte spread nuclei immunostained for SYCP3 (red) and RAD18 (green). RAD18 accumulates on the XY body and on the incompletely synapsed 1^{13} bivalent (arrow right nucleus), but not on the completely synapsed 1^{13} bivalent (arrow left nucleus). Bar represents 10μm. (d) Control (left) and irradiated (right) T/T' diplotene spermatocyte spread nuclei immunostained for SYCP3 (red) and RAD18 (green). In diplotene, RAD18 also accumulates on the XY body and on the incompletely synapsed 1^{13} bivalent (arrow right nucleus), but not on the completely synapsed 1^{13} bivalent (arrow left nucleus). Open arrowheads point to possible unrepaired DSBs on the autosomes. Bar represents 10μm. (e) The morphology of the 113 bivalent was classified as incompletely synapsed or completely synapsed, and the graph shows the percentage of nuclei with incompletely synapsed 113 bivalent in mid-pachytene spermatocytes from control (n = 400 analysed nuclei / 4 mice) and irradiated (n = 486 analysed nuclei / 5 mice) T/T' mice. Error bars represent the standard error of the mean. * Indicates a significant difference (p<0.05) as compared to the control group. (f) Graph shows RAD18 accumulation on the 1^{13} bivalent during pachytene and diplotene in the control (n = 280 analysed nuclei / 4 mice) and irradiated (n = 300 analysed nuclei / 5 mice) T/T'mouse spermatocytes. Error bars represent the standard error of the mean. * indicates a significant difference (p<0.05) as compared to the control group.

Next, we used an antibody against the protein RAD18, which we have identified as a marker of MSUC from pachytene until mid-diplotene [20]. RAD18 is the mouse homologue of *Saccharomyces cerevisiae* RAD18, and this ubiquitin ligase functions in the replicative damage bypass (RDB) pathway together with the ubiquitin-conjugating enzyme RAD6 [35]. Its role during meiotic prophase is unknown, but might involve function(s) in MSUC and suppression of recombination [20]. In control and irradiated pachytene and diplotene nuclei, RAD18 localizes to the XY body and incompletely synapsed 1^{13} bivalents [20] (Figure 5cd). We found that in the irradiated group, the number of RAD18 positive 1^{13} bivalents was significantly increased in mid-pachytene nuclei that were exposed to radiation during the previous leptotene (Figure 5f). This effect was similar to the increase in the frequency of incompletely synapsed 1^{13} bivalent configurations after irradiation (Figure 5e). However, in late pachytene and diplotene nuclei from irradiated mice, we observed additional RAD18 staining at a few sites (Figure 5d). These sites also accumulate γH2AX (not shown) and most likely represent unrepaired DSBs that were induced during early pachytene.

It is possible that only those breaks which are introduced before pachytene can be incorporated into the meiotic recombination pathway, implying that the time-window of break formation influences the behaviour of the translocation bivalents and the process of MSUC. Therefore, we tested whether cells that had already completed leptotene and zygotene at the time of irradiation behave similar in irradiated and control mice, with respect to the frequency of MSUC associated with the 1^{13} bivalent. We analysed spermatocytes that were in early pachytene at the time of irradiation and have progressed to diplotene at the time of analysis (Figure 2). At this time point, the morphology of the 1^{13} bivalent is difficult to classify, and, therefore, we again analysed RAD18 staining, which still marks silenced unsynapsed chromatin during diplotene [20]. In these diplotene nuclei we found no significant difference in RAD18 staining of the 1^{13} bivalent between irradiated and control mice (Figure 5d,f).

We cannot formally exclude that our findings on MSUC of the 1^{13} bivalent are caused by a stress-related response of the cells to irradiation. However, the results of the analyses of RAD51 and MLH1 foci, and the absence of residual damage in mid-pachytene nuclei, indicate that the surviving spermatocytes have been able to repair the DSBs. Therefore, our data suggest that the detection and associated asynapsis of nonhomologous chromatin could be linked to the presence of meiotic DSBs, localized in the nonhomologous region, and induced during a certain time window, most likely limited to leptotene and zygotene. We and others [16,18] find a tight correlation between asynapsis and activation of MSUC. Therefore, it is at present not possible to discriminate between the possibilities that either persistent DSBs or the asynapsed configuration trigger MSUC. In fact,

the persistence of DSBs as well as a failure to synapse both may act as critical factors, in the mechanism that activates MSUC. Li and Schimenti [56] recently showed that mutation of *Trip13* leads to a meiotic defect that is characterised by persistence of several DNA repair proteins on normally synapsed chromosomes, and normal XY body formation. Apparently, the incomplete repair of DSBs in this mouse model does not interfere with MSCI. It is not known whether the sites, which contain persistent γH2AX staining, activate ectopic MSUC. In various other mouse mutants with defective repair of meiotic DSBs, γH2AX is associated with these breaks, but no XY body is formed [25]. It could be suggested that in these mouse models with a certain level of incomplete repair of meiotic DSBs, and an additional lack of chromosome pairing, the second wave of H2AX phosphorylation is initiated at too many sites to achieve effective MSCI. This implies that there is a limiting amount of one or more of the components that establish MSCI/MSUC. A recent report also suggests that silencing of autosomal unsynapsed chromatin (MSUC) partially disrupts MSCI [57].

Analysis of the larger 13¹ translocation bivalent with the same heterologous region
The large 13¹ bivalent carries the same nonhomologous region as the 1¹³ bivalent, but pairing problems are observed at much lower frequencies [30, 58]. If heterologous synapsis is inhibited by the presence of meiotic DSBs and associated repair proteins, induction of extra DSBs by irradiation should also increase the frequency of asynapsis and meiotic silencing of the nonhomologous chromatin of the 13¹ bivalent. To analyse this, we first identified this bivalent using a combined anti-SYCP3 immunostaining with a DNA FISH identifying chromosomes 1 and 13 (Figure 6a). Subsequently, we measured the length of the SCs that showed a positive signal for the FISH probes. These analyses confirmed that the 1¹³ bivalent has the shortest SC present in pachytene spread nuclei and that the 13¹ bivalent represents the longest SC. Previous reports have shown that both the 1¹³ and 13¹ translocation chromosomes can form unsynapsed loops that become visible around late zygotene [26, 51, 58]. For the 13¹ bivalent, this loop is rarely observed in mid pachytene, and it has been suggested that the disappearance of this loop is due to synaptic adjustment [58]. In contrast, asynapsis of the 1¹³ bivalent is frequently observed throughout pachytene [59]. When we carefully analysed late zygotene/early pachytene nuclei, we sometimes observed nuclei that contained a 13¹ bivalent with an unsynapsed loop, positive for γH2AX (Figure 6b). However, less then 1% of the nuclei showed this 13¹ configuration. In addition, no RAD18 staining on the 13¹ bivalent was observed in 160 irradiated and 120 control mid-pachytene nuclei.

Together, the data on the 13¹ bivalent show that this bivalent almost always escapes from MSUC, even if extra DSBs are induced, in contrast to the observed
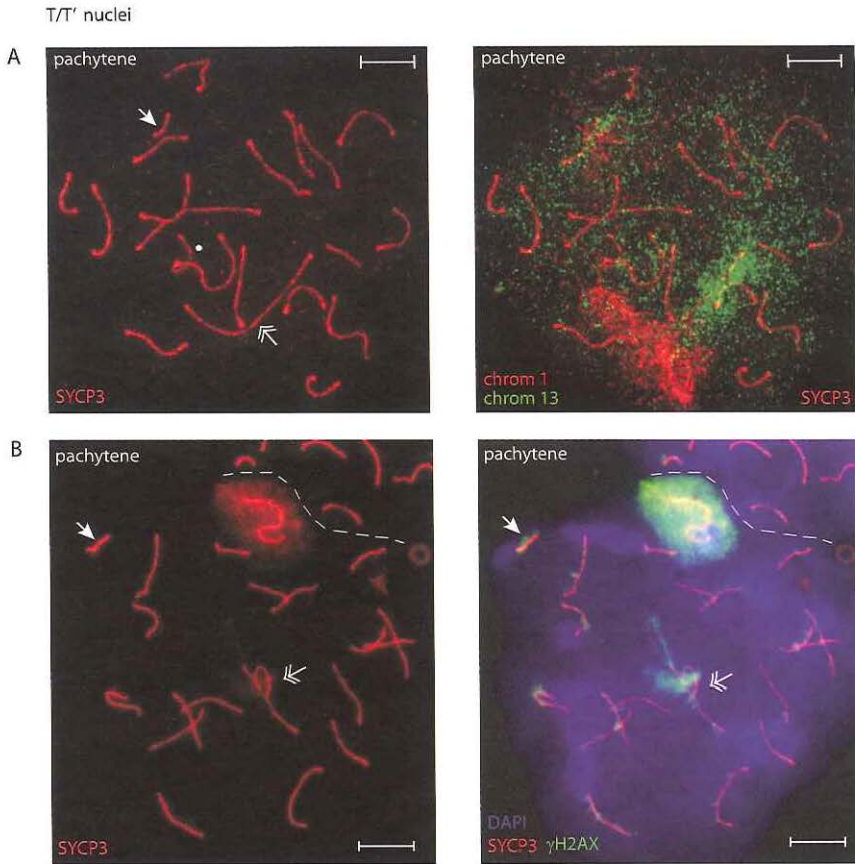
Figure 6. Analysis of 13^1 bivalents in T/T' meiotic prophase spermatocytes. (a) Irradiated T/T' pachytene spermatocyte spread nuclei DNA FISH with painting probes for chromosomes 1 (red) and 13 (green) (right), and immunostained for SYCP3 (red) (left and right). This allows identification of the 13^1 (double arrow) and 1^{13} (single closed arrow) bivalents. Asterisk indicates the XY body. Bar represents 10μm. (b) Irradiated T/T' pachytene spermatocyte spread nuclei immunostained for SYCP3 (left/right), γH2AX and DAPI (right). γH2AX accumulates on an incompletely synapsed 13^1 bivalent. Double arrow indicated the 13^1 and the single closed arrow the 1^{13} bivalent. Bar represents 10μm.

association between extra DSBs and increased frequency of asynapsis and associated MSUC of the small 1^{13} bivalent.

Concluding remarks

Pairing sites have been identified in species like *Drosophila melanogaster* and *Caenorhabitis elegans*, that show synapsis prior to DSB formation (reviewed in [60]). For mouse and human, this is less clear, but a recent study showed that SC

initiation occurs in distal subtelomeric regions [61]. It has been suggested that DSB repair sites may function as such SC initiation sites [35]. This could imply that irradiation-induced DSBs act in two ways. First, irradiation-induced extra DSBs in homologous parts of the genome may lead to formation of extra sites of strand invasion on a non-sister chromatid, and this could facilitate the process of synapsis. Second, if induced in heterologous regions, the lack of a homologous partner precludes strand invasion and this may result in asynapsis and subsequent activation of the MSUC pathway.

The onset and spreading of SC formation initiated from regions of homology may act as an opposing force against MSUC, promoting heterologous synapsis irrespective of the presence of persistent DSBs. RAD51 foci, indicative of sites of DSB repair, disappear from synapsed regions in pachytene [5]. This most likely also occurs when synapsis is nonhomologous on both the 1^{13} and 13^1 bivalent. It could be that DSBs that are still present following heterologous synapsis, are repaired via homologous recombination with the sister chromatid. Alternatively, repair proteins may dissociate while the DSB persists. The large 13^1 translocation bivalent was found to escape from MSUC in almost 100% of the nuclei, irrespective of the induction of extra DSBs. The nonhomologous region in the 13^1 bivalent comprises only 13% of the total length of the bivalent, as compared to 50% for the 1^{13} bivalent (Figure 1). In view of this, it can be understood that the increased number of DSBs induced by irradiation in the present experiments has significantly altered the balance between heterologous synapsis and MSUC for the 1^{13} bivalent, whereas the behaviour of the longer 13^1 bivalent is subject to additional mechanisms, which may cause heterologous synapsis and escape from MSUC.

Herein, we have shown for the first time that extra irradiation-induced DSBs during leptotene, can be incorporated into the meiotic recombination pathway of mouse spermatocytes. The extra DSBs lead to more frequent asynapsis and associated MSUC of the small 1^{13} bivalent, and this suggests that unrepaired DSBs in heterologous regions may inhibit the progression of synapsis. However, structural adaptations of the chromosomal axes and heterologous synapsis also occur, in association with an escape from silencing, even in the presence of DSBs.

MATERIALS AND METHODS

Mice

Adult wild type FVB and T(1;13)70H/T(1;13)1WA (T/T') double-heterozygous mice [30] (T/T') were subjected to whole body γ-irradiation with ^{137}Cs Gammacell-40 / Elekta linear accelerator (Crawley, UK). Mice received a total dose of 4 Gy at a rate of respectively 0.74 Gy/min and 0.5 Gy/min. Mice were killed at 2 hours, 30

hours (wild type) and 120 hours (T/T') after treatment, and testes were collected as described below.

Meiotic spread nuclei preparations, immunocytochemistry and FISH analysis
Testes were isolated from T/T' and wild type mice. Spread nuclei preparations of mouse spermatocytes were prepared using a modification of the drying-down technique described by Peters et al. [62]. For immunocytochemistry, frozen slides were defrosted at room temperature and washed with PBS. The slides were blocked with PBS containing 0.5% w/v BSA and 0.5% w/v milk powder, and were double stained with rat polyclonal anti-SYCP3 [63], mouse monoclonal anti-MLH1 (BD Pharmingen, San Diego, USA), rabbit polyclonal anti-RAD18 [20], rabbit polyclonal anti-RNA polymerase II (Abcam, Cambridge, United Kingdom) and rabbit anti-human RAD51 [64]. For rabbit polyclonal primary antibodies, the secondary antibodies were fluorescein isothiocyanate (FITC) (Sigma, St Louis, USA)-labeled goat anti-rabbit IgG antibodies; the secondary antibodies used for the rat polyclonal anti-SYCP3 (IgG) and mouse monoclonal anti-MLH1 (IgG) were Alexa 594-labeled goat anti-rat IgG and FITC-labeled goat anti-mouse IgG respectively. Primary antibodies were diluted in 10% w/v BSA in PBS and incubated overnight in a humid chamber. Thereafter, slides were washed in PBS, blocked in 10% v/v normal goat serum (Sigma) in blocking buffer (5% milk powder (w/v in PBS, centrifuged at 13,200 rpm for 10 min), and incubated with secondary antibodies in 10% v/v normal goat serum in blocking buffer at room temperature for 2 hours. Next, the slides were washed in PBS and embedded in Vectashield containing DAPI (4',6'-diamindino-2-phenylindole) (Vector Laboratories, Burlingame CA, USA).

Fluorescent in situ hybridisation
Painting probes of chromosome 1 and 13, respectively labelled with Cy3 and FITC (Cambio, Cambridge, UK) were warmed at 37 C. 3 µl of each concentrated chromosome paint was added to 12 µl of hybridisation buffer (Cambio, Cambridge, UK). Slides were treated with 0,2% pepsin for 4 minutes at 37 C, washed in 4% paraformaldehyde in PBS at room temperature for 5 minutes, and finally dehydrated in an ethanol series consisting of 3 minutes washes in 70%, 90% and 100%. Slides were air-dried and denatured for 3 minutes in 70% formamide, 30% 2xSSC at 85 C. This was followed by quenching the slides in ice-cold 70% ethanol and dehydration. The probe mixture was placed on the slide and covered with a coverslip. The slides were placed in a pre-heated sealed slide box and incubated overnight at 37 C. After incubation, the slides with coverslip were placed in 2xSSC at 45 C for 5 minutes. After removal of the coverslip, slides were then rinsed twice in 50% formamide and 50% 1xSSC for 5 minutes,

followed by rinsing twice in 1xSSC at 45 C for 5 minutes and 4 minutes in 0,05% Tween-20 and 100% 4xSSC. Finally, a droplet of Vectashield mounting medium with DAPI (Vector Laboratories) was placed on the slide and covered with a coverslip.

*Fluorescence microscopy analysis, digital image preparation and analysis*
Analysis of the spermatocyte nuclei was performed using a Carl Zeiss Axioplan 2 imaging microscope (Jena, Germany) with a plan-neofluar objective 100x/1.3 oil immersion. Images were taken with a Coolsnap-pro digital camera (Photometrics, Waterloo, Canada). The acquired digital images were processed with Photoshop software (Adobe Systems). The number of RAD51-foci on digital images was determined using the image analysis software package ImageJ (http://www.rsb.info.nih.gov/ij/). First, we measured the mean intensity and its standard deviation per nucleus with ImageJ. Next, we set the foci detection threshold for each nucleus on the mean plus 2 x the standard deviation, and analyzed the same nucleus for total area of foci. We calculated the average focus area by analysing 20 manually selected foci. Subsequently, we determined the number of foci per nucleus using the total area of foci divided by the average focus size. Measurement of synaptonemal complex lengths and distances within nuclei was performed using the ImageJ plugin NeuronJ (http:www.imagescience.org/meijering/software/neuronj/). We visually selected the 10 longest bivalents in each nucleus, tracked the SCs, and measured the lengths using NeuronJ software. With aid of ImageJ we measured the longest diameter from each nucleus (named Feret's diameter), and divided the calculated SC lengths by Feret's diameter to correct for variations in spreading of nuclei.

Statistical analysis
Statistical analyses were carried out using SPSS 11 (SPSS Inc., Illinois, USA). A nonparametric or independent sample T-test was used to analyse differences between the groups. The differences were considered statistically significant at 95% confidence limit ($p < 0.05$).

ACKNOWLEDGEMENTS
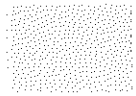
REFERENCES

1. Zickler D. From early homologue recognition to synaptonemal complex formation. *Chromosoma.* 2006;115(3):158-174.
2. Padmore R, Cao L, Kleckner N. Temporal comparison of recombination and synaptonemal complex formation during meiosis in S. cerevisiae. *Cell.* Sep 20 1991;66(6):1239-1256.
3. Mahadevaiah SK, Turner JM, Baudat F, et al. Recombinational DNA double-strand breaks in mice precede synapsis. *Nat Genet.* 2001;27(3):271-276.
4. Neale MJ, Keeney S. Clarifying the mechanics of DNA strand exchange in meiotic recombination. *Nature.* 2006;442(7099):153-158.
5. Moens PB, Chen DJ, Shen Z, et al. Rad51 immunocytology in rat and mouse spermatocytes. *Chromosoma.* 1997;106(4):207-215.
6. Keeney S, Giroux CN, Kleckner N. Meiosis-specific DNA double-strand breaks are catalyzed by Spo11, a member of a widely conserved protein family. *Cell.* 1997;88(3):375-384.
7. Baudat F, Manova K, Yuen JP, Jasin M, Keeney S. Chromosome synapsis defects and sexually dimorphic meiotic progression in mice lacking Spo11. *Mol Cell.* Nov 2000;6(5):989-998.
8. Romanienko PJ, Camerini-Otero RD. The mouse Spo11 gene is required for meiotic chromosome synapsis. *Mol Cell.* Nov 2000;6(5):975-987.
9. Grelon M, Vezon D, Gendrot G, Pelletier G. AtSPO11-1 is necessary for efficient meiotic recombination in plants. *Embo J.* Feb 1 2001;20(3):589-600.
10. Loidl J, Klein F, Scherthan H. Homologous pairing is reduced but not abolished in asynaptic mutants of yeast. *J Cell Biol.* Jun 1994;125(6):1191-1200.
11. Bhuiyan H, Schmekel K. Meiotic chromosome synapsis in yeast can occur without spo11-induced DNA double-strand breaks. *Genetics.* Oct 2004;168(2):775-783.
12. Monesi V. Differential rate of ribonucleic acid synthesis in the autosomes and sex chromosomes during male meiosis in the mouse. *Chromosoma.* 1965;17:11-21.
13. Hendriksen PJM, Hoogerbrugge JW, Themmen APN, et al. Postmeiotic transcription of X and Y chromosomal genes during spermatogenesis in the mouse. *Dev. Biol.* 1995;170:730-733.
14. Namekawa SH, Park PJ, Zhang LF, et al. Postmeiotic sex chromatin in the male germline of mice. *Curr Biol.* Apr 4 2006;16(7):660-667.
15. Turner JM, Mahadevaiah SK, Ellis PJ, Mitchell MJ, Burgoyne PS. Pachytene asynapsis drives meiotic sex chromosome inactivation and leads to substantial postmeiotic repression in spermatids. *Dev Cell.* Apr 2006;10(4):521-529.
16. Baarends WM, Wassenaar E, van der Laan R, et al. Silencing of unpaired chromatin and histone H2A ubiquitination in mammalian meiosis. *Mol Cell Biol.* 2005;25(3):1041-1053.
17. Schimenti J. Synapsis or silence. *Nat Genet.* 2005;37(1):11-13.
18. Turner JM, Mahadevaiah SK, Fernandez-Capetillo O, et al. Silencing of unsynapsed meiotic chromosomes in the mouse. *Nat Genet.* 2005;37(1):41-47.
19. Turner JM, Aprelikova O, Xu X, et al. BRCA1, histone H2AX phosphorylation, and male meiotic sex chromosome inactivation. *Curr Biol.* Dec 14 2004;14(23):2135-2142.
20. van der Laan R, Uringa EJ, Wassenaar E, et al. Ubiquitin ligase Rad18Sc localizes to the XY body and to other chromosomal regions that are unpaired and transcriptionally silenced during male meiotic prophase. *J Cell Sci.* 2004;117(Pt 21):5023-5033.
21. Shiu PK, Raju NB, Zickler D, Metzenberg RL. Meiotic silencing by unpaired DNA. *Cell.* Dec 28 2001;107(7):905-916.
22. Shiu PK, Metzenberg RL. Meiotic silencing by unpaired DNA: properties, regulation and suppression. *Genetics.* Aug 2002;161(4):1483-1495.

23. Costa Y, Speed RM, Gautier P, et al. Mouse MAELSTROM: the link between meiotic silencing of unsynapsed chromatin and microRNA pathway? *Hum Mol Genet.* Aug 1 2006;15(15):2324-2334.

24. Bellani MA, Romanienko PJ, Cairatti DA, Camerini-Otero RD. SPO11 is required for sex-body formation, and Spo11 heterozygosity rescues the prophase arrest of Atm-/- spermatocytes. *J Cell Sci.* Aug 1 2005;118(Pt 15):3233-3245.

25. Barchi M, Mahadevaiah S, Di Giacomo M, et al. Surveillance of different recombination defects in mouse spermatocytes yields distinct responses despite elimination at an identical developmental stage. *Mol Cell Biol.* Aug 2005;25(16):7203-7215.

26. Plug AW, Peters AH, Keegan KS, Hoekstra MF, de Boer P, Ashley T. Changes in protein composition of meiotic nodules during mammalian meiosis. *J Cell Sci.* Feb 1998;111 (Pt 4):413-423.

27. Thorne LW, Byers B. Stage-specific effects of X-irradiation on yeast meiosis. *Genetics.* 1993;134(1):29-42.

28. Dernburg AF, McDonald K, Moulder G, Barstead R, Dresser M, Villeneuve AM. Meiotic recombination in C. elegans initiates by a conserved mechanism and is dispensable for homologous chromosome synapsis. *Cell.* 1998;94(3):387-398.

29. Celerin M, Merino ST, Stone JE, Menzie AM, Zolan ME. Multiple roles of Spo11 in meiotic chromosome behavior. *Embo J.* 2000;19(11):2739-2750.

30. de Boer P, Searle AG, van der Hoeven FA, de Rooij DG, Beechey CV. Male pachytene pairing in single and double translocation heterozygotes and spermatogenic impairment in the mouse. *Chromosoma.* 1986;93(4):326-336.

31. Bergerat A, de Massy B, Gadelle D, Varoutas PC, Nicolas A, Forterre P. An atypical topoisomerase II from Archaea with implications for meiotic recombination. *Nature.* Mar 27 1997;386(6623):414-417.

32. Gasior SL, Wong AK, Kora Y, Shinohara A, Bishop DK. Rad52 associates with RPA and functions with rad55 and rad57 to assemble meiotic recombination complexes. *Genes Dev.* Jul 15 1998;12(14):2208-2221.

33. Bowring FJ, Yeadon PJ, Stainer RG, Catcheside DE. Chromosome pairing and meiotic recombination in Neurospora crassa spo11 mutants. *Curr Genet.* Aug 2006;50(2):115-123.

34. de Vries FA, de Boer E, van den Bosch M, et al. Mouse Sycp1 functions in synaptonemal complex assembly, meiotic recombination, and XY body formation. *Genes Dev.* Jun 1 2005;19(11):1376-1389.

35. Moens PB, Kolas NK, Tarsounas M, Marcon E, Cohen PE, Spyropoulos B. The time course and chromosomal localization of recombination-related proteins at meiosis in the mouse are compatible with models that can resolve the early DNA-DNA interactions without reciprocal recombination. *J Cell Sci.* 2002;115(Pt 8):1611-1622.

36. Oakberg EF, Diminno RL. X-ray sensitivity of primary spermatocytes of the mouse. int. *Int J Radiat Biol.* Apr 1960;2:196-209.

37. Ahmed EA, van der Vaart A, Barten A, et al. Differences in DNA double strand breaks repair in male germ cell types: Lessons learned from a differential expression of Mdc1 and 53BP1. *DNA Repair (Amst).* Sep 1 2007;6(9):1243-1254.

38. Chicheportiche A, Bernardino-Sgherri J, de Massy B, Dutrillaux B. Characterization of Spo11-dependent and independent phospho-H2AX foci during meiotic prophase I in the male mouse. *J Cell Sci.* May 15 2007;120(Pt 10):1733-1742.

39. Goedecke W, Eijpe M, Offenberg HH, van Aalderen M, Heyting C. Mre11 and Ku70 interact in somatic cells, but are differentially expressed in early meiosis. *Nat Genet.* Oct 1999;23(2):194-198.

40. Roeder GS. Meiotic chromosomes: it takes two to tango. *Genes Dev.* 1997;11(20):2600-2621.

41. Ruiz de Almodovar JM, Steel GG, Whitaker SJ, McMillan TJ. A comparison of methods for calculating DNA double-strand break induction frequency in mammalian cells by pulsed-field gel electrophoresis. *Int J Radiat Biol.* 1994;65(6):641-649.

42. Rogakou EP, Pilch DR, Orr AH, Ivanova VS, Bonner WM. DNA double-stranded breaks induce histone H2AX phosphorylation on serine 139. *J Biol Chem.* 1998;273(10):5858-5868.

43. Forand A, Dutrillaux B, Bernardino-Sgherri J. Gamma-H2AX expression pattern in non-irradiated neonatal mouse germ cells and after low-dose gamma-radiation: relationships between chromatid breaks and DNA double-strand breaks. *Biol Reprod.* 2004;71(2):643-649.

44. Zheng H, Olive PL. Influence of oxygen on radiation-induced DNA damage in testicular cells of C3H mice. *Int J Radiat Biol.* Mar 1997;71(3):275-282.

45. Max B. This and that: hair pigments, the hypoxic basis of life and the Virgilian journey of the spermatozoon. *Trends Pharmacol Sci.* Jul 1992;13(7):272-276.

46. Oakberg EF. Duration of spermatogenesis in the mouse and timing of stages of the cycle of the seminiferous epithelium. *Am J Anat.* Nov 1956;99(3):507-516.

47. Baker SM, Plug AW, Prolla TA, et al. Involvement of mouse Mlh1 in DNA mismatch repair and meiotic crossing over. *Nat Genet.* 1996;13(3):336-342.

48. Anderson LK, Reeves A, Webb LM, Ashley T. Distribution of crossing over on mouse synaptonemal complexes using immunofluorescent localization of MLH1 protein. *Genetics.* 1999;151(4):1569-1579.

49. Ashley T, Gaeth AP, Creemers LB, Hack AM, de Rooij DG. Correlation of meiotic events in testis sections and microspreads of mouse spermatocytes relative to the mid-pachytene checkpoint. *Chromosoma.* Sep 2004;113(3):126-136.

50. van der Heijden GW, Derijck AA, Posfai E, et al. Chromosome-wide nucleosome replacement and H3.3 incorporation during mammalian meiotic sex chromosome inactivation. *Nat Genet.* Feb 2007;39(2):251-258.

51. Wauben-Penris PJ, van der Hoeven FA, de Boer P. Chiasma frequency and nondisjunction in heteromorphic bivalents: meiotic behavior in T(1;13)70H/T(1;13)1Wa mice as compared to T(1;13)70H/T(1;13)70H mice. *Cytogenet Cell Genet.* 1983;36(3):547-553.

52. Jones GH. The control of chiasma distribution. *Symp Soc Exp Biol.* 1984;38:293-320.

53. Hillers KJ. Crossover interference. *Curr Biol.* 2004;14(24):R1036-1037.

54. Baart EB, de Rooij DG, Keegan KS, de Boer P. Distribution of Atr protein in primary spermatocytes of a mouse chromosomal mutant: a comparison of preparation techniques. *Chromosoma.* 2000;109(1-2):139-147.

55. van der Laan R, Roest HP, Hoogerbrugge JW, et al. Characterization of mRAD18Sc, a mouse homolog of the yeast postreplication repair gene RAD18. *Genomics.* 2000;69(1):86-94.

56. Li X, Schimenti JC. Mouse pachytene checkpoint 2 (trip13) is required for completing meiotic recombination but not synapsis. *PLoS Genet.* Aug 10 2007;3(8):e130.

57. Homolka D, Ivanek R, Capkova J, Jansa P, Forejt J. Chromosomal rearrangement interferes with meiotic X chromosome inactivation. *Genome Res.* Oct 2007;17(10):1431-1437.

58. Peters AH, Plug AW, de Boer P. Meiosis in carriers of heteromorphic bivalents: sex differences and implications for male fertility. *Chromosome Res.* 1997;5(5):313-324.

59. Moses MJ, Poorman PA. Synaptosomal complex analysis of mouse chromosomal rearrangements. II. Synaptic adjustment in a tandem duplication. *Chromosoma.* 1981;81(4):519-535.

60. Joyce EF, McKim KS. When specialized sites are important for synapsis and the distribution of crossovers. *Bioessays.* Mar 2007;29(3):217-226.

61. Brown PW, Judis L, Chan ER, et al. Meiotic synapsis proceeds from a limited number of subtelomeric sites in the human male. *Am J Hum Genet.* Oct 2005;77(4):556-566.
62. Peters AH, Plug AW, van Vugt MJ, de Boer P. A drying-down technique for the spreading of mammalian meiocytes from the male and female germline. *Chromosome Res.* Feb 1997;5(1):66-68.
63. Baarends WM, Wassenaar E, Hoogerbrugge JW, Schoenmakers S, Sun ZW, Grootegoed JA. Increased phosphorylation and dimethylation of XY body histones in the Hr6b-knockout mouse is associated with derepression of the X chromosome. *J Cell Sci.* Jun 1 2007;120(Pt 11):1841-1851.
64. Essers J, Hendriks RW, Wesoly J, et al. Analysis of mouse Rad54 expression and its implications for homologous recombination. *DNA Repair (Amst).* Oct 1 2002;1(10):779-793.
65. de Boer P, van Gijsen M. The location of the positions of the breakpoints involved in the T26H and T70H mouse translocations with the aid of Giemsa-banding. *Can J Genet Cytol.* Dec 1974;16(4):783-788.
66. Brunet JF, Denizot F, Luciani MF, et al. A new member of the immunoglobulin superfamily--CTLA-4. *Nature.* Jul 16-22 1987;328(6127):267-270.
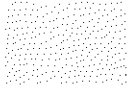
CHAPTER 4

FEMALE MEIOTIC SEX CHROMOSOME INACTIVATION IN CHICKEN

ABSTRACT

During meiotic prophase in male mammals, the heterologous X and Y chromosomes remain largely unsynapsed, and meiotic sex chromosome inactivation (MSCI) leads to formation of the transcriptionally silenced XY body. In birds, the heterogametic sex is female, carrying Z and W chromosomes (ZW), whereas males have the homogametic ZZ constitution. During chicken oogenesis, the heterologous ZW pair reaches a state of complete heterologous synapsis, and this might enable maintenance of transcription of Z- and W chromosomal genes during meiotic prophase. Herein, we show that the ZW pair is transiently silenced, from early pachytene to early diplotene using immunocytochemistry and gene expression analyses. We propose that ZW inactivation is most likely achieved via spreading of heterochromatin from the W on the Z chromosome. Also, persistent meiotic DNA double-strand breaks (DSBs) may contribute to silencing of Z. Surprisingly, γH2AX, a marker of DSBs, and also the earliest histone modification that is associated with XY body formation in mammalian and marsupial spermatocytes, does not cover the ZW during the synapsed stage. However, when the ZW pair starts to desynapse, a second wave of γH2AX accumulates on the unsynapsed regions of Z, which also show a reappearance of the DSB repair protein RAD51. This indicates that repair of meiotic DSBs on the heterologous part of Z is postponed until late pachytene/diplotene, possibly to avoid recombination with regions on the heterologously synapsed W chromosome. Two days after entering diplotene, the Z looses γH2AX and shows reactivation. This is the first report of meiotic sex chromosome inactivation in a species with female heterogamety, providing evidence that this mechanism is not specific to spermatogenesis. It also indicates the presence of an evolutionary force that drives meiotic sex chromosome inactivation independent of the final achievement of synapsis.

INTRODUCTION

During meiotic prophase, homologous chromosomes pair and are held together by the synaptonemal complex (reviewed in [1]). In spermatocytes of male mammals, the heterologous X and Y chromosomes pair and synapse only in small pseudoautosomal regions (PARs). The presence of the largely unsynapsed X and Y chromosomal axes is associated with meiotic sex chromosome inactivation (MSCI) [2,3]. The two X chromosomes in meiotic prophase in oocytes show complete synapsis and are transcriptionally active.

In birds, females are heterogametic, carrying Z and W chromosomes (ZW), whereas males have the homogametic ZZ constitution. The chicken Z chromosome is the larger of the two chromosomes (http://www.ensembl.org/Gallus_gallus/index.html). Similar to the mammalian X and Y sex chromosomes, the Z and W chromosomes share only a small pseudoautosomal region [4]. However, the behaviour of the ZW pair during female oogenesis in the chicken differs from that of the XY pair in mammalian spermatocytes, in that the ZW chromosomes appear to reach a stage of complete synapsis. Based on electron micrographs, Solari [5] analysed the pairing between Z and W throughout the pachytene stage and found that the chromosomal axes of the Z chromosome thickens and shortens (most likely by folding back on itself), and wraps itself around the W chromosome to achieve complete synapsis during the brief so-called equalized stage. Subsequently, the Z and W chromosomes desynapse but remain attached at their tips when the oocytes enter diplotene. The morphological changes of the Z and W axes have been explained by a mechanism called synaptic adjustment [5]. This mechanism describes the process of resolving an axial length difference between aligned chromosomes to achieve complete synapsis [6,7].

During mitotic prophase in female chicken cells, the small W chromosome appears to be heterochromatic [8] indicating that the W chromosome is mostly inactive in somatic cells. During early meiotic prophase in leptotene and zygotene oocytes, such a heteropycnotic area appears to be absent [9-11]. Subsequently, Z and W pair completely. Although the pairing is mainly heterologous, Jablonka and Lamb [12] have suggested that pairing, synapsis and subsequent retention of an active state is preferred above meiotic inactivation of Z and W, because of a requirement for Z- and/or W-linked genes for maintenance and growth of the large and long-living oocytes. However, Solari [11] describes the appearance of a more dense chromatin structure surrounding the ZW pair in late pachytene and early diplotene oocytes, and the appearance of a heteropycnotic body in some late pachytene and diplotene nuclei of chicken oocytes. This observation suggests that some form of Z and/or W inactivation may occur during late meiotic prophase.

MSCI in mammals is thought to be a specialization of a more general process that silences unsynapsed chromatin during meiotic prophase, named MSUC (meiotic silencing of unsynapsed chromatin) [13-15]. Similar, but mechanistically distinct mechanisms (meiotic silencing by unpaired DNA; MSUD) are operative in a variety of distant species such as *Caenorhabditis elegans* and *Neurospora crassa* (reviewed in [16]).

In mammalian meiosis, chromosomal alignment and pairing is preceded by induction of DNA double strand breaks (DSBs) by the topoisomerase-like protein SPO11, and these DSBs are thought to participate in homology recognition [17, 18]. After formation of DSBs, the homologous recombination repair protein RAD51 rapidly forms filaments on the 3' end single-strand DNA overhangs of meiotic DSBs (reviewed in [19, 20]). The presence of persistent RAD51 foci on the unpaired X chromosome of mouse and man indicates that DSBs in heterologous regions show delayed repair [20-22]. This is most likely due to the fact that a non-sister chromatid from a homologous chromosome is not available for strand invasion and recombination repair. Ashley et al. [21] reported a high concentration of RAD51 foci on the unsynapsed axis of the Z chromosome in chicken oocytes during early pachytene, which disappear as the oocytes progress through pachytene. Unsynapsed sex chromatin, persistent DSBs, and meiotic silencing are always associated in mice [13, 15, 23]. In chicken oocytes, however, the ZW pair reaches a state of complete synapsis, but possibly with persistent DSBs. In the present paper, we have investigated whether meiotic DSBs in chicken oocytes persist on the Z chromosome, analogous to persistence of X-chromosomal meiotic DSBs in mouse spermatocytes, and whether or not this would be associated with MSCI.

RESULTS

The equalized ZW is completely synapsed in mid-pachytene oocytes
We analysed the progression of meiotic prophase in chicken oocytes by immunostaining for SYCP3, which visualizes the lateral axial elements of the synaptonemal complex (SC). At leptotene, small SYCP3 fragments started to appear throughout the nucleus (Figure 1a). In addition to Z and W, the chicken genome is distributed over 38 autosomal chromosome pairs, including 10 pairs of microchromosomes. During zygotene, most microchromosomes are found at the periphery of one part of the nucleus, where they are aligned and have initiated pairing, whereas macrochromosomes are more confined to the center and opposite site of the nucleus, and appear entangled and disorganized (Figure 1a). At early pachytene, when all autosomes have completed synapsis, the ZW pair starts to synapse (Figure 1ab). Around mid-pachytene, the ZW pair reaches the complete synapsed or so-called equalized stage (Figure 1b), and frequently
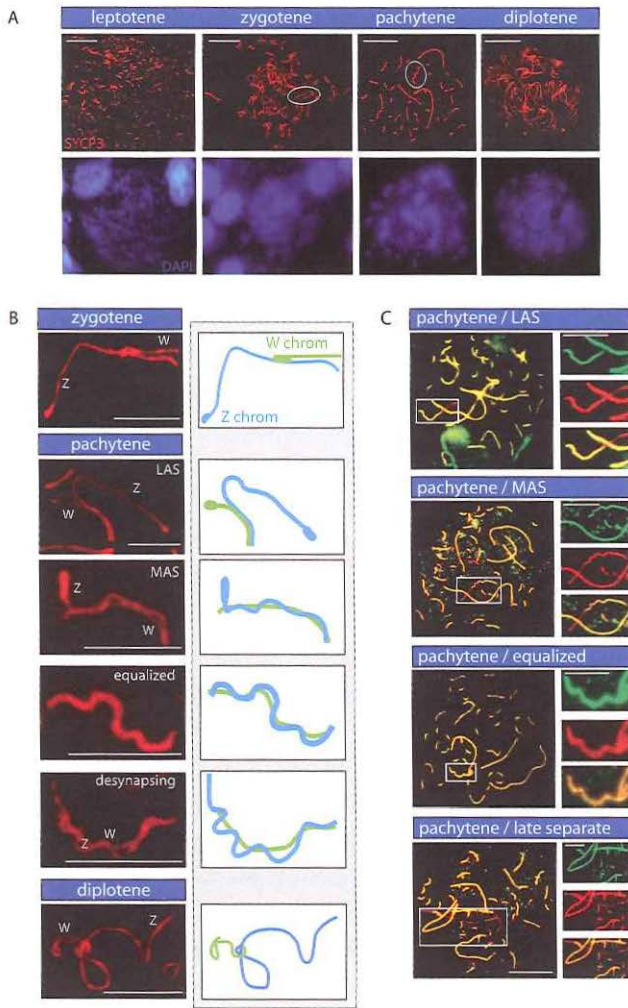
Figure 1. Synaptonemal complex formation and ZW pairing during meiotic prophase in chicken oocyte nuclei. (a) Overview of meiotic prophase in chicken oocytes. The upper panel shows the different substages, based on the morphology of the lateral elements of the synaptonemal complexes immunostained for SYCP3 (red). The lower panel shows the corresponding DAPI stained nuclei. The ZW pair is encircled in the zygotene and pachytene oocytes. Bar represents 10 μm. (b) Overview of the different synaptic configurations of the ZW pair during zygotene, pachytene, and diplotene, visualized by anti-SYPC3 (red). LAS = long asynaptic segment, MAS = medium asynaptic segment [38]; W indicates W chromosome, Z indicates Z chromosome. The panels on the right show schematic drawings of the morphological configurations of Z and W (Z chromosome in blue, W chromosome in green). Bar represents 5 μm. (c) Progress of ZW synapsis during pachytene visualized by immunostaining for SYCP1 (green) and SYCP3 (red). Bar represents 10 μm. The higher magnifications show separate immunostainings for SYCP1 (green, upper), SYCP3 (red, middle) and the merge (bottom) for the ZW pair. Bar represents 5 μm.

localizes to the periphery of the nucleus (Figure 2a). These findings are consistent with the configurations of the Z and W chromosomes described by Solari [5] (Figure 1b), and we used the consecutive configurations of the ZW pair to subdivide the pachytene stage.

During early pachytene, the Z and W chromosomes appear to be separate ('early type'). This is followed by ZW pairing and synapsing in the short pseudo-autosomal regions. Subsequently the long asynaptic segment (LAS) of Z, starts to condense and shorten (most likely by folding back on itself), becoming the medium asynaptic segment (MAS). At mid-pachytene, the Z chromosome starts to wind itself around the relatively straight W axis, resulting in a fully equalized ZW pair (Figure 1b). Next, the Z and W start to desynapse and rapidly separate again ('late separate'). At early diplotene, Z and W display end-to-end attachment (Figure 1b). Subsequently, all bivalents desynapse, elongate and become intertwined, making it almost impossible to distinguish and follow the individual Z and W chromosomes. However, in some diplotene nuclei, the Z and W chromosomes were found to display an end-to-end pairing in a typical ζ (zeta)-like configuration (Figure 1b and 2b).

Next, we investigated if the Z and W chromosomes actually reach a state of full synapsis during the equalized stage. For this purpose, we stained for SYCP1. In contrast to SYCP3, which localizes to the chromosomal axes of meiotic chromosomes, SYCP1 is a component of the central element of the SC, which is only assembled on completely synapsed chromosomes (reviewed in [26]. During the LAS and MAS stages, SYCP1 stains only the synapsed regions of the ZW pair. As soon as the Z chromosome starts to wrap itself around the W chromosome, we observed that the SYCP1 signal followed the twists of the Z chromosome (Figure 1c). At the equalized stage, the SYCP3 and SYCP1 staining fully overlapped, except for the occasionally free tip of the Z chromosome. As pachytene progresses further, Z and W begin to desynapse, and this was accompanied by disappearance of SYCP1 from these regions (Figure 1c). At the 'late separate' stage, SYCP1 was no longer present on Z and W. Based on these observations, we conclude that the equalized stage indeed represents a completely synapsed configuration of Z and W.

The equalized ZW chromosome pair is transcriptionally silent in pachytene oocytes
To analyse the transcriptional activity of the Z and W chromosomes during the different stages of meiotic prophase, we immunostained oocytes for RNA polymerase II (RNA pol II) and SYCP3. During leptotene and zygotene, we found positive staining for RNA pol II throughout the nucleus, but from early pachytene onwards, there is a depletion of RNA pol II surrounding the ZW pair (Figure 2a). The absence of RNA pol II was most prominent during the
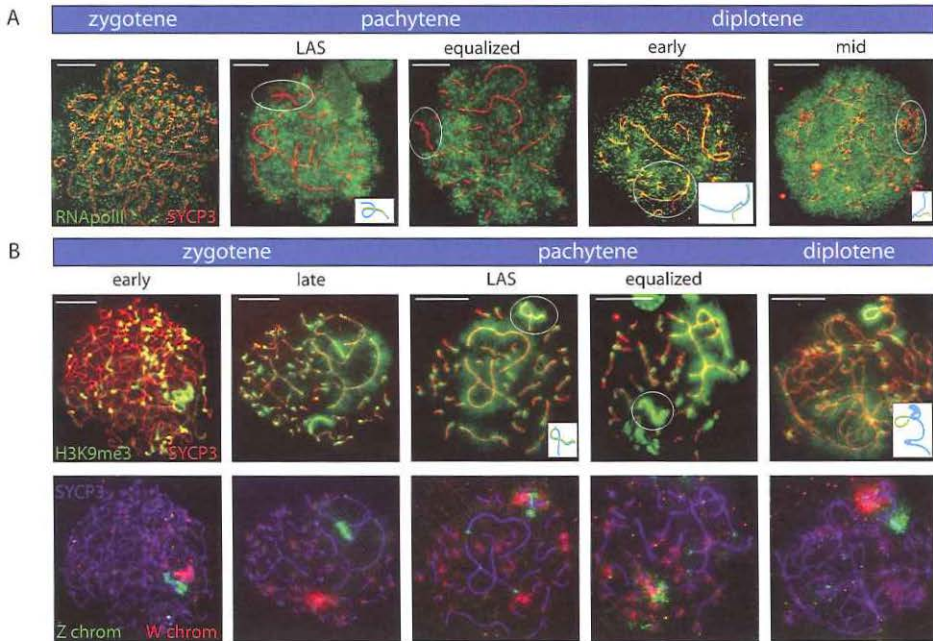
Figure 2. Lack of RNA polymerase II and enrichment for H3K9me3 mark the ZW pair. (a) Oocyte spread nuclei immunostained for RNA polymerase II (green) and SYCP3 (red). The RNA pol II signal is evenly spread in the zygotene nucleus. In pachytene nuclei (LAS and equalized configuration of the ZW pair) and in diplotene, RNA pol II signal is reduced around the ZW pair. Bar represents 10 μm. (b) Oocyte spread nuclei immunostained for H3K9me3 (green) and SYCP3 (red) (upper panel), and DNA FISH with painting probes for the heterochromatic part of the Z (green) and W (red) chromosomes (lower panel). W and the heterochromatic part of Z are enriched for H3K9me3 already in early zygotene. The highest H3K9me3 signal is seen on the fully synapsed ZW pair in pachytene. In diplotene, as Z and W have desynapsed, H3K9me3 remains highly positive on W and is lost from Z, with the exception of the constitutive heterochromatic part of the Z that is recognized by the painting probe which is still positive for H3K9me3, although with much lower intensity than W. Bar represents 10 μm.

equalized stage. As pachytene progresses into diplotene, the exclusion of RNA pol II around the ZW pair persists, and a reduction of RNA pol II surrounding the SC was also observed for other macrobivalents (Figure 2a). In mid diplotene, the overall signal of RNA pol II increased, but the level in the area around ZW remained relatively low. These data indicate that the Z and W chromosomes are subjected to meiotic silencing. In late diplotene, RNA pol II staining is no longer reduced on Z and W (not shown).

To obtain further evidence for transcriptional silencing of Z and W during chicken oogenesis, we analysed the localization of the known heterochromatin

marker H3K9me3 [27], in combination with a FISH specific for the W chromosome and the heterochromatic part of the Z chromosome. In oogonia, and in leptotene and zygotene oocytes, we observed several regions enriched for H3K9me3, but the region with the highest signal always colocalized with the FISH signal for W (Figure 2b). The Z painting probe colocalized with a region of Z that was also enriched for H3K9me3, but to a lesser extent compared to the enrichment of H3K9me3 on the W chromosome. During the equalized stage, the chromatin surrounding the ZW pair could easily be recognized as the region that displayed the strongest H3K9me3 staining in the nucleus (Figure 2b). As the ZW pair desynapses, H3K9me3 is lost from the Z chromosome, with the exception of the heterochromatic region that is recognised by the painting probe (Figure 2b). These findings indicate that the W chromosome is already inactive before entry into meiotic prophase, while the inactivation of the whole Z seems to be a transient process from early pachytene until diplotene. Based on our observations and earlier reports, we estimate that the duration from pachytene till early diplotene takes approximately 3-4 days [28].

γH2AX appears in two separate waves during meiotic prophase
Next, we analysed the behaviour of histone H2AX phosphorylated at serine 139, (γH2AX), a well-known marker of DNA double strand breaks (DSBs) [17, 29]. This is also the earliest histone modification that appears on the silenced XY body in mouse (reviewed in [3]. In chicken oocytes, γH2AX was found to be present throughout the nucleus with areas showing more intense staining in leptotene and zygotene (Figure 3a). These areas most likely correspond to sites of meiotic DSBs, similar to what has been observed for mouse oocytes and spermatocytes [17]. At the end of zygotene, remaining γH2AX foci localize to sites associated with synaptonemal complexes (SCs). Persistent γH2AX foci were observed along the unsynapsed arm of the Z chromosome (Figure 3bc), as confirmed by subsequent FISH with specific probes against the heterochromatic part of Z and the whole W chromosome. During mid pachytene, when the ZW pair is fully synapsed, γH2AX foci along the length of the SCs have disappeared, but all telomeres showed a bright focus (Figure 3d). During mid-late pachytene, when the Z and W start to desynapse, a second wave of γH2AX starts to accumulate in a distal to proximal fashion on all the desynapting regions of Z (Figure 3ef). In diplotene, γH2AX covers the whole Z chromosome, with the exception of the heterochromatic part, which looses γH2AX during the late separate stage (compare diplotene in Figure 3e with Figure 3f). In addition, all other chromosomes maintain γH2AX at the telomeres. Approximately two days after entering diplotene, as seen in part of the diplotene oocytes isolated from 7-day-old chickens, γH2AX is lost from the Z chromosome (Figure 3a).
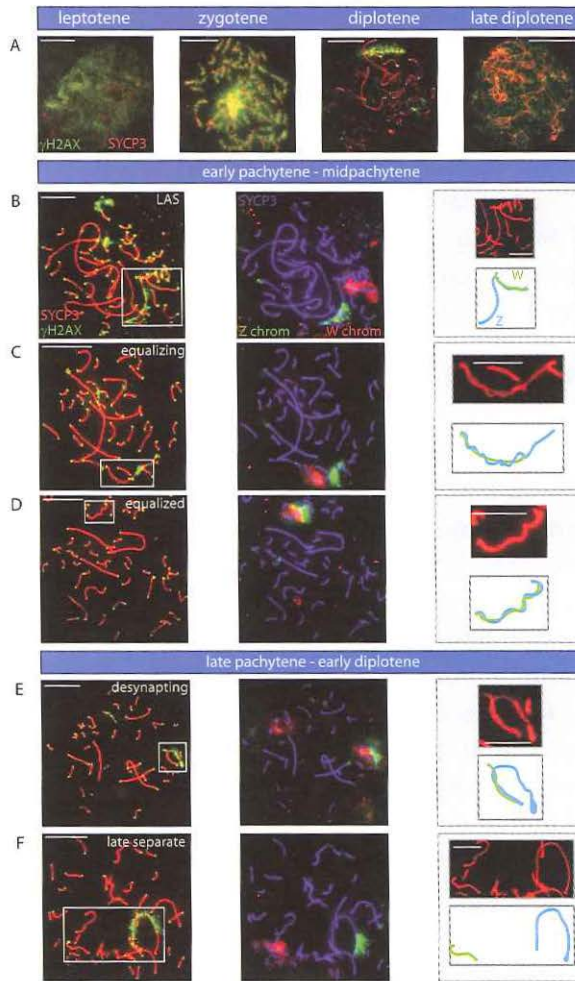
Figure 3. Two separate waves of γH2AX on Z during meiotic prophase in chicken oocytes. (a – f)(a) Oocyte spread nuclei immunostained for γH2AX (green) and SYCP3 (red) (b – f) Oocyte spread nuclei immunostained for γH2AX (green) and SYCP3 (red) (left panels), DNA FISH with painting probes for the heterochromatic part of the Z (green) and W (red) chromosomes (middle panels) and schematic drawings of the synaptic configurations of Z (blue) and W (green) (right panels). At leptotene, γH2AX starts to appear, and in zygotene it is present throughout the nucleus (a). In pachytene, γH2AX marks all telomeres and is present as big foci on several chromosomes (b). γH2AX also coats the unsynapsed part of Z during early pachytene, but disappears from Z as synapsis between Z and W progresses (bc). At the equalized stage, around midpachytene, only the telomeres are γH2AX positive (d). Upon unwinding or desynapsis of the Z and W, a second wave of γH2AX starts to coat the desynapsed part of Z (e). The heterochromatic part of Z has lost γH2AX from late pachytene onwards (f). In diplotene, only the telomeres and the desynapsed Z chromosome are highly enriched for γH2AX (a). At later stages of diplotene, γH2AX disappears also from the telomeres and Z (a). Bar represents 10 μm.

Together with the RNA polymerase II and H3K9me3 staining patterns, these data show that the second wave of γH2AX accumulation starts after silencing of the ZW pair has been established. Moreover, the second wave of γH2AX labelling appears to be restricted to the Z chromosome. These findings contrast with observations during mouse meiosis, where γH2AX accumulation is essential for, and occurs concomitant with, silencing of the sex chromosomes [30]. To obtain more insight in the trigger for γH2AX accumulation on the Z chromosome during late pachytene in chicken oocytes, we analysed the immunolocalization of the DSB-repair protein RAD51.

DNA double strand break repair associated proteins transiently disappear from the ZW pair

We found RAD51 foci on the synapsed autosomes and the unsynapsed axis of the Z chromosome during early pachytene. However, we never observed RAD51 foci on the W chromosome during pachytene (Figure 4a-f). During progression of pachytene, RAD51 foci gradually disappeared from the autosomes. As synapsis between Z and W progresses, RAD51 foci start to disappear from the synapsed part, but remain present on the part of Z that is still unsynapsed (Figure 4b-d). During the equalized stage, only a diffuse RAD51 signal persists at the distal tip of Z (Figure 4e). When the Z and W start to desynapse, we noticed a reappearance of RAD51 foci along the desynapsing Z chromosomal axis (Figure 4f). When Z and W were almost completely separated ('late separate' subtype), RAD51 foci covered the complete Z chromosome (Figure 4g), whereas the W chromosome remained devoid of these foci. Upon entering diplotene, all SC-associated RAD51 foci gradually disappear (Figure 4a). The observed temporal disappearance of RAD51 foci (and γH2AX) during progression of synapsis between Z and W in pachytene could indicate that the repair proteins are transiently lost, while the breaks are not repaired. However, the lack of detectable RAD51 foci could also be due to the tight winding and twisting of Z around W, which may render the RAD51 proteins inaccessible to the antibody. Still, the absence of γH2AX from the synapsed ZW indicates that the DSBs may also be temporarily undetectable for the machinery that couples processing of these breaks to γH2AX formation. Final repair of these breaks may therefore be suppressed until Z and W desynapse.

H2A ubiquitylation marks the ZW pair from early pachytene until diplotene

Next, we investigated the localization of several known other mammalian and marsupial XY body markers in chicken oocyte nuclei. First, we evaluated H2Ak119ub1, a histone modification which is generally associated with gene silencing, in combination with FISH for Z and W. It marks the inactive X
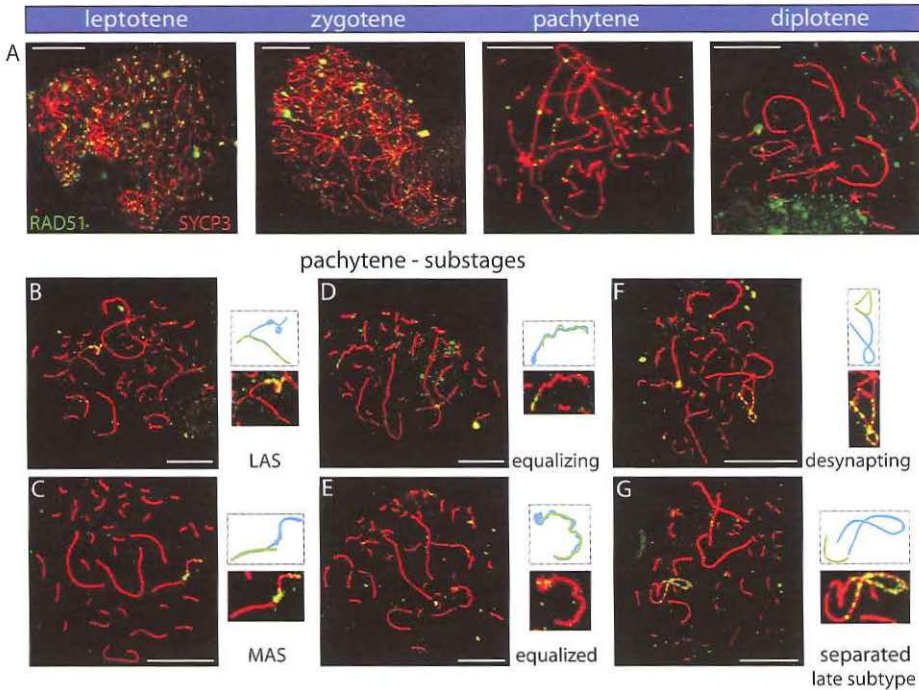
Figure 4. Reappearance of RAD51 foci on the desynapsing Z chromosome. (a – g) Oocyte spread nuclei immunostained for RAD51 (green) and SYCP3 (red). At leptotene and zygotene, RAD51 foci are dispersed throughout the nucleus (a). At early pachytene, some RAD51 foci are present on almost all synaptonemal complexes, most prominently on the unsynapsed part of the Z chromosome (ab). With progression of pachytene, RAD51 foci disappear from the autosomes, but remain present on the unsynapsed segment of the Z chromosome (cd). As synapsis between Z and W proceeds (MAS to equalized), RAD51 foci disappear along the synapsed region of Z and W (cde). When Z starts to unwrap itself, RAD51 foci reappear on the desynapsed part of Z (fg) and remain present until diplotene (a). Enlargements and the schematic drawings (Z in blue, W in green) of the synaptic configurations of the ZW pair are shown. Bar represents 10 μm.

chromosome in female somatic cells [13, 31, 32], and the mammalian XY body from mid-pachytene to early diplotene [33]. In chicken zygotene oocytes, this histone modification marks the W chromosome (Figure 5b) and from late zygotene onwards also accumulates on centromeric chromatin. In early pachytene, H2Ak119ub1 starts to spread from the centromeres on a few microbivalents. It also begins to accumulate on the already synapsed part of the ZW pair, and part of the distal unsynapsed arm of the Z chromosome (Figure 5c). Around mid-pachytene, when the ZW pair is fully synapsed, the H2Ak119ub1 signal increases and intensifies specifically on the ZW pair (Figure 5d). When the Z and W start to desynapse, H2Ak119ub1 remains present on the desynapting Z chromosomal
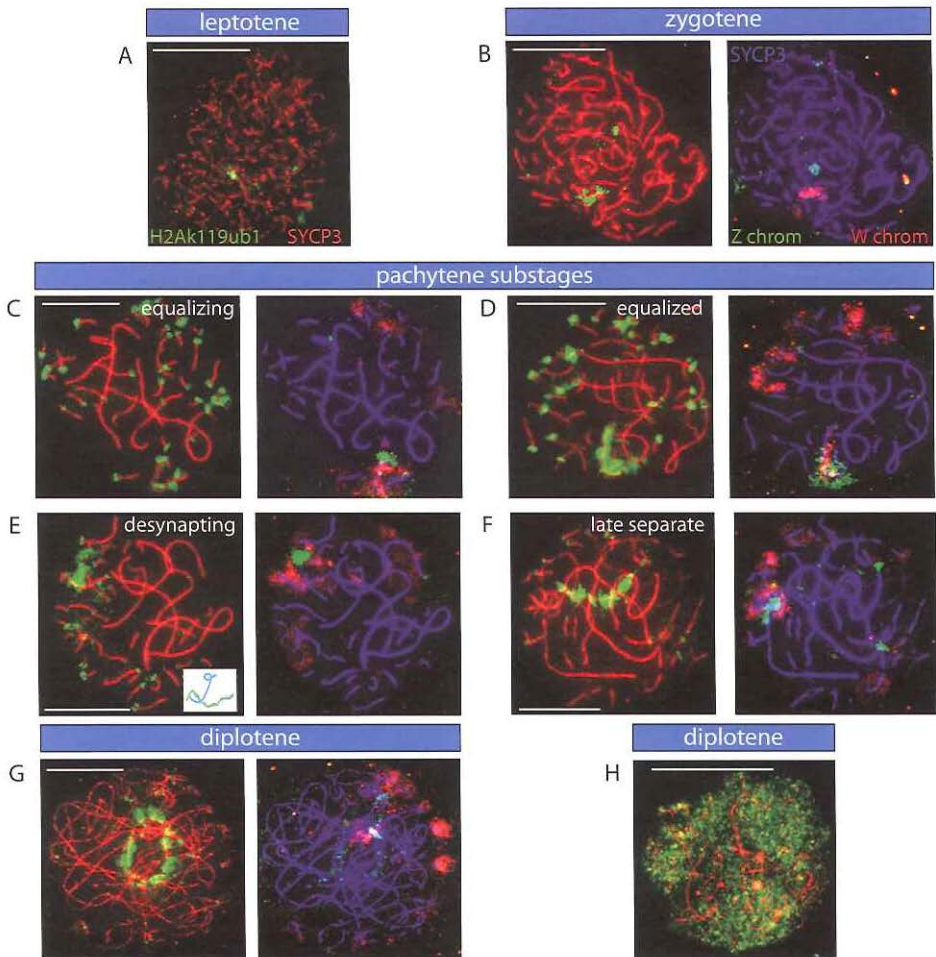
Figure 5. Analysis of H2Ak119ub1 on the ZW pair during meiotic prophase. (a – h) (a) + (h) Immunostaining for H2Ak119ub1 (green) and SYCP3 (red) on spread oocyte nuclei. (b – g) Immunostaining for H2Ak119ub1 (green) and SYCP3 (red) on spread oocyte nuclei (left) and DNA FISH with painting probes for the heterochromatic part of the Z (green) and W (red) chromosomes (right). In leptotene, some H2Ak119ub1 areas are visible (a). H2Ak119ub1 already marks the W chromosome during early zygotene (b) and accumulates at all centromeres at late zygotene (not shown). In pachytene, H2Ak119ub1 still marks the centromeres, and H2Ak119ub1 starts to coat the Z and W chromosomes, covering both parts of the synapsed regions as well as the heterochromatic part of the unsynapsed Z (c). The ZW pair is completely covered by H2Ak119ub1 at its equalized stage (d). When the Z and W start to desynapse, H2Ak119ub1 only persists on the Z chromosome (e) (inset shows schematic drawing of Z (blue) and W (green) pair). At late pachytene, H2Ak119ub1 remains present on the Z, but is lost from its heterochromatic part (f). In diplotene oocytes from 7-day-old chickens (g), H2Ak119ub1 briefly persists on Z, but eventually disappears and is distributed throughout the nucleus (h). Bar represents 10 μm.

axis, but is eventually lost from the W (Figure 5e). At the late separate stage and during early diplotene, H2Ak119ub1 covers the Z chromosome (Figure 5fg), with exception of the heterochromatic part recognized by the FISH probe. A few days after entering diplotene, H2AK119ub1 is lost from the Z chromosome, and appears in an evenly distributed manner throughout the whole nucleus (Figure 5h).

Trimethylation of lysine 27 of histone H3 is a prominent marker of the W chromosome during meiotic prophase

H3K27me3, an early marker of X chromosome inactivation in the female mouse embryo [34], is reduced on the XY body in mammals [35] and marsupials [36]. In chicken leptotene oocyte nuclei, this modification is virtually absent, whereupon the signal in zygotene nuclei increases on W and some microbivalents (Figure 6a). During pachytene, H3K27me3 is enriched on three microbivalents, but this modification most prominently marks a subregion of the W chromosome (Figure 6a). This enrichment of H3K27me3 on the W chromosome was found to remain prominent only on the W chromosome, even in late diplotene (Figure 6a).

Acetylation of H4K16 on the ZW pair is reduced from mid pachytene until diplotene

Acetylation of H4K16 is associated with active transcription, and in nuclei of female chicken somatic cells, a subregion of the Z chromosome is specifically enriched for this histone modification [37]. We performed double-immunostainings of oocytes for H4K16ac and SYCP3, followed by a FISH for Z and W. During zygotene, H4K16ac stained the nucleus more prominent then during leptotene and pachytene, which could indicate a transient global upregulation of transcription (not shown). Similar to what was observed for RNA polymerase II, reduced H4K16ac staining is observed on the completely synapsed ZW pair (Figure 6b). As pachytene progresses, H4K16ac is also reduced around long autosomal SCs. The low level of H4K16ac on ZW appears to persist until mid diplotene. We also performed double-stainings for γH2AX and H4K16ac and observed that when γH2AX accumulates on the desynapting Z, H4K16ac is reduced, and this persists up to diplotene (Figure 6c). Concomitantly, H4K16ac signal increases on the rest of the genome. Together, these observations show that the Z and W chromosome lose H4K16ac around the midpachytene stage, indicating transcriptional silencing, in accordance with our other observations.

mRNAs of Z and W genes show transient downregulation in oocytes during early postnatal ovary development

If the Z and W chromosome are silenced during pachytene and early diplotene, mRNAs for Z and W-encoded genes should be decreased in these cells, compared
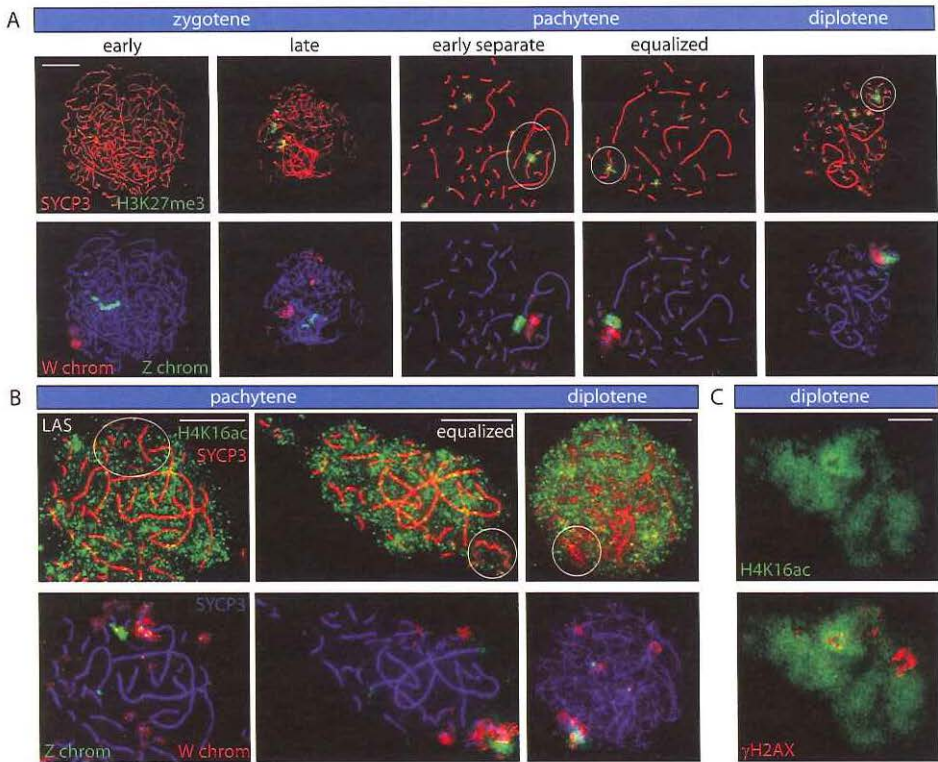
Figure 6. Analysis of histone modifications on Z and / or W during meiotic prophase. Immunostaining of oocyte spread nuclei preparations for H3K27me3 (green) and SYCP3 (red) (upper panel) and DNA FISH with painting probes for the heterochromatic part of the Z (green) and W (red) chromosomes (lower panel). With progression of zygotene, part of the W chromosome becomes positive for H3K27me3. During pachytene, H3K27me3 is present on several microbivalents and coats a specific part of the W chromosome. This pattern persists up into diplotene. Bar represents 10 μm. (b) Oocyte spread nuclei preparations immunostained for H4K16ac (green) and SYCP3 (red). From around midpachytene onwards, H4K16ac is reduced around the ZW pair. In pachytene, also other chromosomes appear to have reduced levels of H4K16ac. Bar represents 10 μm. (c) Oocyte spread nuclei preparations immunostained for H4K16ac (green) and γH2AX (red). In diplotene, γH2AX and H4K16ac signals are mostly mutually exclusive. Bar represents 10 μm.

to earlier and/or later stages of oocyte development. To analyse this, we performed real-time RT-PCR experiments using total RNA isolated from purified oocyte fractions and total ovaries isolated on 3 different time points (embryonic day 20, post hatching day 4 and day 7). Real time RT-PCR was performed for 10 Z-encoded genes, 4 W-encoded genes (Figure 7a) and 2 autosomal meiosis-specific genes, namely the synaptonemal complex component *SYCP3* and meiotic-DNA

double strand break-inducing enzyme *SPO11*. The expression profiles of *SYCP3* and *SPO11* followed the expected pattern (Figure 7b, Figure 8). The Z genes, *HINT1*, *TXN*, *NIPBL* and *SMAD2* all show a relative decrease in expression in oocytes of post hatching day 4, followed by an increase in expression at day 7 (Figure 7b); Expression of the Z gene *SLCA1A3* is measured in oocytes for the first time at day 7. The W gene *HINTW* also shows a decrease on post hatching day 4, and subsequently increased expression at day 7. The other analysed Z- en W-encoded genes showed no expression in oocytes at any timepoint, indicating that they are inactive during meiotic prophase. Based upon earlier descriptions of ovary development [5, 10, 11, 37] and our own observations, most oocytes are still in zygotene during embryonic day 20, whereas the vast majority of the oocytes is in late pachytene on post hatching day 4, and in late diplotene on day 7. The observed decrease in mRNA levels of Z- and W-encoded genes supports our immunocytochemical findings and confirms that Z and W are transiently silenced during oocyte development.
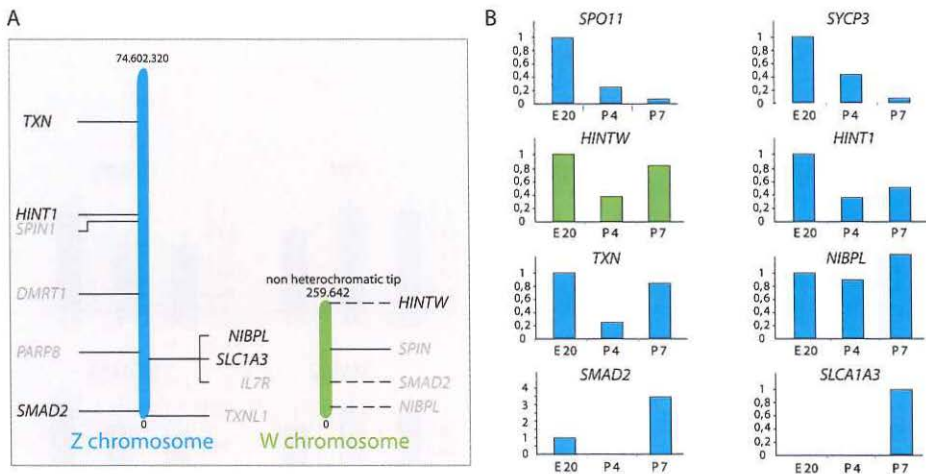
Figure 7. Gene expression profile in oocytes in different stages of meiotic prophase. (a) Schematic drawing of the location of the analyzed genes on the Z and W chromosomes. The genes in gray did not show expression in oocytes at any of the analysed timepoints. The intermittent lines from the W chromosome indicate that the exact location of the genes is unknown [41]. (b) Gene expression graphs as analyzed by real time RT PCR for two autosomal meiosis-specific genes; *SPO11* and *SYCP3*, for 1 W chromosome gene (*HINTW*) and 5 Z chromosomal genes (*HINT1*, *TNX*, *NIPBL*, *SMAD2*, and *SLCA1A3*). Data were collected at 3 different time-points: embryonic day 20 (E20), 4 (P4) and 7 days post-hatching (P7), and expression in oocytes was estimated as described in Materials and Methods. Finally, expression at E20 was set at 1, except for *SLCA1A3*, which was expressed in oocytes only on day 7 post hatching.

The ZZ chromosome pair behaves similar to the autosomal chromosome pairs during male meiotic prophase

To establish that the ZW pair in oocytes behaves different from the ZZ pair in spermatocytes, we also performed immunocytochemical analyses on chicken spermatocytes isolated from adult testes. Similar to what we observed in oocytes, , γH2AX was present throughout the nucleus with areas showing more intense staining in leptotene and zygotene spermatocytes (Figure 9a). At the end of zygotene, remaining γH2AX foci localize to sites associated with synaptonemal complexes, also resembling the pattern observed in chicken oocytes. However, during pachytene, all chromosomes were fully synapsed and γH2AX was present only on telomeres, and this pattern persisted up to late diplotene (Figure 9a).

Next, we analyzed the presence of H3K9me3 in combination with a FISH specific for the heterochromatic regions of the Z chromosomes (Figure 9b). Several regions in leptotene and zygotene spermatocytes were enriched for H3K9me3, but they never colocalized with the FISH signal(s) of Z (Figure 9b). In pachytene, the heterochromatic region of Z showed some enrichment for H3K9me3, and this signal decreased again during diplotene (Figure 9b).

H3K27me3 was present on a few microchromosome throughout meiotic prophase, but not on Z (not shown).
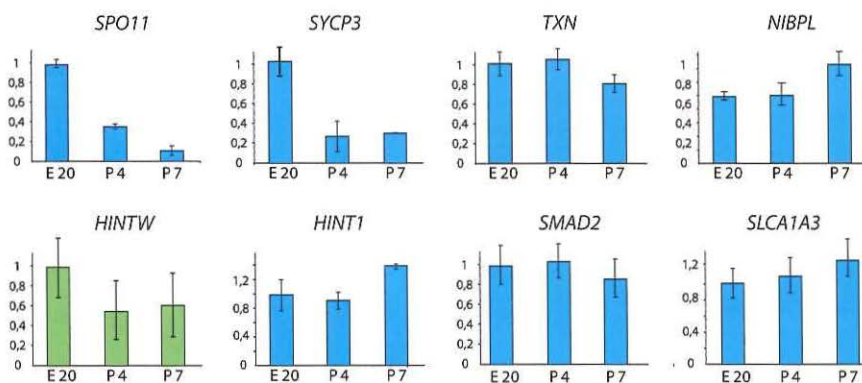
Figure 8. Gene expression profile in ovaries in different stages of meiotic prophase. Gene expression graphs with SEM as analyzed by real time RT PCR using total ovary RNA for two autosomal meiosis specific genes; *SPO11* and *SYCP3*, for 1 W chromosome gene (*HINTW*) and 5 Z chromosomal genes (*HINT1, TNX, NIBPL, SMAD2,* and *SLCA1A3*). Data were normalized to actin at 3 different time-points: embryonic day 20 (E20), 4 (P4) and 7 days post-hatching (P7). Expression at E20 was set at 1.
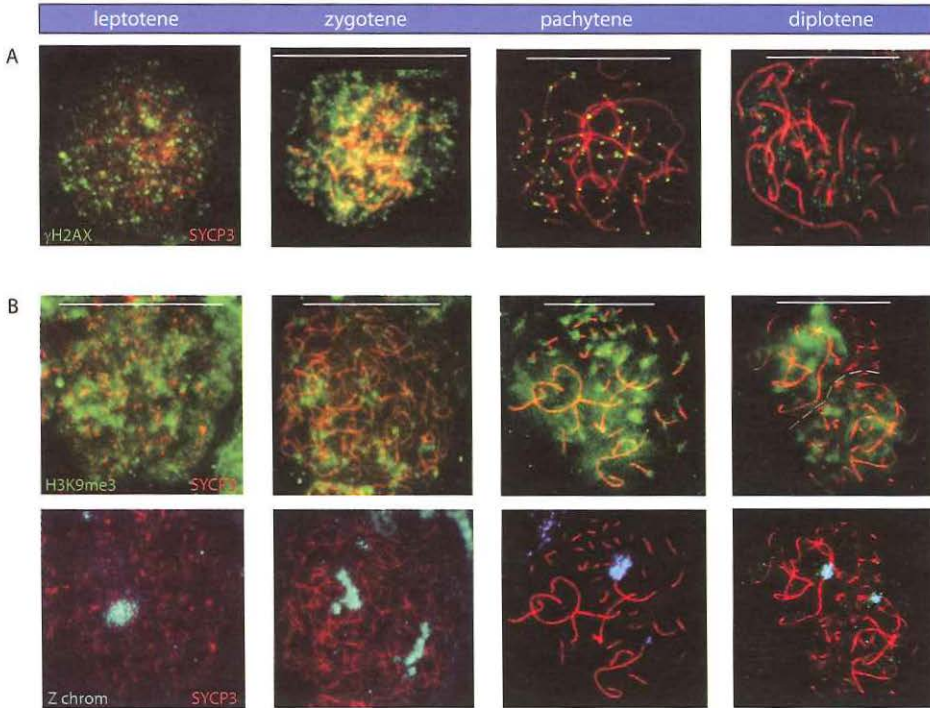
Figure 9. Analysis of histone modifications during meiotic prophase of male chicken spermatocytes. (a) Spermatocyte spread nuclei immunostained for γH2AX (green) and SYCP3 (red). At leptotene γH2AX starts to appear and in zygotene it is present throughout the nucleus. In pachytene, γH2AX marks all telomeres, then it gradually disappears from telomeres in diplotene. Bar represents 10 μ. (b) Spermatocyte spread nuclei immunostained for H3K9me3 (green) and SYCP3 (red) (upper panel) and DNA FISH with painting probes for the heterochromatic part of the Z (light blue) and SYCP3 (red) (lower panel). In leptotene and zygotene, H3K9m3 is present throughout the nucleus with several regions of higher signal intensity, and the Z chromosomal regions show the same H3K9me3 signal as the majority of the nucleus. In mid pachytene, some microchromosomes and the heterochromatic part of Z have a slightly higher signal. In diplotene (2 nuclei are shown), H3K9me3 signal is found in a patchy pattern on some macrochromosomes and minichromosomes, and it is lost from the heterochromatic part of Z.

DISCUSSION

Meiotic inactivation of the synapsed ZW pair in chicken oocytes

Meiotic sex chromosome inactivation (MSCI) in male mammals is thought to be triggered by the presence of unsynapsed axes of the X and Y chromosome (reviewed in [3]. Recently, it was discovered that in marsupial spermatocytes the unsynapsed X and Y chromosomes are also inactivated in a manner similar to

what has been observed in mouse [36, 38]. Herein, we show inactivation of sex chromosomes during meiosis in the female *Gallus gallus domesticus*, a species with female heterogamety and a ZW sex chromosome system that evolved independent of XY. Female oocytes undergo a much longer developmental process between the initiation of meiotic prophase and ovulation, compared to the time course that is involved during development of spermatocytes to mature sperm. Therefore, it was suggested that meiotic inactivation of Z (and W) would not occur because it would be incompatible with the lengthy oocyte developmental process [12]. Herein, we have shown to the contrary that MSCI does occur, but is transient in chicken oocytes; in diplotene, the Z chromosome loses its specific "silencing" histone modifications (γH2AX and H2Ak119ub1). In addition, the mRNA of several Z-encoded genes is higher in oocytes isolated at posthatching day 7 compared to day 4. Reactivation of Z may allow Z-encoded genes to assist in further oocyte development. *HINTW* is a W chromosomal multicopy gene [39, 40] that also shows increased expression in day 7 oocytes. It localizes to the non-heterochromatic tip of W [41]. Based on its female specificity and expression in differentiating ovaries of early embryos, *HINTW* has been implicated in female sex differentiation, but its exact function is unclear [41]. The W chromosome is gene poor, and to date, only a few genes have been described to be W-specific (ICBN Mapviewer, [40, 42]. In addition, the actual size of the pseudo-autosomal region between Z and W has not been established. Based on the persistent presence of H3K9me3 on W in diplotene oocytes, it could be suggested that the W remains inactive throughout oocyte development, perhaps with the exception of the non-heterochromatic tip that contains the multicopy gene *HINTW*. This nicely parallels the recent findings by Mueller et al [43], who describe that X- linked multicopy genes that are subjected to MSCI are specifically re-expressed in postmeiotic spermatids in mouse, whereas the vast majority of single-copy genes remain inactive.

In early mouse pachytene spermatocytes, the X and Y chromosome show more extensive synapsis compared to the later pachytene stages, when desynapsis progresses until the X and Y show only an end to end association in some diplotene nuclei [44]. This resembles the dynamics of ZW association during chicken oogenesis, with exception of the fact that complete synapsis is never achieved in mouse, and always in chicken. Our data now show that despite the complete (heterologous) synapsis, sex chromosome inactivation is not prevented, and repair of meiotic DSBs is delayed (see below).

*No compensation for Z inactivation by retrogene expression from autosomal sites*
During mammalian MSCI, silencing of some essential X chromosomal genes is compensated by expression from retroposed copies on autosomal chromosomes. The expression of these copies is male-specific and initiates concomitant with

MSCI [45]. However, in the chicken genome, very few functional retroposed genes appear to be present [46]. For the 15 identified functional retroposed genes in chicken, no bias for genes from specific chromosomes was detected. Due to the transient nature of the ZW inactivation, Z-encoded mRNAs and proteins may be in large enough supply to allow maintenance of function of essential Z-linked genes during this short period. Genomic analyses and analyses of EST databases have revealed that ovary-specific genes are underrepresented on the chicken Z chromosome. In addition, microarray analyses of gene expression in different chicken tissues have shown that the average expression of Z-linked genes versus autosomal genes is lowest in the embryonic ovary [47]. This phenomenon could have different causes. In principle, so-called sexually antagonistic genes (genes beneficial to one sex, detrimental to the other), are expected to accumulate on the sex chromosomes. In species with male heterogamety, recessive male beneficial genes would be expected to accumulate on the X. In accordance with this notion, the mouse and human X chromosome are enriched for spermatogenesis-genes expressed prior to meiotic prophase. Due to MSCI and PMSC (post meiotic sex chromatin), the X is depleted for spermatogenesis-genes expressed during later stages, with the exception of some single-copy and multicopy genes, that show postmeiotic reactivation [43, 48, 49]. Since retroposition of Z genes to autosomes does not seem to occur in chicken [46], it might be suggested that the evolutionary force to drive oocyte-specific genes off the Z during evolution is relatively weak, perhaps due to the transient nature of MSCI in chicken. Still, the relative lack of ovary-specific genes, and the generally low level of Z-encoded gene expression in embryonic ovary may indicate that MSCI in chicken reduces the likelihood of oocyte-specific genes that function during meiotic prophase to evolve on the Z. However, the properties of the chicken Z chromosome can also be explained by a dominant model of sexual antagonistic genes, whereby dominant genes encoding proteins that are beneficial to males would be downregulated in females to minimize antagonism [50]. More detailed analyses of ovary-specific genes is required, including separate analyses of genes expressed in somatic and germ line cells of the ovary, to determine whether MSCI in chicken affects gene content on Z.
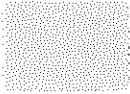
Z inactivation precedes the second wave of γH2AX formation

The inactivation of Z and W during chicken oogenesis shows marked differences and similarities to MSCI in marsupial and mouse (summarized in Figure 10). The timing of Z inactivation (early pachytene) is similar to what has been observed in the other vertebrates. However, the W chromosome appears to enter the zygotene stage already in a (partially) inactivated configuration. γH2AX appears as foci on the Z chromosome during zygotene, and these foci appear to persist
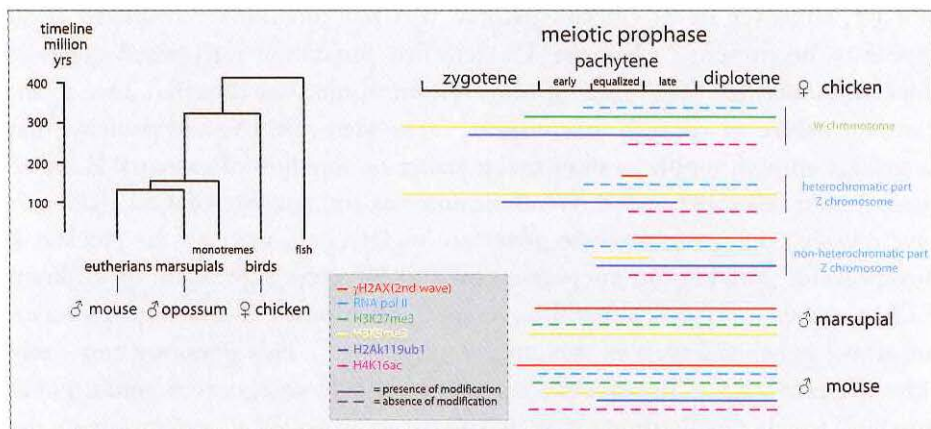
Figure 10. Phylogenetic tree, and overview of marsupial and mammalian XY body and chicken ZW pair markers. Timescale for the avian (chicken) and mammalian (mouse, marsupials) vertebrates [58-62]. Overview of the localization of different markers on XY (mouse [3, 35, 63] and marsupial [36]) and ZW (chicken) during meiotic prophase.

longer on the Z compared to the autosomes, similar to what has been observed on the X chromosome during zygotene in mouse [17, 51]. However, during the stage of complete synapsis, γH2AX is absent from the ZW pair. Then, a second wave of γH2AX formation appears around late pachytene on the desynapsed Z, and only after silencing has been established. This is in marked contrast with the second wave of γH2AX formation in mouse, which occurs on both X and Y, and immediately as spermatocyes enter pachytene. The appearance of γH2AX on the desynapting Z chromosome is accompanied by a reappearance of RAD51. At this stage autosomal axes also begin to desynapse, but do not show a reappearance of RAD51 foci, and do not accumulate γH2AX. Thus, repair of meiotic DSBs on the Z chromosome may be inhibited to avoid recombination with the synapsed W chromosome, and postponed until desynapsis. This provides a clear link between the second wave of γH2AX formation and DSB-repair rather than with an unsynapsed axis per se. At this late pachytene/early diplotene stage, H2Ak119ub1 formation is also specifically enhanced on the Z chromosome. This modification is known to be associated with inactive chromatin, but has also been implicated in DSB-repair [52]. Perhaps silencing is induced at sites containing persistent DSBs to prevent aberrant (truncated) transcription through the damaged region in somatic as well as germ-line cells. In somatic cells, DSB repair can also be associated with the recruitment of silencing factors [53]. We reported a link between the presence of persistent DSBs and the frequency of meiotic silencing of unsynaped chromatin (MSUC) in mouse [23].

Inactivation of Z during pachytene is most likely accomplished by spreading of heterochromatin from W

With the identification of meiotic sex chromosome inactivation in a species that shows female heterogamety as well as complete nonhomologous synapsis during pachytene, we provide indications for the presence of an evolutionary force that drives meiotic sex chromosome inactivation independent of the final achievement of synapsis. The absence of homologous chromatin (as a template
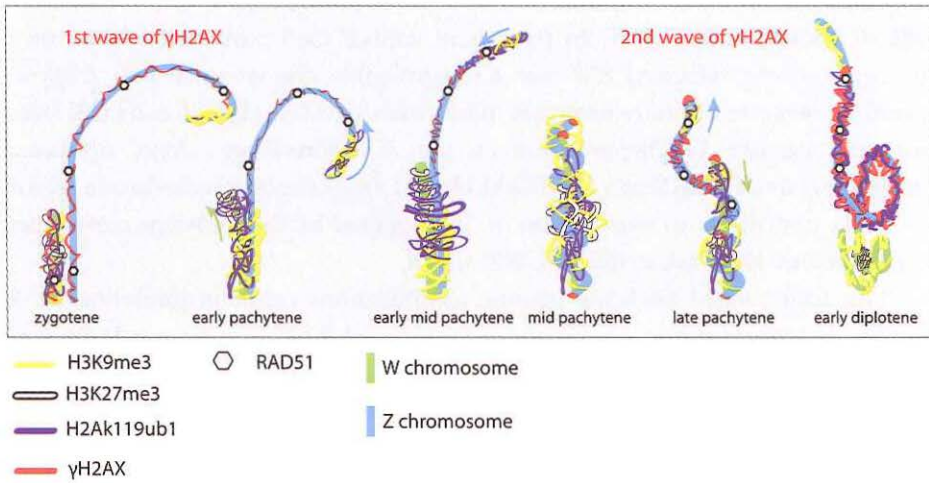
Figure 11. Model for transient sex chromosome inactivation in the chicken oocyte. In zygotene, parts of the W chromosome are already inactive and marked by increased H3K9me3 and H2Ak119ub1. In addition, part of the W chromosome acquires H3K27me3. The Z chromosome is enriched for H3K9me3 and H2Ak119ub1 only in the region that is known to be heterochromatic. During this phase, RAD51 foci are present and the first wave of γH2AX accumulation has occurred clearly on Z and most likely also to a lesser extent on W. Upon entrance of pachytene, Z starts to condense and folds back on itself, while the W chromosome lengthens slightly, and RNA pol II and the first wave of γH2AX gradually disappear. With progression of pachytene, the ZW pair reaches full synapsis, H3K9me3 and H2AK119ub1 most likely spread *in trans* from W on Z while H4K16ac is lost. Also, silencing may spread on Z *in cis*, triggered by the presence of persistent meiotic DSBs. As the ZW starts to desynapse, RAD51 reappears on the desynapting Z, and a second wave of γH2AX on the whole Z chromosome follows. H2AK119ub1 also spreads on the desynapting Z. During this period, meiotic DNA double-strand breaks on Z are most likely repaired, and transcriptional silencing of Z is maintained by γH2AX and H2AK119ub1. Shortly after desynapting, both γH2AX and H2AK119ub1 are lost from the heterochromatic part of Z, while H3K9me3 is lost from Z, except from its heterochromatic region. In diplotene, both sex chromosomes lengthen, and γH2AX and H2AK119ub1 are gradually lost, allowing re-activation of the Z chromosome, while W remains positive for H3K27me3 and H3K9me3, most likely indicating a maintenance of its inactive state.

for the repair of DNA double-strand breaks) could be instrumental in initiating this silencing, since synapsis is only achieved after silencing has been established. Based on the observations described herein, we propose the following model for the inactivation of the sex chromosome in the heterogametic female oocyte during meiotic prophase (Figure 11).

The W chromosome enters meiosis in an inactive configuration, which includes hypermethylation of H3K9 and ubiquitylation of H2AK119. H3K27me3 is also present on the W chromosome from zygotene onwards. H3K27me3 may recruit the polycomb protein complex PRC1, which could then help to enhance ubiquitylation of H2AK119, as has been observed during X inactivation in somatic cells of female mammals [32]. In pachytene, H3K27me3 remains enriched on a subregion of the synapsed ZW pair. Concomitantly, the synapsis with Z allows spreading *in trans* of heterochromatic marks such as H2Ak119ub1 and H3K9me3 from the inactive W chromosome on the Z chromosome. Also, additional spreading *in cis* of H3K9me3 and H2Ak119ub1 from the heterochromatic region of Z may contribute to inactivation of Z, triggered by the transient persistence of the meiotic DSB-associated γH2AX-signal.

The accumulated silencing histone modifications result in inhibition of Z and W gene transcription, as visualized by reduced RNA polymerase II staining around ZW, and reduced mRNA expression of selected Z and W genes. During the compact arrangement of the Z-chromosomal axis around the W axis, DSB-repair is inhibited, and γH2AX and possibly also RAD51 are lost from the DSB-repair sites. Subsequent desynapsis is accompanied by reappearance of RAD51, a second wave of γH2AX formation and enhanced H2Ak119ub1 formation on Z. The latter modification may maintain silencing (despite the absence of H3K9me3 on the desynapsed Z) until the breaks are repaired. The W chromosome remains inactive due to the high levels of H3K9me3 and H3K27me3.

Transcriptional inactivation of the ZW pair was first observed in oocytes when Z and W show the LAS to MAS configuration, at day 1 after hatching. Disappearance of γH2AX and H2Ak119ub1 from Z in diplotene was observed in oocytes isolated at the 7th day after hatching. This indicates that the period of Z inactivation lasts approximately 5.5 – 6 days.

Meiotic sex chromosome inactivation and dosage compensation.
A wide variety of mechanisms exist that compensate for unequal gene dosage in species with chromosomal sex determination. Female marsupials show inactivation of the paternal X chromosome in somatic cells, to equalize the expression level of X-encoded genes with that of males. The recent discovery of MSCI and maintenance of X inactivation in postmeiotic cells of male marsupials supports the hypothesis that inheritance of a "pre-inactivated" X chromosome could

contribute to the establishment of paternal X-inactivation in female embryos [36]. Our findings on transient ZW inactivation argue against the existence of such a mechanism in birds. This is in accordance with data from the literature that show that male birds do not show inactivation of one of the two Z chromosomes [47, 54, 55]. In fact, dosage compensation in birds appears to be far less complete than in mammals, and it is not yet known whether dosage compensation, if it occurs, is achieved via upregulation of Z-genes in females, or downregulation in males. It cannot be excluded however, that the transient inactivation of Z leads to epigenetic modifications that persist and may influence gene expression in male (ZZ) offspring.

Meiotic silencing in evolution

During male meiosis in mice, a general mechanism named meiotic silencing of unsynapsed chromatin (MSUC) silences all unsynapsed chromosomes [13, 15]. This mechanism could be evolutionary related to meiotic silencing by unpaired DNA (MSUD) which operates in *Neurospora crassa* [56]. However, MSUD is a posttranscriptional silencing mechanism that acts at the single gene level. It is not clear whether components of MSUD are conserved and used in MSUC, which acts at a much larger scale and is far less efficient. Meiotic silencing of sex chromosomes (MSCI) in mammals is most likely a specialized form of MSUC. The driving force behind MSUD and MSUC may be that it is beneficial for the species to silence foreign DNA. Although sex chromosomes are no foreign DNA, recognition as such may also be beneficial, because it will help to suppress recombination between the heterologous regions of the sex chromosomes. This suppression of sex chromosome recombination could also be a strong driving force to silence single or heterologous sex chromosomes. Spreading of heterochromatin from W on Z in female chicken oocytes to achieve meiotic sex chromosome inactivation may be mechanism that evolved independent from MSCI in mammals. In XO male grasshoppers, the single X chromosome also enters spermatogenesis in an already inactive configuration [57]. In chicken, the heterologous synapsis between Z and W may be required to escape from a synapsis checkpoint, and not to avoid meiotic silencing.

MATERIALS AND METHODS

Isolation of oocytes from chicken ovaries

Oocytes were isolated from embryonic day 20 (E20), day 4 (P4) and 7 (P7) post hatching female chickens. Ovaries were collected and incubated for 30 min in 20 ml Dulbecco's-PBS medium containing 1 mg/ml collagenase, 1 mg/ml trypsin and 0,5 mg/ml hyaluronidase (Worthington, Lakewood, USA) in a

shaking waterbath with an amplitude of 1 cm at 37°C (60 cpm/min). A single cell suspension was obtained by repeated pipetting of the suspension. After filtration through 70 mm gauze, the cell suspension was centrifuged for 3 min at 800 g. 1ml of cell suspension in DMEMF12 was loaded on 9 ml of a 3-step gradient of 1.012, 1.037 and 1.071 mg/ml Nycodenz (Nycoprep™ Universal, Axis Shield PoC AS, Oslo, Norway) and centrifuged at 2400 g for 20 min at 20°C. The oocyte fraction was collected from the 1,037 mg/ml layer, centrifuged for 3 min at 800g and the pellet was snap-frozen in liquid nitrogen and stored at −80°C. Based on SYCP3 staining of spread nuclei preparations from the purified fractions we calculated a purity of 70%, 40% and 50% oocytes in fractions isolated from E20, P4 and P7, respectively.

Spreads and immunocytochemistry
Chicken (*Gallus gallus domesticus*) eggs were incubated at 37 °C and a humidity of 70-80% until hatching. Chickens were killed by CO_2 intoxication. The functional left ovary or left and right testes were dissected and placed in Hanks' solution. Spread nuclei preparations of chicken oocytes and spermatocytes were prepared using a modification of the drying-down technique described by Peters et al. [24]. Briefly, ovaries and testes were minced in pieces with forceps and cells were suspended in 500 ml of 100 mM sucrose, containing EDTA-free complete protease inhibitor cocktail (Roche Diagnostics, Almere, The Netherlands). Oocytes and spermatocytes were dispersed on a glass slide dipped in 1% paraformaldehyde fixative with 0.1% Triton X100. After two hours in a humid chamber at room temperature, the slides were allowed to dry for 30 minutes at room temperature, followed by a single wash in 0.08% Photoflo (Kodak, Paris, France) and air-dried. The slides were stored at −80 °C.

For immunocytochemistry, frozen slides were defrosted at room temperature and washed with PBS. The slides were blocked with PBS containing 0.5% w/v BSA and 0.5% w/v milk powder, and double stained with different combinations of the following antibodies: rabbit polyclonal anti-SYCP3 (1:1000), rabbit polyclonal anti-SYCP1 (1:200) (gifts from C. Heyting, Wageningen), mouse polyclonal anti-γH2AX (1:1000) (Upstate, Walthum, MA, USA), rabbit polyclonal anti-γH2AX (1:1000) (Upstate), mouse monoclonal IgM anti-H2AK119ub1 (1:1000) (Upstate), mouse monoclonal anti-RNA polymerase II, (8WG16) directed against the RNA polymerase II CTD repeat YSPTSPS (1:600) (Abcam, Cambridge, United Kingdom), mouse monoclonal anti-H4K16ac (1:200) (Upstate), mouse monoclonal anti-H3K27me3 (1:100) (Abcam), rabbit polyclonal anti-H3K9me3 (1:500) (Upstate), and rabbit anti-human RAD51 (1:500) [25]. For mouse monoclonal primary antibodies, the secondary antibodies were fluorescein isothiocyanate (FITC)-labeled goat anti-mouse IgG antibodies

(1:128) (Sigma, St Louis, USA) for anti-RNA polymerase II, anti-γH2AX, and anti-H3K27me3, FITC-labeled goat anti-mouse IgM (1:128) (Sigma) for anti-H2AK119ub1 and tetramethylrhodamine isothiocyanate (TRITC)-labeled goat anti-mouse IgG antibodies (1:128) (Sigma) for anti-γH2AX. The secondary antibody for polyclonal rabbit primary antibodies was tetramethylrhodamine isothiocyanate (TRITC)-labeled goat anti-rabbit IgG antibodies (1:200) (Sigma) for anti-SYCP3 and fluorescein isothiocyanate (FITC)-labeled goat anti-rabbit IgG antibodies (1:80) (Sigma) for anti-Rad51, anti-SYCP1, and anti-γH2AX. Primary antibodies were diluted in 10% w/v BSA in PBS and incubated overnight in a humid chamber. Thereafter, slides were washed in PBS, blocked in 10% v/v normal goat serum (Sigma) in blocking buffer (5% milk powder (w/v) in PBS, centrifuged at 13.200 rpm for 10 min), and incubated with secondary antibodies in 10% v/v normal goat serum in blocking buffer at room temperature for 2 hours. Next, the slides were washed in PBS and embedded in Vectashield containing DAPI (4',6'-diamindino-2-phenylindole) (Vector Laboratories, Burlingame CA, USA). Double stainings of SYCP1 with SYCP3, of RAD51 with SYCP3, and of SYCP3 with H3K9me3 (all rabbit polyclonal antibodies) were obtained by sequential immunostainings with the single antibodies. Images of SYCP1, RAD51 and SYCP3 stainings respectively, were obtained prior to immunostaining with anti-SYCP3 or H3K9me3 of the same nuclei.
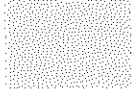
Real-time RT-PCR

For real-time RT-PCR, RNA was prepared from embryonic female liver, embryonic day (E20), post hatching day 4 (P4) and day 7 (P7) ovaries and oocyte fractions by Trizol (Invitrogen, Breda, The Netherlands), DNase-treated and reverse transcribed using random hexamer primers and Superscript II reverse transcriptase (Invitrogen). PCR was carried out with the Fast SYBR green PCR mastermix (Applied Biosystems, Foster City, USA) in the DNA engine Opticon 2 real-time PCR detection system (Bio-Rad, Hercules, USA). For *ACTB, SYCP3, SPO11*, W genes: *NIBPL, SPIN, SMAD2, HINTW* and Z genes: *NIBPL, SPIN1, SMAD2, HINT1, DMRT1, TXNL1, TXN, ILR7, PARP8, SLCA1A3* we used the following conditions: 3 minutes 95°C, then 10 seconds 95°C, 30 seconds 58°C, 30 seconds 72°C for 40 cycles, experiments were performed in triplicate. For data analysis, the average threshold cycle (*Ct*) was converted to absolute amount of transcript (E^{-Ct}) (E=efficiency determined via a standard curve) and presented as $E^{\text{Ct Actin} - Ct \text{ gene of interest}}$. To estimate the expression of Z and W encoded genes in oocytes and to correct for differences in purity, we used the following formulas:

$$Ex_{po} = P \cdot Ex_{oc} + (1-P)Ex_{r}$$
$$Ex_{ov} = F \cdot Ex_{oc} + (1-F)Ex_{r}$$

Ex$_{po}$ = measured expression level in the purified oocyte sample, P= purity of the oocytes (0.7, 0.4 and 0.5 for E20, P4 and P7 respectively), Ex$_{oc}$ = expression level in oocytes, Ex$_r$ = expression level in the rest of the ovarian cells, Ex$_{ov}$ = measured expression level in the ovary, F = oocyte fraction in the ovary. We equalized the Ex$_r$ for *SYCP3* to the expression measured in embryonic liver. This allowed us to calculate the value of F in the different ovary samples. The median value of F was found to be 0.06, and this number was used to calculate Ex$_{oc}$. All –RT reactions were negative. Forward and reverse primers (5' to 3'): See Table 1.

Fluorescent in situ hybridisation (FISH)

First, immunocytochemistry was performed as described above, and images were made of selected nuclei. Probe mixture of digoxigenin-labelled GGA (Gallus GAllus) W and biotin-labelled GGA Z chromosome (heterochromatic part) painting probes (Farmachrom, Kent, UK), salmon sperm DNA and hybridisation buffer were mixed and denatured at 75 °C. Slides were treated with 0.005 % pepsine solution for 5 minutes at 37 °C, washed in 2xSSC at room

Table 1. Primers used for real-time RT-PCR analyses

Gene	Forward primer (5' – 3')	Reverse primer (5'-3')
autosomal		
SYCP3	AGAGCATGGAAGAGCTAGAG	AGAGCATGGAAGAGCTAGAG
SPO11	AGAAGTGACTGCCCTGCAAC	TGGCTACCAAACAGGAGCTT
W chromosomal genes		
NIBPL	AAAGTCCTGCGGGATATGTG	ATGGGACTGGACACTGAAGC
SPIN	TCAGCCACGAAGAAACATTG	TGTCCCTTCCATTGTGTTA
SMAD2	ACCAGAAACACCACCTCCAG	TTGGTTCAACTGCTGGTCAC
HINTW	CTTCTTGGGCGTTTGATGAT	GCGGTAGTCTGAAGGGACTG
Z chromosomal genes		
NIBPL	CAGGGTCTCATCCATCCTGT	TCGCATAGAAGGCTCTGGAT
SPIN1	GTCTCTGCCAGCATGATGAA	CACTCCCTTCTTTCCATCCA
SMAD2	GTCTCTGCCAGCATGATGAA	GTCCCCAAATTTCAGAGCAA
HINT1	GTTTTGAATGAAGGGCCTGA	CATGCAGCATCTCTTGTGGT
DMRT1	AGTGGCAGATGAAAGGGATG	CGAGGCCAGTATCTGTGTGA
TXNL1	GCCCTGGAACTAACACCAGA	TCCCCGTGATTAGACTGGAC
TXN	AGAACGGAAAGAAGGTGCAG	AGACATGCTCCGATGTCTCC
IL7R	TTCCTACAGCAGCCTGACCT	TGGTACACACAGCCAGGGTA
PARP8	CACCAGCCAAAGAATCCAAT	CAGGATGGAATGCCAGTTTT
SLC1A3	TCTTGGATCGTCTCCGTACC	CTTCAGCTCATGCCGTGATA

temperature for 5 minutes, rinsed in distilled water and then air dried. Next, they were dehydrated, air-dried and incubated for 1 hour at 75 °C. Again, slides were dehydrated and air dried. Subsequently, RNAse mix (100µg/ml in PBS) was placed on each slide, and slides were incubated in a humid chamber at 37 °C. After 1 hour, slides were again air dried. Slides were denatured in 70% formamide with 30% 2xSSC for 160 seconds at 75 °C. This was followed by quenching the slides in ice-cold 70% ethanol, then at room temperature in 80% ethanol and finally in 100% ethanol. Probe mixture was placed on the slide, covered with a coverslip and sealed. The slides were placed in a pre-heated humid chamber and incubated overnight at 37 °C. After incubation, the slides with coverslip were placed in 2xSSC at room temperature for 5 minutes. After removal of the coverslip, slides were then rinsed twice in 50% formamide and 50% 2xSSC for 10 minutes at 37 °C, followed by rinsing in 2xSSC with 0.1% Triton X-100 at room temperature for 1 minute. Subsequently, the slides where placed 1 hour in 4xSSC with 0,05% Triton X-100. Finally, the slides were placed in 4xSCC, 0.05% Triton X-100, 3% BSA for 25 minutes at room temperature. Slides were incubated with anti-biotin-labelled Cy3 and anti-digoxigenin Avidine Alexa Fluor 488-labelled antibodies (Invitrogen) in a dark humid chamber for 35 minutes at room temperature. After removing the coverslips, slides were washed 3 times for 3 minutes in 4xSSC with 0.05% Triton X-100, rinsed in distilled water and air dried before a droplet of Vectashield mounting medium with DAPI (4',6'-diamidino-2-phenylindole) (Vector Laboratories) was placed on the slide and covered with a coverslip.
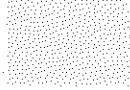
Fluorescence microscopy, digital image preparation and analysis
Analysis of the chicken oocyte nuclei was performed using a Carl Zeiss Axioplan 2 imaging microscope (Jena, Germany) with a plan-neofluar objective 100x/1.3 oil immersion. Images were taken with a Coolsnap-pro digital camera (Photometrics, Waterloo, Canada). The acquired digital images were processed with Photoshop software (Adobe Systems).

ACKNOWLEDGEMENTS

REFERENCES

1. Zickler D. From early homologue recognition to synaptonemal complex formation. *Chromosoma.* Jun 2006;115(3):158-174.
2. Monesi V. Differential rate of ribonucleic acid synthesis in the autosomes and sex chromosomes during male meiosis in the mouse. *Chromosoma.* 1965;17(1):11-21.
3. Helena Mangs A, Morris BJ. The Human Pseudoautosomal Region (PAR): Origin, Function and Future. *Curr Genomics.* Apr 2007;8(2):129-136.
4. Solovei I, Gaginskaya E, Hutchison N, Macgregor H. Avian sex chromosomes in the lampbrush form: the ZW lampbrush bivalents from six species of bird. *Chromosome Res.* Sep 1993;1(3):153-166.
5. Solari AJ. Equalization of Z and W axes in chicken and quail oocytes. *Cytogenet Cell Genet.* 1992;59(1):52-56.
6. Moses MJ, Poorman PA. Synaptosomal complex analysis of mouse chromosomal rearrangements. II. Synaptic adjustment in a tandem duplication. *Chromosoma.* 1981;81(4):519-535.
7. Moses MJ, Poorman PA, Roderick TH, Davisson MT. Synaptonemal complex analysis of mouse chromosomal rearrangements. IV. Synapsis and synaptic adjustment in two paracentric inversions. *Chromosoma.* 1982;84(4):457-474.
8. Stefos K, Arrighi FE. Heterochromatic nature of W chromosome in birds. *Exp Cell Res.* Sep 1971;68(1):228-231.
9. Becak ML, Becak W. Behaviour of the ZW sex bivalent in the snake Bothrops jararaca. *Chromosoma.* 1981;83(2):289-293.
10. Ohno S. [Sex chromosomes and microchromosomes of Gallus domesticus.]. *Chromosoma.* 1961;11:484-498.
11. Solari AJ. Ultrastructure of the synaptic autosomes and the ZW bivalent in chicken oocytes. *Chromosoma.* 1977;64:155-165.
12. Jablonka E, Lamb MJ. Meiotic pairing constraints and the activity of sex chromosomes. *J Theor Biol.* Jul 8 1988;133(1):23-36.
13. Baarends WM, Wassenaar E, van der Laan R, et al. Silencing of unpaired chromatin and histone H2A ubiquitination in mammalian meiosis. *Mol Cell Biol.* Feb 2005;25(3):1041-1053.
14. Schimenti J. Synapsis or silence. *Nat Genet.* 2005;37(1):11-13.
15. Ellis PJ, Clemente EJ, Ball P, et al. Deletions on mouse Yq lead to upregulation of multiple X- and Y-linked transcripts in spermatids. *Hum Mol Genet.* Sep 15 2005;14(18):2705-2715.
16. Kelly WG, Aramayo R. Meiotic silencing and the epigenetics of sex. *Chromosome Res.* 2007;15(5):633-651.
17. Mahadevaiah SK, Turner JM, Baudat F, et al. Recombinational DNA double-strand breaks in mice precede synapsis. *Nat Genet.* Mar 2001;27(3):271-276.
18. Padmore R, Cao L, Kleckner N. Temporal comparison of recombination and synaptonemal complex formation during meiosis in S. cerevisiae. *Cell.* Sep 20 1991;66(6):1239-1256.
19. Keeney S, Giroux CN, Kleckner N. Meiosis-specific DNA double-strand breaks are catalyzed by Spo11, a member of a widely conserved protein family. *Cell.* Feb 7 1997;88(3):375-384.
20. Moens PB, Chen DJ, Shen Z, et al. Rad51 immunocytology in rat and mouse spermatocytes and oocytes. *Chromosoma.* Sep 1997;106(4):207-215.
21. Ashley T, Plug AW, Xu J, et al. Dynamic changes in Rad51 distribution on chromatin during meiosis in male and female vertebrates. *Chromosoma.* Oct 1995;104(1):19-28.

22. Moens PB, Kolas NK, Tarsounas M, Marcon E, Cohen PE, Spyropoulos B. The time course and chromosomal localization of recombination-related proteins at meiosis in the mouse are compatible with models that can resolve the early DNA-DNA interactions without reciprocal recombination. *J Cell Sci.* Apr 15 2002;115(Pt 8):1611-1622.

23. Schoenmakers S, Wassenaar E, van Cappellen WA, et al. Increased frequency of asynapsis and associated meiotic silencing of heterologous chromatin in the presence of irradiation-induced extra DNA double strand breaks. *Dev Biol.* May 1 2008;317(1):270-281.

24. Peters AH, Plug AW, van Vugt MJ, de Boer P. A drying-down technique for the spreading of mammalian meiocytes from the male and female germline. *Chromosome Res.* Feb 1997;5(1):66-68.

25. Essers J, Hendriks RW, Wesoly J, et al. Analysis of mouse Rad54 expression and its implications for homologous recombination. *DNA Repair (Amst).* Oct 1 2002;1(10):779-793.

26. Bolcun-Filas E, Costa Y, Speed R, et al. SYCE2 is required for synaptonemal complex assembly, double strand break repair, and homologous recombination. *J Cell Biol.* Mar 12 2007;176(6):741-747.

27. Nakayama J, Rice JC, Strahl BD, Allis CD, Grewal SI. Role of histone H3 lysine 9 methylation in epigenetic control of heterochromatin assembly. *Science.* Apr 6 2001;292(5514):110-113.

28. Hughes GC. The Population of Germ Cells in the Developing Female Chick. *J Embryol Exp Morphol.* Sep 1963;11:513-536.

29. Rogakou EP, Pilch DR, Orr AH, Ivanova VS, Bonner WM. DNA double-stranded breaks induce histone H2AX phosphorylation on serine 139. *J Biol Chem.* Mar 6 1998;273(10):5858-5868.

30. Fernandez-Capetillo O, Mahadevaiah SK, Celeste A, et al. H2AX is required for chromatin remodeling and inactivation of sex chromosomes in male mouse meiosis. *Dev Cell.* Apr 2003;4(4):497-508.

31. de Napoles M, Mermoud JE, Wakao R, et al. Polycomb group proteins Ring1A/B link ubiquitylation of histone H2A to heritable gene silencing and X inactivation. *Dev Cell.* Nov 2004;7(5):663-676.

32. Fang J, Chen T, Chadwick B, Li E, Zhang Y. Ring1b-mediated H2A ubiquitination associates with inactive X chromosomes and is involved in initiation of X inactivation. *J Biol Chem.* Dec 17 2004;279(51):52812-52815.

33. Baarends WM, Hoogerbrugge JW, Roest HP, et al. Histone ubiquitination and chromatin remodeling in mouse spermatogenesis. *Dev Biol.* Mar 15 1999;207(2):322-333.

34. Plath K, Fang J, Mlynarczyk-Evans SK, et al. Role of histone H3 lysine 27 methylation in X inactivation. *Science.* Apr 4 2003;300(5616):131-135.

35. Namekawa SH, Park PJ, Zhang LF, et al. Postmeiotic sex chromatin in the male germline of mice. *Curr Biol.* Apr 4 2006;16(7):660-667.

36. Namekawa SH, VandeBerg JL, McCarrey JR, Lee JT. Sex chromosome silencing in the marsupial male germ line. *Proc Natl Acad Sci U S A.* Jun 5 2007;104(23):9730-9735.

37. Bisoni L, Batlle-Morera L, Bird AP, Suzuki M, McQueen HA. Female-specific hyperacetylation of histone H4 in the chicken Z chromosome. *Chromosome Res.* 2005;13(2):205-214.

38. Franco MJ, Sciurano RB, Solari AJ. Protein immunolocalization supports the presence of identical mechanisms of XY body formation in eutherians and marsupials. *Chromosome Res.* 2007;15(6):815-824.

39. Mizuno S, Kunita R, Nakabayashi O, et al. Z and W chromosomes of chickens: studies on their gene functions in sex determination and sex differentiation. *Cytogenet Genome Res.* 2002;99(1-4):236-244.

40. O'Neill M, Binder M, Smith C, et al. ASW: a gene with conserved avian W-linkage and female specific expression in chick embryonic gonad. *Dev Genes Evol.* May 2000;210(5):243-249.

41. Smith CA. Sex determination in birds: HINTs from the W sex chromosome? *Sex Dev.* 2007;1(5):279-285.

42. Hori T, Asakawa S, Itoh Y, Shimizu N, Mizuno S. Wpkci, encoding an altered form of PKCI, is conserved widely on the avian W chromosome and expressed in early female embryos: implication of its role in female sex determination. *Molecular biology of the cell.* Oct 2000;11(10):3645-3660.

43. Mueller JL, Mahadevaiah SK, Park PJ, Warburton PE, Page DC, Turner JM. The mouse X chromosome is enriched for multicopy testis genes showing postmeiotic expression. *Nat Genet.* Jun 2008;40(6):794-799.

44. Tres LL. Extensive pairing of the XY bivalent in mouse spermatocytes as visualized by whole-mount electron microscopy. *J Cell Sci.* Jun 1977;25:1-15.

45. Turner JM, Aprelikova O, Xu X, et al. BRCA1, histone H2AX phosphorylation, and male meiotic sex chromosome inactivation. *Curr Biol.* Dec 14 2004;14(23):2135-2142.

46. Sequence and comparative analysis of the chicken genome provide unique perspectives on vertebrate evolution. *Nature.* Dec 9 2004;432(7018):695-716.

47. Ellegren H, Hultin-Rosenberg L, Brunstrom B, Dencker L, Kultima K, Scholz B. Faced with inequality: chicken do not have a general dosage compensation of sex-linked genes. *BMC Biol.* 2007;5:40.

48. Khil PP, Oliver B, Camerini-Otero RD. X for intersection: retrotransposition both on and off the X chromosome is more frequent. *Trends Genet.* Jan 2005;21(1):3-7.

49. Khil PP, Smirnova NA, Romanienko PJ, Camerini-Otero RD. The mouse X chromosome is enriched for sex-biased genes not subject to selection by meiotic sex chromosome inactivation. *Nat Genet.* Jun 2004;36(6):642-646.

50. Mank JE, Ellegren H. Sex-Linkage of Sexually Antagonistic Genes Is Predicted by Female, but Not Male, Effects in Birds. *Evolution.* Jan 14 2009.

51. Hamer G, Roepers-Gajadien HL, van Duyn-Goedhart A, et al. DNA double-strand breaks and gamma-H2AX signaling in the testis. *Biol Reprod.* Feb 2003;68(2):628-634.

52. Mailand N, Bekker-Jensen S, Faustrup H, et al. RNF8 ubiquitylates histones at DNA double-strand breaks and promotes assembly of repair proteins. *Cell.* Nov 30 2007;131(5):887-900.

53. O'Hagan HM, Mohammad HP, Baylin SB. Double strand breaks can initiate gene silencing and SIRT1-dependent onset of DNA methylation in an exogenous promoter CpG island. *PLoS Genet.* Aug 2008;4(8):e1000155.

54. Itoh Y, Melamed E, Yang X, et al. Dosage compensation is less effective in birds than in mammals. *J Biol.* 2007;6(1):2.

55. Melamed E, Arnold AP. Regional differences in dosage compensation on the chicken Z chromosome. *Genome Biol.* 2007;8(9):R202.

56. Bowring FJ, Yeadon PJ, Stainer RG, Catcheside DE. Chromosome pairing and meiotic recombination in Neurospora crassa spo11 mutants. *Curr Genet.* Aug 2006;50(2):115-123.

57. Cabrero J, Teruel M, Carmona FD, Jimenez R, Camacho JP. Histone H3 lysine 9 acetylation pattern suggests that X and B chromosomes are silenced during entire male meiosis in a grasshopper. *Cytogenet Genome Res.* 2007;119(1-2):135-142.

58. Bininda-Emonds OR, Cardillo M, Jones KE, et al. The delayed rise of present-day mammals. *Nature*. Mar 29 2007;446(7135):507-512.
59. Kumar S, Hedges SB. A molecular timescale for vertebrate evolution. *Nature*. Apr 30 1998;392(6679):917-920.
60. Pereira SL, Baker AJ. A mitogenomic timescale for birds detects variable phylogenetic rates of molecular evolution and refutes the standard molecular clock. *Mol Biol Evol*. Sep 2006;23(9):1731-1740.
61. Veyrunes F, Waters PD, Miethke P, et al. Bird-like sex chromosomes of platypus imply recent origin of mammal sex chromosomes. *Genome Res*. Jun 2008;18(6):965-973.
62. Woodburne MO, Rich TH, Springer MS. The evolution of tribospheny and the antiquity of mammalian clades. *Mol Phylogenet Evol*. Aug 2003;28(2):360-385.
63. van der Heijden GW, Derijck AA, Posfai E, et al. Chromosome-wide nucleosome replacement and H3.3 incorporation during mammalian meiotic sex chromosome inactivation. *Nat Genet*. Feb 2007;39(2):251-258.
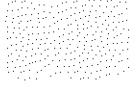
CHAPTER 5

MEIOTIC SILENCING AND FRAGMENTATION OF
THE MALE GERMLINE RESTRICTED CHROMOSOME
IN ZEBRA FINCH

ABSTRACT

During male meiotic prophase in mammals, X and Y are in a largely unsynapsed configuration, which is thought to trigger meiotic sex chromosome inactivation (MSCI). In avian species, females are ZW, and males ZZ. Although Z and W in chicken oocytes show complete, largely heterologous synapsis., they too undergo MSCI, albeit only transiently. The W chromosome is already inactive in early meiotic prophase, and inactive chromatin marks may spread on to the Z upon synapsis. Mammalian MSCI is considered as a specialized form of the general meiotic silencing mechanism, named meiotic silencing of unsynapsed chromatin (MSUC). Herein, we studied the avian form of MSUC, by analysing the behaviour of the peculiar germline restricted chromosome (GRC) that is present as a single copy in zebra finch spermatocytes. In the female germline, this chromosome is present in two copies, which normally synapse and recombine. In contrast, during male meiosis, the single GRC is always eliminated. We found that the GRC in the male germline is silenced from early leptotene onwards, similar to the W chromosome in avian oocytes. The GRC remains largely unsynapsed throughout meiotic prophase I, although patches of SYCP1 staining indicate that part of the GRC may self-synapse. In addition, the GRC is largely devoid of meiotic double-strand breaks. We observed a lack of the inner centromere protein INCENP on the GRC and elimination of the GRC following metaphase I. Subsequently, the GRC forms a micronucleus in which the DNA is fragmented. We conclude that in contrast to MSUC in mammals, meiotic silencing of this single chromosome in the avian germline occurs prior to, and independent of DNA double strand breaks and chromosome pairing, hence we have named this phenomenon meiotic silencing prior to synapsis (MSPS).

INTRODUCTION

In vertebrate species, male and female meiotic prophase starts with the introduction of genome wide meiosis-specific DNA double strand breaks (DSBs) during (pre)leptotene. Meiotic DSBs are detected and repaired by the homologous recombination repair machinery, using the homologous chromosomal partner as template (reviewed in [1] and [2]). The DSB repair protein RAD51 and its meiosis-specific paralogue DMC1, rapidly form filaments on the 3' end single-strand DNA tails that result from processing of the meiotic DSBs, and these filaments can be identified as distinct RAD51 foci (reviewed in [3]).

The presence of RAD51 and DMC1 mark the initiation of meiotic recombination, which involves homologous chromosome alignment, pairing, synapsis and the formation of crossovers. All these steps are necessary to obtain correct DSB repair and subsequent proper segregation of the chromosomes during the meiotic divisions, with the haploid gametes as a final result. With progression of meiotic prophase (zygotene), the number of RAD51 foci gradually decreases to almost zero on the synapsed autosomal chromosomes at early pachytene [4]. During synapsis, the synaptonemal complex (SC) keeps the homologous chromosomes physically connected along their axes (reviewed [1]) and ultimate complete synapsis is essential for normal continuation of the meiotic prophase. Failure of homologous chromosomes to reach full synapsis leads to meiotic arrest and apoptosis (reviewed in [5]). The male mammalian X and Y chromosomes and the female avian Z and W sex chromosomes form a pair but are largely nonhomologous. Therefore, these sex chromosomes are confronted with a pairing problem during meiosis. The avian Z and W have solved this problem by wrapping the much longer Z chromosome around the short W chromosome during pachytene, resulting in a brief state of heterologous, but complete synapsis at mid pachytene [6,7]. Hereafter, during late pachytene, the Z and W start to desynapse again [6,7]. Although the mammalian XY pair shows extensive (heterologous) synapsis in early pachytene, this is followed by gradual desynapsis, and only the small homologous pseudoautosomal region remains synapsed in late pachytene, leaving the rest of the X and Y chromosomal arms unsynapsed [8]. In addition to the pairing problem, the nonhomologous sex chromosomes also face the presence of persistent unrepaired meiotic DSBs. These arise because the homologous template needed for recombination repair is lacking, and repair via the sister-chromatid is most likely repressed [9]. Consequently, RAD51 foci persist on the unsynapsed region of the mammalian X chromosome until late pachytene [10], and reappear on the desynapsing avian Z chromosome at mid - late pachytene [6].

During male mammalian meiotic prophase, the unsynapsed arms of the X and Y chromosomes are detected, and meiotic sex chromosome inactivation (MSCI) causes transcriptional silencing of the sex chromosomes, resulting in the formation of the heterochromatic XY body [11, 12]. Initiation and maintenance of MSCI in mammals is always associated with the combination of persistent DSBs and asynapsis. Recently, we found that, although the avian ZW pair synapses completely, it is still subjected to a transient form of MSCI [6].

MSCI is considered as a more efficient and specialized form of the general mechanism of meiotic silencing of unsynapsed chromatin (MSUC), which transcriptionally inactivates all unsynapsed (nonhomologous autosomal) chromatin. MSCI always silences the X and Y chromosomes, but MSUC in mammals can be circumvented through heterologous (self)synapsis, which probably conceals the nonhomologous regions (reviewed in [5]). When autosomal chromosomal regions without a homologous partner remain unsynapsed, these regions become silenced by MSUC and also show persistent RAD51 foci indicative of unrepaired DSBs [13, 14].

In birds, the mechanism of MSCI may be essentially different from that in mammals. Heterochromatinization by hypermethylation of H3K9 [6] implying the inactivation of W, precedes the introduction of DSBs and initiation of synapsis of homologous chromosomes, indicating a DNA repair and synapsis-independent recognition of the single W chromosome. Indeed, the ZW pair is silenced despite its complete heterologous, synapsis. We have proposed that the heterochromatin of W spreads onto Z during the intimate wrapping of Z around W during pachytene [6]. However, in chicken as well as mammalian meiotic cells, there appears to be a link between the presence of unrepaired DSBs and transcriptional silencing. In mammals, this is already apparent at the initiation of silencing, whereas in chicken oocytes, such a link is observed later, when Z and W desynapse during late pachytene. At this stage, RAD51 foci reappear on the unsynaped part of Z, together with accumulation of γH2AX and ubiquitylated H2A on these parts [6]. These histone modifications may help to maintain Z chromosome silencing until the DSBs have been repaired.

Since both Z and W are silenced in the female germline of birds by MSCI, we next asked how the mechanism of MSUC operates in avian species. To answer this question, we chose the zebra finch (*Taeniopygia guttata*) as a model system. This avian species carries a peculiar additional chromosome, which is only present in the germline, named germline restricted chromosome (GRC). The GRC is present as a single copy in the male germline, whereas two copies are detected in most oocytes [15, 16]. In the female germline, the two copies synapse and form a bivalent, which normally participates in pairing and meiotic recombination [15, 16].

In the male germline, the single GRC lacks a homolog and remains unsynapsed. In addition, it is heterochromatic, resembling the mammalian XY body, and Pigozzi and Solari [15, 16] reported that the GRC is eliminated from the nucleus around metaphase I. To investigate the general process of meiotic silencing in birds, we analysed the behaviour of the GRC in the male and female zebrafinch germline.

RESULTS

The GRC forms a heterochromatic body at the end of preleptotene that persists until early diplotene

Two previous reports described the formation of a DAPI dense body (DDB) during meiotic prophase in zebra finch spermatogenesis [15, 16]. We observed that the DDB or GRC body almost always localizes in the periphery of the nucleus and is, except in diplotene, easily identifiable as the intense DAPI field that clearly stands out from the rest of the chromosomes (Figure 1a).

To discriminate between the different substages of meiotic prophase, we immunostained for the presence of the lateral element of the synaptonemal complex, using antibodies targeting SYCP3. At preleptotene, SYPC3 foci start to appear in the nucleus. A DDB is visible in only part of the preleptotene nuclei (Figure 3a), indicating that preleptotene is a transitory stage during which the DDB is formed. At leptotene and zygotene, a DDB is visible in all nuclei and small SYCP3 fragments occasionally localized in the DDB, while thick and long SC axial elements are present on assembling chromosome pairs in the rest of the nucleus. In pachytene, the GRC chromosomal axis is coated by SYCP3, but the signal is not always continuous. The axial SYCP3 element of the GRC is relatively thin compared to the SYCP3 axes associated with the other chromosomes, due to the fact that only one axial element has been assembled.

Despite the absence of a pairing partner for the GRC, we sometimes observed patches of SYCP1 assembly on the GRC (Figure 1c), most likely representing small regions of self-synapsis.

γH2AX does not mark the GRC during meiotic prophase, but accumulates on the eliminated micronucleus

It is well-known that shortly after the formation of DSBs, histone H2AX is phosphorylated at serine 139, forming γH2AX [17, 18]. In addition, γH2AX marks the silenced sex chromosomes from late zygotene until diplotene in mouse (XY) and marsupial (XY) spermatocytes. In female (ZW) chicken oocytes, it marks the Z chromosome during desynapsis from the W, from late pachytene until diplotene [6]. In zebra finch spermatocytes, γH2AX was found to accumulate in leptotene
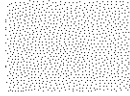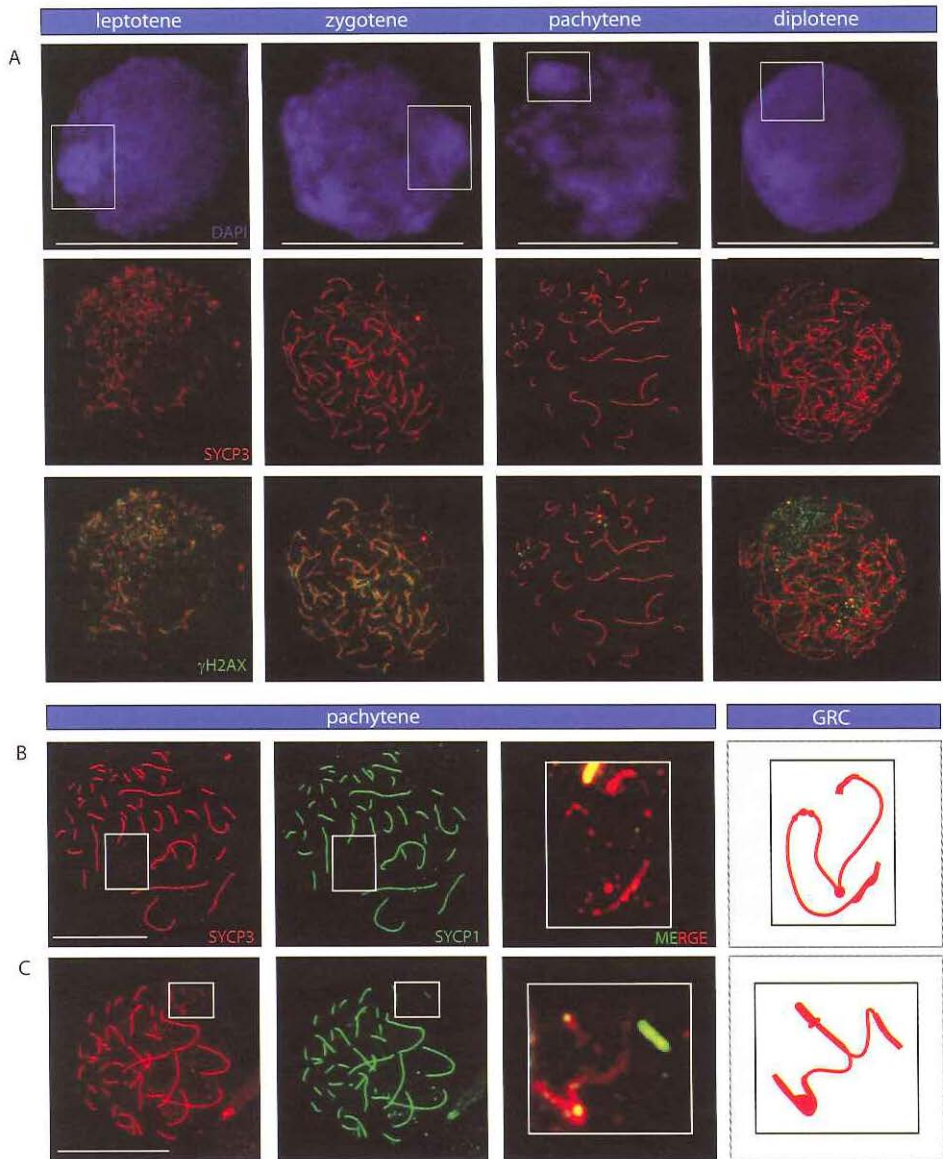
Figure 1. The GRC throughout meiosis in zebra finch spermatocytes. (a) Overview of the different stages of meiotic prophase I of zebra finch spermatocytes. The top panel shows the DAPI staining of the different nuclei, the lower panel shows the corresponding nuclei stained for SYCP3 (red), the bottom panel shows the same nuclei stained for both SYCP3 (red) and γH2AX (green). The position of the GRC is indicated by a box. Bar represents 10 μm. (b,c). Spermatocyte spread nuclei immunostained for SYCP3 (red) and SYCP1 (green). The GRC is boxed. Enlargement and the schematic drawing of GRC are shown. No (b) or a small fragment (c) of SYCP1 signal is present on the GRC. Bar represents 5 μm.

nuclei, mainly confined to the areas where SYCP3 had already assembled, most likely representing sites of meiosis specific induced DSBs. Also, in zygotene and pachytene, γH2AX mostly colocalizes with the SYCP3 filaments. In pachytene, only a few γH2AX foci and some larger γH2AX-positive areas remained. In diplotene, the γH2AX signal was found to increase and to disperse throughout the nucleus (Figure 1a).

In early meiotic prophase, the area of the GRC was found to be mostly devoid of γH2AX (Figure 1a). However, some weak γH2AX foci are present on the axial element in zygotene and pachytene, indicating the presence of some (unrepaired) DSBs. The much lower intensity and limited presence of γH2AX (foci) on the GRC as compared to the rest of the nucleus indicates that only very few meiotic DSBs are induced on the heterochromatic GRC. At metaphase, an intense γH2AX signal covers the whole nucleus, including the relatively DAPI dense GRC (Figure 2a).

When the nuclei progress from metaphase I through the first meiotic division and transform into secondary spermatocytes, the GRC appears to be eliminated from the nucleus, while its γH2AX signal increases strongly (Figure 2a).

The GRC and its participation in meiotic recombination during spermatogenesis
To analyse the processing of meiotic DSBs on the GRC and the rest of the chromosomes in more detail, we immunostained for the homologous recombination repair protein RAD51. In leptotene spermatocytes, many small foci are present throughout the nucleus. During zygotene, the total number of RAD51 foci drops, and the remaining foci are larger and more intensely stained. In late zygotene, a few bright foci remain present, mainly on the unsynapsed parts of chromosome pairs. We also identified several RAD51 foci on the GRC, although the number and intensity of the foci is much less, and the foci itself appear smaller compared to the RAD51 foci on the other chromosomes (Figure 2b).

A small fraction of the introduced meiotic DSBs are processed into crossovers. The DNA mismatch repair protein MLH1 marks the locations of these crossovers in spread meiotic nuclei of most species analysed to date. In mammals, MLH1 foci appear during midpachytene, and disappear before entering diplotene [19, 20]. In chicken oocytes MLH1 foci are already observed around mid to late zygotene [21].

In spermatocytes of the zebrafinch, many small MLH1 foci form aggregates around SYCP3 filaments of different chromosomes already at early zygotene. These aggregates appear to transform into bright MLH1 foci on the SCs around mid zygotene. Surprisingly, also the GRC shows a MLH1 focus in a minority of the nuclei (Figure 2c), which provides an additional indication for the formation of meiotic DSBs in the GRC of some nuclei during leptotene. The MLHI foci on
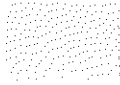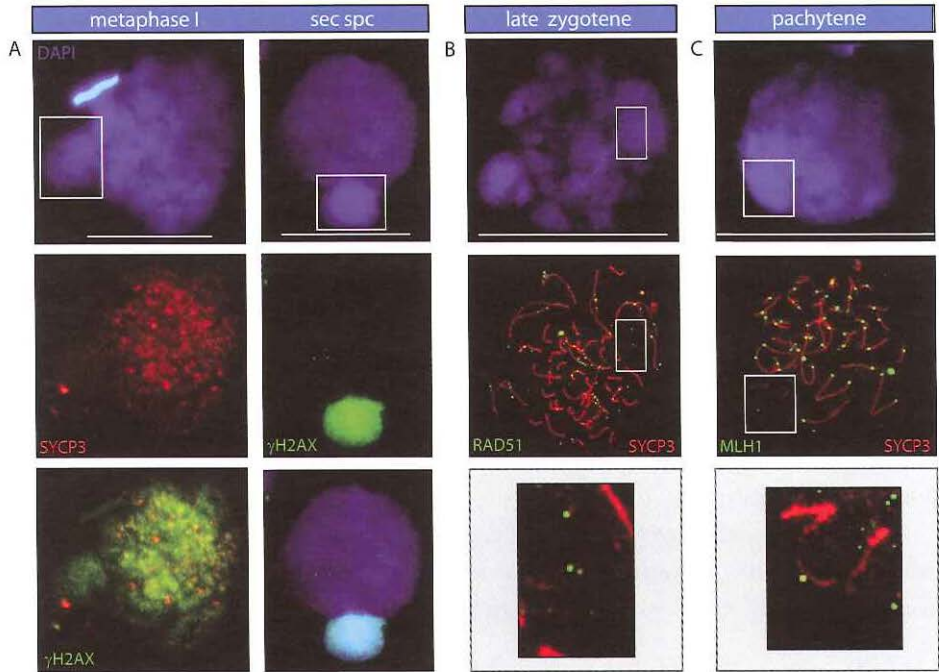
Figure 2. The GRC and meiotic recombination. (a) Spread nuclei immunostained for DAPI (blue), γH2AX (green) and SYCP3 (red). After metaphase I, the GRC becomes strongly positive for γH2AX. The GRC is boxed. Bar represents 5 μm. Sec spc, secondary spermatocyte. (b) Spermatocyte spread nucleus immunostained for SYCP3 (red), RAD51 (green) and DAPI (blue). The GRC is boxed. Most RAD51 foci localize on axial elements of the SC. The bottom image represents a magnification of the area of the boxed GRC. Few small RAD51 foci are visible on the GRC. Bar represents 10 μm. (c) Spermatocyte spread nucleus immunostained for SYCP3 (red), MLH1 (green) and DAPI (blue). The area of the GRC is boxed. The bottom image represents a magnification of the area of the boxed GRC, and shows the presence of a MLH1 focus on the GRC. Bar represents 10 μm.

the autosomes remain present until diplotene, followed by dispersion of MLH1 signal throughout the nucleus towards the end of diplotene (not shown).

The GRC is silenced early during male meiotic prophase

The appearance of the DAPI-dense GRC body during preleptotene indicates that it acquires a heterochromatic configuration upon entrance into meiotic prophase. To confirm this, we immunostained for a well-known marker of inactivation and heterochromatin, H3K9me3. We identified preleptotene nuclei as the stage in which SYPC3 foci start to appear (Figure 3ab). Furthermore, the combined staining for SYPC3 and DAPI allowed us to distinguish between the different substages (early, mid and late) of preleptotene based on the appearance of a DDB
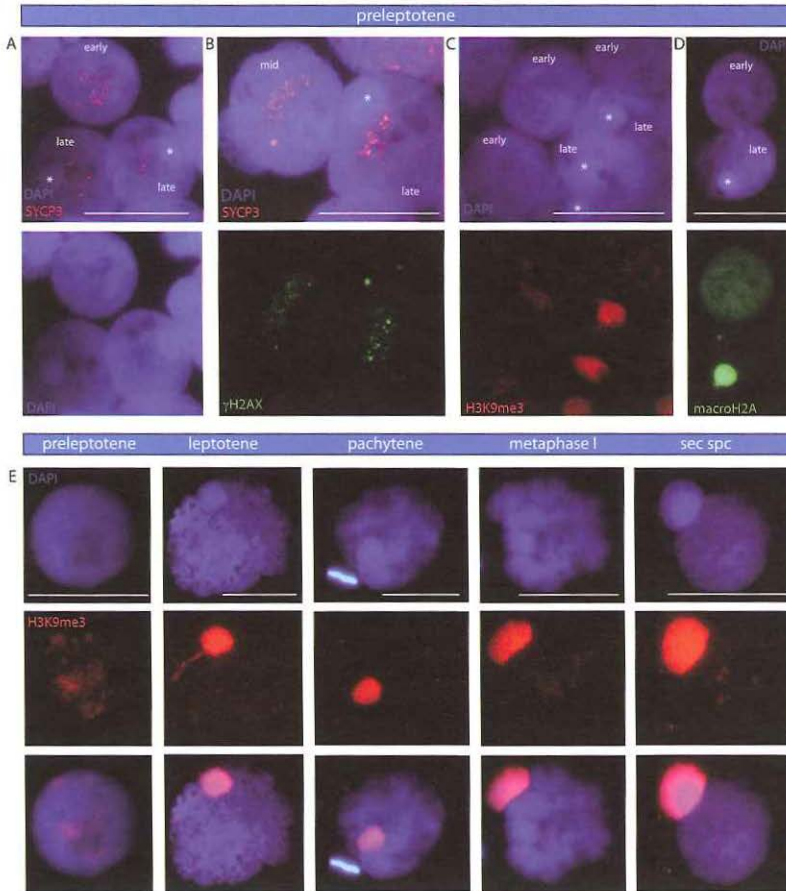
Figure 3. The GRC is silenced during early meiotic prophase. (a – d): Preleptotene spermatocyte spread nuclei. Bar represents 5 μm. (a) Top panel shows early and late preleptotene nuclei stained for SYCP3 (red) and DAPI (blue). The DAPI dense GRC localisation in late preleptotene stages is indicated with an asterix; the lower panel shows only the DAPI staining. The early preleptotene nucleus shows no heterochromatic area, indicating that the DDB has not yet formed. The formation of a few SYCP3 axial element fragments in all nuclei marks the preleptotene stage. (b) The top panel shows a mid and late preleptotene nucleus stained for SYCP3 (red) and DAPI (blue). The asterix indicates the DAPI dense GRC. The lower panel shows the same nuclei, but immunostained for γH2AX (green), indicative of the presence of the first DNA double strand breaks, that more or less colocalise with SYCP3. (c,d) The top panel shows early and late preleptotene stages with DAPI staining. The asterix indicates the DAPI dense GRC. The lower panels shows the corresponding nuclei stained for H3K9me3 (c) and macroH2A (d). Early preleptotene nuclei lack intense H3K9me3 (c) and macroH2A (d) staining, and no DDB is observed. (e) The top panel shows DAPI staining of the different nuclei, the middle panel shows the corresponding nuclei stained for H3K9me3 (red), and the bottom panel shows the merge. In preleptotene, a faint staining is present throughout the nucleus. In all consecutive meiotic prophase stadia, the GRC is positive for H3K9me3. Sec spc secondary spermatocyte. Bar represents 5 μm.

(Figure 3a–e). In the earlier preleptotene nuclei, we never observed a distinct subnuclear region containing such a strong H3K9me3 signal as was observed for the GRC body in leptotene spermatocyes (Figure 3c, e). However, at the end of preleptotene, we observed colocalization of the DDB and H3K9me3 (Figure 3c, e). For macroH2A, another heterochromatin marker, we observed a similar staining pattern as for H3K9me3 (Figures 3d and 7). This indicates that the GRC becomes heterochromatized upon entry into meiotic prophase.

The highly intense H3K9me3 staining, colocalizing with the DDB remained present until its elimination. In metaphase I, H3K9me3 also marks the area of the centromeres (Figure 3e).

We often observed a somewhat separate localisation of the GRC from the rest of the chromosomes around metaphase I, indicating that this chromosome may not be aligned with the rest of the chromosomes. In secondary spermatocytes, identified by the presence of a few SYPC3 filaments per nucleus (Figure 4a), we observed nuclei with and without a DAPI dense area, representing presence or absence of the GRC. To investigate this further, we quantified the number of nuclei without the GRC DAPI dense chromatin, nuclei with the GRC still minimally attached to the nucleus and nuclei still containing the GRC DDB (Figure 4a). We scored 180 secondary spermatocyte nuclei and the vast majority (131 out of 180 nuclei) had lost the GRC. A minority of the secondary spermatocytes appeared with a round, small DAPI dense GRC body still attached to the nucleus (36 out of 180 nuclei), and these bodies were still positive for H3K9me3 (Figure 4a). We also observed secondary spermatocyte nuclei still containing an H3K9me3 positive area, indicating that the GRC is not always eliminated at metaphase I (13 out of 180 nuclei) (Figure 3a).

We also immunostained for H3K9ac and H3K4me3 (Figure 5), as markers for active transcription. As expected, based on the staining for H3K9me3 and macroH2A, the GRC body lacked both markers of active chromatin from early leptotene until late diplotene. Whereas the GRC body remained devoid of H3K4me3, the H3K9ac signal on the DAPI dense GRC body, was no longer reduced compared to the rest of the chromatin from late diplotene onwards, indicating that the GRC acquires a mixed pattern of histone modifications at H3K9 around this stage.

Analyses of known MSUC/MSCI markers on the GRC body
Next, we investigated if markers of meiotic silencing of unsynapsed chromatin (MSUC) or more specifically, sex chromosomes (MSCI) also localise to the GRC body. The most well-known marker of the XY body in mammals is γH2AX. However, as mentioned above, γH2AX is mostly absent from the GRC until metaphase. Still, γH2AX starts to mark the GRC body from metaphase onwards,
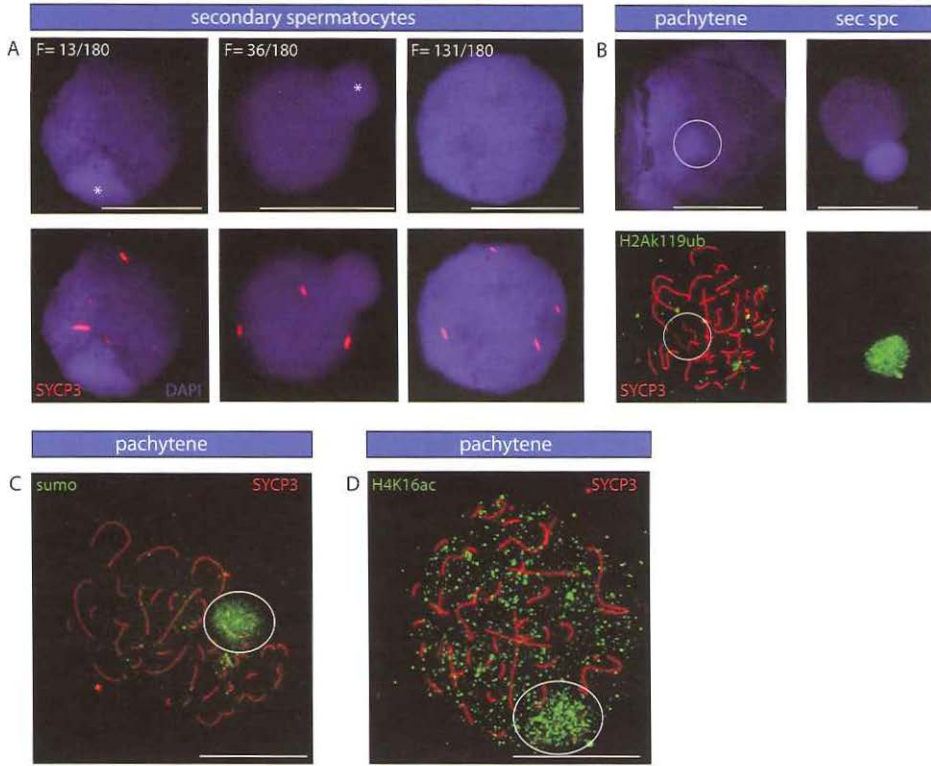
Figure 4. The silenced GRC is eliminated at metaphase I in the vast majority of spermatocytes. (a) Spermatocyte spread nuclei stained for DAPI (blue, upper and lower panel) and SYCP3 (lower panel, red). The left image shows a secondary spermatocyte with the GRC still inside the nucleus, the middle image with the GRC still attached to the outside of the nucleus, and the right image shows a secondary spermatocyte lacking the GRC. The typical SYCP3 filaments/dots mark the secondary spermatocyte stage. F = the number of positive nuclei / the total number of scored secondary spermatocyte nuclei. Bar represents 5 µm. (b,c,d) Male meiotic prophase spread nuclei stained for H2AK119 ubiquitylation (green, b), sumoylation (green, c), H4K16ac (green, d) and SYCP3 (red). At pachytene, the GRC becomes increasingly sumoylated, and acetylated on H4K16. However, no H2AK119 ubiquitylation signal is present on the GRC at this stage. When the GRC is almost eliminated, it becomes increasingly ubiquitylated at H2AK119, (b). The area of the GRC is encircled. Bar represents 5 µm.

and the GRC remains γH2AX positive until it is expelled from the nucleus (Figure 2a).

H2AK119 ubiquitylation, another XY and ZW body marker, also marked the GRC, starting just after metaphase I and reaching its maximum in secondary spermatocytes, when it is still attached to the nucleus (Figure 4b). Free GRC bodies were mostly negative for H2AK119 ubiquitylation (not shown).
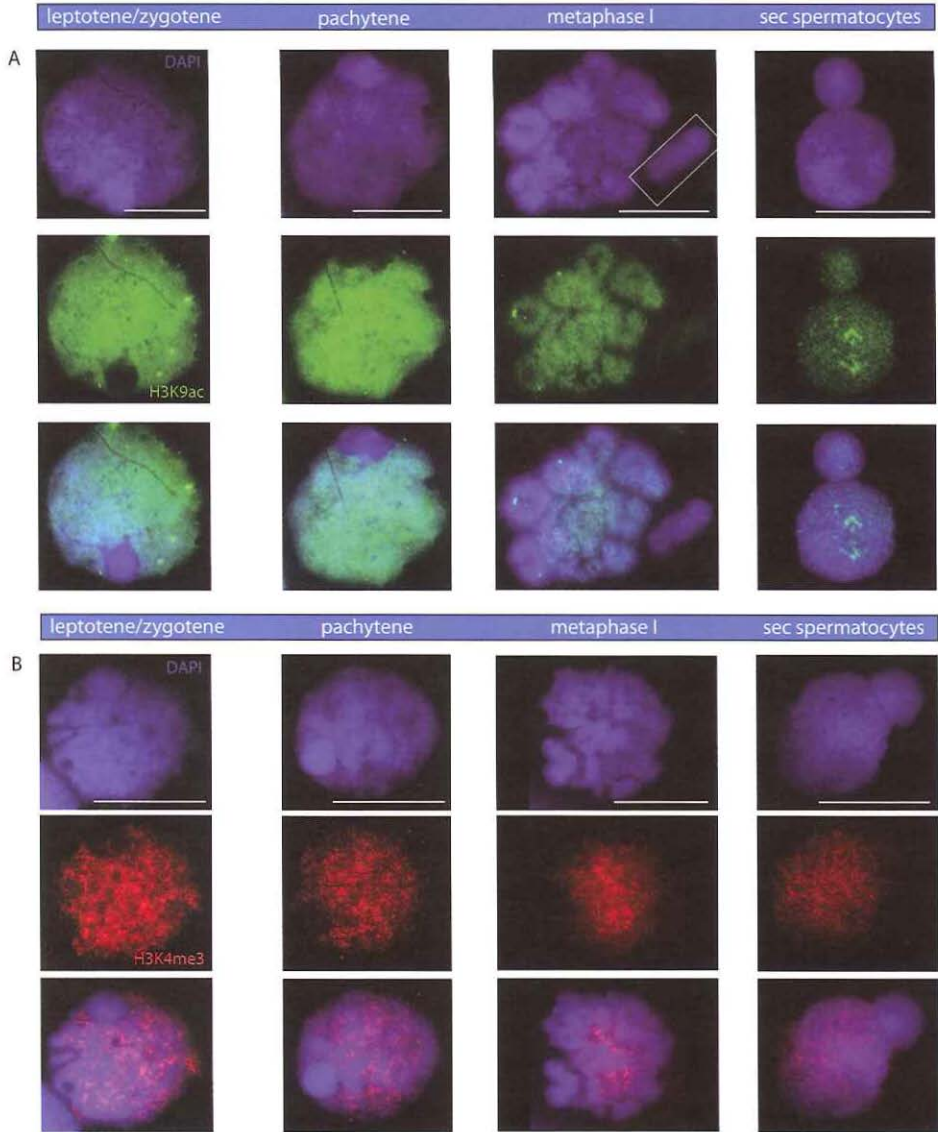
Figure 5. Overview of histone modifications on the GRC in the different stages of meiotic prophase I of zebra finch spermatocytes. (a) The top panel shows DAPI staining of the different nuclei, the middle panel shows the corresponding nuclei stained for H3K9ac (green), and the bottom panel shows the merge. The area of the GRC is always devoid of H3K9ac until diplotene. During metaphase I, the GRC becomes positive for H3K9ac, and when it is almost expelled, the GRC is as positive as the rest of the nucleus. Sec spc, secondary spermatocyte. (b) The top panel shows DAPI staining of the different nuclei, the middle panel shows the corresponding nuclei stained for H3K4me3 (red), and the bottom panel shows the merge. The GRC is devoid of the active marker H3K4me3 during all stages of meiotic prophase. Sec spc, secondary spermatocyte.

In mouse [22, 23], the XY body is marked by increased protein sumoylation from late zygotene onwards, whereas the XY body in human [24] and the ZW body in chicken (not shown) show no increased sumoylation. We found strong staining for sumoylation on the GCR body from leptotene onwards, and the signal remained present until late pachytene (Figure 4c).

Lack of H4K16ac marks the inactive ZW pair at during pachytene in chicken oocytes [6]. However, we observed marked H4K16ac staining, colocalizing with the GRC body during leptotene, zygotene and reaching a maximum at pachytene (Figure 4d). From metaphase onwards, H4K16ac staining was evenly distributed throughout the nucleus, including the GRC body (not shown).

Absence of INCENP from the GRC

During metaphase I, attachment of spindle microtubules to the kinetochores enables segregation of dyads during the first meiotic division.

We found that the GRC mostly localises to the periphery of the nucleus during meiotic prophase. In metaphase I, we noticed that the GRC often appears separate from the other chromosomes. Earlier reports also described that the GRC becomes separate from the rest of the DNA during metaphase I [15, 16]. The distant position of the GRC and its apparent separation could be caused by defective or absent attachment of the GRC to the spindle. To analyse this, we immunostained for the centromeric protein INCENP (inner centromere protein). During male meiosis in mouse, INCENP localizes on the central elements of the synaptonemal complex from zygotene onwards. In late pachytene, it relocalizes to the centromeres [25]. In zebra finch spermatocytes, we first observed the appearance of INCENP on the SC fragments around late zygotene – early pachytene and as bright foci throughout the nuclei (Figure 6a). However, the area containing the GRC lacked INCENP staining. Around metaphase I, most of the INCENP foci disappeared and the protein relocalized to the center of the nucleus. During progression of metaphase I, we observed intense INCENP staining indicating the positions of the centromeres. In the vast majority of the nuclei, the GRC lacked all INCENP signals. However, rarely, the GRC did show INCENP staining, which could indicate that the GRC participates in the first meiotic division in a small minority of the cells (not shown).

DNA fragmentation of the GRC during and after its elimination from the nucleus

Both phosphorylation of H2AX, and ubiquitylation/de-ubiquitylation of H2A have been associated not only with DSB repair and chromatin silencing, but also with initiation and execution of apoptosis, which involves the generation of DNA breaks and finally results in DNA fragmentation [26-29]. The appearance of increasing γH2AX and H2AK119 ubiquitylation staining on the GRC from
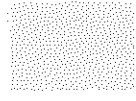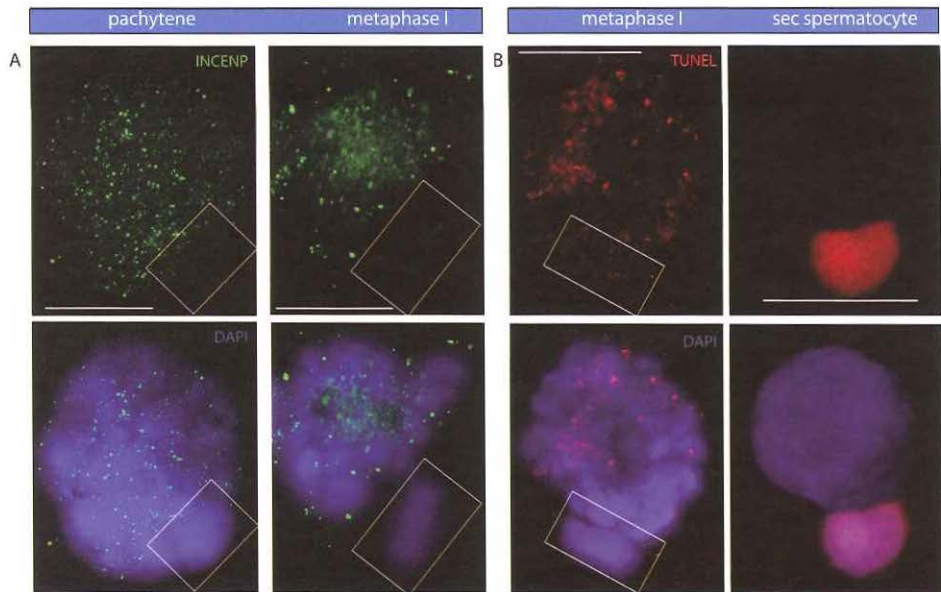
Figure 6. The GRC lacks INCENP protein and its DNA is degraded. (a) Male meiotic prophase spread nuclei stained for INCENP (green) and DAPI (blue). In pachytene, INCENP foci most likely follow the axial elements, which can be inferred from the DAPI staining. Also, many INCENP-foci are present throughout the nucleus. The GRC remains largely devoid of INCENP staining. From diplotene onward, INCENP-foci relocalize and concentrate mainly around the centromeres in metaphase. The GRC mostly shows no INCENP-staining at its centromere. The area of the GRC is boxed. Bar represents 5 μm. (b) Spermatocyte spread nuclei stained for TUNEL (terminal deoxynucleotidyl transferase dUTP nick end labelling) (red) and DAPI (blue). Early in meiosis the GRC is largely devoid of TUNEL staining. When the GRC is almost expelled from the nucleus, it becomes strongly TUNEL-positive. The area of the GRC is boxed. Bar represents 5 μm.

metaphase I onwards (Figure 2a and 4b), combined with initial lack of γH2AX and H2AK119 ubiquitylation staining during pachytene, indicated that the DNA of the GRC may be degraded during and after its release from the nucleus. TUNEL (terminal deoxynucleotidyl transferase) dUTP nick end labelling) staining is a common method used for the detection of DNA fragmentation. We observed faint TUNEL staining in early meiotic prophase spermatocytes, which most likely represents the presence of meiotic DSBs. The GRC body showed less TUNEL staining compared to the rest of the chromosomes during these stages, which is in agreement with the relative lack of RAD51 and γH2AX foci on the GRC we observed previously. When the GRC body becomes more separate from the rest of the chromosomes, TUNEL signal increases, and when the GRC has formed a separate body, the TUNEL staining is maximal, again indicating that
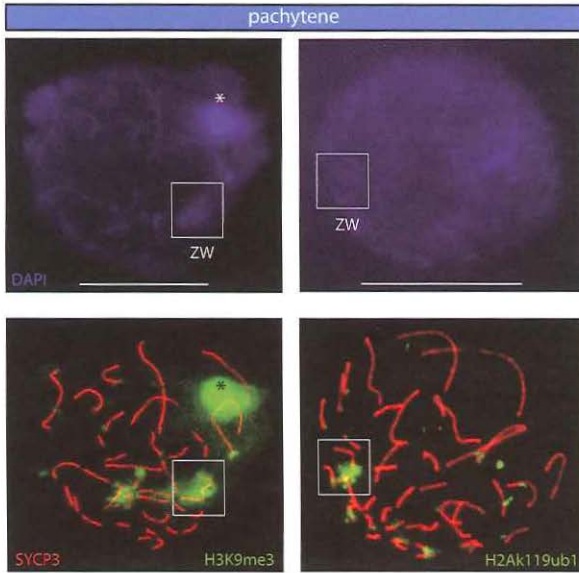
Figure 7. Analyses of the ZW pair and GRC chromosomes during female meiotic prophase. Oocyte spread nuclei stained for SYCP3 (red), H3K9me3 (green), H2AK119ub (green) and DAPI (blue). At pachytene, the ZW pair is strongly positive for H3K9me3 and H2Ak119ubiquitylation.
* indicates the middle part of the GRC, which is also positive for H3K9me3, indicating that the GRC is also (partially) silenced during female meiotic prophase. GRC is boxed. Bar represents 5 μm.

the DNA of the GRC is fragmented during and after its exclusion from the nucleus (Figure 6b).

Analyses of the GRC during female meiotic prophase of the zebra finch

To compare the behaviour of the single GRC in male spermatocytes with that of the paired GRC and the ZW chromosome pair in oocytes, we immunostained oocyte spread preparations of zebra finch females for SYCP3 and H3K9me3 and for SYCP3 and H2AK119 ubiquitylation (Figure 7).

As we observed previously in chicken oocytes [6], a H3K9me3-positive ZW body is visible during pachytene in zebra finch oocytes. H2AK119 ubiquitylation also marks part of the ZW pair around mid pachytene. In addition, we observed that the middle part of the GRC pair is also positive for H3K9me3, shows a dense DAPI signal, and mostly localizes in the periphery of the nucleus. Throughout the female meiotic prophase, the GRCs remain partially positive for H3K9me3 (Figure 7), although the signal is much less intense compared to what we observed for the single GRC in spermatocytes. In pachytene and diplotene, part of the GRC shows a very strong H3K9me3 signal and this part of the GRC often colocalises with the H3K9me3 positive ZW pair in the periphery of the nucleus.

DISCUSSION

During male and female meiotic prophase in mammals, the presence of unsynapsed chromatin is associated with silencing of these areas by MSUC.

The heterologous XY pair remains largely unsynapsed, and is always subjected to a specialized form of MSUC: meiotic sex chromosome inactivation (MSCI) (reviewed in [5]). In mammals, MSUC and MSCI appear to be triggered by the presence of unsynapsed chromatin in combination with persistent meiotic DSBs [5, 30]. Recently we showed that the avian sex chromosomes in chicken oocytes also display MSCI, albeit transient, despite the fact that Z and W show complete synapsis [6]. Here, we asked how, in addition to the avian form of MSCI, meiotic silencing of unsynapsed chromatin (MSUC) functions in the avian germline. We chose to analyse the meiotic behaviour of the single copy of the GRC in the germline of the male zebrafinch. Our data show that this chromosome is silenced upon entry into meiotic prophase, first detectable in preleptotene spermatocytes. This resembles what we observed for the W chromosome in chicken and zebra finch oocytes. Apparently, the inactivation of both the GRC and W chromosomes precedes the introduction of meiotic DSBs and synapsis. Furthermore, the GRC does appear to accumulate only few meiotic DSBs during leptotene. Therefore, it is unlikely that the mechanisms that silence W and the GRC are linked to meiotic DSB repair. In addition, since silencing of W (in oocytes) and the GRC (in spermatocytes) occurs prior to initiation of chromosome pairing, discrimination between synapsis/asynapsis can also not be the initiating trigger for this transcriptional silencing.

In male grasshoppers, *Eyprepocnemis plorans* and *Locusta migratoria,* the single facultative heterochromatic X chromosome (and a constitutive heterochromatic B chromosome) remain unsynapsed throughout meiotic prophase and are also silenced at the onset of meiotic prophase [31, 32] as visualised by the loss of H3K9 acetylation [31, 33]. Apparently, in spermatocytes of grasshoppers, silencing of these single chromosomes is also DSB and synapsis-independent. Based on these observations, we would like to propose to refer to this type of early meiotic silencing of chromosomes as Meiotic Silencing Prior to Synapsis (MSPS), to indicate that the initiating events and timing in this type of meiotic silencing may be different from MSUC in mammals.

Cabrero et al. [33] suggested the existence of a counting mechanism operating at the start of meiosis, enabling detection and direct subsequent inactivation of single chromosomes. The clustering of telomeres in the nuclear envelope that occurs upon entry in meiotic prophase I (reviewed in [34]) could play a role in the detection of these univalents. For zebra finch and chicken, such a counting mechanism seems unlikely, since the single Z chromosome behaves different from the single W and GRC.

W and the GRC appear euchromatic in premeiotic germ cell stages, but may be largely transcriptionally silent due to the fact that very few functional genes

appear to be present. In fact, these chromosomes seem to be highly enriched for repeat sequences [35], and their inactive status may be associated with late replication during the final S phase before entry into meiotic prophase. Recently, Lande-Diner et al. [36] showed that replication-time switching, from late to early or vice versa, is linked to the acetylation state of the chromatin, and thus may direct nucleosome structure regulation. Perhaps the nucleosomes that assemble on GRC and W chromatin during the final S phase are specifically modified, for example by acetylation of H4K16, to mark them for global silencing and heterochromatization, and, in case of the GRC, to prepare it for its ultimate expulsion. Apart from, or in addition to, late replication, small non-coding RNA pathways may also be involved, since these have been linked to silencing of transposable elements and repeats in meiosis. The elimination of the GRC during male meiosis shows some resemblance to homology dependent programmed (single copy) DNA elimination that is also mediated by non-coding RNAs during sexual reproduction in ciliates (reviewed in [37-39]).

Surprisingly, we found that in contrast to what has been described for the grasshopper X and B chromosomes, the GRC occasionally accumulates a few meiotic DSBs, as shown by the presence of both RAD51 and γH2AX foci. Its compact heterochromatic configuration most likely prevents access of DSB-inducing proteins to most of the GRC, minimizing the number of DSBs in the GRC. Rarely, we noticed the presence of a MLH1 focus on the GRC. The existence of intrachromosomal recombination could explain this observation, and this is supported by the recent finding that the GRC is rich in repeat sequences [35] and our observation of small regions of self-synapsis, visualised by the presence of small SYCP1 stretches on the GRC during pachytene.

H4K16 acetylation is generally associated with an open chromatin configuration and a transcriptionally active state (reviewed in [40]). However, we find increased H4K16 acetylation on the heterochromatic GRC. Although there are a few reports describing that histone acetyltransferases could be involved in maintaining silencing of certain loci, this most likely results from shifting of heterochromatic boundaries and not from direct silencing activity induced by the histone acetylation (reviewed in [40]). Therefore, it is unlikely that the observed increased H4K16 acetylation is linked to GRC silencing. Histone acetyltransferases (HATs) have also been implicated in the detection of DSBs and DNA repair processes [41]. It might be suggested that the induction of even a few DSBs on the GRC could cause (hyper)acetylation of H4, since these breaks cannot be repaired.

As the cells progress towards the diplotene stage, DAPI staining of the GRC was found to become indistinguishable from the rest of the nucleus. This may

indicate that the GRC undergoes a brief stage of chromatin relaxation, facilitated by the observed increased H3K9 acetylation on the GRC around diplotene. The less condensed configuration could then provide access to the GRC for the kinase (most likely ATR or ATM) that phosphorylates H2AX and the ubiquitin ligase that induces ubiquitylation of H2A, which accompany the observed fragmentation of the GRC.

INCENP, is part of the conserved chromosomal passenger complex, which regulates chromosomal segregation and ensures correct kinetochore-microtubule interactions (reviewed in [42]). The lack of INCENP loading on the GRC indicates that the separation of the GRC from the rest of the chromosomes around metaphase I is at least partly due to the fact that proper microtubule attachment to the GRC kinetochore may not occur, resulting in aberrant localisation of the chromosome. In addition, the fact that the GRC is not attached to a homolog will contribute to its aberrant behaviour; the lack of tension from opposing pulling forces will destabilize the attached microtubules. Abberant regulation of the kinetochore/centromere is also apparent from the lack of H2AK119 ubiquitylation (not shown), which marks the centromeres on other chromosomes. Around the first meiotic metaphase-to-anaphase transition, the GRC is truly separated from the two haploid genomes and will no longer be incorporated in the nucleus in the vast majority of secondary spermatocytes. Instead, the GRC forms a micronucleus.

When the GRC does not move to the metaphase plate, DNA fragmentation that selectively affects the GRC could be triggered, as visualized by increasing γH2AX, H2AK119 ubiquitylation and TUNEL-staining. Subsequently, de-ubiquitylation of H2A follows, which is a feature of ongoing apoptosis [26]. These events are schematically summarized in Figure 8. Recently, Terradas et al. [43] showed that also in human cells, DNA with unrepaired DSBs can be separated in a micronucleus, in which DNA degradation occurs, followed by elimination. Elimination of the single GRC may have evolved to avoid activation of the spindle checkpoint. For example, in mantid spermatocytes, sex chromosomes occasionally remain unpaired, and this leads to phosphorylation of the kinetochore, checkpoint activation, and meiotic arrest [44]. In contrast, in XO grasshopper species, the always single X has a special kinetochore that apparently is not recognized by the checkpoint machinery [44].

In the female germline, the GRC is present as a bivalent, in most oocytes. It can be easily recognized because it is the longest bivalent [15, 16]. We noticed that it is also partly heterochromatic, which may be caused by a low gene content and/or the presence of repetitive DNA on these chromosomes. In chicken oocytes, we have also observed increased H3K9me3 staining on parts of the
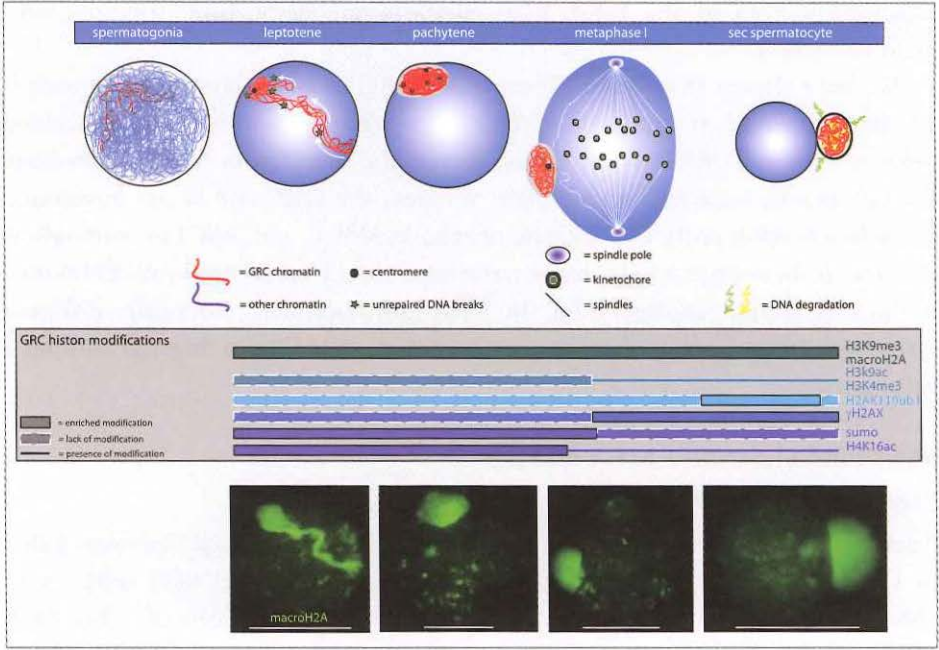
Figure 8. Schematic overview of the behaviour of the GRC during the male meiotic prophase of the zebra finch. In the transition phase between spermatogonia and the start of the male meiotic prophase, the GRC is identified and from preleptotene, it becomes heterochromatized and gains specific chromatin modifications such as H3K9me3, macroH2A, sumoylation and H4K16ac. With progression through meiotic prophase, all chromatin of the GRC is drawn into a heterochromatic body at the periphery of the nucleus. Few DSBs are induced on the GRC, and these remain unrepaired. Also, H2A on its centromere is not ubiquitylated. Sumoylation of chromatin and acetylation at H4K16 accumulate on the GRC and reach a maximum around mid pachytene. At diplotene, the GRC becomes acetylated at H3K9 and starts to decondense. During metaphase I, the nuclear membrane is degraded, the centromere and kinetochore of the GRC are aberrant, and proper attachment to the spindles fails. This may cause DNA degradation of the GRC, and the chromatin to become phosphorylated, ubiquitylated, and again de-ubiquitylated. In addition, the GRC forms a micronucleus with ongoing DNA fragmentation in the cytoplasm of the secondary spermatocyte.

macrochromosomes [6]. In contrast to the single GRC in males, the GRC bivalent in oocytes normally participates in meiotic recombination. It has been suggested that recombination of the GRC-pair in the female germline prevents the loss of the GRC and ensures the transmission through females [16]. From this perspective, recombination of Z with W in the pseudoautosomal region may rescue W from a fate similar to that of the single GRC in males. Alternatively, failure of pairing leading to a single W may trigger meiotic arrest. A special feature intrinsic to the GRC may be responsible for the aberrant kinetochore/centromere structure,

causing initiation of the DNA fragmentation and elimination from the male meiotic nucleus.

We have shown that the single unpaired GRC in male zebra finch meiosis is efficiently silenced, and propose to refer to this phenomenon as Meiotic Silencing Prior to Synapsis (MSPS). The timing of meiotic silencing in birds differs from that of meiotic silencing in mammals: Whereas the GRC and W are inactivated immediately upon entry into meiotic prophase, MSUC and MSCI in mammals is initiated at the zygotene/pachytene transition, strictly correlating with the timing of an unsynapsed configuration. In birds and mammals, essentially different machineries may have evolved to trigger meiotic silencing of regions without a pairing partner.

MATERIALS AND METHODS

Spreads and immunocytochemistry

Adult male and 2 - 7 day old female zebra finches (*Taeniopygia guttata*) were killed by CO_2 intoxication. The functional left ovary and left and right testes were dissected and placed in PBS solution. Spread nuclei preparations of zebra finch oocytes and spermatocytes were prepared using a modification of the drying-down technique described by Peters et al [45]. Briefly, ovaries and testes were minced with forceps, and ovarian cells were suspended in 500 ml of 100 mM sucrose, containing EDTA-free complete protease inhibitor cocktail (Roche Diagnostics, Almere, The Netherlands), whereas testicular cells were placed in hypobuffer solution, and after centrifugation, cells were resuspended in 100 mM sucrose. Oocytes and spermatocytes were dispersed on a glass slide dipped in 1% paraformaldehyde fixative with 0.1% Triton X100. After two hours in a humid chamber at room temperature, the slides were allowed to dry for 30-60 minutes at room temperature, followed by a single wash in 0.08% Photoflo (Kodak, Paris, France) and air-dried. The slides were stored at −80 °C.

For immunocytochemistry, frozen slides were defrosted at room temperature and washed with PBS. The slides were blocked with PBS containing 0.5% w/v BSA and 0.5% w/v milk powder, and double stained with different combinations of the following antibodies: rabbit polyclonal anti-SYCP3 (1:1000), rabbit polyclonal anti-SYCP1 (1:200) (gifts from C. Heyting, Wageningen), mouse polyclonal anti-γH2AX (1:1000) (Upstate, Walthum, MA, USA), mouse monoclonal IgM anti-H2AK119ub1 (1:1000) (Upstate), mouse monoclonal anti-H4K16ac (1:200) (Upstate), mouse monoclonal MLH1 (1:25) (BD Pharmingen, San Diego, USA), rabbit polyclonal anti-H3K9me3 (1:500) (Upstate), rabbit anti-human RAD51 (1:500) [24], rabbit polyclonal macroH2A (1:500) (Upstate), rabbit monoclonal H3K9ac (1:50) (Sigma, USA), H3K4me3 (1:1000) (Upstate), mouse monoclonal

GMP-1 (SUMO) (1:100) (Zymed, San Francisco, USA) rabbit polyclonal INCENP (1:100) (Abcam, UK). For mouse monoclonal primary antibodies, the secondary antibodies were fluorescein isothiocyanate (FITC) (1:128) (Sigma, St Louis, USA)-labelled goat anti-mouse IgG antibodies for anti-γH2AX, anti-MLH1, anti-macroH2A and anti-GMP-1, FITC -labelled goat anti-mouse IgM (1:128) (Sigma) for anti-H2AK119ub1 and tetramethylrhodamine isothiocyanate (TRITC) (1:128) (Sigma)-labelled goat anti-mouse IgG antibodies for anti-γH2AX. The secondary antibody for polyclonal rabbit primary antibodies was tetramethylrhodamine isothiocyanate (TRITC) (1:200) (Sigma)-labelled goat anti-rabbit IgG antibodies for anti-SYCP3 and fluorescein isothiocyanate (FITC) (1:80) (Sigma)-labelled goat anti-rabbit IgG antibodies for anti-RAD51, anti-SYCP1, anti-H3K9ac and anti-INCENP. Primary antibodies were diluted in 10% w/v BSA in PBS and incubated overnight in a humid chamber. Thereafter, slides were washed in PBS, blocked in 10% v/v normal goat serum (Sigma) in blocking buffer (5% milk powder (w/v in PBS, centrifuged at 13.200 rpm for 10 min), and incubated with secondary antibodies in 10% v/v normal goat serum in blocking buffer at room temperature for 2 hours. Next, the slides were washed in PBS and embedded in Vectashield containing DAPI (4',6'-diamindino-2-phenylindole) (Vector Laboratories, Burlingame CA, USA). Double stainings of SYCP1 with SYCP3 and of RAD51 with SYCP3 (all rabbit polyclonal antibodies) were obtained by sequential immunostainings with the single antibodies. Images of SYCP1, RAD51 and SYCP3 stainings respectively, were obtained prior to immunostaining with anti-SYCP3 of the same nuclei.

ACKNOWLEDGEMENTS

REFERENCES

1. Zickler D. From early homologue recognition to synaptonemal complex formation. *Chromosoma.* Jun 2006;115(3):158-174.
2. Keeney S, Giroux CN, Kleckner N. Meiosis-specific DNA double-strand breaks are catalyzed by Spo11, a member of a widely conserved protein family. *Cell.* Feb 7 1997;88(3):375-384.
3. Neale MJ, Keeney S. Clarifying the mechanics of DNA strand exchange in meiotic recombination. *Nature.* Jul 13 2006;442(7099):153-158.
4. Moens PB, Chen DJ, Shen Z, et al. Rad51 immunocytology in rat and mouse spermatocytes and oocytes. *Chromosoma.* Sep 1997;106(4):207-215.
5. Turner JM. Meiotic sex chromosome inactivation. *Development.* May 2007;134(10):1823-1831.
6. Schoenmakers S, Wassenaar E, Hoogerbrugge JW, Laven JS, Grootegoed JA, Baarends WM. Female meiotic sex chromosome inactivation in chicken. *PLoS Genet.* May 2009;5(5):e1000466.
7. Solari AJ. Equalization of Z and W axes in chicken and quail oocytes. *Cytogenet Cell Genet.* 1992;59(1):52-56.
8. Tres LL. Extensive pairing of the XY bivalent in mouse spermatocytes as visualized by whole-mount electron microscopy. *J Cell Sci.* Jun 1977;25:1-15.
9. Roeder GS. Meiotic chromosomes: it takes two to tango. *Genes Dev.* Oct 15 1997;11(20):2600-2621.
10. Ashley T, Plug AW, Xu J, et al. Dynamic changes in Rad51 distribution on chromatin during meiosis in male and female vertebrates. *Chromosoma.* Oct 1995;104(1):19-28.
11. Monesi V. Differential rate of ribonucleic acid synthesis in the autosomes and sex chromosomes during male meiosis in the mouse. *Chromosoma.* 1965;17(1):11-21.
12. Turner JM, Mahadevaiah SK, Ellis PJ, Mitchell MJ, Burgoyne PS. Pachytene asynapsis drives meiotic sex chromosome inactivation and leads to substantial postmeiotic repression in spermatids. *Dev Cell.* Apr 2006;10(4):521-529.
13. Plug AW, Peters AH, Keegan KS, Hoekstra MF, de Boer P, Ashley T. Changes in protein composition of meiotic nodules during mammalian meiosis. *J Cell Sci.* Feb 1998;111 (Pt 4):413-423.
14. Turner JM, Mahadevaiah SK, Fernandez-Capetillo O, et al. Silencing of unsynapsed meiotic chromosomes in the mouse. *Nat Genet.* Jan 2005;37(1):41-47.
15. Pigozzi MI, Solari AJ. Germ cell restriction and regular transmission of an accessory chromosome that mimics a sex body in the zebra finch, Taeniopygia guttata. *Chromosome Res.* Feb 1998;6(2):105-113.
16. Pigozzi MI, Solari AJ. The germ-line-restricted chromosome in the zebra finch: recombination in females and elimination in males. *Chromosoma.* Dec 2005;114(6):403-409.
17. Mahadevaiah SK, Turner JM, Baudat F, et al. Recombinational DNA double-strand breaks in mice precede synapsis. *Nat Genet.* Mar 2001;27(3):271-276.
18. Rogakou EP, Pilch DR, Orr AH, Ivanova VS, Bonner WM. DNA double-stranded breaks induce histone H2AX phosphorylation on serine 139. *J Biol Chem.* 1998;273(10):5858-5868.
19. Anderson LK, Reeves A, Webb LM, Ashley T. Distribution of crossing over on mouse synaptonemal complexes using immunofluorescent localization of MLH1 protein. *Genetics.* Apr 1999;151(4):1569-1579.
20. Baker SM, Plug AW, Prolla TA, et al. Involvement of mouse Mlh1 in DNA mismatch repair and meiotic crossing over. *Nat Genet.* Jul 1996;13(3):336-342.

21. Pigozzi MI. Distribution of MLH1 foci on the synaptonemal complexes of chicken oocytes. *Cytogenet Cell Genet.* 2001;95(3-4):129-133.
22. Vigodner M. Sumoylation precedes accumulation of phosphorylated H2AX on sex chromosomes during their meiotic inactivation. *Chromosome Res.* 2009;17(1):37-45.
23. Vigodner M, Morris PL. Testicular expression of small ubiquitin-related modifier-1 (SUMO-1) supports multiple roles in spermatogenesis: silencing of sex chromosomes in spermatocytes, spermatid microtubule nucleation, and nuclear reshaping. *Dev Biol.* Jun 15 2005;282(2):480-492.
24. Metzler-Guillemain C, Depetris D, Luciani JJ, Mignon-Ravix C, Mitchell MJ, Mattei MG. In human pachytene spermatocytes, SUMO protein is restricted to the constitutive heterochromatin. *Chromosome Res.* 2008;16(5):761-782.
25. Parra MT, Gomez R, Viera A, et al. Sequential assembly of centromeric proteins in male mouse meiosis. *PLoS Genet.* Mar 2009;5(3):e1000417.
26. Mimnaugh EG, Kayastha G, McGovern NB, et al. Caspase-dependent deubiquitination of monoubiquitinated nucleosomal histone H2A induced by diverse apoptogenic stimuli. *Cell Death Differ.* Dec 2001;8(12):1182-1196.
27. Sluss HK, Davis RJ. H2AX is a target of the JNK signaling pathway that is required for apoptotic DNA fragmentation. *Mol Cell.* Jul 21 2006;23(2):152-153.
28. Zhou W, Wang X, Rosenfeld MG. Histone H2A ubiquitination in transcriptional regulation and DNA damage repair. *Int J Biochem Cell Biol.* Jan 2009;41(1):12-15.
29. Rogakou EP, Nieves-Neira W, Boon C, Pommier Y, Bonner WM. Initiation of DNA fragmentation during apoptosis induces phosphorylation of H2AX histone at serine 139. *J Biol Chem.* Mar 31 2000;275(13):9390-9395.
30. Schoenmakers S, Wassenaar E, van Cappellen WA, et al. Increased frequency of asynapsis and associated meiotic silencing of heterologous chromatin in the presence of irradiation-induced extra DNA double strand breaks. *Dev Biol.* May 1 2008;317(1):270-281.
31. Viera A, Calvente A, Page J, et al. X and B chromosomes display similar meiotic characteristics in male grasshoppers. *Cytogenet Genome Res.* 2004;106(2-4):302-308.
32. Viera A, Santos JL, Page J, et al. DNA double-strand breaks, recombination and synapsis: the timing of meiosis differs in grasshoppers and flies. *EMBO Rep.* Apr 2004;5(4):385-391.
33. Cabrero J, Teruel M, Carmona FD, Jimenez R, Camacho JP. Histone H3 lysine 9 acetylation pattern suggests that X and B chromosomes are silenced during entire male meiosis in a grasshopper. *Cytogenet Genome Res.* 2007;119(1-2):135-142.
34. Scherthan H. Telomere attachment and clustering during meiosis. *Cell Mol Life Sci.* Jan 2007;64(2):117-124.
35. Itoh Y, Kampf K, Pigozzi MI, Arnold AP. Molecular cloning and characterization of the germline-restricted chromosome sequence in the zebra finch. *Chromosoma.* Aug 2009;118(4):527-536.
36. Lande-Diner L, Zhang J, Cedar H. Shifts in replication timing actively affect histone acetylation during nucleosome reassembly. *Mol Cell.* Jun 26 2009;34(6):767-774.
37. Bernstein E, Allis CD. RNA meets chromatin. *Genes Dev.* Jul 15 2005;19(14):1635-1655.
38. Mochizuki K, Gorovsky MA. Small RNAs in genome rearrangement in Tetrahymena. *Curr Opin Genet Dev.* Apr 2004;14(2):181-187.
39. Lepere G, Betermier M, Meyer E, Duharcourt S. Maternal noncoding transcripts antagonize the targeting of DNA elimination by scanRNAs in Paramecium tetraurelia. *Genes Dev.* Jun 1 2008;22(11):1501-1512.

40. Shahbazian MD, Grunstein M. Functions of site-specific histone acetylation and deacetylation. *Annu Rev Biochem*. 2007;76:75-100.

41. Murr R, Loizou JI, Yang YG, et al. Histone acetylation by Trrap-Tip60 modulates loading of repair proteins and repair of DNA double-strand breaks. *Nat Cell Biol*. Jan 2006;8(1):91-99.

42. Vagnarelli P, Earnshaw WC. Chromosomal passengers: the four-dimensional regulation of mitotic events. *Chromosoma*. Nov 2004;113(5):211-222.

43. Terradas M, Martin M, Tusell L, Genesca A. DNA lesions sequestered in micronuclei induce a local defective-damage response. *DNA Repair (Amst)*. Aug 13 2009.

44. Li X, Nicklas RB. Tension-sensitive kinetochore phosphorylation and the chromosome distribution checkpoint in praying mantid spermatocytes. *J Cell Sci*. Mar 1997;110 (Pt 5):537-545.

45. Peters AH, Plug AW, van Vugt MJ, de Boer P. A drying-down technique for the spreading of mammalian meiocytes from the male and female germline. *Chromosome Res*. Feb 1997;5(1):66-68.
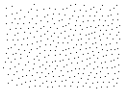
CHAPTER 6

CANINE MEIOTIC SEX CHROMOSOME
INACTIVATION IN COMBINATION WITH COMPLETE
HETEROLOGOUS SYNAPSIS

ABSTRACT

Pairing problems between autosomal chromosomes during the meiotic prophase in mouse spermatogenesis result in meiotic silencing of unsynapsed chromatin (MSUC), which causes transcriptional inactivation. However, if heterologous autosomal regions manage to synapse, by a mechanism called synaptic adjustment, MSUC is avoided and transcription continues.

Mammalian and avian heterologous sex chromosomes are always faced with pairing problems due to evolutionary physical and genetic divergence. Therefore, the sex chromosomes synapse only partially and are transcriptionally silenced through meiotic silencing of sex chromosomes (MSCI), a specialized form of MSUC. However, where X and Y chromosomes remain largely unsynapsed, the ZW pair becomes completely synapsed, although temporarily, but is still subjected to MSCI.

Herein, we investigated the behaviour of X and Y chromosomes during canine male meiotic prophase in order to study the possible variability in sex chromsome behaviour during meiotic prophase between different mammalian species. Such knowledge may help to identify critical components of the MSCI/MSUC pathway that are common among mammals.

In contrast to the male mouse sex chromosomes, the canine XY pair was found to synapse completely in the meiotic prophase, possibly in part through some self-synapsis of X. The canine X chromosome also shows persistent foci of the homologous recombination repair protein RAD51, but with progression of the heterologous synapsis between X and Y during pachytene, the number of RAD51 foci decreases At late pachytene, all RAD51 foci and γH2AX as a general marker of DNA damage, have disappeared, whereas the mouse X chromosome maintains RAD51 foci throughout pachytene and γH2AX until late diplotene. This indicates more rapid repair of meiotic DSBs on the canine X.

We postulate that once mammalian and avian MSCI is trigged, it remains activated, even in the presence of heterologous synapsis. Heterologous synapsis of X and Y in canine pachytene spermatocytes may facilitate homologous recombination repair of persistent meiotic DSBs, using the sister chromatid as a template for repair.

Since the canine XY can accomplish synapsis that is far more extensive and stable compared to what is observed for the mouse XY pair, this provides a previously unrecognized parallel between avian and mammalian MSCI.

INTRODUCTION

During vertebrate gametogenesis the homologous chromosomes have to pair and recombine during the meiotic prophase to obtain proper segregation during the two successive meiotic divisions. Failure of homologs to pair and/or synapse during meiotic prophase is associated with meiotic arrest and fertility problems (reviewed in [1]).

In mammals, males are heterogametic, carrying X and Y sex chromosomes, whereas females have two X chromosomes. In contrast, avian species have a female heterogametic sex with Z and W chromosomes, and males are ZZ. Although both XY and ZW sex chromosome pairs have evolved from an autosomal chromosome pair, they do not originate from the same pair of autosomes (reviewed in [2]). The evolutionary degeneration of both the Y and W chromosomes has led to a physical as well as a genetic divergence of Y and W from X and Z, respectively (reviewed in Chapter 2, [3]). Therefore, the heterogametic sex in both mammals and birds is faced with a sex chromosome pairing problem during meiotic prophase. The X and Y chromosomes share significant homology only in the small pseudoautosomal regions (PARs) (reviewed in [4]). Pairing and synapsis only takes place in the PARs and an obligatory crossover is formed in this region, ensuring proper segregation of both chromosomes during the meiotic divisions. The rest of the sex chromosomal arms remains unsynapsed. The unsynapsed state of X and Y is detected early during the meiotic prophase and leads to complete transcriptional inactivation, a process called meiotic sex chromosome inactivation (MSCI) (reviewed in [1]). The XY chromatin usually resides in the periphery of the nucleus and forms the socalled XY body [5].

MSCI is viewed as a specialized form of a more general silencing mechanism that also detects pairing problems of autosomal chromosomes, named meiotic silencing of unsynapsed chromatin (MSUC) [6-8]. MSCI is always triggered during meiotic prophase in the heterogametic sex, but the degree of MSUC is variable, and if autosomal heterologous regions manage to synapse, MSUC does not occur [6, 8, 9]. Such heterologous synapsis is achieved through an adaptive process called synaptic adjustment, in which the chromatin loop length is adjusted to equalize the axis length of the two chromosomal regions that are heterologous [10].

During meiotic prophase of avian oocytes, the heterologous Z and W chromosomes initially also only pair in their PARs, but with progression into pachytene, synapsis between Z and W extends progressively and at midpachytene they show complete heterologous synapsis. Since mammalian MSUC can be circumvented by heterologous synapsis, heterologous ZW synapsis was explained as a mechanism to prevent meiotic inactivation. Due to the longevity of oocytes, it was suggested that continued expression of Z and/or W-linked genes was

necessary for maintenance and growth, and inactivation by MSCI should be incompatible with survival until ovulation [12]. However, recently, we showed that although the ZW pair shows complete heterologous synapsis, it is still subjected to a transient form of MSCI [13]. In pachytene, Z and W-linked gene expression is repressed, but Z-genes and at least one W-linked gene show re-expression from diplotene onwards. The W chromosome is already heterologous upon entrance into meiotic prophase, and remains largely inactive in diplotene oocytes. Heterochromatization and inactivation immediately upon entrance of meiotic prophase was also observed for a very special single chromosome in zebra finch spermatocytes [14]. This socalled germline restricted chromosome (GRC), is present as a univalent and hence lacks a pairing partner [15,16]. However, even before homologous chromosome pairing is initiated, the GRC becomes heterochromatic and transcriptionally silenced. We named this mechanism meiotic silencing prior to synapsis (MSPS) [14]. Based upon the differences in timing and chromosome behaviour, the mechanisms to silence heterologous sex chromosomes in avian and mammalian meiotic prophase seem to be rather different, and could have evolved independently. However, there could be parallels between the two systems. First, there are indications that the mammalian Y chromosome may be in an already partially inactive state in spermatogonia [17]. Second, in mouse spermatocytes, the Y chromosome synapses almost completely with the X in early pachytene, and desynapses subsequently [18], whereas the larger part of the X chromosome remains unsynapsed throughout this process.

The pairing behaviour of the sex chromosomes during meiotic prophase in male mice and men have been documented and investigated [5,19,20]. However, even though the XY pair is subject to inactivation in these two mammalian species, the appearance and (dis)assembly of the synaptonemal complex on X and Y shows striking differences between the two species during mid and late pachytene (Reviewed in Chapter 2, [18,21]).

The behaviour of the mouse XY pair during meiosis is used as a model for sex chromosome dynamics representing the mammalian class. We wanted to establish how representative the mouse is for other mammals with respect to meiotic sex chromosome behaviour. Therefore, we decided to investigate the behaviour of another mammalian XY pair, namely that of the domestic dog (*Canis familiaris*). In evolution, the domestic dog descended from the common mammalian ancestor 50 million years ago [22], approximately 10 million years before the mouse did. Dogs are of particular interest in this respect, since mouse and man belong to the Euarchontoglires clade of placental mammals whereas dogs represent the Laurasiatheria. This clade also includes cats, cows, horses and pigs.

The diploid genome of the dog consists of 38 autosomal pairs and the sex chromosomal pair (http://www.ncbi.nlm.nih.gov/sites/entrez?Db=genomep

rj&cmd=ShowDetailView&TermToSearch=10726). Formation of the obligate crossover on the XY pair during meiotic prophase has been visualized through staining of spread spermatocyte nuclei for the mismatch repair proteins MLH1, that also marks crossover sites in mouse and man meiotic prophase cells [23]. However, no detailed analyses of the pairing behaviour and meiotic DNA double strand break (DSBs) repair dynamics of the dog X and Y during meiotic prophase have been described.

Here, we provide a detailed description of the assembly and disassembly of the synaptonemal complex during canine spermatogenesis. We show that the caninie XY pair achieves complete heterologous synapsis during pachytene. However, this synapsis does not lead to an escape from MSCI, and it may involve self-synapsis of X. In addition, meiotic DSB repair on the canine X appears to be completed around late pachytene, which is faster compared to the completion in diplotene in the mouse. Our data indicate that once MSCI is initiated, subsequent synapsis cannot alleviate the repression.

RESULTS AND DISCUSSION

The heterologous X and Y chromosomes of Canis familiaris completely synapse in pachytene

First, we visualized the progression of meiotic prophase and synapsis in canine spermatocytes. We immunostained for SYCP3, a component of the lateral element of the synaptonemal complex (SC), which assembles first along the chromosomal axes. In addition, we analysed the appearance of SYCP1, a component of the central element of the SC. The presence of SYCP1 indicates complete synapsis between chromosomal pairs.

At leptotene, short fragments of SYCP3 appear throughout the nucleus, shortly followed by the appearance of fragments of SYCP1, that colocalize with SYCP3, but are initially fewer in number (Figure 1a). This indicates that already early in leptotene, synapsis is achieved in small regions. In zygotene, long stretches of co-localized SYCP3 and SYCP1 fragments are present, in agreement with the known progression of synapsis between the homologous chromosomes (reviewed in Chapter 2). During zygotene in male mouse meiosis, thin continuous stretches of SYCP3 represent the chromosomal axes, and synapsis seems to starts from one or both ends and progresses towards the centre or the other end. During zygotene in canine spermatocytes, the SYCP3-SYCP1 assembly between the homologs is often interrupted at several places along the axes, giving the complexes a dashed-like appearance. In pachytene, the SC assembly is complete on all autosomes and SYCP3 and SYCP1 completely co-localize, indicating full synapsis.
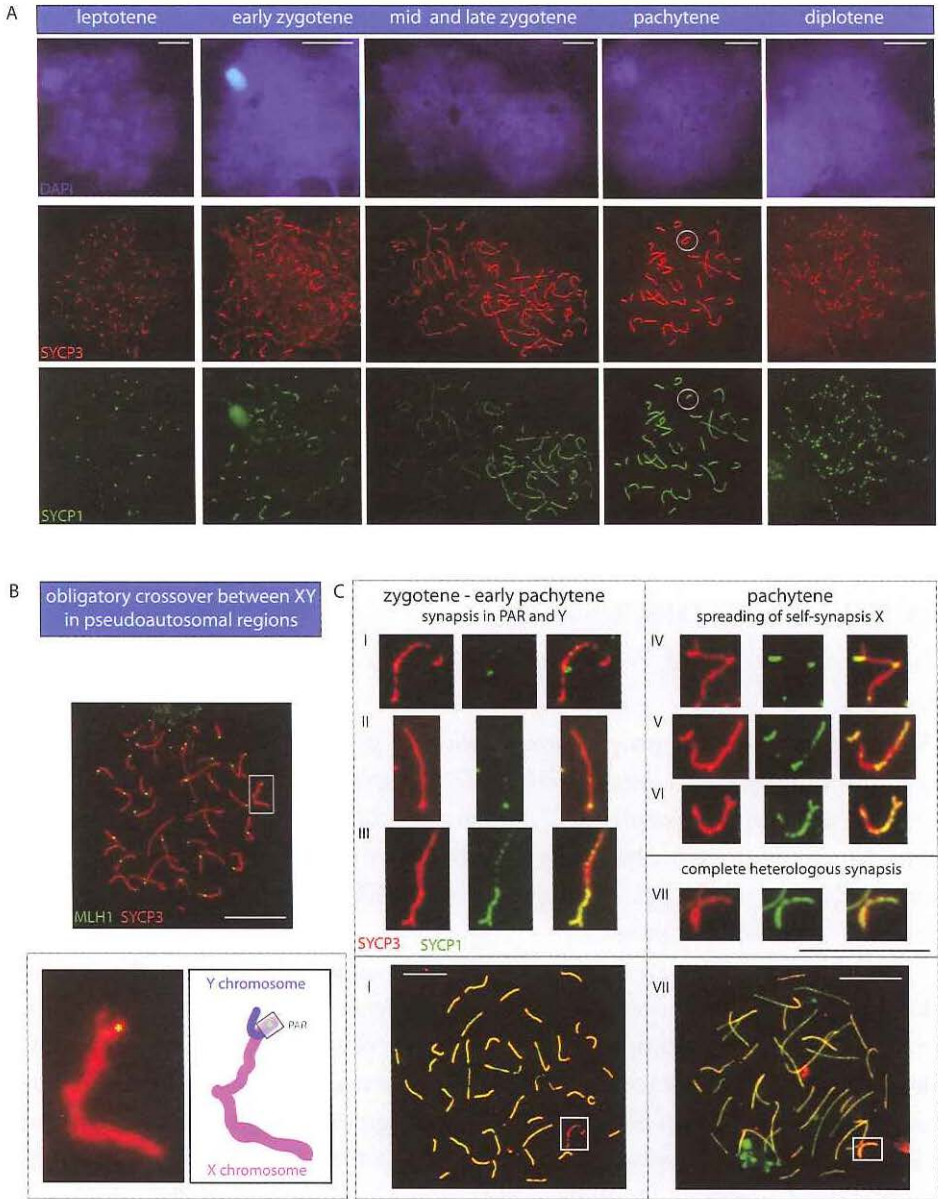
Figure 1. Overview of the canine male meiotic prophase and the progression of synapsis between the XY pair. (a) The different stages of the first meiotic prophase in canine spermatogenesis. The upper panel shows DAPI staining of the different canine meiotic nuclei, the middle and lower panel show the corresponding nuclei stained for respectively the synaptonemal complex lateral element of the SYCP3 (red) and the central element SYCP1 (green). The partially synapsed XY pair, which can be identified by the presence of the thick part of X and its horseshoe shape, is encircled. Bar represents 10 µm. (b) Spermatocyte spread nucleus stained for MLH1 (green) and SYCP3 (red). ▷

To identify the pseudoautosomal regions (PARs) and the location of the Y chromosome, we decided to immunostain for the DNA mismatch protein, MLH1. This protein is known to localize to the future crossover sites in pachytene nuclei of different mammalian species, including dog [23-25]. The obligatory crossover between X and Y takes place in the PARs (Figure 1b) during pachytene, and we observed a single MLH1-focus on the tip of the XY pair in almost all nuclei that also displayed MLH1 foci on the autosomes. Based upon this observation, we conclude that the small protruding part from these PARs, represents part of Y (Figure 1b).

At the beginning of pachytene, SYCP1 is only present at the tip of the XY pair, which represents the PARs. The rest of the X chromosome is positive for SYCP3, but not for SYCP1. Interestingly, the small part of Y that protrudes from the PARs is positive for SYCP1 (Figure 1c). It is unclear how SYCP1 can accumulate along this part of the Y chromosomal axes.

As pachytene progresses, the chromosomal axis of the long unpaired region of the X chromosome seems to lengthen and this is followed by shortening, which appears to be caused by the X chromosome folding back on itself (Figure 1c; IV). At midpachytene, the length of the XY pair is much shorter compared to early pachytene, and the intensity and thickness of the SYCP3 signal on the X is much higher and broader than on the autosomes, reminiscent of the avian Z behaviour during pachytene in the female meiotic prophase [13].

This behaviour of the canine X during the meiotic prophase is paralled by the appearance of both small fragments of SYCP1 on the unpaired part of X and spreading of SYCP1 from the PARs into the rest of the X chromosome. At this stage, the small SYCP1-positive part of the Y is still protruding. Around mid-pachytene, the Y chromosome has completely synapsed with X since the tip can
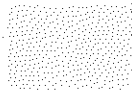
▷ The XY pair is boxed and the lower panel represents an enlargement of the boxed area; next to it a schematic drawing of the X and Y chromosomes is shown (X in pink, Y in bleu). The localization of the MLH1 focus indicates the area of the PARs and the tip of Y. Bar represents 10 µm. (c) Progression of heterologous synapsis between X and Y chromosomes from late zygotene until midpachytene. Spread nuclei were immunostained for SYCP3 (red) and SYCP1 (green). Initially, X and Y are completely unsynapsed (I; no SYCP1 colocalisation with SYCP3), followed by synapsis starting at the tip where the PARs are situated (II), recognisable by the protruding tip of Y, and from there it spreads towards the other tip (III). Simultaneously, small areas of SYCP1 appear on the unpaired part of X. Individual variations in de presence of SYCP1 on both the PARs-area and X can be seen (compare III, IV and V). In pachytene, X appears to fold back on itself (IV), after which longer stretches of SYCP1 appear on X (V, VI). At mid-to-late pachytene, SYCP1 and SYCP3 colocalize in 100% of cases (VII), indicating full heterologous synapsis between X and Y. The lower panel show the whole spread nuclei for respectively I and VII. Bar represents 5 µm.

sometimes no longer be seen, and the XY pair is completely positive for SYCP1 (Figure 1c; VII).

Hereafter, the SC must disassemble quickly, since we never observed nuclei corresponding to a transition stage between pachytene and diplotene. At diplotene, mostly intense SYCP1 and SYCP3 dots are visible, sometimes accompanied by thin stretches of SYCP3. Occasionally, we observed a remaining continuous SYCP3 complex in diplotene, while the rest of the nucleus exists only out of dots. The presence of H3K9me3 and the lack of H3K4me2 (see below) around this complex, indicate that this persistent complex represents the region that contains the XY pair.

H2BT119ph marks the axial axes of the completely synapsed XY pair at late pachytene

During pachytene in mouse spermatocytes, H2BT119ph marks the unpaired axes of autosomes and X and Y chromosomes, and is absent from the synapsed PARs [26]. To verify the completely synapsed state of the canine XY pair, we investigated the presence of H2BT119ph during the meiotic prophase.

H2BT119ph initially only marks the first half of the unsynapsed region of X (Figure 2), and we observed no presence on the synapsed PARs, nor on the Y. As mentioned above, we see the appearance of small patches of SYCP1 when the unpaired part of X has shortened, indicating that X has initiated some form of self-synapsis (Figure 1c). However despite the progression of synapsis,
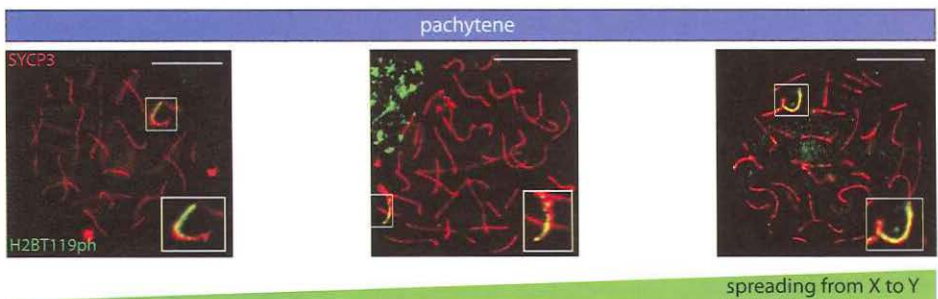
Figure 2. H2BT119ph, a marker of mouse mammalian unsynapsed chromosomal axes, is present on the synapsed axes of X and Y. Spermatocyte spread nuclei were immunostained for H2BT119ph (green) and SYCP3 (red). Initially, in early pachytene, H2BT119ph marks an area of the X. With progression of pachytene, H2BT119ph spreads towards the PARs, and during the completely synapsed stage it marks the whole XY pair. The XY pair is boxed and the enlargement represents the boxed XY pair. Bar represents 10 μm.

H2BT119ph spreaded gradually until it covered the complete XY chromosomal axes. At the end of pachytene, H2BT119ph is present all along the axes of the XY pair, despite the fact that we earlier showed that SYCP1 is present along all the XY axes, indicating a completely synapsed state (Figure 2).

DNA double strand break repair on XY follows the progression of heterologous synapsis between XY

Due to the largely nonhomologous state of X and Y and Z and W, SPO11-induced meiotic DNA double strand break repair is generally delayed on the sex chromosomes ([27] and Chapter 2). To visualize the dynamics of DNA double strand break formation and repair on the canine XY, we first analysed the presence of the homologous recombination repair protein, RAD51 (Figure 3a). At leptotene, many RAD51 foci, indicative for the presence of DNA double strand breaks (DSBs) appear throughout the nucleus and the number of foci decreases during zygotene (not shown). In pachytene, only a few foci remain present on the synapsed axes of autosomes, whereas the X chromosome still carries a lot of bright RAD51 foci (Figure 3a). With progression of pachytene, and the process of heterologous synapsis between X and Y, the number of foci on X declines. When X and Y are completely synapsed around midpachytene, all foci have disappeared. Since we never observed reappearance of RAD51 foci, as we did during female meiotic prophase in chicken [13], this indicates that the DSBs on the canine X have been repaired already before the end of pachytene, which is much earlier than during meiotic prophase in female chicken and male mouse, when RAD51 foci persist throughout pachytene and only disappear during diplotene.
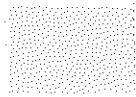
Simultaneously with the appearance of RAD51 foci, a general marker of DSBs, γH2AX appears. γH2AX represents the phosphorylated form of H2AX. This variant of H2A can be phosphorylated by the checkpoint kinases ATR and ATM or by DNA-PKcs in somatic cells in response to DNA damage [28]. During meiotic prophase in mouse, ATM phosphorylates H2AX at meiotic DSBs [28-30]. Later, ATR is responsible for the formation of γH2AX at the XY body [29]. In canine leptotene spermatocytes, γH2AX covers the whole nucleus, indicative of the presence of the numerous unrepaired meiotic DSBs (not shown), and at the end of zygotene, it concentrates mainly on the X and Y. Contrary to the autosomes, X and Y are often still separate at this stage. In pachytene, γH2AX covers the now paired X and Y, and increases in intensity. The unsynapsed part of X, mostly displays a higher intensity of γH2AX than the synapsed region (Figure 3b, early-mid pachytene). This could be due to either the presence of the unrepaired DSBs on X or the activation of MSCI by the the unsynapsed state of X.
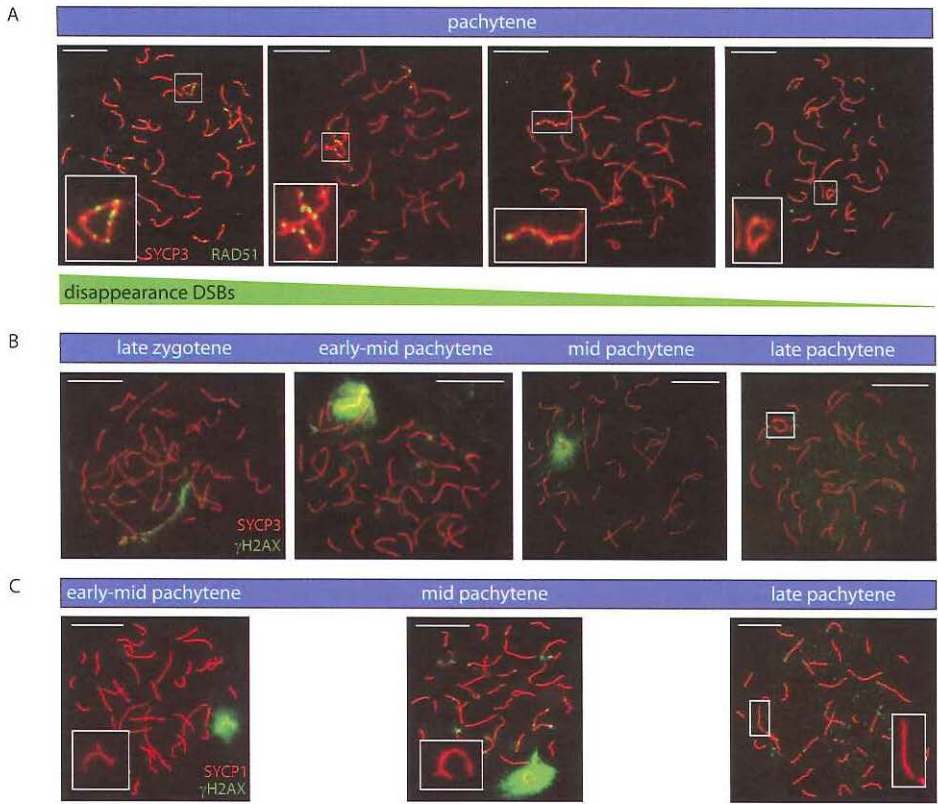
Figure 3. DNA double strand breaks on the XY pair are repaired during synapsis. Canine spermatocyte spread nuclei were immunostained for RAD51 (green) and SYCP3 (red) (upper panel), γH2AX (green) and SYPC3 (red) (middle panel) and γH2AX (green) and SYCP1 (red) (lower panel). (a) In early pachytene, only few RAD51 foci are present on the autosomes, whereas many foci remain present on the XY pair. With progression of synapsis between X and Y, the number of RAD51 foci on XY is reduced and when the XY pair is completely synapsed, all RAD51 foci have disappeared. The XY pair is boxed. Enlargement represents the boxed XY pair. Bar represents 10 μm. (b) At late zygotene, γH2AX levels on the autosomes decrease, indicating completion of repair of meiotic DNA double strand breaks at these sites. However, the intensity of γH2AX increases on the unpaired X and Y chromosomes, indicative of either the presence of unrepaired DNA double strand breaks or initiation of MSCI, or both. The intensity of γH2AX on X and Y increases in early pachytene and remains present during the progression of DNA double strand break repair and the process of synapsis. At midpachytene, γH2AX increases intensively on the completely synapsed XY. At late pachytene, γH2AX is lost from the XY pair. Bar represents 10 μm. (c) In pachytene, γH2AX is present on the XY pair while synapsis progresses (SYCP1). When SYPC1 is present along all the axes, γH2AX starts to disappear, and in late pachytene no γH2AX is present. Bar represents 10 μm.

γH2AX is also the earliest known marker of MSCI in mouse spermatocytes [31], and although the canine X and Y become completely synapsed at midpachytene, the intensity of γH2AX increases and is highest and uniform at midpachytene. At the end of pachytene, γH2AX is lost from the YX pair, and γH2AX can be observed as a diffuse nuclear staining, which remains present in diplotene. The complete loss of high intensity γH2AX accumulation from the XY pair further supports the conclusion that all DSBs on X have been repaired at the end of pachytene.

Complete heterologous synapsis of the XY pair is associated with normal MSCI
In addition to being the earliest known marker of the mouse XY body, γH2AX is required for the initiation of MSCI in mouse spermatocytes [31]. Since the canine XY-pair is highly positive for γH2AX, we next investigated other markers of mammalian and avian MSCI.

First, we analysed the presence of RNA polymerase II, a general marker for active transcription. The overall level of RNA polymerase II was relatively low in pachytene nuclei. However, the XY-pair still appeared relatively devoid of RNA polymerase II as compared to the rest of the nucleus (Figure 4a), indicating a lack of transcriptional activity.

H3K27me3, which is reduced on the mammalian and marsupial sex body [17, 19] but is a prominent marker of the avian W chromosome [13], appears in a foci-like fashion around the XY pair in pachytene (Figure 4b), with its highest concentration around the region that represents the Y chromosome and the PARs.

Ubiquitylation of lysine 119 of H2A is associated with gene silencing and marks the inactive mammalian and avian sex chromosomes in pachytene and diplotene [13, 32]. However, we did not observe enrichment of H2AK119ub1 on the chromatin of the canine XY pair. Intriguingly, an antibody that recognizes all conjugated ubiquitin (Figure 4b; FK2) showed a focal staining pattern on the unsynapsed region of X in pachytene, resembling the pattern of H3K27me3.

The ubiquitin-conjugating enzyme HR6B/UBE2B is a prominent marker of the silenced XY-body in mouse spermatocytes and plays a role in the maintenance of inactivation of the sex chromosomes during the postmeiotic stages [9, 26]. Here, we observed a bright focal pattern of HR6B/UBE2B covering the whole canine XY pair in pachytene (Figure 4b; HR6A/B-S120ph).

The concentration of a marker for transcriptionally potentiated chromatin, H3K4me2, is much lower on the canine XY pair compared to the signal in the rest of the chromatin in pachytene (Figure 4b), resembling what is also observed for the XY body in pachytene mouse spermatocytes [26]. In diplotene, an area with a relatively low concentration of H3K4me2 persists, and often co-localizes with a continuous SYCP3 complex (not shown), indicating that
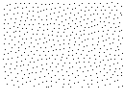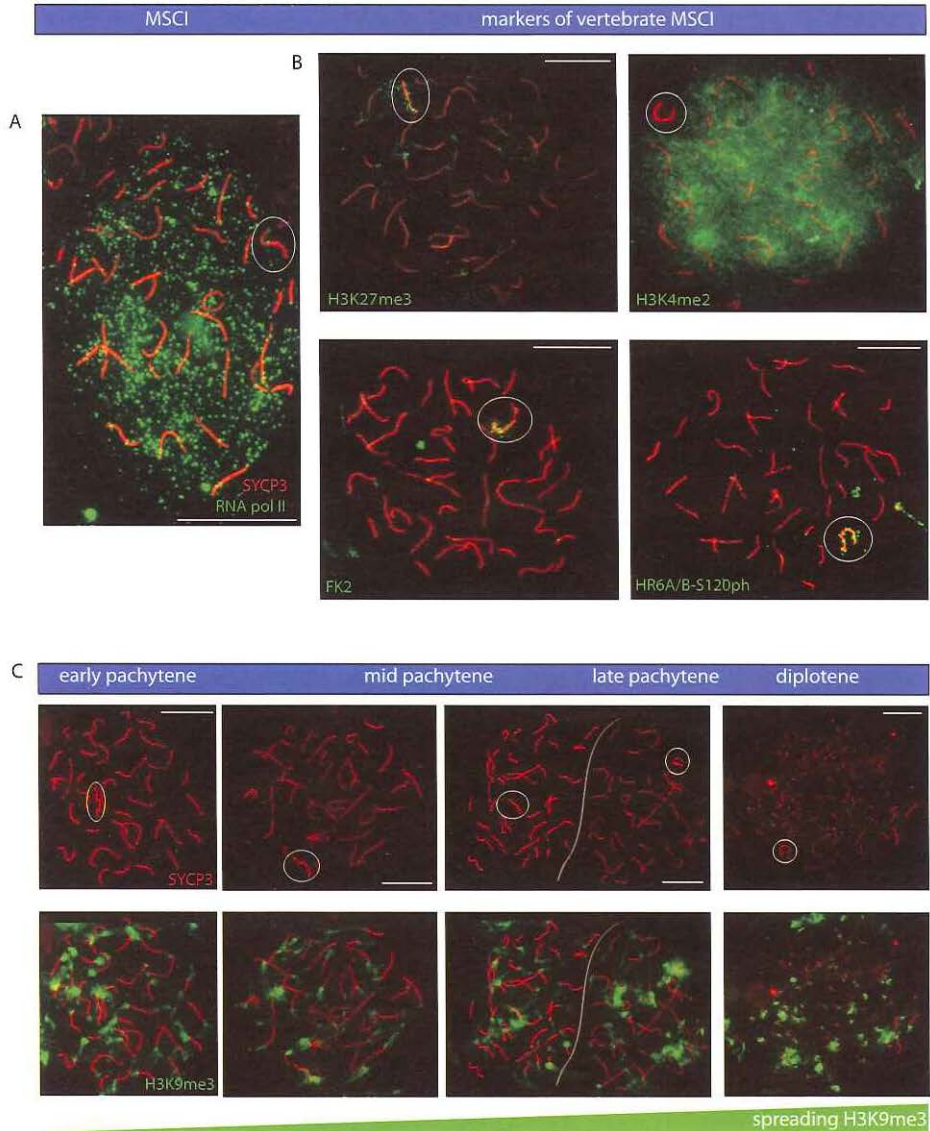
Figure 4. Presence of mammalian and avian MSCI markers on canine XY pair.
Spermatocyte spread nuclei were immunostained for (a) RNA polymerase II (green);
(b) H3K27me3 (green), FK2 (green), H3K4me2 (green), HR6A/B-S120ph (green) and
SYCP3 (red); (c) H3K9me3 (green) and SYCP3 (red). (a) The RNA pol II signal is evenly
spread throughout the nucleus, and is reduced around the XY pair. Bar represents 10
μm. (b) During pachytene, H3K27me3, H3K4me3 and HR6A/B-S120ph are present
on the XY pair, while H3K4me2 is strongly reduced around XY. Bar represents 10 μm.
(c) H3K9me3, which initially marks the Y and the PARs, spreads during the process
of heterologous synapsis distally towards the X. Spermatocyte spread nuclei were
immunostained for H3K9me3 (green) and SYCP3 (red). Early in pachytene, H3K9me3 ▷

MSCI might persist beyond pachytene. Together, these data indicate that once MSCI has been triggered during early canine meiotic prophase, when X and Y have not yet synapsed, MSCI is maintained even during the phase of complete heterologous synapsis. This shows some resemblance to the avian ZW pair. In chicken oocytes, the first signs of MSCI of the ZW pair can be visualized around early pachytene, and repression continues and is most evident during the state of complete heterologous synapsis at mid pachytene [13]. However, in contrast to the apparent postponement of DSB-repair until diplotene in chicken oocytes, repair of meiotic DSBs at the canine X appear to occur during pachytene.

H3K9me3 originates from Y and then spreads to X during their synapsed state

Another general marker of transcriptional inactivation and heterochromatin is the histone modification H3K9me3. This modification specifically marks the inactive germline restricted chromosome (GRC) in spermatocytes of the zebra finch and the avian W chromosome upon entry in meiotic prophase [13, 14].

Early in pachytene, only the protruding tip of Y and the PARs are positive for H3K9me3, but this appears to spread distally along the expanding synapsed area to the X during the process of heterologous synapsis (Figure 4c). When X and Y are completely synapsed, H3K9me3 is enriched on the whole XY body, resembling the heterologously synapsed avian ZW pair [13]. In diplotene, an area containing the remaining SYCP3 complex is still positive for H3K9me3 (Figure 4c), which resembles the region in which we found the relatively low concentration of H3K4me2 (not shown). However, these findings are pending to be verified by fluorescent in situ hybridization, using probes for canine X and Y.

CONCLUSIONS

At late zygotene, the canine X and Y chromosomes are the last chromosomal pair that remains unpaired as compared to the fully synapsed autosomes. In addition, X and Y are both marked by unrepaired DSBs and an increasing presence of γH2AX. The presence of γH2AX at this stage most likely represents the second wave of γH2AX formation, associated with the initiation of mammalian MSCI, which might be triggered by the presence of unrepaired DSBs and the unsynapsed configuration. Despite progression of synapsis between the heterologous X and Y chromosomes during pachytene, markers of avian and mammalian MSCI

▷ marks the centromeres of the autosomes and the protruding tip of Y intensively. H3K9me3 then seems to spreads towards the PARs and further along the X chromosome. When X and Y are completely synapsed and form a horse-shoe shape, H3K9me3 completely covers the XY pair. In diplotene, a same horse-shoe shaped SYCP3 complex, is also completely covered with H3K9me3. The XY pair is encircled. Bar represents 10 μm.

accumulate and spread on the silenced canine XY pair. In contrast to described escape from MSUC of heterologous synapsed chromatin in mouse meiotic prophase [6, 8, 9], heterologous synapsis between the canine X and Y cannot undo MSCI. In addition, the persistent DSBs on X appear to be repaired during the process of synapsis.

Based on the length of the Y axial element visualized by SYCP3-immunostaining, the canine Y is much smaller relative to X, comparable to how the length of the chicken W relates to the chicken Z chromosome. While we proposed that H3K9me3 spreads from the chicken W onto the Z during their complete synapsed state [13], such a scenario seems unlikely for the canine Y and X. However, it cannot be excluded that the heterochromatic Y causes chromatic alteration during its heterologous synapsis with X, allowing heterochromatization of the XY pair. Most likely, the initiation of MSCI in dogs occurs in a manner that is similar to what occurs in mouse and man, and functionally involves the early accumulation of γH2AX on the unsynapsed X and Y. The lack of H3K4me2 and the presence of H3K9me3 around the remaining SYCP3 complex during diplotene suggest maintenance of MSCI beyond pachytene, which would also resemble the behaviour of mouse and marsupial XY [17, 19, 33].

Although marsupial, mouse and canine sex chromosome behaviour resemble each other, such as the initiating accumulation of γH2AX and the lack of RNA polymerase II, the extensive heterologous synapsis, most likely including self-synapsis of X of the dog XY pair, provides novel information. First, heterologous synapsis does not lead to a release from MSCI once this has been established. Second, the disappearance of RAD51 and γH2AX during XY synapsis indicates that heterologous synapsis may facilitate meiotic DSB repair in heterologous regions. It might be suggested that achieving synapsis releases the inhibition to repair meiotic DSBs via the sister chromatids. Finally, the achievement of complete synapsis between X and Y in a mammalian species, such as the dog studied herein, and possibly also in other mammalian species, provides a strong parallel to meiotic silencing in avian species

MATERIALS AND METHODS

Meiotic spread nuclei preparations, immunocytochemistry and FISH analysis
Testes were isolated from adult dog. Spread nuclei preparations of dog spermatocytes were prepared from fresh and frozen testis fragments using a modification of the drying-down technique described by Peters et al. [34]. For immunocytochemistry, frozen slides were defrosted at room temperature and washed with PBS. The slides were blocked with PBS containing 0.5% w/v BSA

and 0.5% w/v milk powder, and were double stained with rabbit polyclonal anti-SYCP3 (1:1000) (gifts from C. Heyting, Wageningen), or goat anti-SYCP3 (1:100) (R&D System, Minneapolis, USA), rabbit polyclonal anti-SYCP1 (1:200) (gifts from C. Heyting, Wageningen), mouse monoclonal anti-MLH1 (1:250 (BD Pharmingen, San Diego, USA), rabbit polyclonal anti-RNA polymerase II (8WG16) directed against the RNA polymerase II CTD repeat YSPTSPS (1:600) (Abcam, Cambridge, United Kingdom), rabbit anti-human RAD51 (1:500) [35], rabbit anti- HR6A/B-S120ph [36], mouse monoclonal IgM anti-H2AK119ub1 (1:1000) (Upstate, Walthum, MA, USA), mouse monoclonal anti-H3K27me3 (1:100) (Abcam), rabbit polyclonal anti-H3K9me3 (1:500) (Upstate), rabbit polyclonal anti-H2BT119ph (1:100)[26], rabbit polyclonal anti-H3K4me2 1:500 (Upstate), rabbit polyclonal anti-H3K9me3 (1:500) (Upstate), rabbit polyclonal anti-FK2 1:1000 (Millipore, MA, USA).

For rabbit polyclonal primary antibodies, the secondary antibodies were fluorescein isothiocyanate (FITC)-labeled goat anti-rabbit IgG antibodies (1:128) (Sigma, St Louis, USA) and tetramethylrhodamine isothiocyanate (TRITC)-labeled goat anti-mouse IgG antibodies (1:128) (Sigma) ; the secondary antibodies used for mouse monoclonal anti-MLH1 (IgG) were Alexa 594-labeled goat anti-mouse IgG (Molecular Probes/Invitrogen, CA, USA) and FITC-labeled goat anti-mouse IgG (Sigma) respectively; for goat primary antibody, the secondary antibody was Alexa 543-labeled donkey anti-goat IgG (Molecular Probes/ Invitrogen, CA, USA). Primary antibodies were diluted in 10% w/v BSA in PBS and incubated overnight in a humid chamber. Thereafter, slides were washed in PBS, blocked in 10% v/v normal goat serum (Sigma) or swine serum (Sigma) in blocking buffer (5% milk powder (w/v in PBS, centrifuged at 13,200 rpm for 10 min), and incubated with secondary antibodies in 10% v/v normal goat serum or swine serum respectively in blocking buffer at room temperature for 2 hours. Next, the slides were washed in PBS and embedded in Vectashield containing DAPI (4',6'-diamindino-2-phenylindole) (Vector Laboratories, Burlingame CA, USA).

Fluorescence microscopy analysis, digital image preparation and analysis
Analysis of the spermatocyte nuclei was performed using a Carl Zeiss Axioplan 2 imaging microscope (Jena, Germany) with a plan-neofluar objective 100x/1.3 oil immersion. Images were taken with a Coolsnap-pro digital camera (Photometrics, Waterloo, Canada). The acquired digital images were processed with Photoshop software (Adobe Systems).

REFERENCES

1. Turner JM. Meiotic sex chromosome inactivation. *Development.* May 2007;134(10):1823-1831.
2. Ezaz T, Stiglec R, Veyrunes F, Marshall Graves JA. Relationships between vertebrate ZW and XY sex chromosome systems. *Curr Biol.* Sep 5 2006;16(17):R736-743.
3. Marshall Graves JA. Weird animal genomes and the evolution of vertebrate sex and sex chromosomes. *Annu Rev Genet.* 2008;42:565-586.
4. Graves JA. Sex chromosome specialization and degeneration in mammals. *Cell.* Mar 10 2006;124(5):901-914.
5. Solari AJ. The behavior of the XY pair in mammals. *Int Rev Cytol.* 1974;38(0):273-317.
6. Baarends WM, Wassenaar E, van der Laan R, et al. Silencing of unpaired chromatin and histone H2A ubiquitination in mammalian meiosis. *Mol Cell Biol.* Feb 2005;25(3):1041-1053.
7. Schimenti J. Synapsis or silence. *Nat Genet.* Jan 2005;37(1):11-13.
8. Turner JM, Mahadevaiah SK, Fernandez-Capetillo O, et al. Silencing of unsynapsed meiotic chromosomes in the mouse. *Nat Genet.* Jan 2005;37(1):41-47.
9. van der Laan R, Uringa EJ, Wassenaar E, et al. Ubiquitin ligase Rad18Sc localizes to the XY body and to other chromosomal regions that are unpaired and transcriptionally silenced during male meiotic prophase. *J Cell Sci.* Oct 1 2004;117(Pt 21):5023-5033.
10. Moses MJ, Poorman PA. Synaptosomal complex analysis of mouse chromosomal rearrangements. II. Synaptic adjustment in a tandem duplication. *Chromosoma.* 1981;81(4):519-535.
11. Homolka D, Ivanek R, Capkova J, Jansa P, Forejt J. Chromosomal rearrangement interferes with meiotic X chromosome inactivation. *Genome Res.* Oct 2007;17(10):1431-1437.
12. Jablonka E, Lamb MJ. Meiotic pairing constraints and the activity of sex chromosomes. *J Theor Biol.* Jul 8 1988;133(1):23-36.
13. Schoenmakers S, Wassenaar E, Hoogerbrugge JW, Laven JS, Grootegoed JA, Baarends WM. Female meiotic sex chromosome inactivation in chicken. *PLoS Genet.* May 2009;5(5):e1000466.
14. Schoenmakers S, Wassenaar E, Laven JS, Grootegoed JA, Baarends WM. Meiotic silencing and fragmentation of the male germline restricted chromosome in zebra finch. *Chromosoma.* Jun;119(3):311-324.
15. Pigozzi MI, Solari AJ. Germ cell restriction and regular transmission of an accessory chromosome that mimics a sex body in the zebra finch, Taeniopygia guttata. *Chromosome Res.* Feb 1998;6(2):105-113.
16. Pigozzi MI, Solari AJ. The germ-line-restricted chromosome in the zebra finch: recombination in females and elimination in males. *Chromosoma.* Dec 2005;114(6):403-409.
17. Namekawa SH, Park PJ, Zhang LF, et al. Postmeiotic sex chromatin in the male germline of mice. *Curr Biol.* Apr 4 2006;16(7):660-667.
18. Tres LL. Extensive pairing of the XY bivalent in mouse spermatocytes as visualized by whole-mount electron microscopy. *J Cell Sci.* Jun 1977;25:1-15.
19. Namekawa SH, VandeBerg JL, McCarrey JR, Lee JT. Sex chromosome silencing in the marsupial male germ line. *Proc Natl Acad Sci U S A.* Jun 5 2007;104(23):9730-9735.
20. Oliver-Bonet M, Ko E, Martin RH. Male infertility in reciprocal translocation carriers: the sex body affair. *Cytogenet Genome Res.* 2005;111(3-4):343-346.
21. Chandley AC, Goetz P, Hargreave TB, Joseph AM, Speed RM. On the nature and extent of XY pairing at meiotic prophase in man. *Cytogenet Cell Genet.* 1984;38(4):241-247.

22. Kumar S, Hedges SB. A molecular timescale for vertebrate evolution. *Nature*. Apr 30 1998;392(6679):917-920.
23. Basheva EA, Bidau CJ, Borodin PM. General pattern of meiotic recombination in male dogs estimated by MLH1 and RAD51 immunolocalization. *Chromosome Res*. 2008;16(5):709-719.
24. Anderson LK, Reeves A, Webb LM, Ashley T. Distribution of crossing over on mouse synaptonemal complexes using immunofluorescent localization of MLH1 protein. *Genetics*. Apr 1999;151(4):1569-1579.
25. Baker SM, Plug AW, Prolla TA, et al. Involvement of mouse Mlh1 in DNA mismatch repair and meiotic crossing over. *Nat Genet*. 1996;13(3):336-342.
26. Baarends WM, Wassenaar E, Hoogerbrugge JW, Schoenmakers S, Sun ZW, Grootegoed JA. Increased phosphorylation and dimethylation of XY body histones in the Hr6b-knockout mouse is associated with derepression of the X chromosome. *J Cell Sci*. Jun 1 2007;120(Pt 11):1841-1851.
27. Inagaki A, Schoenmakers S, Baarends WM. DNA double strand break repair, chromosome synapsis and transcriptional silencing in meiosis. *Epigenetics*. May 16;5(4).
28. Rogakou EP, Boon C, Redon C, Bonner WM. Megabase chromatin domains involved in DNA double-strand breaks in vivo. *J Cell Biol*. Sep 6 1999;146(5):905-916.
29. Bellani MA, Romanienko PJ, Cairatti DA, Camerini-Otero RD. SPO11 is required for sex-body formation, and Spo11 heterozygosity rescues the prophase arrest of Atm-/-spermatocytes. *J Cell Sci*. Aug 1 2005;118(Pt 15):3233-3245.
30. Mahadevaiah SK, Turner JM, Baudat F, et al. Recombinational DNA double-strand breaks in mice precede synapsis. *Nat Genet*. Mar 2001;27(3):271-276.
31. Fernandez-Capetillo O, Mahadevaiah SK, Celeste A, et al. H2AX is required for chromatin remodeling and inactivation of sex chromosomes in male mouse meiosis. *Dev Cell*. Apr 2003;4(4):497-508.
32. Baarends WM, Hoogerbrugge JW, Roest HP, et al. Histone ubiquitination and chromatin remodeling in mouse spermatogenesis. *Dev Biol*. Mar 15 1999;207(2):322-333.
33. Turner JM, Mahadevaiah SK, Ellis PJ, Mitchell MJ, Burgoyne PS. Pachytene asynapsis drives meiotic sex chromosome inactivation and leads to substantial postmeiotic repression in spermatids. *Dev Cell*. Apr 2006;10(4):521-529.
34. Peters AH, Plug AW, de Boer P. Meiosis in carriers of heteromorphic bivalents: sex differences and implications for male fertility. *Chromosome Res*. Aug 1997;5(5):313-324.
35. Essers J, Hendriks RW, Wesoly J, et al. Analysis of mouse Rad54 expression and its implications for homologous recombination. *DNA Repair (Amst)*. Oct 1 2002;1(10):779-793.
36. Mulugeta Achame E, Wassenaar E, Hoogerbrugge JW, et al. The ubiquitin-conjugating enzyme HR6B is required for maintenance of X chromosome silencing in mouse spermatocytes and spermatids. *BMC genomics*. 2010;11:367.

CHAPTER 7

INCREASED PHOSPHORYLATION AND
DIMETHYLATION OF XY BODY HISTONES IN THE
HR6B-KNOCKOUT MOUSE IS ASSOCIATED WITH
DEREPRESSION OF THE X CHROMOSOME

ABSTRACT

Mono-ubiquitylated H2A marks the transcriptionally silenced XY body during male meiotic prophase. Concomitant with H2AK119ub1, the ubiquitin-conjugating enzyme HR6B is also enriched on the XY body. We analysed H2A and H2B ubiquitylation in *Hr6b* knockout mouse spermatocytes, but no global changes were detected. Next, we analyzed phosphorylation of the threonine residues T120 and T119 that are adjacent to the K119 and K120 target sites for ubiquitylation in H2A and H2B, respectively. In wild type cells, H2AT120ph and mark meiotically unpaired and silenced chromatin, including the XY body. In *Hr6b* knockout spermatocytes, the signal was unchanged, but H2AT120ph was enhanced from late pachytene until metaphase I. Furthermore, we found increased H3K4 dimethylation on the X and Y chromosomes of diplotene *Hr6b* knockout spermatocytes, persisting into postmeiotic round spermatids. In these cells, the X and Y chromosomes maintained an unchanged H3K9me2 level, even when this modification was lost from centromeric heterochromatin. Analysis of gene expression showed derepression of X-chromosomal genes in postmeiotic *Hr6b* knockout spermatids. We conclude that HR6B exerts control over different histone modifications in spermatocytes and spermatids, and that this function contributes to the postmeiotic maintenance of X chromosome silencing.

INTRODUCTION

Chromatin structure regulation requires the concerted actions of different histone modifying enzymes and ATP-dependent chromatin remodeling complexes. The combined presence of specific histone modifications, such as acetylation, phosphorylation, methylation, ubiquitylation, and sumoylation, on the four core histones (H2A, H2B, H3, H4) that constitute the nucleosome, has been termed the histone code which is "read" by regulatory effector proteins [1].

Histone mono-ubiquitylation [2] and histone sumoylation [3] involve addition of a peptide rather than a smaller organic group. Ubiquitin is a M_r 7000 peptide that is attached to lysine residues of substrates through the subsequent action of ubiquitin-activating (E1), ubiquitin-conjugating (E2) and ubiquitin-ligating (E3) enzymes. Poly-ubiquitylation usually targets a substrate for degradation by the proteasome [4] whereas mono-ubiquitylation is involved in various processes including DNA repair and regulation of gene expression [5].

The ubiquitin-conjugating enzymes HR6A and HR6B are two very similar mouse homologs of the *S. cerevisiae* RAD6 protein [6,7]. In yeast, RAD6 is required for ubiquitylation of H2BK123, together with an E3 named BRE1 [8-10]. H2AK119 is not ubiquitylated in yeast, but it is a prominent ubiquitylation substrate in mammalian cells, since as much as 10% of H2A, as compared to 0.1-2% of H2B, is ubiquitylated in most mammalian cell types investigated [11,12]. To study the possible role of HR6A and HR6B in histone ubiquitylation in mammalian cells, knockout or knock-down approaches are required. In mouse, the *Hr6a* gene is located on the X chromosome, and *Hr6b* localizes to chromosome 11. Knockout mice for each individual gene were generated, but *Hr6a-Hr6b* double-knockouts are not viable, indicating that the two encoded proteins perform essential redundant functions [6]. In most cell types, HR6A and HR6B protein levels are approximately equal, but oocytes contain a relatively high HR6A dose, explained by the presence of two active X chromosomes [6]. Conversely, male germline cells show a relatively low HR6A expression associated with inactivation of the X and Y chromosomes during male meiotic prophase (see below), while HR6B expression is maintained at a high level [13]. In the female and male germlines, there is a specific requirement for *Hr6a* and *Hr6b*, respectively, as reflected by the infertility phenotypes of *Hr6a* knockout females and *Hr6b* knockout males [6,7].

During male meiotic prophase, the X and Y chromosomes remain largely unpaired, with exception of the so-called pseudoautosomal regions. The XY body is formed when the X and Y chromosomes are transcriptionally inactivated, by a mechanism named "meiotic silencing of unsynapsed chromatin" (MSUC) [14]. Proteins that are specifically associated with the XY body during meiotic prophase, may play a role in MSUC. In particular, recruitment of the checkpoint

kinase ATR by the BRCA1 protein and subsequent phosphorylation of serine 139 of H2AX have been shown to be essential for MSUC [15-17]. Interestingly, H2AK119ub1 is also enriched on the XY body, concomitant with accumulation of the HR6B enzyme [18, 19]. However, HR6A- or HR6B-dependent histone modifications in mammalian cells have not been described.

Hr6b knockout spermatocytes display an increased frequency of meiotic recombination, possibly related to disruption of the structural organization of the paired chromosomes as a consequence of dysregulation of histone modifications [20]. In yeast, RAD6 dependent H2BK123 ubiquitylation is required for H3K4 and H3K79 methylation in a trans-histone regulatory mechanism [21-23]. In addition, neighboring amino acid residues can be modified by different posttranslational modifications, and this was proposed to function as a binary switch [24]. The existence of such a binary switch in H3 was recently shown to involve stable methylation on Lys9 and transient phosphorylation of Ser10 [25]. The H2A and H2B ubiquitin-accepting lysines together with their respective adjacent threonine residues may also form binary switches [24]. It is not known whether H2BT119 is phosphorylated, but H2AT120 is phosphorylated by nucleosomal histone kinase-1 (NHK-1) in *Drosophila* [26]. Based on the findings of trans-histone regulation in yeast and the binary switch model, we have analysed histone ubiquitylation, as well as H2AT120 and H2BT119 phosphorylation, and H3K4 and H3K9 methylation in wild type and *Hr6b* knockout animals. Finally, we have analysed changes in X-chromosomal gene expression in wild type and *Hr6b* knockout meiotic and postmeiotic spermatogenic cells.

RESULTS

Histone H2AK119 and H2BK120 ubiquitylation

In analogy to the function of RAD6 in yeast, ubiquitylation of H2BK120 is the most obvious candidate histone modification that could be affected in *Hr6b* knockout mice. To study the effect of loss of HR6B on H2BK120 ubiquitylation in spermatogenesis we analysed H2BK120 ubiquitylation in spermatocytes and spermatids isolated from wild type and *Hr6b* knockout testes. Antibodies that specifically recognize ubiquitylated H2BK120 are not available, and we used anti-H2B to detect both H2B and H2BK120ub1 (Figure 1a). In addition, the use of antibodies against ubiquitin and H2AK119ub1 allowed us to compare the amounts of H2AK119ub1 and H2BK120ub1 (Figure 1b). The results show that the global levels of H2AK119 and H2BK120 ubiquitylation are not affected in *Hr6b* knockout spermatogenic cells (Figure 1b).
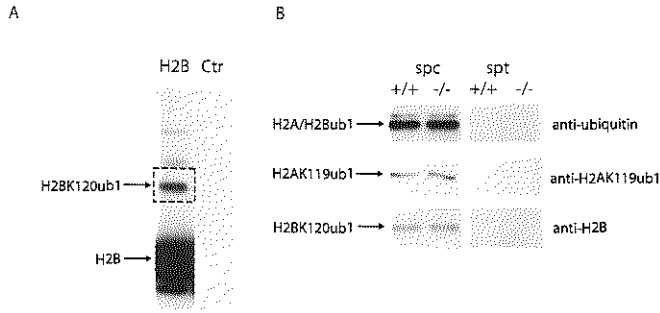
Figure 1. HR6B is not required for histone ubiquitylation in spermatocytes. (a) Basic nuclear proteins were isolated from purified spermatocytes, and analysed on Western blots using anti-H2B. The antibody recognizes unmodified H2B and H2BK120ub1 (both indicated by arrows). In the control lane (Ctr), the first antibody was omitted from the incubation mixture. The boxed area is presented for each immunostaining in (b). (b) Histone ubiquitylation was analysed in spermatocytes (spc) and spermatids (spt) isolated from wild type (+/+) and *Hr6b* knockout (-/-) mice. From top to bottom, antibodies were targeting ubiquitin, H2AK119ub1, and H2B as indicated on the right side of the blots, and the modified histones are indicated by arrows. Representative results are shown; each experiment was repeated at least twice with germ cell preparations isolated from a different pool of mice. Equal amounts of protein were present in each lane, as verified by Ponceau S staining of the blot (not shown).

Histone H2AT120 and H2BT119 phosphorylation

The binary switch model predicts that phosphorylation of the threonines that are immediately adjacent to Lys119 and Lys120 in H2A and H2B, respectively, would take part in a mechanism to regulate binding of effectors of the histone code [24]. In this mechanism, the pattern of ubiquitylation and phosphorylation at these neighbouring residues may be interdependent. To analyse these modifications in wild type and *Hr6b* knockout spermatocytes, we performed immunocytochemical analysis using specific antibodies against phosphorylated H2AT120 and H2BT119. To identify the different substages of meiotic prophase, we co-stained with an antibody that recognizes SYCP3. This protein is a component of the axial elements (before synapsis) or lateral elements (during synapsis) of the synaptonemal complex (SC) that forms between the chromosomal axes of pairing homologous chromosomes during meiotic prophase (reviewed by [27]). Round spermatids are recognized using DAPI staining of DNA, which also visualizes the chromocenter, a heterochromatic dense-staining round area containing the centromeric DNA in the center of the spermatid nucleus.

The highest level of H2BT119ph was observed along the unpaired axial elements of the X and Y chromosomes of pachytene and diplotene spermatocytes, and a lower level extended over the rest of the XY body chromatin (Figure 2a).
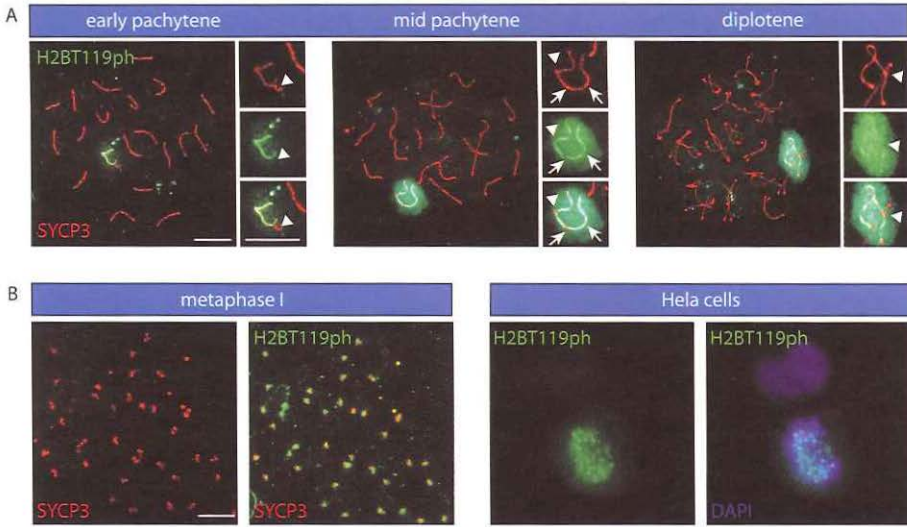
Figure 2. H2BT119ph on the XY body and on meiotic and mitotic metaphase chromosomes. (a) Double immunostaining of pachytene and diplotene spermatocyte nuclei with anti-SYCP3 (red) and anti-H2BT119ph (green). The insert shows a larger magnification of the area containing the XY body. Arrowhead: pseudoautosomal synapsed region; arrows: patches of synaptonemal complex lateral elements that are H2BT119ph negative. Scale bars represent 10 μm. (b) H2BT119ph (green) and SYCP3 (red) on meiotic metaphase (left), and H2BT119ph (green) on Dapi-stained (blue) mitotic Hela cell nucleus (right). Scale bar represents 10 μm.

Interestingly, H2BT119ph was strongly reduced on a few foci along the unpaired axial elements of pachytene nuclei. All other spermatogenic cell nuclei were negative, except for metaphases of mitotic spermatogonia and meiotic spermatocytes, where was mainly detected on centromeric DNA (Figure 2b, and results not shown). In nuclei of *Hr6b* knockout spermatocytes, the staining pattern and level of H2BT119ph were not different from wild type (not shown). In cultured human somatic cells (HeLa), H2BT119 phosphorylation was restricted to centromeric DNA of metaphase nuclei (Figure 2b). All observed signals could be competed by the phosphorylated peptide that was used to generate the antibody and not by similar amounts of non-phosphorylated peptide, indicating that the antibody selectively recognized H2BT119ph on nuclei (data not shown).

Next, we analysed H2AT120ph in spread nuclei of testes from wild type and *Hr6b* knockout mice. In wild type cells, H2AT120ph was found to be high in leptotene/zygotene spermatocyte nuclei, with the exception of regions containing centromeric DNA. Most H2AT120ph is lost at early pachytene, but it remains present on the XY body. During late pachytene and diplotene development,

H2AT120 phosphorylation decreases further, and the staining disappears also from the XY body. Hereafter, H2AT120ph increases on centromeric DNA during meiotic divisions. Then, early round spermatids show a low level of H2AT120ph, but an increased level of H2AT120ph in the whole nucleus is detected at later stages of round spermatid development, with the highest signal in the chromocenter (Figure 3a). Antibody specificity was again demonstrated through competition with phosphorylated and nonphosphorylated peptides (not shown). In *Hr6b* knockout spermatogenic cells, we observed interesting alterations in the pattern of H2AT120 phosphorylation. In late pachytene and diplotene spermatocyte nuclei, phosphorylation of H2AT120 was increased compared to wild type nuclei of the same stages (Figure 3b). Most strikingly, we observed enhanced signals on the XY body. We also found much higher H2AT120ph on metaphase I chromosomes of *Hr6b* knockout compared to wild type cells. Following the meiotic divisions, H2AT120ph in *Hr6b* knockout round spermatids was back to wild type level. To substantiate these findings, the H2AT120ph signal was quantified in wild type and *Hr6b* knockout diplotene spermatocytes (Figure 3c). The results show an approximately three-fold increase in nuclear H2AT120ph of *Hr6b* knockout diplotene spermatocytes compared to wild type, and a five-fold increase in XY body-associated H2AT120ph.

Previously, we reported accumulation of H2AK119ub1 on the XY body of pachytene spermatocytes of wild type and *Hr6b* knockout mice [18, 28]. The staining for H2AK119ub1 was repeated, and quantification of the immunofluorescent signal confirmed that H2AK119ub1 levels were similar in wild type and *Hr6b* knockout spermatocytes (Figure 3d). Next, we studied the developmental time course of H2AT120ph and H2AK119ub1 in wild type and *Hr6b* knockout meiotic spread nuclei using triple immunocytochemical staining. In wild type early pachytene spermatocytes, H2AT120ph precedes H2AK119ub1 on the XY body. Then, H2AT120ph strongly decreases during mid-pachytene, as H2AK119ub1 increases to a high level that is reached during late pachytene (Figure 4a). In *Hr6b* knockout pachytene spermatocyte nuclei, H2AT120ph also precedes H2AK119ub1, but remains present until diplotene, which results in high signals for the two modifications within the same nucleus (Figure 4b).

To investigate whether H2A molecules are present that contain both the phosphorylation and the ubiquitylation marks, we performed Western blot analysis for basic nuclear protein extracts from testis. In addition to H2AT120ph, a faint but specific band with a size corresponding to H2AK119ub1 was identified, and this likely represents a small fraction of H2A that is both ubiquitylated and phosphorylated at the adjacent Lys119 and Thr120, respectively, in wild type testis (Figure 4c). Spermatocytes of *Hr6b* knockout mice show a higher level of both H2AT120ph and H2AK119ub1T120ph to wild type (Figure 4d). The

A

wild type

zygotene	early pachytene

H2AT120ph / SYCP3

late pachytene	early diplotene

late diplotene	metaphase I

early round spermatid

DAPI / H2AT120ph

late round spermatid

B

***Hr6b* knockout**

zygotene	early pachytene

H2AT120ph / SYCP3

late pachytene	early diplotene

late diplotene	metaphase I

early round spermatid

DAPI / H2AT120ph

late round spermatid

C — H2AT120ph

arbitrary units /um2

early autosomes — wt, ko
late autosomes — wt, ko
early XY body — wt, ko
late XY body — wt, ko

D — H2AK119ub1

autosomes — wt, ko
XY body — wt ko

H2AT120ph signal is higher in spermatids compared to spermatocytes, but we observed no difference between wild type and *Hr6b* knockout spermatids. The pattern of H2AT120ph resembles the known pattern of H2AXS139 phosphorylation during meiotic prophase [15, 16], but we detected no differences for the patterns of H2AXS139 phosphorylation in wild type and *Hr6b* knockout spermatocytes (not shown).

H2AK119ub1 is associated not only with the XY body, but also with other chromatin areas that remain unsynapsed during meiotic prophase [18]. These findings indicated that H2AK119 ubiquitylation could be important for MSUC, the silencing of this chromatin. To establish if H2BT119ph and H2AT120ph are also associated with MSUC, we investigated these modifications in T/T' mice. These mice are double heterozygous for two very similar translocations between chromosomes 1 and 13, and the small 1^{13} bivalent often shows regions of unsynapsed chromatin that are subject to MSUC [18]. The results show that both H2BT119ph and H2AT120ph localize not only to the XY body, but also to the 1^{13} translocation bivalent (Figure 5).

XY body nucleosome replacement
Histone variant H3.1 is deposited on DNA during DNA replication, whereas H3.3 is a replacement histone that can be incorporated into nucleosomes on DNA, independent of the cell cycle phase [29]. Using antibodies against these different histone variants, it was recently shown that all nucleosomes associated with the X and Y chromosomes are replaced during pachytene [30]. During this process, H3.1 gradually disappears from the XY body, concomitant with a gradual increase of the H3.3 level [30]. We analysed XY body nucleosome replacement in *Hr6b*
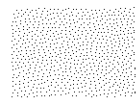
◁ **Figure 3. H2AT120ph is increased in *Hr6b* knockout spermatocyte nuclei.** (a) Double immunostaining of wild type spermatocyte and spermatid nuclei with anti-SYCP3 (red) and anti-H2AT120ph (green). For spermatids, separate images of the H2AT120ph (green) and Dapi (blue) staining are shown. Arrowhead: XY body; Z: zygotene; eP: early pachytene; IP: late pachytene; eD: early diplotene; lD: late diplotene; MI: Metaphase I; eT: early round spermatid; lT: late round spermatid. Scale bar represents 10 µm. (b) As in (a), but for *Hr6b* knockout spermatocyte and spermatid nuclei. (c) Quantification of H2AT120ph immunofluorescent signal in early and late diplotene nuclei of wild type (wt) and *Hr6b* knockout (ko) mouse testes. Arbitrary units per µm2 were calculated for the standard error of the mean (SEM) covering the XY body and for the area covering the autosomes. Error bars represent the SEM values of 20 nuclei that were measured for each genotype from two different animals. (d) Quantification of H2AK119ub1 immunofluorescent signal in pachytene nuclei of wild type (wt) and *Hr6b* knockout (ko) mouse testes. Arbitrary units per µm2 were calculated for the area covering the XY body and for the area covering the autosomes. Error bars represent the SEM values of 20 nuclei that were measured for each genotype from two different animals.
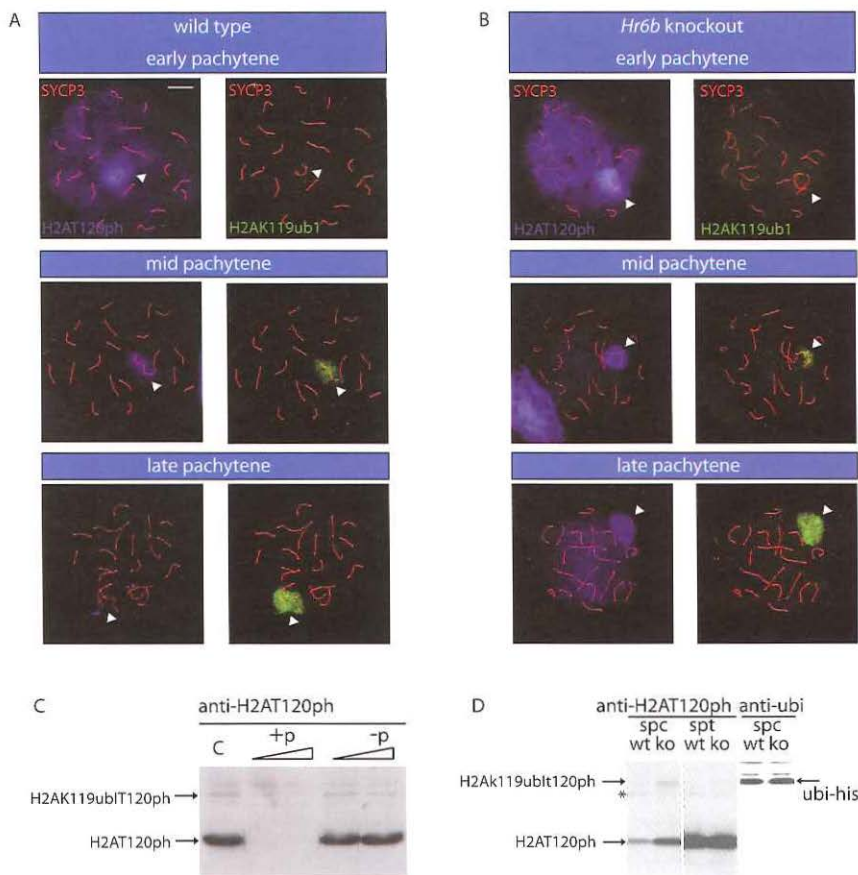
Figure 4. H2AT120 phosphorylation in association with H2AK119 ubiquitylation in *Hr6b* knockout pachytene spermatocytes. (a) Triple immunostaining of wild type early (eP), mid (mP) and late (lP) spread pachytene nuclei with anti-H2AT120ph (blue), anti-H2AK119ub1 (green), and anti-SYCP3 (red). The left panels show the merge of the H2AT120ph signal and SYCP3 signal, and right panels show the merge of the H2AK119ub1 (green) signal and SYCP3 signal (red). The arrowheads indicate the XY body. Scale bar represents 10 μm. (b) As in (a), but for *Hr6b* knockout nuclei. (c) Western blot analysis of H2AT120ph in basic nuclear protein extracts from total testis (C). Specificity of the antibody reaction is shown by competition of the signal with the phosphorylated H2A peptide (+P) but not with the nonphosphorylated peptide (-P). The identities of protein bands are indicated. Equal amounts of protein were present in each lane, as verified by Ponceau S staining of the blot (not shown). (d) Western blot analyses of H2AT120ph and ubiquitinated histones (ubi-his) in basic nuclear protein extracts from spermatocytes (spc) and spermatids (spt) isolated from wild type (wt) and *Hr6b* knockout (ko) mice. *indicates a non-specific protein band enriched in germ cell extracts compared to total testis extracts; the localization of H2AK119ub1T120ph was verified using the localization of ubiquitinated histones visible on the same blot that was stripped and reprobed with anti-ubiquitin as shown. Equal amounts of protein were present in each lane, as verified by Ponceau S staining of the blot (not shown).
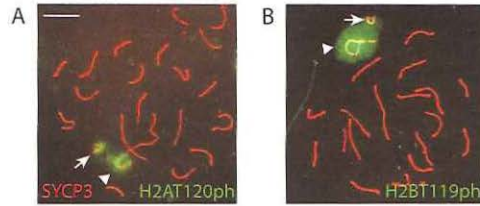
Figure 5. H2AT120ph and H2BT119ph and meiotic silencing of unpaired chromatin (MSUC). (a) Double immunostaining of pachytene nuclei isolated from T/T' mice with anti-H2AT120ph (green) and anti-SYCP3 (red). Arrowhead indicates the XY body, and the arrow indicates the 1^{13} translocation bivalent. Scale bar represents 10 μm. (b) As in (a), but these nuclei were stained with anti-H2BT119ph (green) and anti-SYCP3 (red).

knockout and wild type spermatocytes, to asses whether the altered dynamics of H2AT120ph in *Hr6b* knockout spermatocytes could be caused by disturbances in the general replacement of nucleosomes. Triple immunofluorescent analyses of SYCP3, H2AT120ph and H3.1 show that the disappearance of H3.1 from the XY body in wild type pachytene spermatocytes coincides with the disappearance of H2AT120ph (Figure 6a). However, in *Hr6b* knockout late pachytene spermatocytes, the XY body-associated H2AT120ph signal is still high when H3.1 has disappeared from the XY body (Figure 6b). Thus, although H2AT120ph dynamics have changed in *Hr6b* knockout spermatocytes, H3.1 disappearance from the XY body follows the wild type pattern.

MacroH2A1

MacroH2A1 is also enriched on heterochromatin and the XY body in late pachytene and diplotene spermatocytes [31]. We found a small increase in the overall level of macroH2A1 in *Hr6b* knockout diplotene spermatocytes, compared to wild type cells. This is a global change, with the same relative increase on autosomal and sex chromosomal chromatin (Figure 6cd). In round spermatids, macroH2A1 is gradually lost from autosomes and sex chromosomes, in a pattern which is not different between wild type and *Hr6b* knockout cells (not shown). Western blot analyses for basic nuclear proteins extracted from wild type and *Hr6b* knockout spermatocytes and spermatids, showed no effect of *Hr6b* mutation on macroH2A1 levels, and also not on H3K4me2 and H3K9me2 levels (Figure 6e). As described in the legend to Figure 6e, the Western blots represent a mixed cell population in which sub-nuclear changes that occur in germ cell substages that constitute a small fraction of the total will go undetected. The Western blot results for these histone variants and modifications, therefore, confirm their presence, but cannot provide additional detail about the sub-nuclear and temporal control of these modifications.
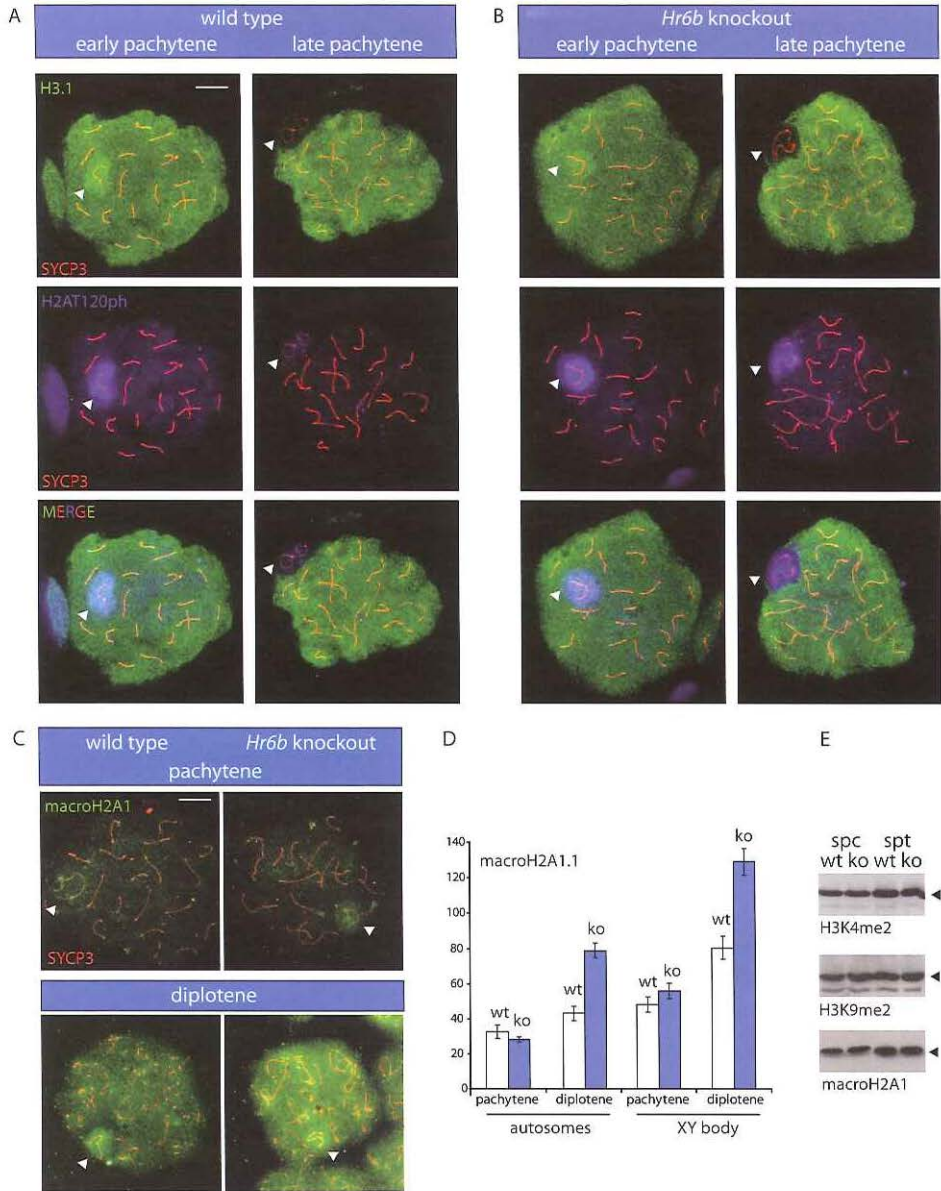
Figure 6. Histone variants in wild type and *Hr6b* knockout spermatocytes. (a) Triple immunostaining with anti-H3.1 (green), anti-SYCP3 (red) and anti-H2AT120ph (blue) in early (eP) and late (lP) pachytene spermatocytes. H3.1 is present on all chromosomes in early pachytene, but has disappeared from the XY body in late pachytene. Concomitantly with the loss of H3.1, H2AT120ph decreases. In *Hr6b* knockout pachytene spermatocytes (b), H3.1 disappears normally from the XY body, but H2AT120ph remains high. Arrowheads point to the XY body. Scale bars represent 10 μm. (c and d) Immunostaining with anti-macroH2A1 (green) and anti-SYCP3 (red) of wild type (leftpanels) and ▷

H3K4 *methylation*

Since H2BT119ph was not changed in *Hr6b* knockout spermatocytes, we next analysed H3K4 methylation in spread nuclei of spermatogenic cells as another possible indirect readout of dynamic changes in H2B ubiquitylation. We have used antibodies targeting H3K4me1, H3K4me2 and H3K4me3, and here we focus on results obtained with anti-H3K4me2. Similar results were obtained with anti-H3K4me1, but H3K4me3 levels were not consistently different between spermatogenic cells of wild type and *Hr6b* knockout (not shown). In agreement with the known general association of H3K4me2 with potentiated or transcriptionally active chromatin, we observed a low level of H3K4me2 in regions containing heterochromatic centromeric DNA (Figure 7a). In meiotic prophase, the overall level of H3K4 dimethylation was highest on euchromatin of leptotene/zygotene spermatocytes. The overall H3K4me2 signal was very low in pachytene and diplotene spermatocyte nuclei, followed by an increase during the meiotic divisions and post-meiotic round spermatid development. The XY body shows an even lower level of H3K4me2 compared to the rest of the pachytene nucleus. During diplotene and subsequent stages, H3K4me2 on the XY body gradually increases to a level that exceeds the H3K4me2 signal on autosomal chromatin (Figure 7a). In haploid round spermatids, either the X or the Y chromosome is located adjacent to the chromocenter. Localization of H3K4me2 on the X or Y chromosomes in round spermatids was verified using FISH (Figure 7c). It should be noted that a significant fraction of round spermatids showed no increased H3K4me2 signal on X or Y, and this most likely reflects H3K4me2 loss from the sex chromosomes in round spermatid at steps
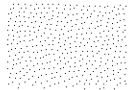
▷ *Hr6b* knockout (right panels) pachytene (P) and diplotene (D) spermatocytes. In *Hr6b* knockout diplotene spermatocytes, the overall level of macroH2A1 is higher compared to wild type spermatocytes. The immunofluorescent macroH2A1 signal was quantified (D) and arbitrary units per μm2 were calculated for the area covering the XY body and for the area covering the autosomes. Error bars represent the SEM values of 20 nuclei that were measured for each genotype from two different animals. (e) Western blot analysis of H3K4me2, H3K9me2 and macroH2A1 in basic nuclear protein extracts from spermatocytes (spc) and spermatids (spt) isolated from wild type (wt) and *Hr6b* knockout (ko) mice. Arrowhead indicates the specific protein bands. Equal amounts of protein were present in each lane, as verified by Ponceau S staining of the blot (not shown). All modifications show approximately equal levels in wild type and *Hr6b* knockout samples. The differences between wild type and *Hr6b* knockout diplotene spermatocytes that were observed using immunocytochemistry may not appear on Western blots, since diplotene spermatocytes represent only approximately 10% of the spermatocyte population. For round spermatids, the immunocytochemical differences in H3K4me2 and H3K9me2 levels are also observed in only a subfraction of the cells, and only in a subregion of the nucleus, and likewise may not appear in Western blot analysis of the whole cell population.
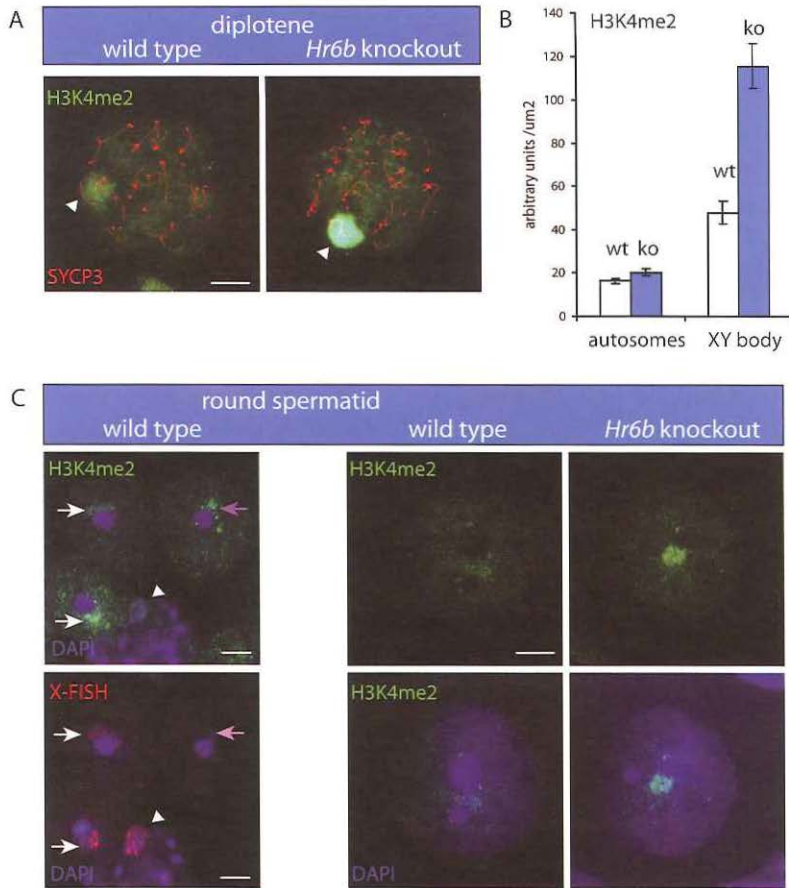
Figure 7. Increased dimethylation of H3K4 on XY chromatin of *Hr6b* knockout spermatocytes and spermatids. (a) Double immunostaining of wild type and *Hr6b* knockout diplotene nuclei with anti-H3K4me2 (green) and anti-SYCP3 (red). Arrowhead indicates the XY body. Scale bar represents 10 μm. (b) Quantification of H3K4me2 immunofluorescent signal on autosomal and XY body chromatin of wild type (wt) and *Hr6b* knockout (ko) diplotene spermatocytes. Arbitrary units per μm2 were calculated for the area covering the XY body and for the area covering the autosomes. Error bars represent the SEM values of 20 nuclei that were measured for each genotype from two different animals. (c) Immunostaining with anti-H3K4me2 (green, upper panels) combined with X chromosome FISH (red, lower panels) on spread chromosomes of MI (one primary spermatocyte) or MII (two secondary spermatocytes) nuclei from wild type and *Hr6b* knockout mice. Chromosomes are stained with Dapi (blue). Arrowhead indicates the X chromosome. Scale bar represents 10 μm. (d) Immunostaining with anti-H3K4me2 (green) combined with X chromosome FISH (red) on wild type spermatocyte and spermatid nuclei (left panel). The right panels show immunostaining of wild type and *Hr6b* knockout spermatid nuclei with anti-H3K4m2 (green). DNA is stained with Dapi (blue). White arrows in the left panel indicate the position of the X chromosome, and the pink arrow denotes the Y chromosome. The arrowhead points to an XY body of a pachytene spermatocyte. Scale bars represent 10 μm.

6-7 (just prior to spermatid elongation), as verified by immunohistochemical analysis (not shown).

When we compared developmental H3K4 dimethylation patterns in wild type and *Hr6b* knockout testis cell preparations, we observed increased H3K4me2 on the X and Y chromosomes from diplotene onwards (Figure 7a-c, Figure 8). This approximately 2.5-fold increase of H3K4me2 was verified by quantification of the fluorescent signal in nuclei and XY bodies of wild type and *Hr6b* knockout diplotene spermatocytes (Figure 7b). The increased H3K4me2 signal persisted in metaphase I and metaphase/anaphase II spermatocytes (Figure 8) and round spermatids (Figure 7c).

H3K9 methylation

Previously, we have found that the synaptonemal complexes (SCs) of late pachytene *Hr6b* knockout spermatocytes are longer and thinner compared to the SCs of wild type cells. In addition, we found a loss of SC components from near telomeric regions in *Hr6b* knockout late pachytene nuclei [20]. These findings most likely reflect a global change in chromatin structure in late pachytene and
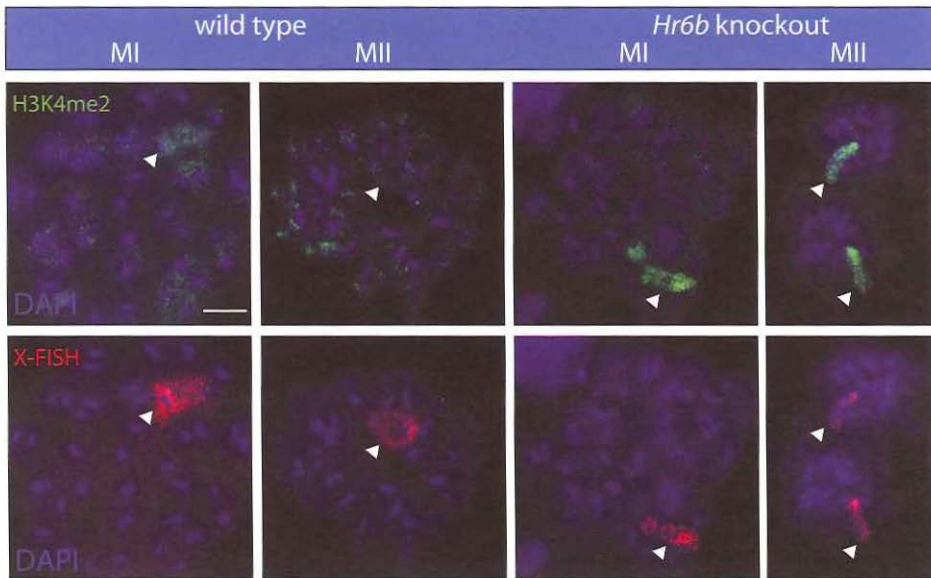
Figure 8. Increased dimethylation of H3K4 on X and Y chromatin of *Hr6b* knockout meiotic metaphase nuclei. Immunostaining with anti-H3K4me2 (green, upper panels) combined with X chromosome FISH (red, lower panels) on spread chromosomes of MI (one primary spermatocyte) or MII (two secondary spermatocytes) nuclei from wild type and *Hr6b* knockout mice. Chromosomes are stained with DAPI (blue). Arrowhead indicates the X chromosome. Scale bar represents 10 μm.

diplotene spermatocytes. To investigate this further, we analysed additional histone modifications generally associated with active (H4K16 and H2AK119 acetylation) or inactive (H3K9me1, H3K9me2, H3K9me3, H3K27me2 and H3K27me3) chromatin during spermatogenesis in wild type and *Hr6b* knockout mice (not shown). Of these, only H3K9me2 appeared to be different between wild type and *Hr6b* knockout spermatocytes. H3K9me2 generally marks silent chromatin, and in wild type diplotene spermatocytes the level is high on centromeric heterochromatin and the XY body. In *Hr6b* knockout diplotene spermatocytes, H3K9me2 is much lower on centromeric heterochromatin compared to wild type nuclei of the same stage, but a normal level is observed on the XY body (Figure 9ab). Also in round spermatids, H3K9me2 is lower on the chromocenter, but not on either X or Y (Figure 9ab).

Postmeiotic maintenance of X-chromosomal silencing

The relatively high level of H3K4me2 on the X and Y chromosomes in *Hr6b* knockout spermatids may be related to changes in transcriptional activity. To investigate this further, we analysed the expression of several X-chromosomal and autosomal genes in cell preparations isolated from wild type and *Hr6b* knockout mice. Genes were selected based on data from Namekawa et al. (2006) who showed that transcription from the X chromosome is largely repressed in meiotic and postmeiotic cells [32]. We selected 4 genes that were reported to remain
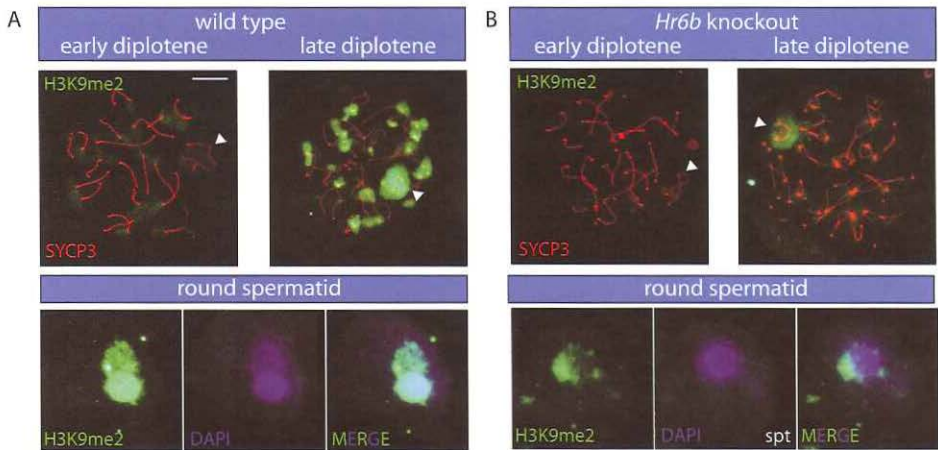
Figure 9. Loss of H3K9me2 from centromeric heterochromatin, but not from X and Y in *Hr6b* knockout diplotene spermatocytes and spermatids. (a) Immunostaining with anti-H3K9me2 (green) and anti-SYCP3 (red) of wild type early (eD) and late (lD) diplotene spermatocytes (upper panels), and round spermatids (spt) (lower panels). DNA is stained with DAPI (blue). Arrowheads point to the XY body. Scale bars represent 10 μm. (b) As in (a), but for *Hr6b* knockout nuclei.

repressed in the postmeiotic spermatids (*Chic1*, *Atp7a*, *Gla* and *Hprt*) and two genes that showed postmeiotic reactivation (*Ube1x* and *Pctk1*) [32]. In addition, we selected 4 autosomal genes that are expressed at meiotic (*Spo11* and *Sycp2*) and postmeiotic (*Tnp1* and *Creb3l4*) spermatogenic developmental steps. Real-time RT-PCR expression data were normalized to *Actb* (b-actin) mRNA, which showed equal expression in the different cell preparations (data not shown). For the autosomal genes, no significant differences between wild type and *Hr6b* knockout cells were detected (Fig 10a). However, five out of the six X-chromosomal genes that were tested show increased expression in *Hr6b* knockout cells compared to wild type (Figure 10b). This effect was most clear for round spermatids. *Pctk1* is
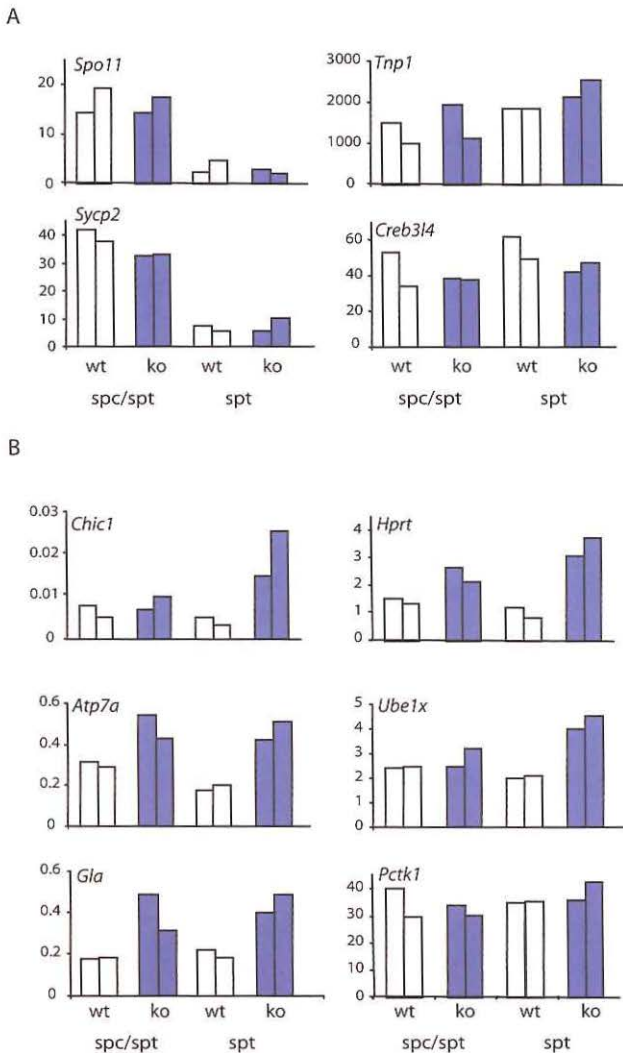
Figure 10. Derepression of X-chromosomal genes in *Hr6b* knockout spermatids. Real-time RT-PCR quantification of mRNA levels of four autosomal genes (A) and six X-chromosomal genes (B) in a mixed spermatocyte/spermatid (spc/spt) and purified spermatid (spt) cell preparation from wild type (wt) and *Hr6b* knockout (ko) mice. The amount of PCR products was normalized to *Actb* (*b-actin*) mRNA (x100). Results from two independent experiments are shown. For each experiment, the value represents the average of a duplicate real-time PCR experiment.

expressed at a relatively high level, compared to the other tested X-chromosomal genes, and no further upregulation of its postmeiotic expression was observed for the *Hr6b* knockout cells (Figure 10b). Taken together, the results indicate that postmeiotic maintenance of X-chromosomal gene silencing is compromised in *Hr6b* knockout spermatids.

DISCUSSION

HR6A/B and histone ubiquitylation

RAD6 is a protein that is highly conserved in evolution. It is most well known for its pivotal function in replicative damage bypass, a pathway that allows replication to proceed in the presence of a damaged template [33]. RAD6 is also essential for sporulation, and this involves H2B ubiquitylation by RAD6, together with BRE1 [8-10]. The present results indicate that HR6A and HR6B do not act as main determinants of global histone ubiquitylation in mammalian cells, since we observe no detectable defects in H2A or H2B ubiquitylation in spermatocytes from *Hr6b* knockout males. HR6A is still expressed in these cells, at a low level [20], and we cannot exclude that this small amount of HR6A is responsible for the observed maintenance of global histone ubiquitylation in *Hr6b* knockout germline cells. In addition, redundancy with other E2 enzymes may prevent detection of some role of HR6B in dynamic control of histone ubiquitylation. Ideally, *Hr6a-Hr6b* double-knockout cells should be used to address the role of HR6A and HR6B in histone ubiquitylation in somatic and germline cells, but these cells are not obtained [6].

Recently, the human E2 enzyme UBCH6 has been shown to be able to ubiquitylate H2B in vitro, together with an E3 complex consisting of RNF20 and RNF40 proteins [34]. RNF20 and RNF40 are orthologs of BRE1, the yeast E3 that ubiquitylates H2B. In addition to the evolutionary conservation of these components, the pathway leading from H2B ubiquitylation to H3K4 methylation also appears to be conserved [34]. Possibly, the role of RAD6 in histone ubiquitylation has been taken over, at least in part, by UBCH6. Given the conservation of the trans-histone regulatory pathway, leading from H2BK120 ubiquitylation to H3K4 methylation, our observation that H3K4 methylation in *Hr6b* knockout spermatogenic cells is not reduced, provides further evidence that H2B ubiquitylation is not affected in HR6B deficient spermatocytes. HR6B localizes primarily to the XY body, and most likely is required to ubiquitylate certain XY body chromatin components, but not H2A or H2B. Somehow, lack of HR6B affects H2AT120ph, and this may subsequently lead to increased H3K4me1 and H3K4me2, specifically in the XY body. Previously, Khalil and Driscoll (2006), reported that H3K4me2 is upregulated on the silent XY body of wild type diplotene spermatocytes [35]. Our data confirm their findings, and we show

that in *Hr6b* knockout spermatocytes this modification is further upregulated on X and Y. We did not detect a consistent increase in H3K4me3 levels, but the anti-H3K4me3 antibodies cross-react to some extent with H3K4me2. Therefore, we cannot exclude that apart from H3K4me2, H3K4me3 is also increased.

Global versus XY specific chromatin regulation

HR6A and HR6B most likely exert multiple functions during spermatogenesis. During meiotic prophase, HR6B concentrates on the XY body, but is also present on autosomal chromatin. Previously, we have shown that *Hr6b* knockout spermatocytes show a higher recombination frequency associated with some dysregulation of the structure of the synaptonemal complex [20]. Changes in the synaptonemal complex might follow after global changes in chromatin structure, and such global changes are indicated by increased macroH2A1 and decreased H3K9me2 levels of meiotic prophase chromatin. This provides a background for the observed differential effects of HR6B deficiency on autosomal versus XY associated histone modifications. Interestingly, however, the loss of H3K9me2 signal in *Hr6b* knockout diplotene spermatocytes and round spermatids occurs on all heterochromatin, but not on XY chromatin. This adds to our observations on the marked XY associated increase in H2AT120ph and H3K4me2 signals

H2AT120ph and regulation of chromatin organization

In *Drosophila*, nucleosomal histone kinase-1 (NHK-1) phosphorylates H2AT120 [26]. Female flies that carry a mutation in the gene encoding NHK-1 are infertile [36]. Loss of H2AT120ph was shown to be associated with a failure to disassemble the synaptonemal complex and with impaired loading of condensin [36]. H2AT120ph in mouse may also be associated with regulation at this level of chromatin organization. During meiosis, we observed a very high level of H2AT120ph not only at metaphase, but also in leptotene/zygotene spermatocytes. This indicates that H2AT120ph may be relevant not only for disassembly of the synaptonemal complex (SC), but also for its assembly. *Hr6b* knockout spermatocytes show SCs that are longer, with some loss of SC proteins from near centromeric regions [20]. Thus, in analogy to what has been observed in *Drosophila*, the modified level and pattern of H2AT120ph in *Hr6b* knockout spermatocytes may be related to a role of HR6B in maintenance of a normal SC structure. Such a relationship may also appear from the observed loss of H3K9me2 from centromeric heterochromatin in *Hr6b* knockout diplotene spermatocytes.

In wild type spermatocytes going through meiotic prophase, H2AT120 phosphorylation decreases as H2AK119 ubiquitylation increases. Also, during spermatid elongation, H2AT120ph decreases again when H2AK119ub1 increases (our own unpublished results).

This indicates that H2AT120 phosphorylation is down-regulated prior to H2AK119 ubiquitylation. Loss of XY body-associated H2AT120 phosphorylation occurs concomitant with the exchange of all nucleosomes from the XY body, as visualized by the loss of H3.1. Therefore, no active dephosphorylation may be required at this stage. In *Hr6b* knockout pachytene spermatocytes, H2AT120ph is not properly removed, but H2AK119 ubiquitylation increases as in wild type. Apparently, H2AT120ph dephosphorylation is not a prerequisite for H2AK119 ubiquitylation.

In *Hr6b* knockout pachytene and diplotene nuclei, H2AT120ph is increased throughout the nucleus, but the combined H2AK119ub1T120ph modification is present mainly on the XY body. This might lead to XY body-restricted recruitment of complexes that recognize this combinatory code, and such a mechanism would provide an explanation for a subsequent increase of H3K4me2 only on the XY body of *Hr6b* knockout diplotene spermatocytes.

H2AT120 and H2BT119 phosphorylation and meiotic silencing of unpaired chromatin (MSUC)

In meiotic prophase nuclei we detect H2BT119ph only on chromatin associated with the unpaired axial elements of the XY body. Then, when cells enter metaphase I, H2BT119ph localizes on centromeric DNA. On Western blots of basic nuclear proteins isolated from testis, no specific signal could be obtained with this antibody (results not shown). This may be due to the fact that the percentage of H2BT119ph is extremely low compared to the amount of unphosphorylated H2B. The localization of H2BT119ph on centromeric DNA of metaphase chromosomes of mitotic somatic cells is similar to the reported localization of H2AT120ph on metaphase chromosomes of mitotic cells from *Drosophila* [26] and human (our own unpublished observations). However, during spermatogenesis the two modifications display different localization patterns and kinetics. H2AT120ph is first present on all chromatin during zygotene, and then persists on unpaired chromatin. In contrast, H2BT119ph is absent during leptotene/zygotene, and subsequently this phosphorylation is specifically induced on chromatin associated with unpaired axial elements. On the XY body, H2AT120ph covers all chromatin, whereas H2BT119ph is mainly concentrated on the axial elements that are unpaired, and it is excluded from pseudoautosomal regions, and a few unidentified small regions on the axial elements, which appear to show enhanced SYCP3 staining.

In spermatocytes from T/T' mice, phosphorylation of H2AT120 and H2BT119 is enhanced on the partially synapsed 1^{13} bivalent. Taken together with the observations on these modifications for the unpaired and silenced XY

chromatin, this indicates that H2AT120ph and H2BT119ph may be functionally relevant for MSUC.

Postmeiotic derepression of X-chromosomal gene expression in Hr6b knockout spermatids

In *Hr6b* knockout spermatocytes, accumulation of specific XY body-associated histone modifications and nucleosome replacement all occur as in wild type cells. The increase in H3K4me2 on X and Y chromatin becomes apparent in late meiotic prophase spermatocytes, and remains present in postmeiotic *Hr6b* knockout cells. Therefore, we conclude that XY body formation in *Hr6b* knockout spermatocytes is not affected; rather, late meiotic and postmeiotic regulation of XY chromatin appears to be disturbed. This is supported by our finding that the most obvious derepression of X-chromosomal genes is detected in postmeiotic spermatids.

H3K4 methylation is generally found in association with active genes, although recent data indicate that certain repressors of gene expression can also bind methylated H3K4 (reviewed by [37]). We find upregulation of five out of six tested X-chromosomal genes in *Hr6b* knockout spermatids, and no downregulation. This effect points to a link between H3K4 methylation and gene activation on the postmeiotic X chromosome. The autosomal genes tested show wild type mRNA levels in the *Hr6b* knockout cells. Although we do not exclude that autosomal gene expression is affected to some extent, the loss of HR6B activity seems to exert a more pronounced effect on transcriptional activity of the X chromosome.

The data presented herein provide evidence for a role of HR6B in regulation of histone modifications in mammalian cells. This has been revealed in *Hr6b* knockout spermatocytes, a cell type with a relatively low level of HR6A. HR6A and HR6B show 96% amino acid similarity, and at present we have no indications that HR6A and HR6B perform different activities, neither in somatic nor in germline cells. In spermatocytes, HR6B localizes mainly on the XY body, together with the putative partner ubiquitin ligase RAD18 [19]. Although H2AK119ub1 also is enriched on the XY body, our findings indicate that HR6B activity is not responsible for this modification. Moreover, HR6B is not required for global H2BK120 ubiquitylation. Instead, we have established that loss of HR6B affects other aspects of histone modifications associated with the XY body, in particular exerting an effect on H2AT120ph and H3K4me2, in association with derepression of X-chromosomal genes in postmeiotic cells.

MATERIALS AND METHODS

Isolation of different cell types from mouse testis

Spermatocytes and round spermatids were isolated from 4-5-week-old wild type (FVB) and *Hr6b* knockout mouse testes after collagenase and trypsin treatment, followed by sedimentation at unit gravity (StaPut procedure) [38]. This yielded a fraction containing approximately equal amounts of spermatocytes and round spermatids (spc/spt), with few other contaminating cells (<10%), and a fraction containing >90% pure spermatids (spt). These fractions were used for analysis of RNA. For protein analysis, cells were further purified (>90%) by density gradient centrifugation through Percoll [38] resulting in preparations of spermatocytes (spc) and spermatids (spt). Cells were snap-frozen in liquid nitrogen and stored at −80C.

Generation of antibodies

Antibody against peptide CPGGRKHSGKSGKPPL representing amino acids 22-37 of mouse SYCP3, with an added N-terminal cysteine, was generated at Eurogentec (Seraing, Belgium) according to their protocols. Antibodies against H2AT120ph H2BT119ph and H2AK119ac$_c$ were generated in rabbits using peptides GTKAVT*KYTSS, LLPKKT*ESHH, and QAVLLPKK*TESH (asterisk indicates phosphorylated or acetylated residue), respectively, using standard protocols. Phosphorylated and non-phosphorylated and acetylated and non-acetylated peptides were used in competition experiments to test antibody specificity.

Isolation of acid soluble nuclear proteins and Western blotting

Nuclei and acid soluble proteins were isolated from cell preparations or total testes according to Chen et al. [39]. The isolated protein fraction was precipitated with 5% (w/v) trichloroacetic acid.

An amount of 20 µg of protein per sample was separated on 12% SDS-polyacrylamide gels and the separated proteins were transferred to nitrocellulose membranes, using the BioRad miniprotean III system and blot cells (Bio-Rad, Veenendaal, Netherlands). Membranes were stained with Ponceau S (Sigma-Aldrich, Zwijndrecht, Netherlands) according to the supplier's protocol.

Modified histones were detected with mouse monoclonal IgM anti-H2AK119ub1 (Upstate, Waltham, MA, USA), rabbit polyclonal anti-ubiquitin (DakoCytomation, Glostrup, Denmark), rabbit polyclonal anti-H2B (Upstate), and rabbit polyclonal anti-H2AT120ph.

Meiotic spread nuclei preparations and immunocytochemistry

Testes were obtained from adult T(1;13)70H/T(1;13)1Wa (T/T') mice (Swiss random bred), and from 5-week-old wild type wild type and *Hr6b* knockout mice (FVB background).

Testis tissues were processed to obtain spread nuclei for immunocytochemistry as described by Peters et al. [40], Spread nuclei of spermatocytes were stained with rat polyclonal anti-Sycp3, mouse monoclonal IgM anti-ubi-H2A (Upstate, Waltham, MA, USA), rabbit polyclonal anti-H3Ke4me1 (Upstate), rabbit polyclonal anti-H3K4me2 (Upstate and Abcam, Cambridge, UK with similar results, Upstate antibody was used in Results section), rabbit polyclonal anti-H3K4me3 (Upstate and Abcam), rabbit polyclonal anti-H3K9me1 (Upstate), rabbit polyclonal anti-H3K9me2 (Upstate), mouse monoclonal anti-H3K9me2 (Abcam, both anti-H3K9me2 antibodies with similar results, Abcam antibody was used in the Results section), rabbit polyclonal anti-H3K27me2 (Upstate), mouse monoclonal anti-H3K27me3 (Abcam), rabbit polyclonal anti-H4K16ac (Abcam), rabbit polyclonal anti-macroH2A1 (Upstate), mouse monoclonal anti-H3.1 [41], rabbit polyclonal anti-H2AT120ph, rabbit polyclonal anti-H2AK119ac, or rabbit polyclonal anti-H2BT119ph. Secondary antibodies were FITC- (Sigma, St Louis, MO, USA), TRITC- (Sigma) , Alexa 350, Alexa 594, or Alexa 488 (Molecular Probes), labeled goat anti-rabbit, goat anti-mouse, or goat anti-rat IgG antibodies; FITC-labeled goat anti-mouse IgM (Sigma) was used as secondary antibody for anti-H2AK119ub1 (IgM). Before incubation with antibodies, slides were washed in PBS (3x10 min), and non-specific sites were blocked with 0.5% w/v BSA and 0.5% w/v milk powder in PBS. First antibodies were diluted in 10% w/v BSA in PBS, and incubations were overnight at room temperature in a humid chamber. Subsequently, slides were washed (3x10 min) in PBS, blocked in 10% v/v normal goat serum (Sigma) in blocking buffer (supernatant of 5% w/v milk powder in PBS centrifuged at 14000 rpm for 10 min), and incubated with secondary antibodies in 10% normal goat serum in blocking buffer at room temperature for 2 hours. Finally, slides were washed (3x10 min) in PBS (in the dark) and embedded in Vectashield containing DAPI to counterstain the DNA (Vector Laboratories, Burlingame, CA, USA) or in Prolong Gold (Molecular probes) when Alexa labeled secondary antibodies were used. DAPI was omitted when triple immunostainings were performed. Fluorescent images from spread nuclei were observed using a fluorescent microscope (Axioplan 2; Carl Zeiss, Jena, Germany) equipped with a digital camera (Coolsnap-pro, Photometrics, Waterloo, Canada). Digital images were processed using Adobe Photoshop software (Adobe Systems). For quantification of immunofluorescent signal, slides were analysed on the same day. Fluorescent images were taken under identical

conditions for all slides, and not further processed in Adobe. The signal present in the total nucleus and in the XY body was measured using Image J software analysis (National Institutes of Health).

FISH

Following immunocytochemistry, the position of selected nuclei on the slide was determined, and FISH was performed to detect the X chromosome using STAR*FISH mouse whole chromosome-specific paints (1200XmCy3; Cambio, Cambridge, UK) according to the manufacturer's protocol. If specific signal was not obtained, the procedure was performed for a second time, and this always resulted in a positive signal in most nuclei. Specificity of hybridization was confirmed using male meiotic spread nuclei preparations; positive signal colocalized with the XY body of pachytene spermatocytes. Digital images were obtained and processed as above. FISH images were combined with immunocytochemical images using Adobe Photoshop software (Adobe Systems).

Real-time RT-PCR

For real-time RT-PCR, RNA was prepared from the isolated germ cell preparations by Trizol, DNAse-treated, and reverse transcribed using random hexamer primers and Superscript II reverse transcriptase (Invitrogen, Breda, The Netherlands). PCR was carried out with the iQ SYBR green PCR mastermix (Applied Biosystems) in the DNA engine Opticon 2 real-time PCR detection system (Bio-Rad). For *Hprt*, *Pctk1* and *Atp7a* we used the following conditions: 3 minutes 95°C - (30 seconds 95°C, 30 seconds 62°C, 30seconds 72°C) x 45cycles. For *Chic1*, we used 3 minutes 95°C - (30 seconds 95°C, 30 seconds 65°C, 30seconds 72°C, 30 seconds 78°C) x 45cycles, For *Gla* we used 3 minutes 95°C - (30 seconds 95°C, 30 seconds 65°C, 30seconds 72°C) x 45cycles and for *Ube1x* conditions were: 3 minutes 95°C - (30 seconds 95°C, 30 seconds 57°C, 30 seconds 72°C, 30 seconds 80°C) x 45 cycles. For *Spo11*, *Sycp2*, *Tnp1* and *Creb3l4* we used 3 minutes 95°C - (30 seconds 95°C, 30 seconds 60°C, 30seconds 72°C) x 45cycles as reaction conditions. *b-actin* was included in each reaction and used to normalize the data. Two independent experiments were performed and each real-time PCR was performed in duplicate. –RT reactions were negative. Forward and reverse primers for *Hprt*, *Pctk1*, *Atp7a*, *Gla*, *Chic1* and *Actb* (*b-actin*) were as described [32]. Forward and reverse primers (5' to 3'):
Ube1x: TGTCCACACCCACTTACT and GCACTCTGCAACTCC
Spo11: GCTCCTGGACGACAACTTCT and ATCTGCATCGACCAGTGTGA
Sycp2: TGGATGTGATGACAGCAAGA and TGGGTCTTGGTTGTCCTTTT
Tnp1: AAGAACCGAGCTCCTCACAA and CATCACAAGTGGGATCGGTA
Creb3l4: CCTCCGATTCGCATAGACAT and GCCAGCAGTTGCTTTTCTTC.

ACKNOWLEDGEMENTS

REFERENCES

1. Jenuwein T, Allis CD. Translating the histone code. *Science.* Aug 10 2001;293(5532):1074-1080.
2. Emre NC, Berger SL. Histone post-translational modifications regulate transcription and silent chromatin in Saccharomyces cerevisiae. *Ernst Schering Res Found Workshop.* 2006(57):127-153.
3. Nathan D, Ingvarsdottir K, Sterner DE, et al. Histone sumoylation is a negative regulator in Saccharomyces cerevisiae and shows dynamic interplay with positive-acting histone modifications. *Genes Dev.* Apr 15 2006;20(8):966-976.
4. Varshavsky A. Regulated protein degradation. *Trends Biochem. Sci.* Jun 2005;30(6):283-286.
5. Pickart CM, Fushman D. Polyubiquitin chains: polymeric protein signals. *Curr Opin Chem Biol.* Dec 2004;8(6):610-616.
6. Roest HP, Baarends WM, de Wit J, et al. The ubiquitin-conjugating DNA repair enzyme HR6A is a maternal factor essential for early embryonic development in mice. *Mol. Cell. Biol.* Jun 2004;24(12):5485-5495.
7. Roest HP, Klaveren van J, Wit de J, et al. Inactivation of the HR6B ubiquitin-conjugating DNA repair enzyme in mice causes a defect in spermatogenesis associated with chromatin modification. *Cell.* 1996;86:799-810.
8. Hwang WW, Venkatasubrahmanyam S, Ianculescu AG, Tong A, Boone C, Madhani HD. A Conserved RING Finger Protein Required for Histone H2B Monoubiquitination and Cell Size Control. *Mol Cell.* Jan 2003;11(1):261-266.
9. Robzyk K, Recht J, Osley MA. Rad6-dependent ubiquitination of histone H2B in yeast. *Science.* 2000;287(5452):501-504.
10. Wood A, Krogan NJ, Dover J, et al. Bre1, an e3 ubiquitin ligase required for recruitment and substrate selection of rad6 at a promoter. *Mol Cell.* Jan 2003;11(1):267-274.
11. West MH, Bonner WM. Histone 2A, a heteromorphous family of eight protein species. *Biochemistry.* 1980;19(14):3238-3245.
12. West MH, Bonner WM. Histone 2B can be modified by the attachment of ubiquitin. *Nucleic Acids Res.* Oct 24 1980;8(20):4671-4680.
13. Koken MHM, Hoogerbrugge JW, Jaspers-Dekker I, et al. Expression of the ubiquitin-conjugating DNA repair enzymes HHR6A and B suggests a role in spermatogenesis and chromatin modification. *Dev. Biol.* 1996;173:119-132.
14. Schimenti J. Synapsis or silence. *Nat. Genet.* Jan 2005;37(1):11-13.
15. Fernandez-Capetillo O, Mahadevaiah SK, Celeste A, et al. H2AX is required for chromatin remodeling and inactivation of sex chromosomes in male mouse meiosis. *Dev Cell.* Apr 2003;4(4):497-508.
16. Turner JM, Aprelikova O, Xu X, et al. BRCA1, histone H2AX phosphorylation, and male meiotic sex chromosome inactivation. *Curr. Biol.* Dec 14 2004;14(23):2135-2142.
17. Turner JM, Mahadevaiah SK, Fernandez-Capetillo O, et al. Silencing of unsynapsed meiotic chromosomes in the mouse. *Nat. Genet.* Jan 2005;37(1):41-47.
18. Baarends WM, Wassenaar E, van der Laan R, et al. Silencing of unpaired chromatin and histone H2A ubiquitination in mammalian meiosis. *Mol. Cell. Biol.* 2005;25:1041-1053.
19. van der Laan R, Uringa EJ, Wassenaar E, et al. Ubiquitin ligase Rad18Sc localizes to the XY body and to other chromosomal regions that are unpaired and transcriptionally silenced during male meiotic prophase. *J. Cell Sci.* Oct 1 2004;117(Pt 21):5023-5033.
20. Baarends WM, Wassenaar E, Hoogerbrugge JW, et al. Loss of HR6B ubiquitin-conjugating activity results in damaged synaptonemal complex structure and increased

crossing-over frequency during the male meiotic prophase. *Mol. Cell. Biol.* Feb 2003;23(4):1151-1162.

21. Dover J, Schneider J, Boateng MA, et al. Methylation of histone H3 by COMPASS requires ubiquitination of histone H2B by RAD6. *J. Biol. Chem.* Jun 17 2002;277:28368-28371.

22. Ng HH, Xu RM, Zhang Y, Struhl K. Ubiquitination of histone H2B by Rad6 is required for efficient Dot1-mediated methylation of histone H3 lysine 79. *J. Biol. Chem.* Sep 20 2002;277(38):34655-34657.

23. Sun ZW, Allis CD. Ubiquitination of histone H2B regulates H3 methylation and gene silencing in yeast. *Nature.* Jun 23 2002;418(6893):104-108.

24. Fischle W, Wang Y, Allis CD. Binary switches and modification cassettes in histone biology and beyond. *Nature.* Oct 2 2003;425(6957):475-479.

25. Fischle W, Tseng BS, Dormann HL, et al. Regulation of HP1-chromatin binding by histone H3 methylation and phosphorylation. *Nature.* Dec 22 2005;438(7071):1116-1122.

26. Aihara H, Nakagawa T, Yasui K, et al. Nucleosomal histone kinase-1 phosphorylates H2A Thr 119 during mitosis in the early Drosophila embryo. *Genes Dev.* Apr 15 2004;18(8):877-888.

27. Heyting C. Synaptonemal complexes: structure and function. *Curr. Opin. Cell. Biol.* 1996;8:389-396.

28. Baarends WM, Hoogerbrugge JW, Roest HP, et al. Histone ubiquitination and chromatin remodeling in mouse spermatogenesis. *Dev. Biol.* 1999;207:322-333.

29. Tagami H, Ray-Gallet D, Almouzni G, Nakatani Y. Histone H3.1 and H3.3 complexes mediate nucleosome assembly pathways dependent or independent of DNA synthesis. *Cell.* Jan 9 2004;116(1):51-61.

30. van der Heijden GW, Derijck AA, Posfai E, et al. Chromosome-wide nucleosome replacement and H3.3 incorporation during mammalian meiotic sex chromosome inactivation. *Nat. Genet.* Feb 2007;39(2):251-258.

31. Hoyer-Fender S, Costanzi C, Pehrson JR. Histone macroH2A1.2 is concentrated in the XY-body by the early pachytene stage of spermatogenesis. *Exp. Cell Res.* 2000;258(2):254-260.

32. Namekawa SH, Park PJ, Zhang LF, et al. Postmeiotic sex chromatin in the male germline of mice. *Curr. Biol.* Apr 4 2006;16(7):660-667.

33. van der Laan R, Baarends WM, Wassenaar E, Roest HP, Hoeijmakers JH, Grootegoed JA. Expression and possible functions of DNA lesion bypass proteins in spermatogenesis. *Int. J. Androl.* Feb 2005;28(1):1-15.

34. Zhu B, Zheng Y, Pham AD, et al. Monoubiquitination of Human Histone H2B: The Factors Involved and Their Roles in HOX Gene Regulation. *Mol Cell.* Nov 23 2005;20(4):601-611.

35. Khalil AM, Driscoll DJ. Histone H3 lysine 4 dimethylation is enriched on the inactive sex chromosomes in male meiosis but absent on the inactive X in female somatic cells. *Cytogenet Genome Res.* 2006;112(1-2):11-15.

36. Ivanovska I, Khandan T, Ito T, Orr-Weaver TL. A histone code in meiosis: the histone kinase, NHK-1, is required for proper chromosomal architecture in Drosophila oocytes. *Genes Dev.* Nov 1 2005;19(21):2571-2582.

37. Becker PB. Gene regulation: a finger on the mark. *Nature.* Jul 6 2006;442(7098):31-32.

38. Grootegoed JA, Jansen R, van der Molen HJ. Effect of glucose on ATP dephosphorylation in rat spermatids. *J. Reprod. Fertil.* 1986;77(1):99-107.

39. Chen HY, Sun JM, Zhang Y, Davie JR, Meistrich ML. Ubiquitination of histone H3 in elongating spermatids of rat testes. *J. Biol. Chem.* 1998;273(21):13165-13169.

40. Peters AH, Plug AW, van Vugt MJ, de Boer P. A drying-down technique for the spreading of mammalian meiocytes from the male and female germline. *Chromosome Res.* 1997;5(1):66-68.

41. van der Heijden GW, Dieker JW, Derijck AA, et al. Asymmetry in histone H3 variants and lysine methylation between paternal and maternal chromatin of early mouse zygotes. *Mech. Dev.* 1022 2005;122(9):1008.

CHAPTER 8

A POSTMEIOTIC AND PATERNAL-EFFECT FUNCTION
OF UBE2B TO PRESERVE GENOME INTEGRITY
IN SPERM AND DURING
EARLY EMBRYONIC DEVELOPMENT

ABSTRACT

Ube2b knockout mice show male-limited infertility due to impaired spermatogenesis, associated with low sperm counts and defective sperm head morphology. The ubiquitin-conjugating enzyme UBE2B plays multiple roles in DNA repair and is involved in regulation of chromatin structure. Herein, we have investigated the role of UBE2B in the control of normal chromatin structure during spermatogenesis.

We generated transgenic mice expressing UBE2B fused to a hemagglutinin tag (HA) in spermatocytes and spermatids, on the *Ube2b* knockout genetic background (*Ube2b-HA/Ube2b$^{-/-}$* / mice). In these mice, spermatogenesis has qualitatively and quantitatively improved compared to the *Ube2b* knockout, although the males are still infertile. Analysis of sperm DNA integrity indicated that sperm from *Ube2b$^{-/-}$* mice showed increased DNA damage as compared to wild type and *Ube2b-HA/Ube2b$^{-/-}$* sperm, indicating accumulation of DNA damage during spermatogenesis in *Ube2b$^{-/-}$* mice.

We compared the outcome of intracytoplasmic injection of *Ube2b$^{-/-}$* or *Ube2b-HA/Ube2b$^{-/-}$* sperm into wild type oocytes (ICSI). After ICSI with *Ube2b* knockout sperm, the paternal pronucleus was fragmented and heavily loaded with the DNA double-strand break-marker γH2AX. In contrast, ICSI with *Ube2b-HA/Ube2b$^{-/-}$* sperm resulted in the formation of a normal paternal pronucleus. However, in vitro embryonic development was associated with progressive accumulation of nuclei with DNA fragmentation, and the embryos blocked before hatching.

To pinpoint the origin of the DNA damage during spermatogenesis in *Ube2b* knockout mice, we selected the earliest haploid germ cells and performed round spermatid injection (ROSI). ROSI with nuclei of *Ube2b$^{-/-}$* spermatids generated zygotes with an unfragmented paternal pronucleus and further *in vivo* embryonic development was successful and indistinguishable from results obtained from ROSI with wild type spermatids.

These data indicate that UBE2B is required in developing spermatids to protect the genome from damage in sperm, and has a paternal-effect function to ensure maintenance of genome integrity during early embryonic development.

INTRODUCTION

Rad6 is an E2 ubiquitin-conjugating enzyme that is required for multiple processes, including meiotic recombination and sporulation [1-3], but it is most well known for its role in replicative damage bypass (RDB) in *S. cerevisae*.

The RDB pathway is initiated when DNA damage is encountered during DNA replication, and allows S phase to proceed (reviewed by [4]). One of the first steps in RDB is ubiquitylation of PCNA (proliferating cell nuclear antigen) by Rad6 in association with the E3 ubiquitin ligase Rad18 [5]. Together with Bre1, another E3 ubiquitin ligase, Rad6 mono-ubiquitylates histone H2B on lysine 123 (H2BK123) [6-10], which is required for the methylation of H3K4 and H3K79 through a "trans tail pathway" [11-14]. Finally, Rad6 participates in protein degradation by the N-end rule pathway through complex formation with Ubr1/2 [15-17].

Two mammalian Rad6 homologs, named UBE2A (previously called HR6A) and UBE2B (previously called HR6B) [18-20], and one mammalian Rad18 homolog, named RAD18 [21] have been identified. UBE2A (encoded by the X chromosome) and UBE2B (autosomally encoded) show 91% amino acid identity, and are ubiquitously expressed. Mutation of both genes in mouse appears to be cell lethal, whereas single *Ube2a* or *Ube2b* knockout cells show no defects in the RDB pathway [19, 20].

In mammalian cells, lysine 120 of histone H2B (H2BK120, homologous to H2BK123 in *S. cerevisae*) is ubiquitylated through the combined action of UBE2A/B and the ubiquitin ligases RNF20/40 (Bre1 homologs) [22-24]. The overall level of H2B ubiquitylation is relatively low, and H2A is the major ubiquitylated histone. In *Ube2b* knockout spermatocytes and spermatids, ubiquitylation of both H2A and H2B appears to be unaffected [25]. Since both UBE2A and UBE2B can ubiquitylate H2B [23], the normal level of ubiquitylated H2B in *Ube2b* knockout germ cell extracts could be due to an overlapping function of UBE2A. However, the level of UBE2A protein in spermatocytes and spermatids is relatively low, compared to that of UBE2B, due to the fact that the X chromosome is transcriptionally silenced during meiotic prophase. The heterologous X and Y chromosomes undergo meiotic sex chromosome inactivation (MSCI) leading to the formation of the XY body [26]. UBE2A/B accumulates on the XY body during male meiotic prophase [4, 27]. After completion of the meiotic divisions, silencing of the sex chromosomes is largely maintained during the postmeiotic stage [28, 29], although a distinct set of single and multi-copy X- and Y-linked genes, including the X-linked *Ube2a* gene, are re-expressed [27, 30, 31].

Interestingly, *Ube2a* and *Ube2b* single knockout mice show diverse fertility problems. *Ube2a* knockout males are fertile, but the females are infertile due to a maternal defect at the 2-cell stage of embryonic development [19]. In contrast,

the *Ube2b* knockout shows male-limited infertility due to severely impaired spermatogenesis [20].

Previously, we have shown that meiotic as well as postmeiotic germ cell development is impaired in *Ube2b* knockout testis [32,33]. During meiotic prophase, the spermatogenic impairment involves increased meiotic recombination frequency, and anomalies of the synaptonemal complex [33]. From late pachytene onwards, *Ube2b* knockout spermatocytes and spermatids show enhanced levels of H3K4me2 on respectively the XY body and the X or Y chromatin, and *Ube2b*-knockout spermatids show derepression of X chromosomal genes [27,32]. This result indicates a role for UBE2B in the maintenance of meiotic and postmeiotic sex chromosome inactivation. Global analysis of gene expression in wild type and *Ube2b* knockout spermatocytes and spermatids revealed that UBE2B-deficiency hardly affects gene expression during the meiotic prophase in spermatocytes, whereas approximately 30% of the genes are differentially expressed in the postmeiotic round spermatids [27]. This global dysregulation of gene expression in *Ube2b* knockout spermatids includes a more pronounced upregulation of the X chromosome.

Following the two meiotic divisions, haploid round spermatids undergo extensive morphological changes and chromatin remodeling in spermiogenesis. When round spermatids start to elongate, histones are replaced by two transition proteins, TP1 and TP2 [34]. The removal of histones and their replacement by transition proteins is accompanied by the transient formation and repair of DNA double strand breaks. The formation of these breaks acts to release topological stress [35-39]. During the final phases of spermatid condensation, the transition proteins are replaced by the arginine-rich protamines 1 and 2 (PMR1 and PMR2). Protamines are essential for fertility, since haploinsufficiency for one of the protamine genes already leads to infertility [40,41]. In the absence of TP1 and TP2 however, histones are still removed and replaced by protamines, but the process of chromatin condensation is aberrant. *Tp1* and *Tp2* double knockout mice are infertile and intracytoplasmic sperm injection (ICSI) of wild type oocytes with epidydimal spermatozoa did not result in offspring. However, ICSI with testicular sperm from these mice resulted in viable offspring, indicating that the genomic integrity is maintained up to release of the sperm cells in the epididymis [42].

To study if genomic derailment of male germ cells might occur before or during the process of spermiogenesis in certain mouse models of male infertility, one possibility would be to inject the earliest haploid nucleus, that of round spermatids, preceeding the chromatin reorganization process, into wild type oocytes (ROSI, round spermatid injection). Recently, Meng et al. [43] showed that ROSI with nuclei carrying a male sterility transgene indeed resulted in life offspring, whereas ICSI did not.

Herein, we generated a transgenic mouse expressing UBE2B fused to a hemagglutinin tag (HA) in spermatocytes and spermatids on the *Ube2b* knockout genetic background (*Ube2b⁻/⁻ / Ube2b-HA* mice) to analyse the specific function of UBE2B in spermatogenesis in more detail. We used ICSI and ROSI to try to rescue the infertility phenotype of *Ube2b* knockout mice, in the presence or absence of germ cell-specific UBE2B-HA expression. We show that UBE2B has an essential role during postmeiotic chromatin reorganisation and that its function during spermatogenesis is also required to ensure maintenance of genome integrity during subsequent early embryonic development.

RESULTS

Testis-specific expression of UBE2B fusion protein in transgenic mice

First we investigated whether we could rescue *Ube2b* knockout infertility through testis-specific transgenic expression of an UBE2B-HA fusion protein. This can yield information about functionality of the tagged proteins, with the aim to use transgenic expression of UBE2B-HA for protein-protein interaction studies.

To direct expression of the *Ube2b-HA* transgene (Figure 1a) specifically to germ cells, we selected a *Calmegin* gene promoter fragment that has been shown to induce transgene reporter expression specifically in pachytene spermatocytes [44].

We obtained a single *Ube2b-HA* transgenic line (Figure 1a). Southern blot analyses indicated that only a single copy of the *Ube2b-HA* transgene was integrated (data not shown), and Western blot analyses confirmed testis-specific expression of the fusion protein in *Ube2b-HA* transgenic mice (Figure 1b). However, expression of the *Ube2b-HA* transgene is low compared to the expression of endogenous *Ube2a/Ube2b* genes. Also, on an *Ube2b⁻/⁻* background in *Ube2b⁻/⁻ / Ube2b-HA* mice, UBE2A expression was higher than UBE2B-HA expression (Figure 1c). In isolated germ cells from *Ube2b⁻/⁻ / Ube2b-HA* mice, UBE2B-HA expression was higher in spermatocytes than in spermatids, but low compared to endogenous UBE2A/UBE2B (Figure 1d).

Localization of UBE2B-HA and SYCP3 in spermatogenic cells

Previously, we have described accumulation of UBE2A/UBE2B on XY body chromatin of pachytene spermatocytes [4]. The antibody used recognizes both UBE2A and UBE2B and, therefore, the only available negative control experiment involved competition with the peptide that was used to generate the antibody. The present generation of transgenic mice that express UBE2B-HA provides a more specific tool to determine the localization of UBE2B in spermatocytes from midpachytene onwards, when the *Calmegin* promoter is activated. Indeed, in spread nuclei of spermatocytes from *Ube2b-HA / Ube2b⁻/⁻* transgenic mice, no UBE2B-HA was detected in leptotene and zygotene spermatocytes.
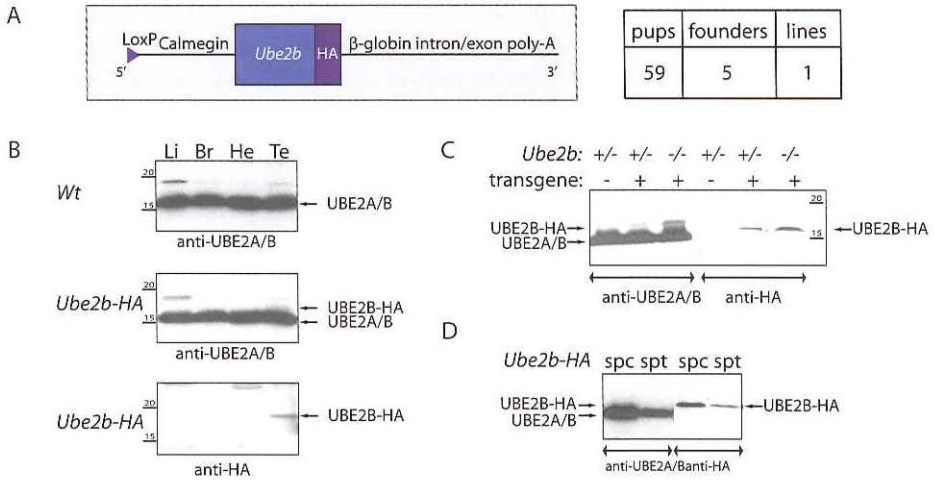
Figure 1. Generation and analyses of the *Ube2b-HA* mouse model. (a) Generation of testis-specific *Ube2b-HA* transgenic mice. The *Ube2b-HA* - DNA construct contained the *Calmegin* promoter placed in front of a cDNA encoding UBE2B-HA fusion protein. To enhance expression, b-globin intron/exon sequences and a polyadenylation signal were fused to 3' to the cDNA sequences. 59 pups were generated of which 5 were positive for the transgene (founders). Of these, only one showed expression of the transgene in testes of male offspring, resulting in a single *Ube2b-HA* line. (b) Testis-specific expression of UBE2B-HA. Expression of UBE2A/B and UBE2B-HA was analysed with anti-UBE2A/B and anti-HA antibodies in liver (Li), brain (Br), heart (He), and testis (Te) tissue extracts from 10-week-old wild-type (*Wt*) and *Ube2b-HA* transgenic mice. Arrows indicate the positions of the detected proteins. We observed the presence of a non-specific band around 18 KDa obtained with anti-UBE2A/B. (c) The expression of UBE2A/B and UBE2B-HA in testis from 25-day-old *Ube2b* heterozygous (+/-) and knockout (-/-) mice with (+) or without (-) the transgene. (d) Analysis of UBE2B-HA expression in isolated germ cells from *Ube2b-HA* transgenic mice. UBE2A/B and UBE2B-HA showed highest expression in germ cell preparations greatly enriched in spermatocytes (spc) compared to spermatids (spt), both isolated from 2-month-old *Ube2b-HA* transgenic animals.

Immunohistochemical analyses of UBE2B-HA expression in *Ube2b* knockout mice showed that the UBE2B-HA protein is expressed from midpachytene onwards (Figure 2a), with lower expression in round and elongating spermatids (Figure 2a).

In pachytene nuclei, UBE2B-HA is detected almost exclusively on the XY body (Figure 2b). Then, in late pachytene and early diplotene nuclei, UBE2B-HA remains high on the XY body, but UBE2B-HA foci become more apparent in the rest of the nucleus (Figure 2b). This staining pattern with anti-HA antibody was not observed in control wild-type mice (not shown). In addition, UBE2B-HA was found to colocalize with RAD18 on the XY body (Figure 2c).
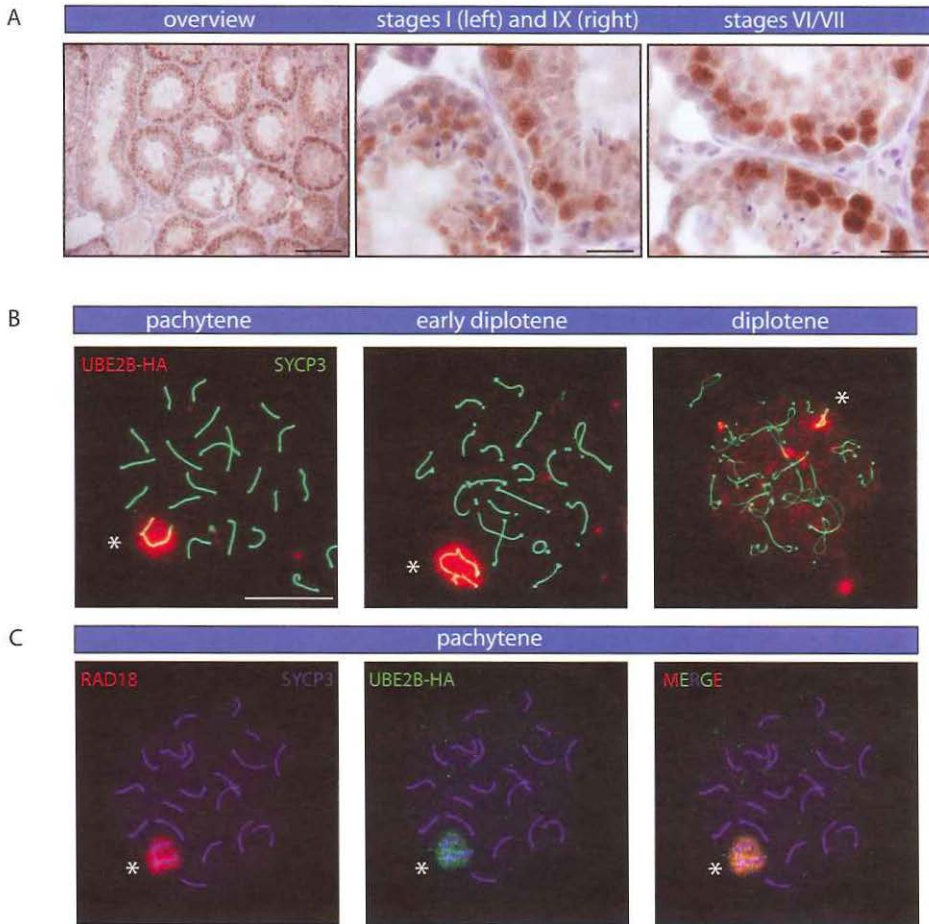
Figure 2. Localisation of UBE2B-HA in mouse testes. (a) Immunohistochemical analyses of UBE2B-HA protein expression in tissue sections of $Ube2b^{-/-}$ /$Ube2b$-HA mouse testis. Bar represents 100mm in the left panel and 20 mm in the two panels on the right. (b) Immunolocalization of UBE2B-HA protein (red) and SYCP3 (green) in spread pachytene, early and late diplotene nuclei from $Ube2b^{-/-}$/$Ube2b$-HA spermatocytes. UBE2B-HA localizes to the XY body. In diplotene, UBE2B-HA gradually shows a more spread distribution of chromatin-associated foci. Pictures were obtained and modified using identical settings. Asterisk indicates the XY body; scale bar represents 20 μm. (c) Immunolocalization of SYCP3 (blue), RAD18 (red) and UBE2B-HA protein (green) in spread nucleus of pachytene spermatocyte from $Ube2b^{-/-}$ /$Ube2b$-HA mouse. Asterisk indicates colocalization of RAD18 and UBE2B-HA on the XY body. Scale bar represents 20 μm.

UBE2B-HA expression in pachytene spermatocytes does not rescue the meiotic phenotype of Ube2b knockout mice.

Previously, we have shown that *Ube2b* knockout pachytene en diplotene spermatocytes show dysregulation of general chromatin structure associated with increased meiotic recombination frequency, anomalies of the synaptonemal complex (SC) [33], and aberrant histone modifications [32].

Since the localization of UBE2B-HA seems to be identical to what we have observed for endogenous, wild type UBE2A/B, we first investigated if the tagged protein expression could rescue the phenotypical characteristics of *Ube2b*^{-/-} knockout spermatocytes. Despite the presence of UBE2B-HA, the average number of MLH1 foci was increased compared to wild type spermatocytes, but comparable with the *Ube2b* knockout (Table 1). In addition, similar SC aberrations were observed in *Ube2b*^{-/-}/*Ube2b-HA* and *Ube2b* knockout spermatocytes (note the numerous separated SC ends in the very early diplotene spermatocye in Figure 2b). We then analyzed spermatocyte apoptosis, and found a similar increase in the number of apoptotic nuclei in sections from transgenic and knockout mouse testis, compared to wild type (Table 1). Also, the increased phosphorylation and dimethylation of XY body histones in *Ube2b*^{-/-} spermatocytes [32], were also observed on the XY body in *Ube2b*^{-/-}/*Ube2b-HA* spermatocytes (not shown).

These results indicate that *Ube2b-HA* transgene expression from pachytene onwards does not rescue the defects of UBE2B-deficient spermatocytes during the meiotic prophase.

Fertility analyses of Ube2b-HA transgenic mouse models

Male *Ube2b-HA* transgenic mice were normally fertile on wild type background (not shown). However, repeated breedings (17) of *Ube2b*^{-/-}/*Ube2b-HA* transgenic mice yielded no offspring. Analysis of testis and epididymal sperm morphology showed that the quality of spermatogenesis was affected in testes from *Ube2b* knockout mice either with or without the *Ube2b-HA* transgene (Figure 3ab). However, testis weights of *Ube2b-HA* transgenic mice were higher compared

Table 1. Analysis of MLH1 foci and apoptosis in wild type, *Ube2b*^{-/-} and *Ube2b-HA/Ube2b*^{-/-} mouse testes.

Genotype	# MLH1 foci	SEM	# apoptotic nuclei*	n
Wild type	25.5	0.35	52	1
Ube2b^{-/-}/*Ube2b*-HA	27.4	0.41	141	2
Ube2b^{-/-}	27.8	0.68	154	2

*average number of apoptotic nuclei per 100 tubule sections

to those of *Ube2b* knockouts lacking the transgene (Figure 3c). A similar partial rescue of the *Ube2b^-/-^* phenotype by the transgene was observed when sperm counts were compared (Figure 3c). Epididymal sperm from *Ube2b* knockout mice shows a large variety of highly abnormal sperm heads (Figure 3bc, [20]) and only a very small percentage of sperm heads with normal, or near normal, morphology can be detected (Figure 3bc). When the *Ube2b-HA* transgene is expressed, the percentage of normal sperm heads increases to approximately 30% (Figure 3c).
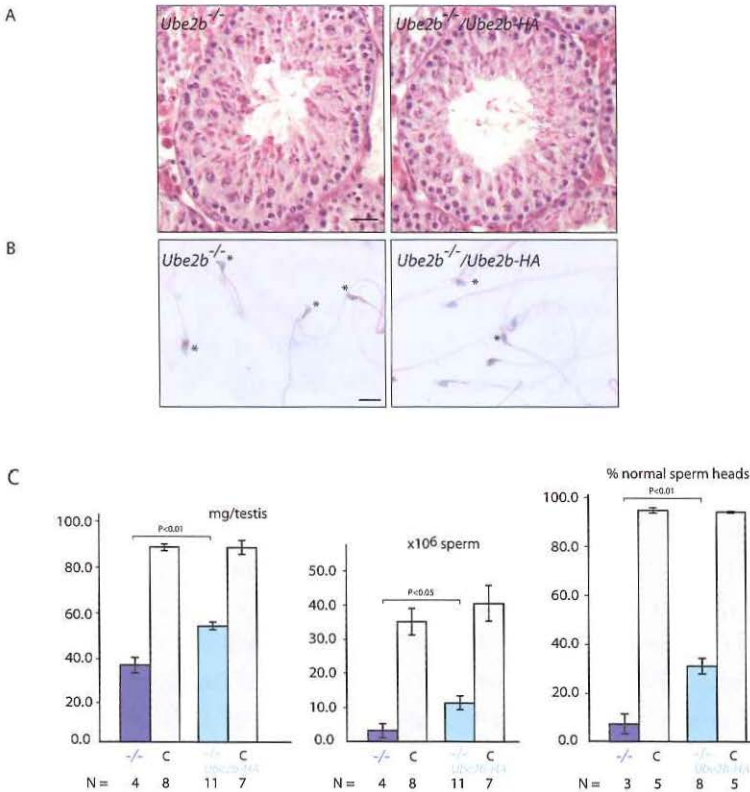
Figure 3. Characterisation of *Ube2b-HA* male mouse model. (a) Hematoxylin/eosin stained stage X-XI testis tubule cross sections from 9-week-old *Ube2b* knockout (*Ube2b^-/-^*) with or without *Ube2b-HA* transgene as indicated. Overall, the quality of spermatogenesis is variable on the *Ube2b* knockout background, with no obvious improvement resulting from the presence of the *Ube2b-HA* transgene. Scale bar represents 25 μm. (b) Epididimal spermatozoa from 9-week-old *Ube2b* knockout mice with (*Ube2b^-/-^/Ube2b-HA*) or without (*Ube2b^-/-^*) transgene. Sperm heads marked with asterisks were classified as abnormal. Note the presence of morphologically normal sperm from *Ube2b^-/-^/Ube2b-HA*. Scale bar represents 10 μm. (c) Testes weight, epididimal sperm cell count and sperm head morphology were assessed for *Ube2b^-/-^* (-/-), *Ube2b-HA/Ube2b* (-/-, *Ube2b-HA*), and control (C) adult mice. n = number of mice. Error bars represent SEM.

The increased testis weight, sperm counts and fraction of morphologically normal sperm of *Ube2b*^{-/-}/*Ube2b-HA* males compared to *Ube2b* knockout males indicates that the spermatocytes that survive beyond the meiotic prophase are at least partly rescued by the postmeiotic *Ube2b-HA* transgene expression. However, UBE2B-HA clearly does not completely rescue the *Ube2b*^{-/-} phenotype, which could be due to either too late and/or too low expression of *Ube2b-HA*. Also, the presence of the HA-tag could interfere with the functionality of UBE2B-HA.

Sperm chromatin structure assay (SCSA) shows that Ube2b^{-/-}*/Ube2b-HA sperm has a normal DNA fragmentation index*

To understand why *Ube2b*^{-/-}/*Ube2b-HA* male mice are still infertile, we performed a sperm chromatin structure assay (SCSA) on *Ube2b*^{-/-}, *Ube2b*^{-/-}/*Ube2b-HA* and wild type sperm originating from the vas deferens. SCSA is a flow cytometric technique that can identify abnormal chromatin packaging in spermatozoa by quantitatively measuring the susceptibility of DNA to low pH-induced denaturation in situ. DNA that contains breaks is more susceptible to the denaturation process, and this will lead to a larger fraction of single-stranded (indicative of breakage) versus double-stranded (intact) DNA. Differential fluorescence of acridine orange (AO) is used to differentiate between denatured, single stranded and native, double-stranded DNA in sperm chromatin. When AO binds to single stranded DNA, fluorescence will be red, and green when AO is associated with double stranded DNA. The extent of DNA denaturation is expressed as the DNA fragmentation index (% DFI), representing the percentage of the sperm with a relatively high level of red fluorescence (% DFI) (for more details see [51]). In several animals and in man, a DFI <15% is associated with normal fertility [55].

SCSA analyses showed a DFI of 7.2% for wild type sperm and 2.8% for *Ube2b*^{-/-}/*Ube2b-HA* sperm, which can be classified as normal. On the other hand, *Ube2b*^{-/-} sperm has a DFI of 39%, indicating the presence of highly damaged DNA. The results from the SCSA indicate that the expression of UBE2B-HA prevents the occurrence or accumulation of DNA damage during spermatogenesis. However, it does not explain the infertility of the *Ube2b*^{-/-}/*Ube2b-HA* males.

The Ube2b^{-/-} *paternal pronucleus shows massive phosphorylation of H2AX and DNA fragmentation, while Ube2b*^{-/-}*/Ube2b-HA sperm induces progressive nucleic fragmentation during early embryonic development*

We investigated if ICSI could rescue the infertility phenotype of the *Ube2b*^{-/-} and *Ube2b*^{-/-}/*Ube2b-HA* mice. Zygotes obtained after ICSI with wild type, *Ube2b*^{-/-} and *Ube2b*^{-/-}/*Ube2b-HA* sperm were fixed at 2 hours and 4 hours (Figures 4, 5 and 6) after injection, and immunostained for the DNA double-strand break (DSB) marker γH2AX. Two hours after injection, zygotes derived from injection

with wild type sperm showed decondensing sperm in almost all cases (13 out of 14) and the second meiotic division of the maternal genome had taken place in all zygotes. Maternal (pre)pronuclei mostly contained one or two distinct γH2AX foci (Figure 4a), whereas several γH2AX foci were observed in paternal (pre)pronuclei. These foci might be caused by DNA breaks that accompany the
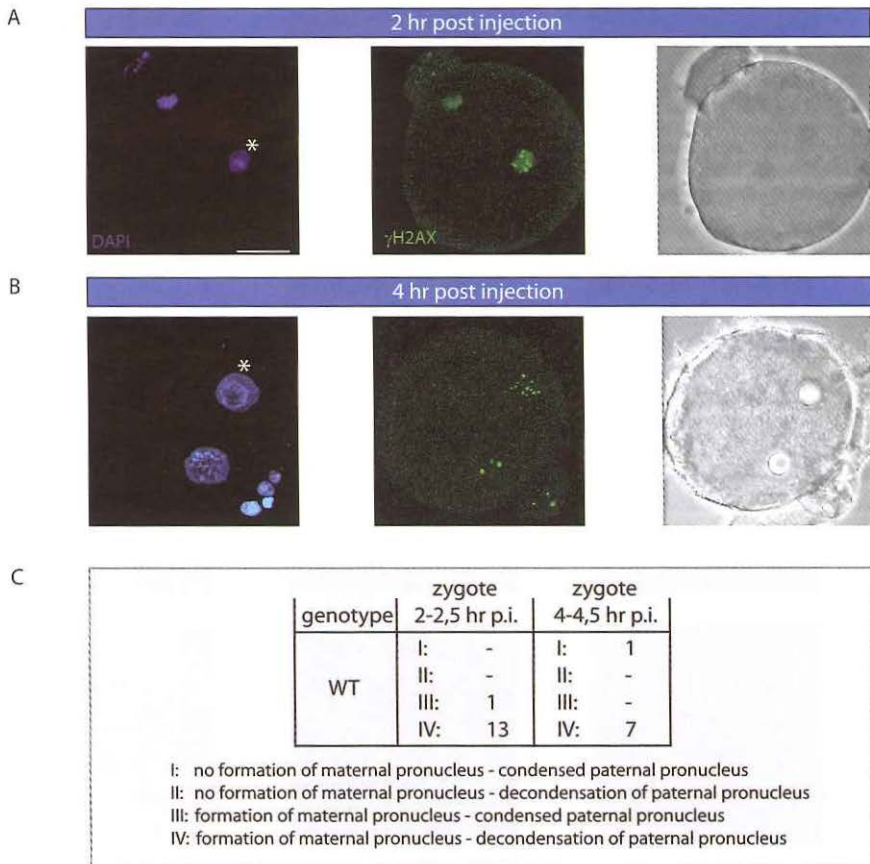
Figure 4. Pronucleus formation and γH2AX foci shortly after intracytoplasmic sperm injection (ICSI) with wild type sperm. Immunostaining for DAPI (blue) and γH2AX (green) of zygotes 2 and 4 hours after injection. The right panel presents differential interference contrast (DIC) images of the same zygote. Asterisks indicate the paternal pronucleus. Bar represents 10 µm. (a) Two hours after injection, the oocyte has completed the second meiotic division and both the developing paternal and maternal pronuclei show some γH2AX foci. (b) Four hours after injection the formation of both paternal and maternal pronucleus is complete. The paternal pronucleus has many γH2AX foci, whereas the maternal pronucleus either shows no γH2AX foci (not shown) or some distinct γH2AX foci (lower panel). (c) Table summarizing the dynamics of the developing paternal and maternal pronuclei two and four hours post injection (p.i.).

A

2 hr post injection

DAPI γH2AX

B

4 hr post injection
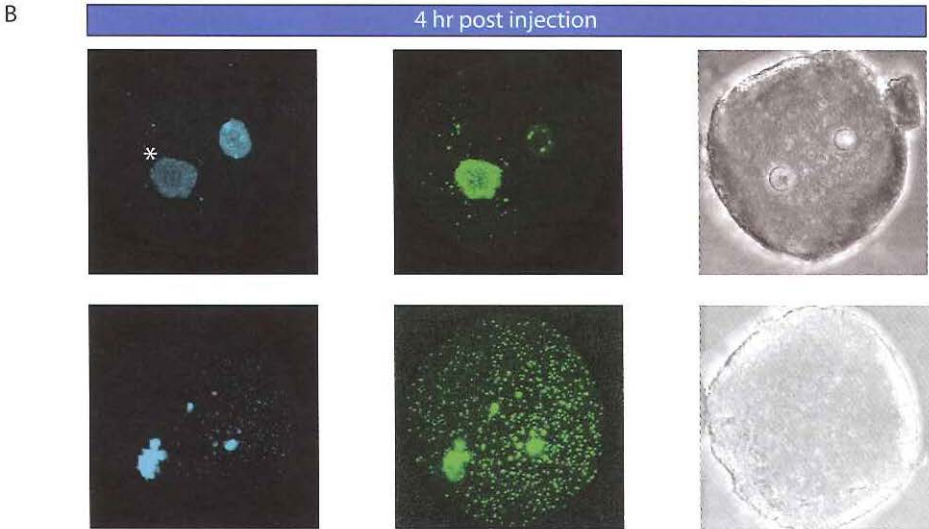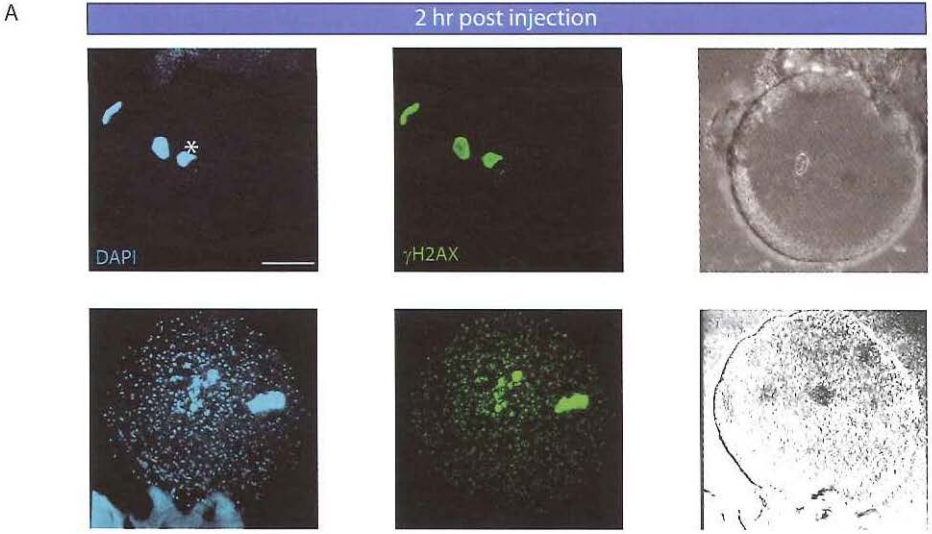
C

genotype	zygote 2-2,5 hr p.i.		zygote 4-4,5 hr p.i.	
Ube2b⁻/⁻	I:	3	I:	1
	II:	4	II:	3
	III:	1	III:	-
	IV:	3	IV:	2

I: no formation of maternal pronucleus - condensed paternal pronucleus
II: no formation of maternal pronucleus - decondensation of paternal pronucleus
III: formation of maternal pronucleus - condensed paternal pronucleus
IV: formation of maternal pronucleus - decondensation of paternal pronucleus

protamine-to-histone transition. Alternatively, or in addition, some DNA damage that has accumulated during sperm storage in the epidydimis might be detected by the maternal DNA repair machinery. Four hours after injection, both the paternal and maternal pronuclei were completely formed; the paternal pronucleus still showed distinct bright γH2AX foci dispersed through the nucleus, and the maternal pronucleus mostly had 3 to 5 large γH2AX foci. Only in 1 out of 22 zygotes at 2 and 4 hours after injection (Figure 4b) the maternal second meiotic division had not taken place.

In the majority of the zygotes from *Ube2b*^{-/-} sperm (7 out of 11), the paternal DNA was fragmented and showed intense staining for γH2AX already at 2 hours after sperm injection (Figure 5a), whereas in the remaining 4 embryos the paternal genome was still completely condensed. The presence of massive H2AX phosphorylation on the *Ube2b*^{-/-} paternal genome in combination with its fragmentation is in agreement with our findings of the SCSA analysis, which indicated the presence of massive DNA damage and/or breakage in *Ube2b*^{-/-} sperm. At 4 hours after injection (Figure 5b), only 2 out of 6 surviving zygotes contained an almost intact (decondensed) paternal pronucleus, although these nuclei were still strongly γH2AX -positive and small DAPI and γH2AX-positive fragments were present. Three embryos contained paternal DNA that showed complete fragmentation, and of one embryo the paternal genome was still condensed. Summarized (Figure 5c), we found that in most of the zygotes (8 out of 10), the paternal genome was completely fragmented and the dispersed patches of DAPI-positive material in the zygote also contained high levels of γH2AX. In addition, in the majority (11 out of 17) of the zygotes, the oocytes had not undergone the second meiotic division (Figure 5ab).

◁ **Figure 5. *Ube2b* knockout sperm derived paternal pronucleus shows fragmentation upon decondensation.** Immunostaining for DAPI (blue) and γH2AX (green) of zygotes fertilized with sperm from *Ube2b* knockout mice. The right panels present differential interference contrast (DIC) images of the same zygote. Asterisks indicate the paternal pronucleus. Bar represents 10 µm. (a) Two hours after injection with *Ube2b*^{-/-} sperm, both the paternal and maternal pronuclei are heavily stained with γH2AX and DAPI, here shown for two different zygotes. In addition, γH2AX and DAPI-positive fragments can be observed apart from the developing paternal pronucleus / decondensing spermhead (upper panel), or the paternal pronucleus is fragmented (lower panel). Note that the second maternal meiotic division has not been completed in the lower panel. (b) Four hours after ICSI with *Ube2b*^{-/-} sperm. In the upper panel, the paternal pronucleus is decondensed, γH2AX-positive and surrounded by small DAPI- and γH2AX-positive parts. The maternal pronucleus has been formed and shows some γH2AX foci. The lower panel shows a completely shattered paternal pronucleus, and maternal metaphase-II arrest. (c) Table summarizing the results for the *Ube2b*^{-/-} paternal pronucleus and wild type maternal pronucleus.
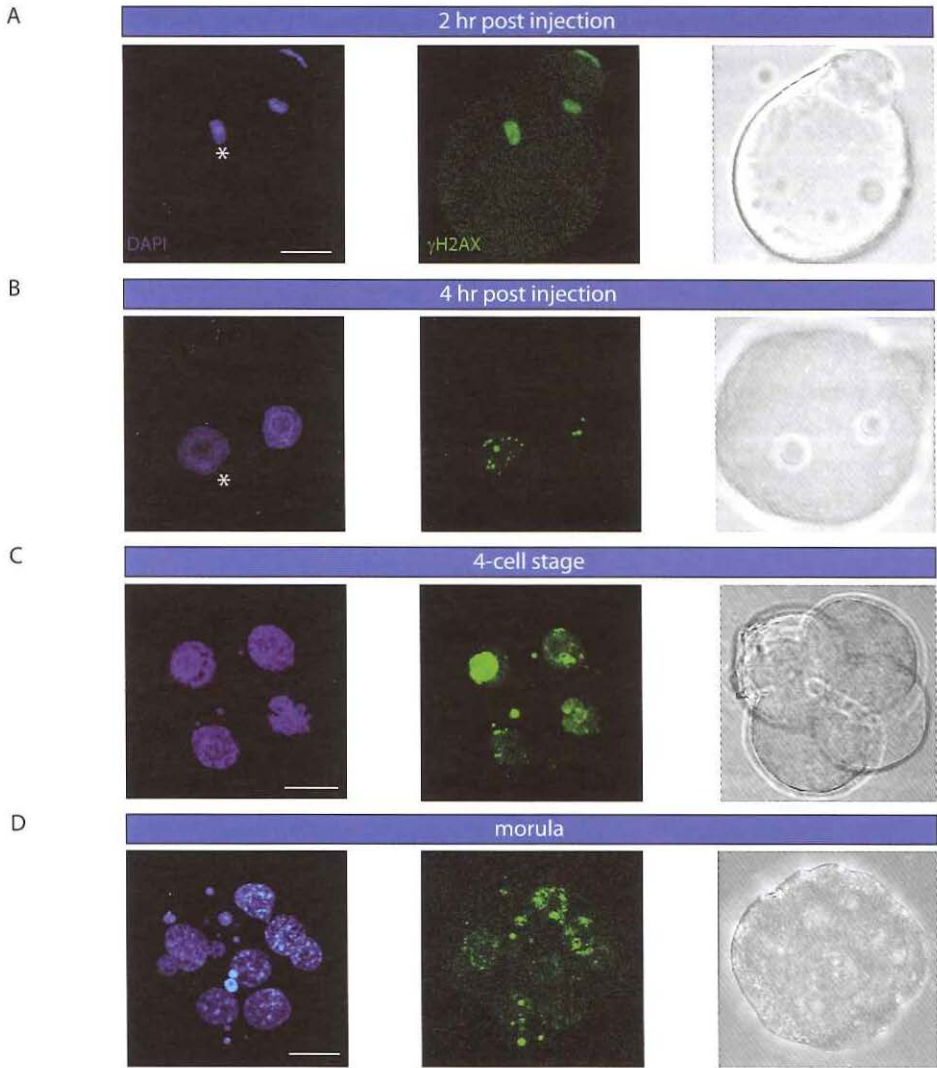
A 2 hr post injection

DAPI | γH2AX

B 4 hr post injection

C 4-cell stage

D morula

E

genotype	zygote 2-2,5 hr p.i.		zygote 4-4,5 hr p.i.		morula 72-90 hr p.i.	blastocyst
Ube2b-HA	I:	-	I:	2	8 8 x DDBs	+, but never hatches
	II:	2	II:	-		
	III:	-	III:	-		
	IV:	4	IV:	5		

I: no formation of maternal pronucleus - condensed paternal pronucleus
II: no formation of maternal pronucleus - decondensation of paternal pronucleus
III: formation of maternal pronucleus - condensed paternal pronucleus
IV: formation of maternal pronucleus - decondensation of paternal pronucleus

Zygotes derived from ICSI with *Ube2b⁻/⁻/Ube2b-HA* sperm showed normal decondensation at 2 (Figure 6a) and 4 hours (Figure 6b) after injection, and the pattern of γH2AX immunostaining in paternal and maternal pronuclei was similar to what was observed in zygotes obtained after ICSI with wild type sperm (Figure 4ab). These results confirmed our SCSA findings, which indicated comparable low levels of DNA damage in both *Ube2b⁻/⁻/Ube2b-HA* and wild type sperm. However, in 4 out of 13 zygotes, the second maternal meiotic division had not occurred (Figure 6e), which could indicate that, although *Ube2b-HA* expression on a *Ube2b* knockout background provides some support during spermiogenesis, the resulting sperm cells are impaired in their ability to activate the oocyte. At the 2-cell stage, we noticed DAPI dense and γH2AX positive bodies (DDBs), in 3 out of the 7 preimplantation embryos (Figure 6e). These DDBs most likely represent nuclear fragmentation, which occurred after the first cleavage division. Each nucleus contained several γH2AX foci, and mitotic metaphases were completely stained with anti-γH2AX. In cultured mitotic cells, γH2AX foci are known to form in S phase, possibly at breaks that result from stalled replication forks [56]. At the 4-cell stage (Figure 6c), 2 out of 5 analysed embryos showed γH2AX DDBs, and again each nucleus contained several γH2AX foci. At the morula stage (Figure 6d), all analysed embryos displayed many γH2AX positive DDBs in almost every cell, and many nuclei showed aberrant morphology compared to the nuclei of blastocysts derived from ICSI with wild type sperm. Although some embryos appeared to reach the blastocyst stage with signs of cavitation, *Ube2b⁻/⁻/Ube2b-HA* sperm derived embryos never hatched (not shown), in contrast to the normal hatching of embryos derived from wild type sperm ICSI.

◁ **Figure 6. ICSI with *Ube2b⁻/⁻/Ube2b-HA* sperm results in normal fertilization but embryos show progressive nuclear fragmentation during early embryonic development.** Pre-implantation embryos at different stages resulting from ICSI with *Ube2b⁻/⁻/Ube2b-HA* sperm were immunostained for γH2AX (green) and DAPI (blue). The right panel presents a differential interference contrast (DIC) image of the same embryo. Asterisks indicate the paternal pronucleus. Bar represents 10 μm. (ab) *Ube2b⁻/⁻/Ube2b-HA* paternal and wild type maternal pronuclei show normal development at 2 (A) and 4 (B) hours after injection. Both pronuclei show γH2AX-foci. Bar represents 10 μm. (cd) Immunostaining of respectively 4-cell and morula stage *Ube2b-HA/Ube2b⁻/⁻* sperm derived embryos for DAPI (blue) and γH2AX (green). (c) Several γH2AX-positive and DAPI dense bodies in two blastomeres of a 4-cell stage embryo. (d) Morula-stage embryo. Some blastomeres show aberrant nuclear morphology and many DAPI dense and γH2AX-positive bodies are present throughout the embryo, indicating progressive nuclear fragmentation. (e) Table with results for the different developmental stage of *Ube2b-HA/Ube2b⁻/⁻* sperm derived embryos. Note that although some reach blastocyst stage, they were never able to hatch.

Ube2b⁻/⁻ testicular sperm shows varying degrees of DNA damage and fragmentation after fertilization but development is blocked before hatching of the blastocyst

Our SCSA results indicated that DNA breaks accumulate throughout the genome in *Ube2b* knockout germ cells during the process of spermatogenesis, or during storage of sperm in the epidydimis. Alternatively, highly aberrant chromatin packaging may render the DNA more susceptible to breakage during the acid denaturation step of the SCSA assay.

Zhoa et al [42] showed that testicular spermatozoa of mice lacking transition nuclear proteins (TP1 and 2) were capable of producing offspring when using ICSI, but epidydimal spermatozoa were not able to fertilize, indicating that aberrant sperm may accumulate DNA damage while stored in the epididymis.

To test whether *Ube2b* knockout sperm isolated from the testis would be able to support embryo development following ICSI, we activated oocytes and then injected *Ube2b⁻/⁻* testicular sperm heads. Five embryos were analysed at 4 hours following fertilization. Of these, three embryos displayed increased γH2AX staining in the paternal pronucleus, compared to controls, and two of these also showed partial DNA fragmentation. Two embryos displayed normal γH2AX staining in the paternal and maternal pronuclei (not shown). Embryos that were kept in culture all reached the 2-cell stage, but blocked before reaching the hatching stage.

Ube2b knockout round spermatids do not accumulate unrepaired DNA double strand breaks

The above results of SCSA and ICSI indicated that *Ube2b* knockout testicular spermatozoa have accumulated DNA damage, or become highly susceptible to DNA breakage, during spermatogenesis, but are further damaged during storage in the epidydimis. We next tried to pinpoint the timing of the occurrence of the defect that leads to the observed DNA damage in early embryos upon ICSI. On testis sections, stained for γH2AX, no differences were detected in the pattern of staining, and fully condensed spermatids were generally γH2AX-negative (not shown). In addition, TUNEL staining patterns on testis sections were similar for wild type and *Ube2b* knockout spermatids (not shown). To study this further, we immunostained *Ube2b⁻/⁻* spread preparations for γH2AX to analyse the presence or occurrence of DNA breaks in secondary spermatocytes, round and elongating spermatids (Figure 7b). The results show that the amount of γH2AX varies between spermatids, in the knockout as well as the wild type. However, a clear focal γH2AX staining observed in wild type spermatids (Figure 7a), was less apparent for the knockout spermatids (Figure 7b).
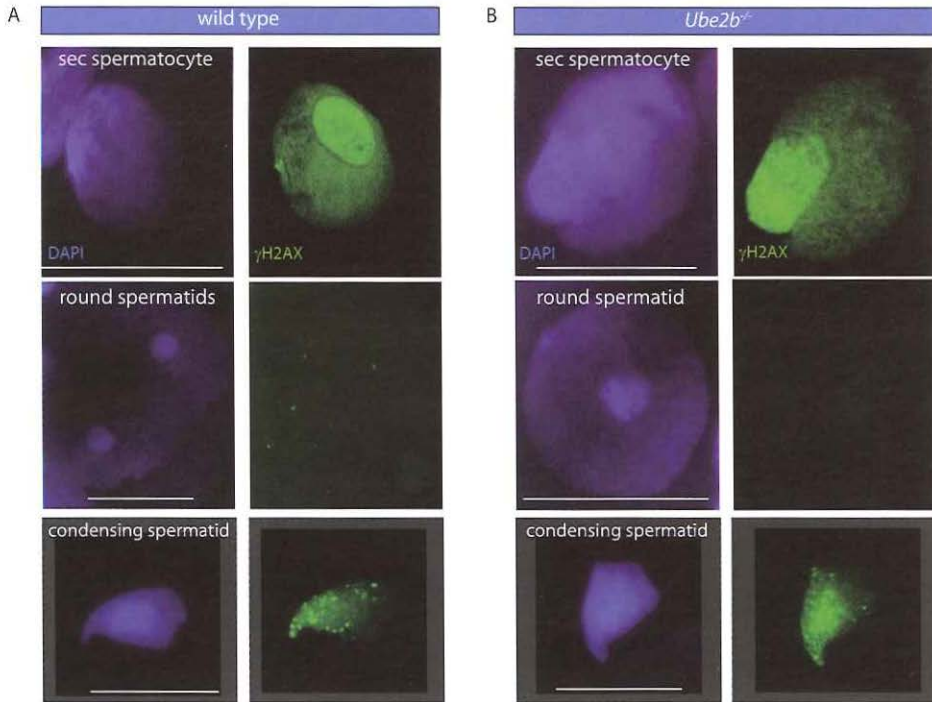
Figure 7. Analysis of γH2AX localization in spread preparations nuclei and spermatozoa of wild type and *Ube2b* knockout mouse testes. Wild type (a) and *Ube2b* knockout (b) secondary spermatocyte, spermatid and spermatozoa nuclei were stained with DAPI (blue) and anti- γH2AX (green). The overall pattern is similar in wild type and knockout nuclei. γH2AX appears somewhat enhanced in knockout spermatocytes and spermatids. Bar represents 10 μm.

Injection of round spermatids from Ube2b knockout mice yields normal embryos.
Based upon the above results, we investigated the fertilization potential of *Ube2b* knockout round spermatids compared to round spermatids from wild type mice through the use of ROSI (Figure 8). Oocytes were injected with nuclei of manually selected round spermatids of *Ube2b⁻/⁻* mice, and the resulting zygotes were fixed 4 hours after injection. Subsequently, the zygotes were immunostained for γH2AX and H3K4me2, and analysed with confocal microscopy. The paternal pronucleus could be identified by the relative lack of H3K4me2 compared to a higher level in the maternal pronucleus (not shown). We found that in the majority of the zygotes (6/11) the developing paternal pronucleus contained some γH2AX foci comparable to what is observed in wild type pronuclei after ICSI (compare Figure 8a to Figure 4b). No nuclear fragments were observed. The remaining paternal pronuclei (5/11) were partially developed (Figure 8b),

Ube2b⁻ᐟ⁻
4 hr post injection

A

DAPI   γH2AX

B

wild type
4 hr post injection

C

DAPI   γH2AX

D

E

Ube2b⁻ᐟ⁻   WT

embryonic day 18
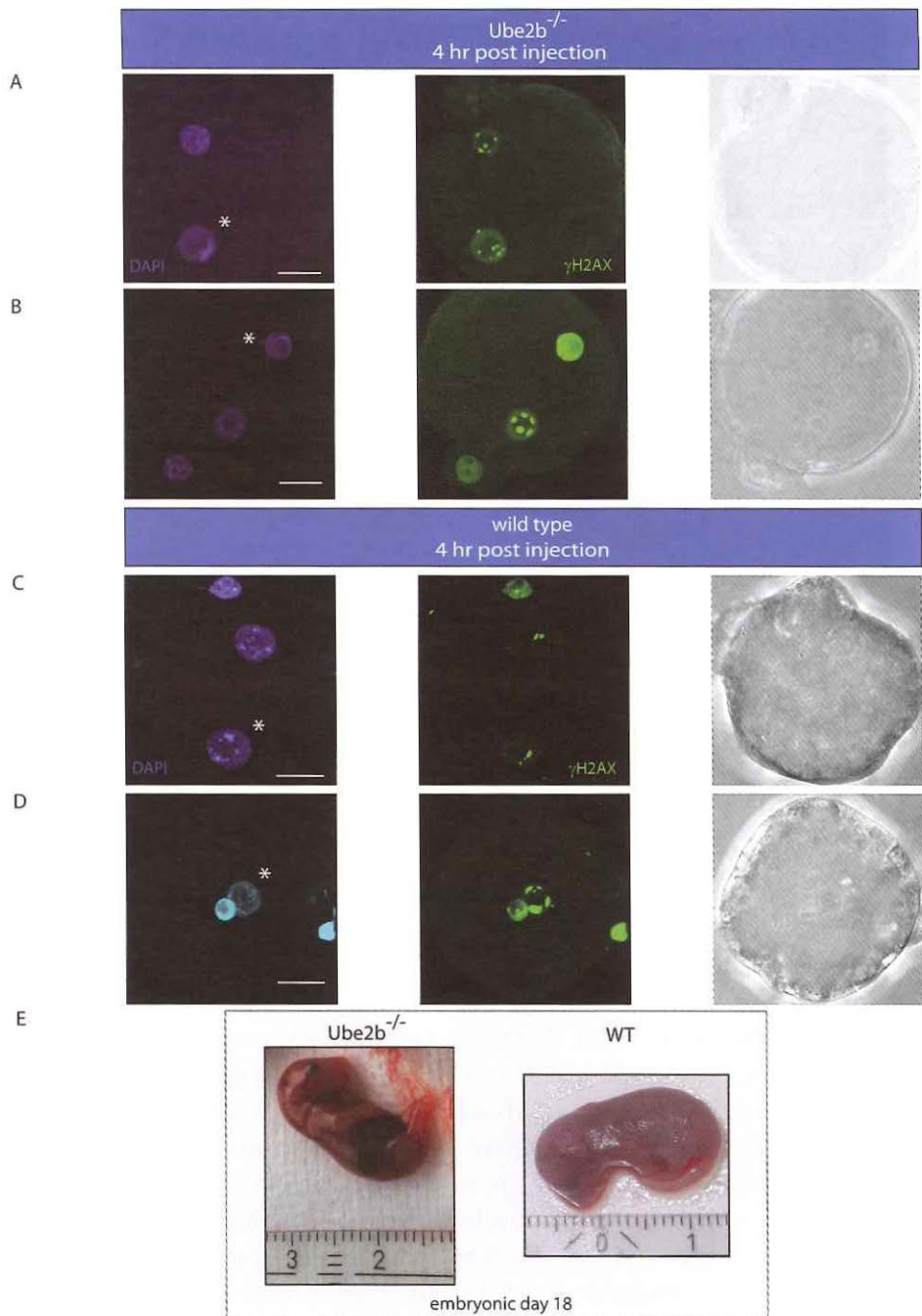
showing a strong overall signal for γH2AX with some bright γH2AX foci. The overall signal seemed to be related to the degree of development: nuclei with more intense DAPI staining showed a stronger γH2AX signal. Similar results were obtained for wild type pronuclei after round spermatid injection (Figure 8cd).

When we cultured the zygotes resulting from ROSI with *Ube2b* knockout spermatids, we observed normal progression to the 2-cell stage (56/58), and subsequent morphologically normal development up to the hatching blastocyst stage (17/28). Analysis with confocal microscopy of these hatching blastocysts showed the presence of normal nuclei and no γH2AX positive DDB, or any sign of nuclear fragmentation. We also noticed that most nuclei contained several γH2AX foci, and mitotic metaphases were completely stained with anti-γH2AX. This is similar to the γH2AX staining pattern that is observed in blastocysts after ROSI or ICSI with wild type sperm.

We transferred 28 2-cell stage embryos derived from injection with *Ube2b* knockout spermatid nuclei into two pseudopregnant mothers, and at day 18 of embryonic development, we observed 2 living embryos with normal appearance and weight in each foster mother (Figure 8e).

DISCUSSION

Intracytoplasmic sperm injection (ICSI) is used to overcome male-factor infertility. Since normal breeding with *Ube2b*^{-/-} males never resulted in live offspring, we used ICSI to try to generate zygotes from *Ube2b*^{-/-} sperm. Shortly after injection, simultaneously with the start of the formation of the maternal and paternal pronuclei, we noticed that the majority of paternal pronuclei derived from UBE2B-deficient sperm showed presence of DNA damage, as visualized by massive H2AX phosporylation, accompanied by progressive paternal pronuclear

◁ **Figure 8. Zygotes resulting from *Ube2b*^{-/-} round spermatid injection show normal embryonic development.** *Ube2b*^{-/-} zygotes after ROSI immunostaining for DAPI (blue) and γH2AX (green). The right panel presents differential interference contrast (DIC) image of the same embryo. Asterisks indicate the paternal pronucleus. Bar represents 10 μm. (ab) Four hours after injection, the zygotes either show the formation of a normal paternal pronucleus with a few γH2AX foci and no fragmentation (a) or a paternal pronucleus that is still developing (b), showing strong γH2AX staining, and this is most likely due to its condensed state. The maternal pronuclei have some bright γH2AX foci. (cd) wild type zygotes after ROSI immunostaining for DAPI (blue) and γH2AX (green). Wild type zygotes four hours after ROSI either show a completely developed paternal pronucleus (c) with few γH2AX-foci, or a partly formed paternal pronucleus (d) which is positive for γH2AX. The maternal pronuclei show some γH2AX spots. (e) 18 days of embryonic development after ROSI with respectively *Ube2b*^{-/-}·*Ube2b*^{-/-} and wild type spermatids.

fragmentation. The results from the SCSA assay showed that $Ube2b^{-/-}$ spermatozoa many carry many unrepaired DNA breaks or their DNA is more receptive to damage, as compared to wild type sperm. The majority of oocytes injected with $Ube2b^{-/-}$ spermatozoa still showed a metaphase II arrest, indicating that the maternal genome did not complete the second meiotic division. Directly after fertilization, the penetrating sperm normally delivers an oocyte-activating factor, which initiates continuation and finalization of the maternal second meiotic division (reviewed in [57]). The impaired methaphase-to-anaphase transition of the maternal genome in the zygotes derived from $Ube2b^{-/-}$ spermatozoa following ICSI could point towards the lack of an oocyte-activating factor in $Ube2b^{-/-}$ sperm. Alternatively, the fragmentated paternal pronucleus could rapidly activate an oocyte-checkpoint that blocks relief of the metaphase II arrest. It could even be suggested that direct communication between the paternal and maternal pronuclei occurs right after fertilization, blocking the maternal second meiotic division in case of a heavily damaged paternal (pro)nucleus. Similar failure to activate the oocyte has been observed upon ICSI of sperm derived from mice carrying two semi-identical translocation chromosomes that is associated with reduced fertility [58]. In addition, in heterologous ICSI experiments using human sperm injected into mouse oocytes, it was also observed that fragmentation of the paternal genome was frequently associated with a failure to activate the oocyte [59].

The results from the $Ube2b^{-/-}/Ube2b$-HA male mice show that even a relatively low level of UBE2B-HA in $Ube2b^{-/-}$ spermatocytes and spermatids significantly improves the qualitative and quantitative output of spermatogenesis, compared to $Ube2b$ knockouts. This indicates that the fusion protein functions at least partially. Therefore, we also tried ICSI to overcome the infertility of the $Ube2b^{-/-}/Ube2b$-HA mouse. We observed the formation of morphologically normal paternal $Ube2b^{-/-}/Ube2b$-HA pronuclei with normal γH2AX staining. The fact that a minority of these zygotes still showed metaphase II arrest, indicates that most likely an oocyte-activating factor is missing or reduced in level in both $Ube2b^{-/-}/Ube2b$-HA transgenic and $Ube2b^{-/-}$ sperm. A possible lack of an oocyte-activating factor in $Ube2b^{-/-}/Ube2b$-HA sperm could partially contribute to the infertility phenotype.

Unfortunately, the obtained transgenic $Ube2b$-HA mouse line shows relatively low levels of UBE2B-HA expression. Shekhar et al. [60] have reported stable overexpression of UBE2B in several mammalian breast cancer cells (MCF10A, WS-15 and MDA-MB-231), which resulted in various abnormalities [60, 61]. These findings indicate that a high level of UBE2B is detrimental to most cells, and transgenic mice that overexpress UBE2B-HA in testis were not obtained. The *Calmegin* promoter is germ cell-specific, and directs expression specifically from pachytene onwards [44], and UBE2B-HA is therefore not present during mitotic

and early meiotic phases of spermatogenesis in *Ube2b-HA* transgenic mice. The incapability to yield offspring with *Ube2b-HA* transgenic sperm could indicate that expression of UBE2B prior to pachytene may be critical. Since none of the known meiotic phenotypical characteristics of the *Ube2b* knockout spermatocytes were rescued by the *Ube2b-HA* transgene, we suggest that UBE2B also performs a function in meiotic prophase cells, most likely during leptotene, zygotene, and/ or early pachytene. Still, this function is not required to obtain an intact haploid genome, since ROSI with *Ube2b* knockout spermatids yielded normal embryos, surviving at least until E18.

As described in the Introduction, in yeast, the ubiquitin-conjugating enzyme Rad6 is known to function together with the E3 ligases Ubr1, Bre1, and Rad18. In mammals, UBE2A and UBE2B also have been shown to interact with the Bre1 homologs RNF20 (huBre1A, [6]) and RNF40 (huBre1B [6]) [22-24], with UBR2 [15] and with RAD18 [62]. Thus, it seems likely that part of the functions of UBE2B in spermatogenesis may depend on the interaction of UBE2B with one or more of these known E3 ligase partners. The expression of Bre1 homologs in mouse testis has not been investigated, but available microarray data indicate that *Rnf40* but not *Rnf20* mRNA levels are high in spermatocytes and spermatids [28]. Previously, we found no difference in H2B ubiquitylation, which most likely depends on UBE2A and UBE2B, in wild type and *Ube2b* knockout spermatocytes and spermatids [32], indicating that this function is not solely dependent on UBE2B during spermatogenesis. Knockouts for *Rnf20* and *Rnf40* are not yet available, precluding comparison of phenotypes. *Ubr2* knockout males are infertile, and display a developmental arrest at late zygotene/early pachytene [15]. Thus, part of the early meiotic functions of UBE2B may depend on its interaction with UBR2. *Rad18* knockout mice have also been described and males were found to have only very minor spermatogenic aberrations [63]. However, detailed analyses of meiosis in these mice have not been performed.

Similar to what has been found using UBE2A/B antibodies [47], UBE2B-HA accumulates on XY body chromatin of pachytene and diplotene spermatocytes. This supports the notion that UBE2B, possibly together with RAD18, acts during meiotic prophase in a role that most likely involves specific aspects of chromatin structure regulation associated with the presence of unsynapsed chromatin [4, 47]. Furthermore, we show that correct timing of UBE2B expression in spermatocytes appears to be critical for normal synaptonemal complex morphology, which is linked to chromatin structure, spermatocyte survival, and postmeiotic maintenance of X and Y chromosome inactivation [32]. Since Western blot analysis has shown that UBE2B and RAD18 are both expressed in spermatids of wild type mice [33, 47], these proteins may also act together at this postmeiotic stage.

The low levels of UBE2B-HA in spermatids of *Ube2b⁻/⁻/Ube2b-HA* mice, together with the finding that the *Ube2b⁻/⁻/Ube2b-HA* epididymis contains an increased percentage of sperm cells with abnormal morphology as compared to wild type, indicates that a high level of UBE2B in postmeiotic spermatids is essential for normal sperm head morphology. Surprisingly, the sperm integrity analysis for spermatozoa from *Ube2b-HA /Ube2b⁻/⁻* mice, showed a DFI comparable to wild type sperm, indicating that UBE2B-HA can rescue this aspect of UBE2B function during postmeiotic development. However, ICSI using *Ube2b⁻/⁻/Ube2b-HA*-sperm did not yield normal hatching blastocysts. Instead, the embryos apparently accumulated increasing genomic damage, since after each cleavage division, more blastomeres are affected. By the time the morula stage was reached, further development was blocked. These data indicate that although the genome of *Ube2b⁻/⁻/Ube2b-HA* -sperm cells may be intact, the chromatin structure is aberrant and more susceptible to damage. It might even be suggested that the role of UBE2B in postmeiotic chromatin reorganization is not to facilitate repair of the breaks that are made during the histone-to-protamine transition, but more likely involves a function in the correct packaging of the genome to protect it from damage during its storage in the epidydimis, and also to allow correct repackaging in the zygote. This idea is supported by our results obtained with zygotes derived from ICSI with testicular sperm of *Ube2b* knockout mice, that showed reduced γH2AX staining and DNA fragmentation compared to zygotes derived from ICSI with epidydimidal sperm. In addition, the fact that the overall sperm head morphology is still aberrant in *Ube2b⁻/⁻/Ube2b-HA* mice provides an indication that the genome is not correctly packaged. Escalier et al. [64] have performed electron microscopic analyses to analyse the nuclear structure of *Ube2b* knockout mice and found no indications for reduced protamine incorporation. In addition, we have previously shown that transition proteins are incorporated during spermatid elongation, and the testis-specific H2B variant TH2B was no longer detectable in condensed spermatids [20]. This indicates that the disturbances in chromatin structure in *Ube2b* knockout sperm are distinct from what is observed in mice that lack the transition proteins or protamines. In this context, it is of interest to note that sperm derived from mice with deletions of large parts of the Y chromosome also contains increased DNA damage that impairs the developmental potential of ICSI-derived embryos [65]. These data point to a possible functional interaction between UBE2B and postmeiotically expressed Y-encoded genes, that is required for proper regulation of the histone-to-protamine transition. Disturbances in the histone-to-protamine transition in spermatids may also cause disturbances in the protamine-to-histone transition in the zygote. This may generate specific problems during DNA replication, causing more stalled replication forks and subsequent collapse of these forks and

the formation of DSBs. This paternal effect of UBE2B upon genome integrity during postfertilization development as revealed in the embryos that were derived from ICSI with *Ube2b^{-/-}*/*Ube2b-HA* sperm, provides evidence for the inheritance of epigenetic disturbances through the male germline.

Although both meiotic and postmeiotic development of male germ cells is impaired in *Ube2b^{-/-}* testes, we initially could not determine if the postmeiotic derailment is a consequence of the lack of UBE2B during the meiotic prophase, or if UBE2B also performs a specific role during spermiogenesis. We argued that if the acquired DNA damage present in *Ube2b^{-/-}* spermatozoa results from a postmeiotic defect, injection with round spermatids (ROSI) from *Ube2b^{-/-}* mice might be able to rescue the defective pronuclear development that was observed upon ICSI with *Ube2b^{-/-}* spermatozoa. We indeed observed formation of a normal paternal pronucleus shortly after ROSI, indistinguishable from pronuclei derived from ROSI with wild type round spermatids or ICSI with wild type sperm, or *Ube2b^{-/-}*/*Ube2b-HA* sperm. Moreover, zygotes from *Ube2b^{-/-}* round spermatids could develop normally *in vivo*, with a similar rate and frequency compared to embryos derived from ROSI with wild type spermatids.

Taken together, these results show that UBE2B has an important role in organizing a chromatin structure, which supports maintenance of genome integrity throughout the last steps of spermatogenesis and early fertilization events, including the histone-to-protamine and protamine-to-histone transitions. The aberrant chromatin structure and histone modifications in *Ube2b^{-/-}* spermatids might perturb the normal exchange of histones for transition proteins and protamines, resulting in enhanced susceptibility to DNA damage. To reveal the exact nature of the postmeiotic UBE2B functions, the UBE2B-HA transgenic mouse model will be useful to purify the E3 enzyme and/or substrates that interact with UBE2B during postmeiotic male germ cell development.

MATERIALS AND METHODS

Mice

All animal experiments were conducted in accordance with the local guidelines and protocols.

Generation of transgenic mice

To produce transgenic mice that show testis-specific expression of UBE2B protein fused to a hemagglutinin tag (HA) we generated a construct (*Ube2b-HA* construct) containing a 330 bp SacI/BamHI fragment of the *Calmegin* promoter (Figure 1) (gift from K. Yamagata, Osaka University Japan), which has been shown to direct specific expression in pachytene spermatocytes and later stages of male germ cell development [44].

This promoter was placed in front of the *Ube2b* cDNA (500 bp fragment) fused in frame to a linker containing the HA immunotag. A BamHI site, generated through site-directed mutagenesis, replaced the *Ube2b* stop codon. To enhance transgene expression, exon 2 (the last 22 bp), intron 2, exon 3, and the 3' untranslated region (including the polyadenylation signal) of the human b-globin gene were inserted at the 3'end. Finally a linker containing a single LoxP site was cloned in front of the *Calmegin* promoter. Linearized DNA was isolated and microinjected into fertilized oocytes from FVB mice. Founders were screened after genomic tail DNA isolation [45] and analyzed with the following forward and reversed PCR primers: 5'CAACATCATGCAGTGGAATGC 3'
5'GCTCAACAATGGCCGAAACT 3'

These primers amplify a fragment of 347 bp only if the transgene is present. A separate multiplex PCR reaction was performed to determine the *Ube2b* genotype. For this, the following primers were used:
5' TTGAAATCCCGCATGAGC 3'
5' CGGAGGGAGACGTCATTG 3'
5' CTTTACGGTATCGCCGCTCCCGAT 3'

Copy number of the transgene per haploid genome was determined using Southern blot analyses according to standard methods with *Ube2b* cDNA as probe. *Ube2b-HA* transgenic male mice were crossed with *Ube2b* knockout females (FVB background) to obtain mice that were transgenic for the testis-specific *Ube2b* fusion gene, and heterozygous for the *Ube2b* knockout allele. These mice were intercrossed to obtain *Ube2b-HA* transgenic mice on a *Ube2b* knockout background.

Fertility analysis
Adult heterozygous *Ube2b-HA* males on *Ube2b* knockout background were bred with control females for a maximum of 6 weeks. Litter number and litter size were recorded. To analyse spermatogenesis, adult males were killed by cervical dislocation, and testes and epididymis were isolated and weighed. To obtain sperm for assessment of morphology, the epididymis were transferred into a plastic Petri dish containing 0.5 ml Dulbecco's medium (Gibco) with 0.5 % BSA, and carefully cut to allow sperm to move out of the tissue. After 10-20 minutes, the medium was carefully stirred, and aliquots were removed for sperm morphology analysis in smears stained by hematoxylin/eosin. Then, the epididymis were transferred into a small glass Potter and homogenized by hand. The total number of sperm present in the epididymis was counted using an improved Neubauer hemocytometer and a phase contrast microscope at a magnification of 400 X. At least 200 sperm in 2 different samples from one animal were counted. Sperm head morphology was assessed using hematoxylin/eosin stained smears and

bright field microscopy at 1000 X magnification. 200 Sperm heads were analyzed per animal.

For morphological analysis of spermatogenesis, testes were fixed overnight in Bouin's fixative and embedded in paraffin. 8μm Sections were cut and stained with hematoxylin/eosin. Statistical analyses were performed using the Student's t-test.

Immunoblot analysis

Mouse testes were obtained from adult mice, and frozen in liquid nitrogen directly after dissection. Cell preparations highly enriched in spermatocytes and round spermatids were isolated from mouse testes after collagenase and trypsin treatment, followed by sedimentation at unit gravity (StaPut procedure) and density gradient centrifugation through Percoll [46].

Protein extracts were prepared by 10 cycles of 10 seconds sonification in 0.25 M sucrose/ 1mM EDTA supplemented with complete protease inhibitor cocktail (Roche). Protein concentrations were determined using Coomassie Plus protein assay reagent (Pierce, Perbio Science, Etten-Leur, Netherlands) as described by the manufacturer.

An amount of 20 μg of protein per sample was separated on 12% SDS-polyacrylamide gels and the separated proteins were transferred to nitrocellulose membranes, using the BioRad miniprotean III system and blot cells (Bio-Rad, Veenendaal, Netherlands). Membranes were stained with Ponceau S (Sigma-Aldrich, Zwijndrecht, Netherlands) according to the supplier's protocol.

UBE2A and UBE2B were detected with a rabbit polyclonal antibody (α-UBE2A/B) raised against a peptide representing the N terminus of UBE2A and UBE2B, which are identical [4]. RAD18 protein was detected using the affinity purified anti-RAD18 antibody described by van der Laan et al. [47]. After blocking non-specific sites with 3 % w/v non-fat milk in PBS/ with 0.1% v/v Tween20 (blotto) for 1 hour at room temperature, antibody was added in fresh blotto, and incubation was continued for an additional hour at room temperature. Subsequently, non-bound antibody was removed through several washes using PBS with 0.1% v/v Tween20. Peroxidase-labeled second antibody (Sigma) was diluted in blotto, and incubation was for 1 hour at room temperature. Antigen-antibody complexes were detected by using a chemoluminescence kit (Du Pont/ NEN, Bad Homburg, Germany) according to the instructions provided by the manufacturer.

Immunostaining of spread meiotic nuclei preparations

Spread nuclei preparations of mouse spermatocytes were made according to the protocol described [48]. The slides containing spread meiotic nuclei were washed

with PBS extensively and nonspecific sites were blocked by incubation in PBS/ 0.5% BSA/ 0.5% w/v non-fat milk, prior to addition of specific antibodies. The primary antibodies; rabbit polyclonal anti-RAD18 (1:50), rat monoclonal anti-HA (Roche, 1:100) mouse monoclonal anti-MLH1 (BD, Alphen aan den Rijn, Netherlands, 1:25) rabbit polyclonal anti-SYCP3 (1:1000) (a gift from C. Heyting) were diluted in 10% BSA/ PBS and incubated overnight at room temperature. Non-bound antibodies were removed by washing in PBS and the slides were incubated with PBS/ 5% w/v non-fat milk/ 10% v/v normal goat serum for 20 minutes at room temperature. The secondary antibodies (FITC-conjugated goat anti-rabbit 1:80, TRITC-conjugated goat anti-mouse 1:130 (Sigma), goat anti-rat Alexa 488 1:200 and goat anti-mouse Alexa 350 1:200 (Molecular Probes, Invitrogen, Breda, Netherlands) were added, and incubation was continued for 2 more hours at room temperature. Finally, after extensive washing with PBS, the slides were mounted in Vectashield (Vector Laboratories, Brunschwig, Amsterdam, Netherlands) containing DAPI. Images were taken with a fluorescence microscope (Axioplan 2; Carl Zeiss, Jena, Germany) equipped with a digital camera (Coolsnap-Pro; Photometrics, Waterloo, Canada).

TUNEL assay

Testes were isolated from adult mice of different genotypes. Tissues were formaldehyde fixed and embedded in paraffin according to standard procedures. Sections were mounted on amino alkylsilane-coated glass slides, dewaxed, and pretreated with proteinase K (Sigma) and peroxidase as described elsewhere [49]. Slides were subsequently washed in terminal deoxynucleotidyl transferase (TdT) buffer [50] for 5 minutes and then incubated for at least 2 hours in TdT buffer containing 0.01 mM Biotin-16-dUTP (Roche) and 0.3 U of TdT enzyme (Promega, Leiden, Netherlands) per μl at RT. The enzymatic reaction was stopped by incubation in TB buffer, and the sections were washed [49]. Slides were then incubated with StreptABComplex-horseradish peroxidase conjugate (Dako) for 30 min and washed in PBS. dUTP-biotin labeled cells were visualized with 3,3'-diaminobenzidine tetrahydrochloride-metal concentrate (Pierce). Tissue sections were counterstained with hematoxylin. For each animal, the number of TUNEL (terminal deoxynucleotidyltransferase-mediated dUTP-biotin nick end labeling)-positive cells was counted in 100 tubule cross sections.

Media

For oocyte collection and injection, 45 ml MEM-alpha complete (Life-technologies/GIBCO Cat.nr. 22571) was supplemented with 10% fetal calf serum, 0.068 g sodium lactate, 0.006 g sodium pyruvaat, 0,25 gr HEPES and 0.007 g L-Glutamine. The pH was adjusted to 7.2 using NaOH. The final solution was

filter sterilized. For oocyte storage, GZ medium was used. For embryo culture, KSOM medium supplemented with amino acids (Chemicon), was used.

Preparation of mouse oocytes

B6D2F1 female mice (Charles River), 6-14 wk old, were each induced to superovulate by i.p. injection of 7.5 IU serum PMSG-Folligonan (Intervet) followed by 7.5 IU hCG-Chorulon (Intervet) 48 h later. Oocytes were collected from oviducts about 13-15 h after hCG injection, freed from cumulus cells by treatment with Hyaluronidase (Sigma, H-4274), thoroughly rinsed in GZ medium and stored at 37°C up to 5 h in GZ medium under 5 % CO_2 and 5 % O_2 in air.

Cryopreservation and preparation of spermatozoa

Spermatozoa were obtained from $Ube2b^{-/-}$, $Ube2b^{-/-}/Ube2b$-HA and wild type male mice. The cauda epididymis and vas deferens were isolated and placed in sperm/cryoprotectant solution (CPA, 8,5 ml MilliQ, 1,8 gr Raffinose (Sigma) and 0,3 gr milkpowder (Campina)). The vas deferens was emptied and the epididymal tubules were cut in several places to allow the spermatozoa to disperse into the medium in a petridish (Greiner Bio-One, Alphen a/d Rijn, Netherlands).

50 - 100 ml of sperm solution was placed in a cooling chamber and rapidly frozen in liquid nitrogen vapour. Tubes were stored in liquid nitrogen.

Thawing occurred for several minutes at room temperature, followed by heating in a waterbath 37°C. This was diluted in 50-100 ml HTF-HEPES-3% BSA, and centrifuged for 5 min at 3000 rpm. The pellet was resuspended in HTF-HEPES-3% BSA, and incubated for 15 min at 37°C, 5% CO_2. Subsequently, the spermheads were separated from the tails by sonication for 15 minutes in a waterbath (Branson 1210). This suspension was kept at room temperature.

4 ml of the spermsuspension was pipeted into PVP-saline (0.9% NaCl containing 12% [w/v] polyvinylpyrrolidone [360 kDa; ICN Biochemicals]). A small drop (about 10 ml) of this mixture was kept under mineral oil (Sigma) in a plastic petri dish on the microscope stage at room temperature before injection into oocytes.

Sperm chromatin structure assay procedure

Sperm was diluted with TNE buffer (0.01 M Tris-HCl, 0.15 M NaCl, 0.001 M ethylenediamine tetraacetic acid, pH 7.4) in a total volume of 200 ml and then mixed with 400 ml of an acid-detergent solution (0.12 N HCl, 0.15 M NaCl, 0.1% Triton X-100, pH 1.2) for 30 seconds and subsequently stained with 1200 ml of staining solution (0.037 M citric acid, 0.126 M Na_2HPO_4, 0.0011 M EDTA, 0.15 M NaCl, pH 6.0, containing 6 mg/mL Acridine Orange (No. A8097, Sigma Chemical, St. Louis, MO, USA). After 3 min at room temperature, sperm cells

were analyzed by flow cytometry using FACScaliber (Becton Dickinson, San Jose, CA). The flow rate was kept below 300 events/second and a total of 5000 events were accumulated for each measurement. The DNA Fragmentation Index (DFI) was measured as the ratio of red fluorescence to total fluorescence [51].

Preparation of round-spermatids for ROSI, and spermatozoa for testicular ICSI
Adult *Ube2b-/-* and wild type male mice were killed by cervical dislocation. The testes were dissected, placed in 1 ml PBS and an incision was made in the testis capsule to allow for the removal of the seminiferous tubules. The content of the seminiferous tubules was liberated by mechanical agitation with forceps, leaving a suspension of cells including round spermatids, which were pipeted into PVP-saline as described above for sperm. To obtain sperm heads from the testicular suspension, the suspension was first sonicated as described above for epididymal sperm and kept at room temperature in PBS until injection.

ICSI and round-spermatid injection (ROSI)
The microinjection procedure was performed as described [52]. In short, oocytes (kept in MEM-alpha complete) were injected using a fine glass capillary with a 10 mm (ICSI) and 5 mm (ROSI) internal diameter, attached to a Piezo microinjection system (PiezoDrill; Burleigh Instruments, Burleigh Park, Fishers, NY, USA). Sperm heads were aspirated and injected into the oocytes. Round spermatids were identified by size and morphology as described by Kimura & Yanagimachi (1995) [53]. The selected spermatids were individually drawn into the injection pipette and by repeated aspiration the nucleus was isolated from the rest of the cell before injected into the oocytes. After ICSI, oocytes were kept at room temperature for 5 min, and then gradually warmed to 37°C and placed in KSOM medium supplemented with amino acids (Chemicon) under 5% CO_2, 5% O_2 in air at 37°C.

For each ROSI-experiment, and for the testicular ICSI experiment, 15 mM $SrCl_2$ (Sigma) was freshly diluted from a 1M stock in calcium-free M16 culture medium. Microdroplets were arranged onto a Petri dish (Falcon, Franklin Lakes, NJ, USA), covered with mineral oil (Sigma) and incubated under 5 % CO_2 and 5 % O_2 in air at 37°C for at least 30 min. For activation, oocytes were washed twice, and cultured in the equilibrated 15 mM $SrCl_2$ solution for 1,5 h.

After ROSI, or after ICSI with testicular sperm, oocytes were washed twice in 15 mM $SrCl_2$ solution, and incubated in this solution for 1,5 h under 5% CO_2, 5% O_2 in air at 37°C. Subsequently, oocytes were washed twice in KSOM medium supplemented with amino acids (Chemicon), and further cultured in this medium in 5% CO_2, 5% O_2 in air at 37°C. Following ICSI or ROSI, embryos were collected at different time points following fertilization. Zygotes were collected at 2 and 4 hr following injection. 2-cell and 4-cell stage embryos were

assessed at respectively 24, and 48 hr after injection. Morulas and blastocysts were collected at either 70 or 96-120 hr after fertilization. Collected embryos were washed several times in PBS and kept at 4°C in a 96-wells plate (Greiner Bio-One)

Embryo transfer into foster mothers

Recipients of the embryos were FVB mice. They were mated with sterile males of the same strain. The day on which a vaginal plug was found was defined as day 1 of pregnancy. At about 14:00 h on that day, females were anaesthetized and their oviducts were exposed through dorso-ventral incisions. Meanwhile, the embryos (2-cell stage) to be transferred were sucked into an embryo transfer pipette and the embryos were transferred into the lumen of the ampulla. The number of embryos transferred into each oviduct was around 10.

Immunocytochemical staining of embryos

Embryos were fixed in 5% PFA for 20 min at 37°C and treated for immunofluorescence as described by Plusa et al. [54] in a 96-well plate (Greiner Bio-One). The primary antibodies mouse monoclonal anti-γH2AX (1:1000) (Upstate, Walthum, MA, USA), rabbit polyclonal H3K4me2 (1:500) (Upstate), rabbit polyclonal anti-RAD18 (1:200) were diluted in 3% BSA/ PBS-Tween 20 (0,15%) and incubated overnight at 4°C. For mouse monoclonal primary antibodies, the secondary antibodies were fluorescein isothiocyanate (FITC)-labeled goat anti-mouse IgG antibodies (1:128) (Sigma, St Louis, USA) and tetramethylrhodamine isothiocyanate (TRITC)-labeled goat anti-mouse IgG antibodies (1:128) (Sigma). For rabbit polyclonal primary antibodies, the secondary antibodies were tetramethylrhodamine isothiocyanate (TRITC)-labeled goat anti-rabbit IgG antibodies (1:128) (Sigma). After antibody incubations and washes, embryos were mounted in DAPI-Vectashield on polylysine-coated slides. To analyze the dynamics of paternal pronucleus formation, ICSI- and ROSI-zygotes were collected two and / or four hours post injection. In addition, we also collected the preimplantation embryonic development stages of 2-cell, 4-cell, morula and blastocyst from ICSI-embryos.

Fluorescence microscopy analysis, digital image preparation and analysis

Confocal microscopic observations of maternal and paternal pronuclei and embryos were made by confocal sectioning at least every 1 μm through the whole embryo, using a Zeiss510 Multiphoton confocal microscope. The acquired digital images were processed with Photoshop software (Adobe Systems).

ACKNOWLEDGEMENTS

REFERENCES

1. Barnhart BJ, Cox SH. Radiation-sensitive and radiation-resistant mutants of Haemophilus influenzae. *J Bacteriol.* Jul 1968;96(1):280-282.
2. Game JC, Zamb TJ, Braun RJ, Resnick M, Roth RM. The role of radiation (rad) genes in meiotic recombination in yeast. *Genetics.* 1980;94:51-68.
3. Lawrence C. The RAD6 DNA repair pathway in Saccharomyces cerevisiae: what does it do, and how does it do it? *Bioessays.* Apr 1994;16(4):253-258.
4. Baarends WM, Wassenaar E, van der Laan R, et al. Silencing of unpaired chromatin and histone H2A ubiquitination in mammalian meiosis. *Mol Cell Biol.* Feb 2005;25(3):1041-1053.
5. Hoege C, Pfander B, Moldovan GL, Pyrowolakis G, Jentsch S. RAD6-dependent DNA repair is linked to modification of PCNA by ubiquitin and SUMO. *Nature.* Sep 12 2002;419(6903):135-141.
6. Hwang WW, Venkatasubrahmanyam S, Ianculescu AG, Tong A, Boone C, Madhani HD. A conserved RING finger protein required for histone H2B monoubiquitination and cell size control. *Mol Cell.* Jan 2003;11(1):261-266.
7. Robzyk K, Recht J, Osley MA. Rad6-dependent ubiquitination of histone H2B in yeast. *Science.* Jan 21 2000;287(5452):501-504.
8. Sung P, Prakash S, Prakash L. The RAD6 protein of Saccharomyces cerevisiae polyubiquitinates histones, and its acidic domain mediates this activity. *Genes Dev.* Nov 1988;2(11):1476-1485.
9. Wood A, Krogan NJ, Dover J, et al. Bre1, an e3 ubiquitin ligase required for recruitment and substrate selection of rad6 at a promoter. *Mol Cell.* Jan 2003;11(1):267-274.
10. Wood A, Schneider J, Dover J, Johnston M, Shilatifard A. The Paf1 complex is essential for histone monoubiquitination by the Rad6-Bre1 complex, which signals for histone methylation by COMPASS and Dot1p. *J Biol Chem.* Sep 12 2003;278(37):34739-34742.
11. Dover J, Schneider J, Tawiah-Boateng MA, et al. Methylation of histone H3 by COMPASS requires ubiquitination of histone H2B by Rad6. *J Biol Chem.* Aug 9 2002;277(32):28368-28371.
12. Foster ER, Downs JA. Methylation of H3 K4 and K79 is not strictly dependent on H2B K123 ubiquitylation. *J Cell Biol.* Mar 9 2009;184(5):631-638.
13. Ng HH, Xu RM, Zhang Y, Struhl K. Ubiquitination of histone H2B by Rad6 is required for efficient Dot1-mediated methylation of histone H3 lysine 79. *J Biol Chem.* Sep 20 2002;277(38):34655-34657.
14. Sun ZW, Allis CD. Ubiquitination of histone H2B regulates H3 methylation and gene silencing in yeast. *Nature.* Jul 4 2002;418(6893):104-108.
15. An JY, Kim EA, Jiang Y, et al. UBR2 mediates transcriptional silencing during spermatogenesis via histone ubiquitination. *Proc Natl Acad Sci U S A.* Jan 11 2010;107(5):1912-1917.
16. Kwon YT, Xia Z, An JY, et al. Female lethality and apoptosis of spermatocytes in mice lacking the UBR2 ubiquitin ligase of the N-end rule pathway. *Mol Cell Biol.* Nov 2003;23(22):8255-8271.
17. Kwon YT, Xia Z, Davydov IV, Lecker SH, Varshavsky A. Construction and analysis of mouse strains lacking the ubiquitin ligase UBR1 (E3alpha) of the N-end rule pathway. *Mol Cell Biol.* Dec 2001;21(23):8007-8021.
18. Koken MH, Hoogerbrugge JW, Jasper-Dekker I, et al. Expression of the ubiquitin-conjugating DNA repair enzymes HHR6A and B suggests a role in spermatogenesis and chromatin modification. *Dev Biol.* Jan 10 1996;173(1):119-132.

19. Roest HP, Baarends WM, de Wit J, et al. The ubiquitin-conjugating DNA repair enzyme HR6A is a maternal factor essential for early embryonic development in mice. *Mol Cell Biol.* Jun 2004;24(12):5485-5495.

20. Roest HP, van Klaveren J, de Wit J, et al. Inactivation of the HR6B ubiquitin-conjugating DNA repair enzyme in mice causes male sterility associated with chromatin modification. *Cell.* Sep 6 1996;86(5):799-810.

21. van der Laan R, Roest HP, Hoogerbrugge JW, et al. Characterization of mRAD18Sc, a mouse homolog of the yeast postreplication repair gene RAD18. *Genomics.* Oct 1 2000;69(1):86-94.

22. Kim J, Hake SB, Roeder RG. The human homolog of yeast BRE1 functions as a transcriptional coactivator through direct activator interactions. *Mol Cell.* Dec 9 2005;20(5):759-770.

23. Kim J, Guermah M, McGinty RK, et al. RAD6-Mediated transcription-coupled H2B ubiquitylation directly stimulates H3K4 methylation in human cells. *Cell.* May 1 2009;137(3):459-471.

24. Zhu B, Zheng Y, Pham AD, et al. Monoubiquitination of Human Histone H2B: The Factors Involved and Their Roles in HOX Gene Regulation. *Mol Cell.* Nov 23 2005;20(4):601-611.

25. Rathke C, Baarends WM, Jayaramaiah-Raja S, Bartkuhn M, Renkawitz R, Renkawitz-Pohl R. Transition from a nucleosome-based to a protamine-based chromatin configuration during spermiogenesis in Drosophila. *J Cell Sci.* May 1 2007;120(Pt 9):1689-1700.

26. Monesi V. Differential rate of ribonucleic acid synthesis in the autosomes and sex chromosomes during male meiosis in the mouse. *Chromosoma.* 1965;17(1):11-21.

27. Mulugeta Achame E, Wassenaar E, Hoogerbrugge JW, et al. The ubiquitin-conjugating enzyme HR6B is required for maintenance of X chromosome silencing in mouse spermatocytes and spermatids. *BMC Genomics.*11:367.

28. Namekawa SH, Park PJ, Zhang LF, et al. Postmeiotic sex chromatin in the male germline of mice. *Curr Biol.* Apr 4 2006;16(7):660-667.

29. Turner JM, Mahadevaiah SK, Ellis PJ, Mitchell MJ, Burgoyne PS. Pachytene asynapsis drives meiotic sex chromosome inactivation and leads to substantial postmeiotic repression in spermatids. *Dev Cell.* Apr 2006;10(4):521-529.

30. Hendriksen PJM, Hoogerbrugge JW, Themmen APN, et al. Postmeiotic transcription of X and Y chromosomal genes during spermatogenesis in the mouse. *Dev. Biol.* 1995;170:730-733.

31. Mueller JL, Mahadevaiah SK, Park PJ, Warburton PE, Page DC, Turner JM. The mouse X chromosome is enriched for multicopy testis genes showing postmeiotic expression. *Nat Genet.* Jun 2008;40(6):794-799.

32. Baarends WM, Wassenaar E, Hoogerbrugge JW, Schoenmakers S, Sun ZW, Grootegoed JA. Increased phosphorylation and dimethylation of XY body histones in the Hr6b-knockout mouse is associated with derepression of the X chromosome. *J Cell Sci.* Jun 1 2007;120(Pt 11):1841-1851.

33. Baarends WM, Wassenaar E, Hoogerbrugge JW, et al. Loss of HR6B ubiquitin-conjugating activity results in damaged synaptonemal complex structure and increased crossing-over frequency during the male meiotic prophase. *Mol Cell Biol.* Feb 2003;23(4):1151-1162.

34. Wouters-Tyrou D, Martinage A, Chevaillier P, Sautiere P. Nuclear basic proteins in spermiogenesis. *Biochimie.* Feb 1998;80(2):117-128.

35. Laberge RM, Boissonneault G. Chromatin remodeling in spermatids: a sensitive step for the genetic integrity of the male gamete. *Arch Androl.* Mar-Apr 2005;51(2):125-133.

36. Laberge RM, Boissonneault G. On the nature and origin of DNA strand breaks in elongating spermatids. *Biol Reprod.* Aug 2005;73(2):289-296.
37. McPherson S, Longo FJ. Chromatin structure-function alterations during mammalian spermatogenesis: DNA nicking and repair in elongating spermatids. *Eur J Histochem.* 1993;37(2):109-128.
38. McPherson SM, Longo FJ. Nicking of rat spermatid and spermatozoa DNA: possible involvement of DNA topoisomerase II. *Dev Biol.* Jul 1993;158(1):122-130.
39. Risley MS, Einheber S, Bumcrot DA. Changes in DNA topology during spermatogenesis. *Chromosoma.* 1986;94(3):217-227.
40. Cho C, Jung-Ha H, Willis WD, et al. Protamine 2 deficiency leads to sperm DNA damage and embryo death in mice. *Biol Reprod.* Jul 2003;69(1):211-217.
41. Cho C, Willis WD, Goulding EH, et al. Haploinsufficiency of protamine-1 or -2 causes infertility in mice. *Nat Genet.* May 2001;28(1):82-86.
42. Zhao M, Shirley CR, Hayashi S, et al. Transition nuclear proteins are required for normal chromatin condensation and functional sperm development. *Genesis.* Apr 2004;38(4):200-213.
43. Meng X, Akutsu H, Schoene K, et al. Transgene insertion induced dominant male sterility and rescue of male fertility using round spermatid injection. *Biol Reprod.* Mar 2002;66(3):726-734.
44. Watanabe D, Okabe M, Hamajima N, Morita T, Nishina Y, Nishimune Y. Characterization of the testis-specific gene 'calmegin' promoter sequence and its activity defined by transgenic mouse experiments. *FEBS Lett.* 1995;368(3):509-512.
45. Laird PW, Zijderveld A, Linders K, Rudnicki MA, Jaenisch R, Berns A. Simplified mammalian DNA isolation procedure. *Nucleic Acids Res.* Aug 11 1991;19(15):4293.
46. Grootegoed JA, Jansen R, van der Molen HJ. Effect of glucose on ATP dephosphorylation in rat spermatids. *J. Reprod. Fertil.* 1986;77(1):99-107.
47. van der Laan R, Uringa EJ, Wassenaar E, et al. Ubiquitin ligase Rad18Sc localizes to the XY body and to other chromosomal regions that are unpaired and transcriptionally silenced during male meiotic prophase. *J Cell Sci.* Oct 1 2004;117(Pt 21):5023-5033.
48. Peters AH, Plug AW, van Vugt MJ, de Boer P. A drying-down technique for the spreading of mammalian meiocytes from the male and female germline. *Chromosome Res.* Feb 1997;5(1):66-68.
49. Gavrieli Y, Sherman Y, Ben-Sasson SA. Identification of programmed cell death *in situ* via specific labeling of nuclear DNA fragmentation. *J. Cell Biol.* 1992;119:493-501.
50. Gorczyca W, Gong J, Darzynkiewicz Z. Detection of DNA strand breaks in individual apoptotic cells by the *in situ* terminal deoxynucleotidyl transferase and nick translation assays. *Cancer Res.* 1993;53:1945-1951.
51. Love CC. The sperm chromatin structure assay: a review of clinical applications. *Anim Reprod Sci.* Oct 2005;89(1-4):39-45.
52. Yanagimachi R. Is an animal model needed for intracytoplasmic sperm injection (ICSI) and other assisted reproduction technologies? *Hum Reprod.* Oct 1995;10(10):2525-2526.
53. Kimura Y, Yanagimachi R. Mouse oocytes injected with testicular spermatozoa or round spermatids can develop into normal offspring. *Development.* 1995;121:2397-2405.
54. Plusa B, Hadjantonakis AK, Gray D, et al. The first cleavage of the mouse zygote predicts the blastocyst axis. *Nature.* Mar 17 2005;434(7031):391-395.
55. Evenson DP, Wixon R. Clinical aspects of sperm DNA fragmentation detection and male infertility. *Theriogenology.* Mar 15 2006;65(5):979-991.
56. Inagaki A, van Cappellen WA, van der Laan R, et al. Dynamic localization of human RAD18 during the cell cycle and a functional connection with DNA double-strand break repair. *DNA Repair (Amst).* Feb 1 2009;8(2):190-201.

57. Malcuit C, Kurokawa M, Fissore RA. Calcium oscillations and mammalian egg activation. *J Cell Physiol.* Mar 2006;206(3):565-573.
58. Baart EB, van der Heijden GW, van der Hoeven FA, Bakker R, Cooper TG, de Boer P. Reduced oocyte activation and first cleavage rate after ICSI with spermatozoa from a sterile mouse chromosome mutant. *Hum Reprod.* May 2004;19(5):1140-1147.
59. Derijck AA, van der Heijden GW, Ramos L, Giele M, Kremer JA, de Boer P. Motile human normozoospermic and oligozoospermic semen samples show a difference in double-strand DNA break incidence. *Hum Reprod.* Sep 2007;22(9):2368-2376.
60. Shekhar MP, Lyakhovich A, Visscher DW, Heng H, Kondrat N. Rad6 overexpression induces multinucleation, centrosome amplification, abnormal mitosis, aneuploidy, and transformation. *Cancer Res.* Apr 1 2002;62(7):2115-2124.
61. Lyakhovich A, Shekhar MP. RAD6B overexpression confers chemoresistance: RAD6 expression during cell cycle and its redistribution to chromatin during DNA damage-induced response. *Oncogene.* Apr 15 2004;23(17):3097-3106.
62. Xin H, Lin W, Sumanasekera W, Zhang Y, Wu X, Wang Z. The human RAD18 gene product interacts with HHR6A and HHR6B. *Nucleic Acids Res.* Jul 15 2000;28(14):2847-2854.
63. Sun J, Yomogida K, Sakao S, et al. Rad18 is required for long-term maintenance of spermatogenesis in mouse testes. *Mech Dev.* Mar-Apr 2009;126(3-4):173-183.
64. Escalier D, Bai XY, Silvius D, Xu PX, Xu X. Spermatid nuclear and sperm periaxonemal anomalies in the mouse Ube2b null mutant. *Mol Reprod Dev.* Jul 2003;65(3):298-308.
65. Yamauchi Y, Riel JM, Stoytcheva Z, Burgoyne PS, Ward MA. Deficiency in mouse Y chromosome long arm gene complement is associated with sperm DNA damage. *Genome Biol.* 2010;11(6):R66.

CHAPTER 9

X CHROMOSOME INACTIVATION
IN THE PRE-IMPLANTATION EMBRYO

ABSTRACT

During early mouse preimplantation development, male XY and female XX embryos are already subject to differential regulatory processes long before the actual sex determination process starts. The difference in X chromosomal dosage between male and female embryos is compensated through the process of imprinted paternal X chromosome inactivation. This is initiated around the four-cell stage resulting in the inactivation of paternally provided X-chromosome. In the inner cell mass (ICM) of the early blastocyst, this imprint is erased and replaced by random X-inactivation whereas inactivation of the paternal X chromosome is maintained in the extra-embryonic lineages. It is not known whether the process of early imprinted X-inactivation could be influenced by existing asymmetry in the early embryo. Differential distribution of asymmetric factors, whose distribution depends on the plane of the first cleavages, might result in intra-embryonic and inter-embryonic differences in the developmental potential of blastomeres and embryos, respectively. Herein, we show that male and female embryos reach the blastocyst stage within a similar time frame. Still, the number of cells is reduced in XX blastocysts compared to XY blastocysts.

RNA FISH analyses of *Xist* expression show that X chromosome inactivation (XCI) appears with increased probability in embryos in which the two divisions that generate the 4-cell embryo from a 2-cell embryo occur along the animal-vegetal axis, whereas XCI is delayed in embryos in which the second cleavage divisions were both equatorial. These data indicate that factors that regulate imprinted XCI may be asymmetrically distributed in the blastomeres of the 2-cell embryo.

INTRODUCTION

The individual blastomeres of the early mammalian embryo have considerable plasticity with respect to their capacities to contribute to the different cell lineages during further development. This is based on the fact that experimental rearrangement of blastomeres, or reduction of the number of blastomeres within an embryo does not terminally compromise normal embryonic development [1-3]. It has long been proposed that the early cell-cleavage divisions occur in an essentially random sequence of events until the formation of the blastocyst. Embryonic polarity is first witnessed by the asymmetric location of the inner cell mass (ICM), that will give rise to the future embryo proper, at the so-called embryonic pole, which is distinct from the opposing abembryonic pole. The formation of this embryonic-abembryonic axis occurs later than equivalents polarities in other species such as insects and amphibians, where anterior-posterior and/ or dorso-ventral polarity is predetermined during oogenesis [4,5] or immediately following fertilization [4].

However, also in mammals early asymmetry can be revealed shortly after fertilization (reviewed in [6]). Coincident with the formation of the paternal pronucleus, the second polar body is extruded and acts as a marker of the animal pole (A), opposing its counterpart, the vegetal pole (V) of the zygote[7,8] (Figure 4, Chapter 1). It is along this AV-axis that the first cleavage division occurs [7,9], results in daughter blastomeres inheriting both animal and vegetal components of the zygote. The asynchronous second cleavage divisions that produce the 4-cell stage embryo, result in daughter blastomeres that can exhibit different developmental potential and capabilities, depending upon the orientation and order of the cell divisions that generated them [10,11].Each two-cell stage blastomere can either divide meridionally (M, in parallel with the AV-axis) producing two similar blastomeres with both animal and vegetal components, or equatorially (E), resulting in dissimilar daughters that either inherit mainly animal or vegetal components of the original zygote (Figure 4, Chapter 1). Approximately 80% of all 4-cell stage embryos are derived from a combination of M and E divisions [10,11]. In ME embryos (the first blastomere divides M and the second E), it is possible to predict the spatial patterning of the eventual blastocyt as the vast majority of M derived progeny contributes to the embryonic part, including the pluripotent inner cell mass (ICM), of the blastocyst. Conversely the E progeny contribute to the abembryonic part. In EM embryos, blastocyst patterning is not as predictable, as the E and M progeny can contribute to either the embryonic or abembryonic parts. This highlights the importance of the order of cell divisions in addition to their orientation. In contrast, the progeny of the blastomeres derived from EE and MM embryos do not form any recognisable pattern and contribute cells randomly throughout the blastocyst [10-12].

The predictable differences in developmental potential of blastomeres from ME embryos appears to be linked to an epigenetic asymmetry. This involves higher levels of H3R17me2 and H3R26me2 in blastomeres derived from the M division, compared to the progeny of the E-dividing blastomere [13]. If the blastomeres derived from the M-dividing cell of different ME embryos are combined, the resulting chimeras are able to efficiently develop to term when transferred back to pseudo-pregnant females. In contrast, chimeras composed of the progeny of the E-division display much poorer developmental success. Especially, chimeras derived from just the 'vegetal' cells of the E dividing blastomere never successfully develop to term and are characterised as trophoblastic vesicles by the blastocyst stage. The developmental deficiency of chimeras created from the progeny of the E dividing blastomere do not necessarily translate to normal development as naturally occuring EE embryos can develop to term, but at much lower frequencies when compared to EM, ME and MM embryos [10, 11] It is interesting that the A/V blastomeres derived from the M cleavage in ME embryos have elevated levels of H3R17me2, H3R26me2 and global transcription compared to those E -division derived A and V blastomeres that have low level of H3R17/26me2 levels [13].

In addition to the apparent different developmental potencies of blastomeres at the 4-cell stage, the sex of an embryo can influence its developmental capacity [14-18]. It has been shown that male preimplantation embryos are often more developmentally advanced when compared to female embryos, with male embryos reaching the blastocyst stage sooner [3, 14, 16-18], and comprising a higher number of blastomeres [14]. It was suggested that the presence of a Y chromosome accelerates embryonic development, and that females development may be comparatively retarded by the presence of two X chromosomes [15] although a potential mechanism was not put forward.

To compensate for the difference in X chromosome dosage between mammalian females (XX) and males (XY), one X chromosome is subjected to transcriptional inactivation during early female embryonic development ([19], reviewed in [20]). In order for X chromosome inactivation (XCI) to occur, the presence of the X inactivation center (Xic) [21, 22], which contains the non-coding RNA genes *Xist* and *Tsix* [23-25], is necessary. *Xist* RNA is specifically expressed from the future inactivate X chromosome (Xi), and spreads across it *in cis* inducing heterochromatinization and subsequent XCI [26, 27]. *Tsix* is transcribed antisense to *Xist,* and overlaps completely with *Xist* in mice. However, *Tsix* is transcribed from the active X chromosome (Xa) and negatively regulates *Xist* expression. During early mouse embryonic development, two separate phases of XCI occur. First, the paternal X chromosome is specifically inactivated between the 4- and 8-cell stage. This paternal specific XCI is then maintained in the extraembryonic

tissues. In the ICM of the early blastocyst, XCI is reversed and then re-initiated to generate random XCI in the progenitor cells of the embryo proper.

From the 2-cell stage onwards, *Xist* is specifically expressed from the paternal X chromosome in female mouse embryos [28, 29]. This paternal specific *Xist* transcription may be facilitated by the overall higher transcriptional activity of the paternal genome compared to that of the maternal genome, following transcriptional activation of the zygotic genome [30]. This most likely results from the fact that during the protamine-to-histone transition of the paternal genome, the maternally provided histones used in the replacement are hypo-posttranslationally modified and hence provide a more transcriptionally permissive chromatin structure [31-34]. Alternatively, or possibly in addition, paternal imprints causing active *Xist* transcription and/or maternal imprints that inhibits *Xist* transcription from the maternal X could also be involved. The accumulation and spreading of *Xist* over the paternal X chromosome is known to occur after the second cleavage division [28, 35] and is accompanied by transcriptional inactivation of the paternal X, verified by RNA polymerase II and Cot1 RNA exclusion from the *Xist* RNA bound domain, and the induction of several epigenetic modifications on the future Xi [28, 35]. Interestingly, analysis of *Xist* expression in blastomeres from 2-, 4-, 8-cell and morulae stage female embryos report that 18-33% of blastomeres actually lack *Xist* signals. This suggests that the timing of XCI differs between blastomeres. Such early heterogeneity between the blastomeres of the early embryo is supported by further experimental evidence showing that two of the blastomeres within an 8-cell embryo contain relatively high levels of *Xist* RNA when compared to the other cells [36].

It is possible that because of (imprinted) XCI, the developmental delay of female embryos may arise due to the extra "task" they must accomplish compared to males. Therefore, we tracked the cell divisions of early male and female embryos to identify whether the reduced size and number of female blastocysts, when compared to males, is due to differences in the timing of cavity formation, or in the duration of the preceding cell cycles. In addition, we asked if observed heterogeneities in *Xist* expression in the early embryo could be correlated to the orientation of the second cleavage divisions as has been shown for some epigenetic marks [13].

RESULTS

Developmental differences between female and male embryos.
Using time-lapse microscopy we analysed the developmental properties of male and female mouse embryos from the 2-cell until the blastocyst stages (defined as the first sign of cavitation). We counted the number of cells at the inititation

of cavitation and found that male embryos developed from the two-cell stage to the stage of initiation of cavitation over an average of 2362.5 min (SEM 79.60 min) and had an average number of 28 cells (SEM 1.3). The developmental duration of female embryos from the two-cell stage to the initiation of cavitation was statistically indistinguishable at 2351.25 min (SEM 124.05) however these blastocysts contained only 24.75 (SEM 4.0) cells on average.

Initiation of X chromosome inactivation differs between individual embryonic groups according to the orientation of the second cleavage division and between blastomeres within the same embryo

We analysed the initiation of X chromosome inactivation (XCI) by assaying for the presence of *Xist* RNA in the blastomeres of the early mouse embryo. Since the first signs of XCI can be detected at the 4-cell stage [35, 37], we started our analyses in the 4-cell stage embryo. We analysed 94 non-sex determined 4-cell stage embryos 3 hours after the division of the second 2-cell stage blastomere (group 1, Table 1) and classified them according to the four cell division orientation groups. The observed distribution across the four groups (ME, MM, ME and EE) was in accordance with earlier reports [11, 12] (Table I). The EE group showed a lower than expected frequency (given an 1:1 ratio of male:female embryos) of initiation of XCI, in that only 1 of 11 analysed embryos (p = 0.034, as compared to ME, MM and ME embryos) showed any positive *Xist* staining and this was only in two of the four blastomeres. In the three other groups there was detectable *Xist* expression in one or more blastomeres per embryo in 30-50% of cases. This is in agreement with the expected male:female ratio of 1:1. Interestingly, in half

A	+3 hours Classes	% of embryos	% *Xist* positive embryos	χ2
⊚	ME	33% (31/94)	48% (15/31)	0.158
⊚	EM	31% (29/94)	41% (12/29)	0.681
⊛	MM	24% (23/94)	35% (8/23)	0.690
⊛	EE	11% (11/94)	9% (1/11)	0.034 *

B	+3 hours Classes	# *Xist* positive embryos	positive blastomere(s) 1	2	3	4
	ME	15 (of 31)	7	6	0	2
	EM	12 (of 29)	7	2	2	1
	MM	8 (of 23)	4	0	2	2
	EE	1 (of 11)	0	1	0	0

Table 1. *Xist*-expression dynamics in 4-cell stage embryos 3 hours after the second cleavage divison. (a) The total number (and % of total) of ME, EM, MM and EE-embryos with *Xist*-cloud 3 hours after the second cleavage division. c2 = p-value between groups, * indicates significant difference (p<0.05). (b) The number of *Xist*-cloud positive blastomere per ME, EM, MM and EE-embryos which have initiated X-chromosome inactivation.

of the *Xist* positive MM embryos, three or four blastomeres had detectable *Xist* expression, whereas only one or two blastomeres from ME and EM embryos had initiated imprinted XCI.

Next, we analysed imprinted XCI in 134 non-sex determined embryos, 6 hours after the completion of second round of cleavage divisions (group 2, Table 2). In this group none of the 15 EE embryos showed initiation of imprinted XCI ($p<0.001$), suggesting that EE cell-division orientation pattern negatively affects *Xist* RNA expression. The majority of the *Xist*-cloud positive ME embryos showed *Xist* expression in all four blastomeres (Figure 1a), which is in accordance with the expected progression of XCI throughout the embryo. The *Xist* positive MM embryos showed either two or four blastomeres with an *Xist* cloud with a similar distribution as observed at 3 hours (Table 1 vs Table 2). In addition, in one of the MM *Xist* positive embryos, we observed two *Xist* clouds in each blastomere, indicating that both X chromosomes were being inactived (Figure 1b). It is interesting to note that the relative developmental success of MM embryos transferred back to pseudo-pregnant females is drastically reduced when compared to ME and EM subgroups [10].

In some of the 4-to-8 cell stage embryos, we noted blastomeres that were mitotic with persistence of *Xist* on the metaphasic X chromosome, indicating that *Xist* RNA does not (always) disappear from the paternal X chromosome as cells enter M-phase. The same observation has been reported in mitotic female
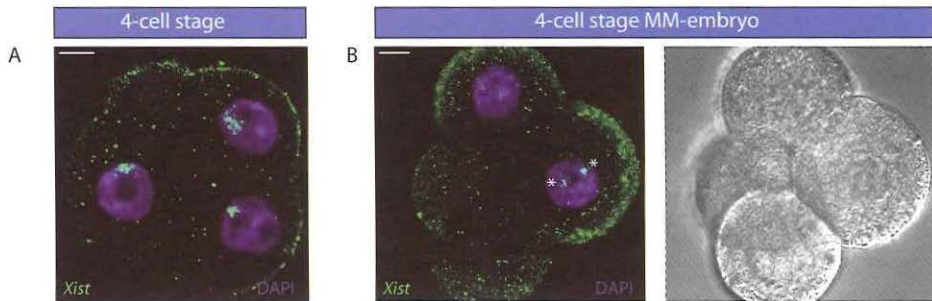
Figure 1. Initiation of X-chromosome inactivation in 4-cell stage pre-implantation embryo six hours after the second cleavage division. (a) Immunostaining for DAPI (blue) and *Xist* (green) in 4-cell stage embryo. Picture represents only one Z-stack showing three blastomeres which all have one positive *Xist*-cloud in the nucleus. Bar represents 10 μm. (b) Left picture presents a Z-stack of a 4-cell stage embryo after two meridional division (MM-embryo) immunostained for DAPI (blue) and *Xist* (green). The nucleus shown has two positive *Xist*-clouds (indicated by asterixes) in one nucleus, indicating that both X-chromosomes have initiated *Xist* expression, leading to X chromosome inactivation. The right picture represents the same Z-stack for bright field microscopy. Bar represents 10 μm.

A

+6 hours Classes	% of embryos	% Xist positive embryos	χ2
ME	43% (58/136)	40% (23/58)	0.992
EM	26% (36/136)	50% (18/36)	0.141
MM	20% (27/136)	48% (13/27)	0.317
EE	11% (15/136)	0% (0/15)	<0.001*

B

+6 hours Classes	# Xist positive embryos	positive blastomere(s)			
		1	2	3	4
ME	23 (of 58)	1	4	5	13
EM	18 (of 36)	2	5	6	5
MM	13 (of 27)	0	6	1	6
EE	0 (of 15)	0	0	0	0

Table 2. *Xist*-expression dynamics in 4-cell stage embryos 6 hours after the second cleavage divison. (a) The total number (and % of total) of ME, EM, MM and EE-embryos with Xist-cloud 6 hours after the second cleavage division. c2 = p-value between groups, * indicates significant difference (p<0.05). (b) The number of *Xist*-cloud positive blastomere per ME, EM, MM and EE-embryos which have initiated X-chromosome inactivation.

ES cells [38]. Also, we noticed that the area covered by *Xist* was larger in group 2 than in group 1 blastomeres, indicating further progression of XCI.

Finally, we analysed imprinted XCI in 8-cell stage embryos, at approximately 14-18 hours after completion of the second round of cleavage divisions. For this purpose, we analysed 29 embryos. Interestingly, at this time point, 3 out of the 5 *Xist* positive EE embryos had initiated XCI in all 8 blastomeres, indicating that EE embryos do inactivate the paternal X, but are delayed as compared to the other types of embryos. The functional significance of this delay is unclear but it is known that of the four classes of embryos, EE embryos develop least successfully [10]. In the EM and MM groups, all of the *Xist* positive embryos had *Xist* signals in all 8 blastomeres indicating complete XCI of the paternal X chromosome in all cells. The 4 *Xist* positive ME embryos displayed Xist expression in only a subset of blastomeres. Again, we noticed an increase in signal and spreading of the *Xist* signal at this later time point, as compared to group 2, indicative of progressive XCI.

Classes	% Xist positive embryos	positive blastomere(s)				
		1	3	4	6	8
ME	50% (4/8)	0	2	1	1	0
EM	60% (3/5)	0	0	0	0	3
MM	62.5% (5/8)	0	0	0	0	5
EE	62.5% (5/8)	1	0	1	0	3

Table 3. *Xist*-expression dynamics in 8-cell stage embryos. The total number (and % of total) of original ME, EM, MM and EE-embryos with *Xist*-clouds in 8-cell stage embryos. Last four columns represent the number of *Xist*-cloud positive blastomeres per embryo.

Although approximately half of the embryos in most groups at all time points showed *Xist* expression, we cannot exclude that some female EM, ME and MM-embryos in our analyses have not initiated XCI, since we did not determine the sex of the embryos. However, considering the embryos in which we observed *Xist* signal, initiation of XCI in EE embryos seems to be delayed. Overall, our data suggests that the onset of XCI could be aided by a M-division orientation and hindered by an E-division. Indeed, we observed an example of aberrant XCI in MM embryos at the 6 hours time point (Figure 1b). Furthermore, it is known that the M-derived blastomeres of ME embryos are more transcriptionally active than those derived from the E-division, therefore providing greater potential for transcription of *Xist*.

DISCUSSION

Early mammalian embryonic development is anticipated as flexible and unbiased, but recent reports indicate the presence of asymmetry and polarization already in the zygote (reviewed in[6, 39]), directing the developmental potency and capacity of the embryo. Another form of asymmetry that appears to influence early embryonic development is the presence of either an XX or XY chromosomal constitution. Several reports mention that female embryos reach the blastocyst stage later than male embryos [14, 16-18], and contain less cells [14, 16]. However, one report shows that during in vivo development, female embryos form a compacted morula earlier than males [16]. Although the number of analysed embryos has to be increased, our first results show that females indeed reach the blastocyst stage with a lower number of blastomeres, but are not slower than male embryos. Although Burgoyne et al. have shown that the Y chromosome plays a role in determining the number of cells at the blastocyst stage [14], the initiation of X chromosome inactivation and its subsequent maintenance in each nucleus in females, can also be viewed as an extra task for these embryos, that may result in a developmental delay. The lower number of cells in female blastocysts compared to males as found in our analyses might be caused by a sex-specific difference in cell cycle length, or by increased cell loss in female embryos, or by the presence of female cells that do not divide at all. Cell loss could occur if cells have inactivated both X chromosomes instead of one. Recently, Monkhorst et al., [40] showed that random X-inactivation is a stochastic process, meaning that every X chromosome has a certain probability to become inactivated. This implies that a certain fraction of cells will inactivate both X chromosomes, and the model predicts that these cells will be lost from the population. During imprinted X inactivation in the female preimplantation embryo, the paternal X chromosome is thought to have a probability of 1 to become inactivated. This is based upon the fact that in XpXp or XpY embryos,

all X chromosomes were shown to express *Xist*[41]. On the other hand, the female X chromosome may also have a certain probability to become inactivated, since (delayed) X-inactivation is observed in parthenogenetic embryos, which consist of two maternal genomes. In these embryos, X-inactivation is not observed until the 8-16-cell stage. In addition, some cells showed *Xist* expression from both alleles [42]. Since we found the presence of two *Xist*-clouds in an MM embryo, this might also suggest that the probality to inactivate the maternal X is >0. The presence of two *Xist*-clouds, suggestive of two inactive X chromosomes, would be incompatible with survival of these cells. This could lead to a loss of such embryos or to a relative decrease in the total cell number at later stages. For example, if this occurs in one of the female blastomeres at the 4-8 cell stage, this would explain the decrease in cell number in female embryos compared to males at the blastocyst stage. It is of interest to establish whether the frequency of blastomeres with two inactive X chromosomes is dependent on the type of early cleavage divisions. Similarly, future experiments with a larger number of embryos should also allow us to make a distinction between the ME, EM, EE, and MM embryos in determining the number of cells at the initiation of cavitation in the blastocyst. This type of analyses, combined with the analyses of *Xist* expression would reveal if cell polarity somehow influences the probability for X-inactivation, and whether this could explain the difference in cell number between embryos of different sex.

Some indications for an effect of the order and plane of the early cleavage divisions on the regulation of *Xist* expression is evident from the fact that blastomeres do not initiate XCI simultaneously [19]. We found that the expression of *Xist* differs between the EM, EE, ME and MM-embryos. The most striking observation was that from the 26 analysed 4-cell EE-embryos (group 1 and 2 combined), only 1 showed signs of XCI. In EE-originated 8-cell stage embryos, XCI is detectable, although in a variable number of blastomeres. However, the total number of embryos analysed at this time point is rather small, and variability in the number of *Xist*-positive blastomeres was also observed for 8-cell stage ME embryos. These results indicate that EE embryos initiate XCI with delayed kinetics compared to the other embryo types. EE embryos show less developmental potential [10, 11], and are less transcriptionally active as compared to ME and EM embryos [13], and perhaps this feature causes delayed accumulation of *Xist* transcripts in these embryos. Conversely, XCI appeared to be enhanced in MM embryos; more blastomeres showed *Xist* clouds at 3 h after reaching the 4-cell stage compared to the other embryo types, and in one MM embryo we observed two *Xist* clouds in all blastomeres.

It is known that the expression of *Xist* is regulated by several factors. Very recently, a dose-dependent, X-linked activator of *Xist*, named RNF12,

has been identified [43]. It will be of interest to analyse RNF12 expression in relation to the *Xist* expression in the different embryo types (EM, ME, EE, MM), to determine if variation in the level of RNF12 might explain the variability in the initiation of imprinted XCI. *Rnf12* mRNA levels are high in oocytes and fertilized eggs (http://genome.ucsc.edu/cgi-bin/hgGene?hgg_chrom=none&org=Mouse&db=mm9&hgg_gene=uc009uaa.1), providing the theoretical possibility for differential distribution of the protein or mRNA to blastomeres upon cleavage. In addition to RNF12 expression, it will be of interest to investigate if the differential timing and maintenance of imprinted XCI in individual blastomeres is also linked to the known epigenetic differences between these cells. If the processes of imprinted XCI, epigenetic regulation of individual blastomeres, and their developmental fate are coupled, this will provide further evidence for biological consequence of epigenetic differences between individual blastomeres.

The capacity of future extra-embryonic cells to maintain imprinted paternal X chromosome inactivation, in contrast to the reactivation of the paternal X chromosomeI in the cells that will give rise to the embryo, could also be related to certain differences between cells of the blastocyst. Recently, it was shown that before the blastocyst stage, pluripotency factors such as NANOG, OCT4 and SOX2 are present in all cells, and expression of these factors becomes downregulated by the transcription factor CDX2 [44]. Around the 8-cell stage, CDX2 mRNA becomes first enriched in the apical part of two polarized blastomeres [45], and following the next round of symmetric cleavage divisions, the number of CDX2-expressing blastomeres, giving rise to the extra-embryonic tissue, increases. This indicates that asymmetrical divisions may lead to differential inheritance of CDX2 mRNA. Decreased presence of CDX2 in the inner cells would relieve the CDX2-mediated downregulation of the pluripotency factors, NANOG, SOX2 and OCT4 in the ICM. These pluripotency factors may directly cause downregulation of *Xist* [46], leading to reactivation of the Xp, whereafter both X chromosomes have the same probability of being subjected to inactivation during initiation of the random XCI process [40]. Conversely, the presence of CDX2 in the outer cells ensures continuous downregulation of the pluripotoency factors, which will result in continued expression and accumulation of *Xist*, allowing no possibility for reactivation. In addition, it has been shown that the blastomeres with higher levels of CDX2 were progeny of the 4-cell stage blastomeres that inherited the vegetal component of the zygote, which showed less development potential and lower levels of H3R17 and H3R26me [13, 45].

Taken together, the enhanced XCI of MM embryos, and the delayed activation of *Xist* expression in EE embryos suggest that factors that regulate *Xist* expression, and thus the probability of XCI, are differentially distributed

in early blastomeres. These data also provide further evidence of considerable heterogeneity in the early mouse embryo and given the known differences in developmental potency of these embryo subgroups, offers a new perspective on the impact of such heterogeneities on early mouse development. The separation, or not, of the animal and vegetal derived poles of the 2-cell embryo may be important in establishing/ delaying imprinted XCI, but it is important to note that the most successful developmental outcomes arise when ME or EM division orientations generate heterogeneity and consequently result in the formation of a developmentally competent blastocysts with a degree of predictable patterning. If both cells behave in a homogenous manner by either separating (EE) or not separating (MM) the A and V poles, this predictability is lost. Future experiments on embryos of defined sex will allow to determine the consequences of the divisions for either sex more thoroughly *e.g.* do male EE and MM embryos develop more successfully than female ones, given they do not need to undertake any XCI?

MATERIALS AND METHODS

Collection and analyses of embryos
2-cell stage embryos were collected from F1 (C57BL/6 ×CBA) females, aged 6 to 8 weeks, induced to superovulation by intraperitoneal injection of 7.5 IU of pregnant mares serum gondotrophin (PMSG, Intervet) followed 48 hours later by 7.5 IU of human chorionic gonadotrophin (hCG, Intervet).

For the purpose of analyses of developmental differences between males and females, the F1 females were mated with transgenic males that express GFP tagged histone H2B [47]. 2-cell embryos were collected 45 hours after hCG injection into M2 medium supplemented with 4 mg/ml BSA and cultured in vitro in drops of KSOM supplemented with amino acids and 4 mg/ml BSA, under paraffin oil in an atmosphere of 5% CO_2 in air at 37.5°C. Time-lapse imaging was performed using a Zeiss Axiovert microscope, Hamamatsu camera and Kinetic-Imaging software. Fluorescence and DIC z-stacks were collected every 15 minutes, on 15 different planes for each time point, from the 2-cell to the blastocyst stage. The PICT files obtained were converted to TIF using VisBio (LOCI, WI) and ImageJ (NIH, Bethesda, MD). All cells were followed manually using SIMI Biocell software [49].

For other purposes, F1 females, aged 6 to 8 weeks, were mated with wild type males. To monitor the order and orientation of the second cleavage divisions, and then at the 4-cell stage to examine the arrangements of blastomeres, embryos were cultured in the 5% CO_2 incubator at 37°C. After a few hours of uninterrupted culture, embryos were observed under light microscopy every 20

minutes to determine plane and order of divisions. Embryos were divided into four groups: ME, EE, MM and ME [11] and cultured until 3, 6 and 14-18 hours (morula stage) after reaching the 4-cell stage. To remove the zona pelludica, 4-cell embryos were placed in an acid tyrode solution until the zona started to dissolve. Next, embryos were fixed for 10 minutes in 4% PFA, rinsed in PBS and stored in 70% ethanol/PBS at 4°C in a 96-well plate (Greiner Bio-One, Alphen a/d Rijn, The Netherlands).

Fluorescent in situ hybridisation
Embryos were dehydrated in 70%, 90% and 100% ethanol. They were permeabilized by placing them in RIPA buffer (150 mM NaCl, 1% Nonidet P-40, 0,5% Na deoxycolate, 0.1% SDS, 1mM EDTA, 50 mM Trish pH 8.0) for 10 minutes at room temperature, and rinsed in PBS. Next the embryos were postfixed in 4% PFA in PBS for 5 minutes.

Xist mRNA was detected with the 5.5-kb cDNA *Xist* probe described by Gribnau et al. [48]. The DNA-probe was labeled with digoxigenin by nick translation (Roche). The nick-translated *Xist*-DNA-probes were dissolved in a hybridization mixture containing 50% formamide, 2XSSC, 50 mM phosphate buffer (pH 7.0), 10% dextran sulfate and 100 ng/μl COT DNA to a final concentration of 1 ng/μl. The probe mixture was denatured for 5 minutes, and prehybridized for 45 minutes at 37 °C. The embryos were placed in the probe mixture overnight in a shaking humid chamber at 37 °C.

After hybridization, the embryos were washed twice in 2 X SSC, three times in 50% formamide/ 2 x SSC at 37 °C, and twice in TNT (0,1 M Tris, 0,15 M NaCl, 0,05% Tween 20) at room temperature. Embryos were blocked in TNBSA for 30 minutes at room temperature. Detection was done by sequential steps of incubation with anti-digoxigenin (Boehringer), anti-sheep FITC (Jackson ImmunoResearch Laboratories) and anti-rabbit FITC (Jackson ImmunoResearch Laboratories) antibodies in blocking buffer for 30 minutes at room temperature. Embryos were washed in TNT between and after the detection steps. Finally, embryos were placed in a droplet of Vectashield mounting medium with DAPI (4',6'-diamidino-2-phenylindole) (Vector Laboratories, Burlingame CA, USA) and stored at 4 °C.

Statistical analyses
To test whether the proportion of *Xist*-positive embryo's in a [group/treatment arm/development stage] was different than the proportion of *Xist*-positive embryos in the combined other [group/treatment arm/development stage] the Pearson Chi-square test was performed. A p-value <0.05 was considered

statistically significant. All statistical analyses were done using SPSS 15.0 for Windows software (SPSS Inc., Chicago, IL, USA).

Fluorescence microscopy analysis, digital image preparation and analysis
Confocal sections were taken every 1 µm through the whole embryo, using Leica-software. The acquired digital images were processed with Photoshop software (Adobe Systems).

ACKNOWLEDGEMENTS

REFERENCES

1. Tarkowski AK. Experiments on the development of isolated blastomers of mouse eggs. *Nature.* Oct 24 1959;184:1286-1287.
2. Tarkowski AK. Studies on mouse chimeras developed from eggs fused in vitro. *Natl Cancer Inst Monogr.* Mar 1963;11:51-71.
3. Tsunoda Y, McLaren A. Effect of various procedures on the viability of mouse embryos containing half the normal number of blastomeres. *J Reprod Fertil.* Sep 1983;69(1):315-322.
4. Gurdon JB. The generation of diversity and pattern in animal development. *Cell.* Jan 24 1992;68(2):185-199.
5. St Johnston D, Nusslein-Volhard C. The origin of pattern and polarity in the Drosophila embryo. *Cell.* Jan 24 1992;68(2):201-219.
6. Zernicka-Goetz M. Cleavage pattern and emerging asymmetry of the mouse embryo. *Nat Rev Mol Cell Biol.* Dec 2005;6(12):919-928.
7. Gray D, Plusa B, Piotrowska K, et al. First cleavage of the mouse embryo responds to change in egg shape at fertilization. *Curr Biol.* Mar 9 2004;14(5):397-405.
8. Zernicka-Goetz M. Patterning of the embryo: the first spatial decisions in the life of a mouse. *Development.* Feb 2002;129(4):815-829.
9. Plusa B, Hadjantonakis AK, Gray D, et al. The first cleavage of the mouse zygote predicts the blastocyst axis. *Nature.* Mar 17 2005;434(7031):391-395.
10. Piotrowska-Nitsche K, Perea-Gomez A, Haraguchi S, Zernicka-Goetz M. Four-cell stage mouse blastomeres have different developmental properties. *Development.* Feb 2005;132(3):479-490.
11. Piotrowska-Nitsche K, Zernicka-Goetz M. Spatial arrangement of individual 4-cell stage blastomeres and the order in which they are generated correlate with blastocyst pattern in the mouse embryo. *Mech Dev.* Apr 2005;122(4):487-500.
12. Bischoff M, Parfitt DE, Zernicka-Goetz M. Formation of the embryonic-abembryonic axis of the mouse blastocyst: relationships between orientation of early cleavage divisions and pattern of symmetric/asymmetric divisions. *Development.* Mar 2008;135(5):953-962.
13. Torres-Padilla ME, Parfitt DE, Kouzarides T, Zernicka-Goetz M. Histone arginine methylation regulates pluripotency in the early mouse embryo. *Nature.* Jan 11 2007;445(7124):214-218.
14. Burgoyne PS. A Y-chromosomal effect on blastocyst cell number in mice. *Development.* Jan 1993;117(1):341-345.
15. Burgoyne PS, Thornhill AR, Boudrean SK, Darling SM, Bishop CE, Evans EP. The genetic basis of XX-XY differences present before gonadal sex differentiation in the mouse. *Philos Trans R Soc Lond B Biol Sci.* Nov 29 1995;350(1333):253-260 discussion 260-251.
16. Peippo J, Bredbacka P. Sex-related growth rate differences in mouse preimplantation embryos in vivo and in vitro. *Mol Reprod Dev.* Jan 1995;40(1):56-61.
17. Valdivia RP, Kunieda T, Azuma S, Toyoda Y. PCR sexing and developmental rate differences in preimplantation mouse embryos fertilized and cultured in vitro. *Mol Reprod Dev.* Jun 1993;35(2):121-126.
18. Zwingman T, Erickson RP, Boyer T, Ao A. Transcription of the sex-determining region genes Sry and Zfy in the mouse preimplantation embryo. *Proc Natl Acad Sci U S A.* Feb 1 1993;90(3):814-817.
19. Huynh KD, Lee JT. Inheritance of a pre-inactivated paternal X chromosome in early mouse embryos. *Nature.* Dec 18 2003;426(6968):857-862.

20. Payer B, Lee JT. X chromosome dosage compensation: how mammals keep the balance. *Annu Rev Genet.* 2008;42:733-772.
21. Brown CJ, Lafreniere RG, Powers VE, et al. Localization of the X inactivation centre on the human X chromosome in Xq13. *Nature.* Jan 3 1991;349(6304):82-84.
22. Rastan S. Non-random X-chromosome inactivation in mouse X-autosome translocation embryos--location of the inactivation centre. *J Embryol Exp Morphol.* Dec 1983;78:1-22.
23. Kalz-Fuller B, Sleegers E, Schwanitz G, Schubert R. Characterisation, phenotypic manifestations and X-inactivation pattern in 14 patients with X-autosome translocations. *Clin Genet.* May 1999;55(5):362-366.
24. Marahrens Y, Panning B, Dausman J, Strauss W, Jaenisch R. Xist-deficient mice are defective in dosage compensation but not spermatogenesis. *Genes Dev.* Jan 15 1997;11(2):156-166.
25. Penny GD, Kay GF, Sheardown SA, Rastan S, Brockdorff N. Requirement for Xist in X chromosome inactivation. *Nature.* Jan 11 1996;379(6561):131-137.
26. Plath K, Fang J, Mlynarczyk-Evans SK, et al. Role of histone H3 lysine 27 methylation in X inactivation. *Science.* Apr 4 2003;300(5616):131-135.
27. Silva J, Mak W, Zvetkova I, et al. Establishment of histone h3 methylation on the inactive X chromosome requires transient recruitment of Eed-Enx1 polycomb group complexes. *Dev Cell.* Apr 2003;4(4):481-495.
28. Okamoto I, Otte AP, Allis CD, Reinberg D, Heard E. Epigenetic dynamics of imprinted X inactivation during early mouse development. *Science.* Jan 30 2004;303(5658):644-649.
29. Zuccotti M, Boiani M, Ponce R, et al. Mouse Xist expression begins at zygotic genome activation and is timed by a zygotic clock. *Mol Reprod Dev.* Jan 2002;61(1):14-20.
30. Aoki F, Worrad DM, Schultz RM. Regulation of transcriptional activity during the first and second cell cycles in the preimplantation mouse embryo. *Dev Biol.* Jan 15 1997;181(2):296-307.
31. Adenot PG, Mercier Y, Renard JP, Thompson EM. Differential H4 acetylation of paternal and maternal chromatin precedes DNA replication and differential transcriptional activity in pronuclei of 1-cell mouse embryos. *Development.* Nov 1997;124(22):4615-4625.
32. Sutovsky P, Schatten G. Paternal contributions to the mammalian zygote: fertilization after sperm-egg fusion. *Int Rev Cytol.* 2000;195:1-65.
33. van der Heijden GW, Derijck AA, Ramos L, Giele M, van der Vlag J, de Boer P. Transmission of modified nucleosomes from the mouse male germline to the zygote and subsequent remodeling of paternal chromatin. *Dev Biol.* Oct 15 2006;298(2):458-469.
34. Wright SJ. Sperm nuclear activation during fertilization. *Curr Top Dev Biol.* 1999;46:133-178.
35. Okamoto I, Heard E. The dynamics of imprinted X inactivation during preimplantation development in mice. *Cytogenet Genome Res.* 2006;113(1-4):318-324.
36. Hartshorn C, Rice JE, Wangh LJ. Differential pattern of Xist RNA accumulation in single blastomeres isolated from 8-cell stage mouse embryos following laser zona drilling. *Mol Reprod Dev.* Jan 2003;64(1):41-51.
37. Patrat C, Okamoto I, Diabangouaya P, et al. Dynamic changes in paternal X-chromosome activity during imprinted X-chromosome inactivation in mice. *Proc Natl Acad Sci U S A.* Mar 31 2009;106(13):5198-5203.
38. Jonkers I, Monkhorst K, Rentmeester E, Grootegoed JA, Grosveld F, Gribnau J. Xist RNA is confined to the nuclear territory of the silenced X chromosome throughout the cell cycle. *Mol Cell Biol.* Sep 2008;28(18):5583-5594.

39. Zernicka-Goetz M, Morris SA, Bruce AW. Making a firm decision: multifaceted regulation of cell fate in the early mouse embryo. *Nat Rev Genet.* Jul 2009;10(7):467-477.
40. Monkhorst K, Jonkers I, Rentmeester E, Grosveld F, Gribnau J. X inactivation counting and choice is a stochastic process: evidence for involvement of an X-linked activator. *Cell.* Feb 8 2008;132(3):410-421.
41. Kay GF, Barton SC, Surani MA, Rastan S. Imprinting and X chromosome counting mechanisms determine Xist expression in early mouse development. *Cell.* Jun 3 1994;77(5):639-650.
42. Nesterova TB, Barton SC, Surani MA, Brockdorff N. Loss of Xist imprinting in diploid parthenogenetic preimplantation embryos. *Dev Biol.* Jul 15 2001;235(2):343-350.
43. Jonkers I, Barakat TS, Achame EM, et al. RNF12 is an X-Encoded dose-dependent activator of X chromosome inactivation. *Cell.* Nov 25 2009;139(5):999-1011.
44. Niwa H, Toyooka Y, Shimosato D, et al. Interaction between Oct3/4 and Cdx2 determines trophectoderm differentiation. *Cell.* Dec 2 2005;123(5):917-929.
45. Jedrusik A, Parfitt DE, Guo G, et al. Role of Cdx2 and cell polarity in cell allocation and specification of trophectoderm and inner cell mass in the mouse embryo. *Genes Dev.* Oct 1 2008;22(19):2692-2706.
46. Navarro P, Chambers I, Karwacki-Neisius V, et al. Molecular coupling of Xist regulation and pluripotency. Science. Sep 19 2008;321(5896):1693-1695.
47. Hadjantonakis AK, Papaioannou VE. Dynamic in vivo imaging and cell tracking using a histone fluorescent protein fusion in mice. BMC Biotechnol. Dec 24 2004;4:33.
48. Gribnau J, Luikenhuis S, Hochedlinger K, Monkhorst K, Jaenisch R. X chromosome choice occurs independently of asynchronous replication timing. J Cell Biol. Jan 31 2005;168(3):365-373.
49. Schnabel R, Hutter H, Moerman D, Schnabel H. Assessing normal embryogenesis in Caenorhabditis elegans using a 4D microscope: variability of development and regional specification. Dev Biol. Apr 15 1997;184(2):234-265.

CHAPTER 10

GENERAL DISCUSSION

In this thesis, we investigated the behaviour of heterologous sex chromosomes during gametogenesis in various vertebrate species. Specifically, we studied the role of HR6B/UBE2B in sex chromosome regulation and maintenance of genome integrity during mouse spermatogenesis. In addition, we analysed the process of X chromosome inactivation in early female mouse embryos. Here, I will focus on three central questions that have arisen during the course of the work described in this thesis. First, we wish to understand what triggers the meiotic silencing of heterologous chromatin during gametogenesis. Second, based on our findings in chicken, we would like to ask here what is the evolutionary benefit of meiotic silencing of sex chromosomes? The third question involves the possible transgenerational effect of meiotic sex chromosome inactivation, is this biologically relevant? Although a definite answer to these three questions is not yet available, the findings described in this thesis have hopefully brought us somewhat closer to the answers, that will undoubtedly also generate new questions.

WHAT TRIGGERS MEIOTIC SILENCING?

Mechanisms that silence DNA sequences, chromosomal regions or whole chromosomes during formation of the gametes operate in a diversity of species and predate the rise of multicellular organisms. Approaching meiotic silencing mechanisms from an evolutionary perspective, to identify if there is a unifying property of this mechanism in the different organisms, could help us to unravel the driving forces that cause the cascade of events leading to transcriptional inactivation. Although the main outcome in all species is inactivation or silencing of specific regions or even whole chromosomes, each species seems to achieve this through their own unique sequence of events, that is of course more dramatically different between species that are more distantly related.

Each meiotic cycle starts with an extensive homology check, comparing chromosomal content to ensure pairing and synapsis of the correct homologous chromosomes, before recombination can occur. Without control for homology, heterologous pairing might occur, leading to incorrect genetic exchange and disruption of genomic integrity.

By means of meiotic transvection [1], the fungus *Neurospora crassa* assesses homology on the level of individual genes between paired alleles. Regions of DNA that remain unpaired, either due to a new genomic insertion (such as a transposable element (TE)), or due to a deletion, are silenced by a mechanism named meiotic silencing of unpaired DNA (MSUD) [2]. MSUD is a post-transcriptional RNA interference (RNAi)-mediated silencing mechanism (PTGS), that silences all DNA homologous to the unpaired region in the genome, even

copies at other genomic locations that are paired. MSUD appears to be an early meiotic event, occurring before and independently of chromosomal pairing and synapsis (reviewed in [3]). Most likely, the resulting mRNA from the unpaired region is processed into short interfering (si)RNA, targeting its original mRNA for degradation (reviewed in [2, 3]), resulting in effective silencing of these genes.

RNAi is a gene-silencing mechanism that depends on homology. It starts with the formation of double stranded RNA (dsRNA) (reviewed in [4, 5]) and is operative in fungi, plants, and animals, including humans [6]. The type III RNase enzyme cleaves dsRNA into siRNAs that are 21-26 nucleotides, and target complementary mRNA for degradation, resulting in effective posttranscriptional silencing [7]. Genes transcribed into noncoding RNAs (ncRNAs) are dispersed throughout the genome, and apart from endogenous siRNAs, several additional classes of ncRNA have been identified: microRNAs (miRNAs), repeat-associated RNAs (rasiRNAs), PIWI-interacting RNAs (piRNAs) (reviewed in [4]), and, more recently, MIWI-independent small RNAs (MSY-RNAs) [8]. Most of these ncRNAs are transcribed by RNA polymerase II ([9], [10] and reviewed in [11]). The resulting dsRNAs are incorporated into silencing-effector complexes, in which the evolutionary conserved small RNA binding protein Argonaute is the core component (reviewed in [12].) In addition, the Argonaute protein Ago1 associates with RNA polymerase II [13, 14]. Apart from posttranscriptional silencing mediated through RNA degradation (siRNAs), such as occurs in MSUD, miRNAs inhibit gene expression mostly via inhibition of mRNA translation. Furthermore, small RNAs may also induce gene silencing at the transcriptional level via RNA-directed DNA methylation (RdDM), or RNAi-mediated heterochromatin formation, (reviewed in [5]). In extreme cases, such pathways may even lead to DNA elimination (reviewed in [5]).

The ciliated protozoans, *Tetrahymena thermophilia* [9] and *Paramecium tetraurelia* [15] use an RNAi pathway to detect nonhomologous regions, but this leads to complete elimination of large (new) DNA sequences, known as internal eliminated segments (IES), during the sexual process of conjugation. Transvection and RNA-mediated silencing have also been described to play roles in somatic cells of *Drosophila melanogaster* (reviewed in [16]). In addition, double-stranded RNA-mediated post-transcriptional gene silencing in the male germline of Drosophila has been reported [17]. An RNA-mediated *trans*-silencing pathway depending on homology has been detected in the germline of female *D. melanogaster* [18]. The insertion of a single transposable element (TE) in a subtelomeric heterochromatic region without the presence of a homolog at the same location causes silencing of all copies of this TE throughout the genome by a *trans*-silencing effect (TSE). The silencing is mediated through a piRNA pathway [18], sharing components of

the siRNA-pathway described to control MSUD in *N. crassa* [3]. Most notably, the silencing of such a TSE is transmitted over generations via piRNA inheritance through maternal deposition in the oocyte [18].

In addition to meiotic homology sensing and silencing at the level of single genes, other silencing mechanisms operate at the level of large chromosomal regions or even whole chromosomes in different species. It is not clear whether the single-gene-based mechanism of MSUD in *N. crassa* is evolutionary related to these chromatin-based mechanisms.

During spermatogensis in *Drosophila*, reduced expression levels of X-linked genes as compared to autosomal genes have been reported [19]. Along with the finding that X-linkage reduces the expression of a testis-specific promoter [20], this indicates that the X chromosome is inactivated during meiosis in *Drosophila* spermatogenesis. This is further supported by the underrepresentation of meiosis- and testis-specific genes on the X [21, 22]. Expression of X-to-autosome retroposed genes during meiosis also points to the existence of a mechanism that compensates for the silencing of genes on the X chromosome during meiosis in the male *Drosophila* [19]. RNA-mediated silencing has been shown to be involved in silencing of TEs during male meiosis in *Drosophila* [17], but it is still unknown if the silencing of the X chromosome is related to MSUD and/ or RNAi-mediated silencing. In contrast to mammals, the Y chromosome of *Drosophila melanogaster* does not determine sex. Since years this it is believed to be achieved by measurement of the ratio of the number of X chromosomes versus the number of sets of autosomes (X:A ratio), but recent results indicate a sex determining role for the X chromosomal dose through an X-chromosome counting system [23]. However, the Y chromosome is essential for male fertility, since XO males are infertile [24]. No single-copy Y-linked genes are shared with X, and all these genes arose by duplication of autosomal genes (reviewed in [25]). Also, the Y chromosome contains male specific fertility genes and active transcription from the Y chromosome is detectable in spermatocytes [26] during *Drosophila* spermatogenesis, despite the fact that it lacks a homologous pairing partner. The difference in activity of X (inactive) and Y (active) during *Drosophila* spermatogenesis can be explained if the silencing of X is triggered by a specific property of the X chromosome, rather than by a mechanism that checks for sequence homology. Alternatively, and more likely in view of the properties of the *Drosophila* Y chromosome, the Y chromosome may somehow escape from a homology-dependent silencing mechanism.

In the hermaphroditic worm *Caenorhabditis elegans*, sex is determined by the X:A ratio. XX animals are hermaphrodites that first produce a few sperm until the last larval stage. Hereafter, the germ cells continue meiosis through

oogenesis (reviewed in [27]). The true males carry only one X chromosome, and this X chromosome remains unpaired in spermatogenesis. In both female and male meiosis, unsynapsed chromosomal regions or chromosomes, including the univalent X in spermatogenesis, become specifically enriched for H3K9me2 and are subjected to meiotic silencing [28], indicating a synapsis-dependent inactivation. Surprisingly, the paired X chromosomes also become temporarily inactivated during *C. elegans* oogenesis and spermatogenesis, but they lack accumulation of H3K9me2, and this inactivation is reversed around late pachytene in oogenesis (reviewed in [3]). The role of RNAi in meiotic silencing during *C. elegans* gametogenesis is still unknown, but the proteins RHA-1 and EGO-1, which are linked to the RNAi-machinery, are also necessary for the formation of H3K9me2 at unsynapsed chromatin (reviewed in [3]).

During mammalian meiosis, unsynapsed chromosomal regions are detected and inactivated at the level of transcription by the mechanism of meiotic silencing of unsynapsed chromatin (MSUC) [29-31]. The heterologous X and Y chromosomes only pair in the small pseudoautosomal regions (PARs), leaving the larger parts of the chromosomes unsynapsed. This unsynapsed state of the mammalian sex chromosomes is thought to trigger a specialized form of MSUC called meiotic sex chromosome inactivation (MSCI) (reviewed in [32], see also Chapter 2), resulting in the formation of the transcriptionally inactive XY body.

In birds, the situation is somewhat different, due to the fact that females are heterogametic (ZW) and males are homogametic (ZZ). Sex is determined by dosage of the Z-linked gene *DMRT1* [33]. We have analysed the behaviour of the heterologous sex chromosomes Z and W in oocytes and found that Z and W are transiently silenced during pachytene, despite their complete synapsis at this stage (Chapter 4, [34]). This indicates that MSCI is not male specific, and heterologous synapsis apparently cannot completely prevent activation of this mechanism. In birds, MSCI may spread from W to Z, since the W chromosome is already inactivated early in meiosis, before the occurrence of pairing and synapsis. Similarly, a germ cell restricted chromosome (GRC) that is present as a single copy in zebra finch spermatocytes, is silenced immediately upon entry into meiosis. We have termed this phenomenon meiotic silencing prior to synapsis (MPSP). Interestingly, the GRC always enters a meiotic degradation pathway and is eliminated around metaphase I (Chapter 5, [35]). MSPS is somewhat reminiscent of the early detection of nonhomologous DNA sequences by MSUD in *Neurospora* [2] and DNA elimination after *trans*-sensing by small RNAs in the ciliate *Tetrahymena* (reviewed in [9]).

A direct link between RNA interference pathways and meiotic silencing as observed in fungi and fly has not been shown for mammals. However, despite

MSCI during mammalian spermatogenesis, it was shown that many X-linked genes transcribed into miRNAs escape MSCI and/or its continuation during the postmeiotic stage as heterochromatic postmeiotic sex chromatin (PMSC) and are *de novo* transcribed in pachytene spermatocytes by RNA polymerase II [36]. Although experimental evidence is lacking, it has been suggested that X-linked miRNAs escaping from MSCI may regulate MSCI [37]. It is known that the piRNA pathway regulates silencing of transposons in meiotic prophase in the mammalian testis. This mechanism is essential for spermatogenesis, as evidenced by the male infertility phenotype of mouse knockouts for the three homologs of *Drosophila Piwi*, *Mili* (*Piwil2*), *Miwi* (*Piwil1*), and *Miwi2* (*Piwil4*). Spermatocytes of *Miwi* knockout mice appear to develop normally during the first wave of spermatogenesis [38], making it unlikely that this gene is involved in MSCI. *Mili* knockout spermatocytes are blocked in early pachytene, with apparently normal formation of a γH2AX-positive XY body [39]. In contrast, *Miwi2* knockout spermatocytes are blocked prior to synapsis, and γH2AX remains high throughout the nucleus, indicating that meiotic DSB repair is blocked [40]. This precludes an analysis of the possible role of this protein in XY body formation. Taken together, it appears unlikely that the piRNA pathway is involved in the initiation or maintenance of MSCI, although a role for MIWI2 cannot be excluded. The significance of X-linked miRNA transcription during pachytene needs to be further investigated.

Irrespective of the possible involvement of small RNAs in MSCI, the question still remains how is MSUC/MSCI triggered? The earliest known initiating event in MSCI and MSUC in mammals is the accumulation of ATR along the asynapsed axes of X and Y, and the subsequent phosphorylation of H2AX in the surrounding chromatin [41,42]. However, during leptotene, before the occurrence of MSCI, ATM already phosphorylates H2AX in association with the meiotic DSBs throughout the genome, making it impossible to clearly distinguish the moment when ATR takes over from ATM at the sex chromosomes [41]. How ATR is recruited is not exactly known, although BRCA1 has been implicated (see Chapter 2). When chromosomal arms remain unsynapsed, specific proteins may remain attached that would otherwise loose affinity for the axial elements when synapsis has been established. Such proteins could then mediate recruitment of silencing proteins to asynapsed chromatin. Strong candidate proteins for such a function are the HORMAD1 and HORMAD2 proteins, which accumulate early during the meiotic prophase on unsynapsed chromosomal axes and are only removed when the SC forms between homologous chromosomes [43]. The presence of persistent DNA double strand breaks (DBSs) on unsynapsed axes could also be involved in the initiation of MSCI, as proposed and described

in detail in Chapter 2. Indeed, Shanbhag et al. (2010) recently showed that the presence of DSBs initiates an ATM-dependent signal that causes transcriptional silencing *in cis*, spreading along several kilobases distal of the DSB in somatic cells [44]. This mechanism has been termed DISC (DNA double-strand break-induced transcriptional silencing *in cis*). After induction of a DSB, ATM quickly phosphorylates the histone H2AX (γH2AX) surrounding the breaks [41, 45, 46], this leads to widespread ubiquitylation of H2A (uH2A) distal to the lesion, leading to transcriptional silencing through shutdown of RNA polymerase II activity, and prevention of chromatin decondensation. Inhibition of ATM, results in deubiquitylation of uH2A, a re-establishment of transcription and decompaction of chromating several kilobases distal to the lesion [44]. Another study also showed transcriptional silencing and accumulation of silencing markers at DSB sites [47].

Although the spreading of silencing after induction of a DSB has not been shown during the meiotic prophase, one could envision that this mechanism also operates during meiosis. With the lack of a repair template, DSBs cannot be repaired and will persist along the axes of X and Y and other unsynapsed chromatin. Due to stalled repair of the DSBs, ubiquitylation of H2A and silencing could gradually continue to spread along the axes. The steady accumulation of histone modifications upon the formation of γH2AX such as uH2A and H3K9me3, could result in a stable lock-in situation allowing maintenance of X and Y silencing. Indeed, the mammalian XY chromosome pair displays accumulation of diverse histone modifications associated with inactivation and heterochromatin formation from the beginning of pachytene, and some are maintained into the postmeiotic phase.

In contrast to the accuracy of gene homology sensing by transvection in *Neurospora* and *Drosophila*, mammalian chromosomal regions without a homologous partner can circumvent MSUC by heterologous synapsis or self synapsis [29, 31, 48]. In Chapter 3, we have shown that the presence of more DSBs in a certain heterologous regions increases recognition and silencing by MSUC of this region [49]. In view of the recent data from Shanhbag et al. (2010) [44], the presence of more DBSs in the same region should cause more accumulation of uH2A and spreading of silencing, making it harder to force heterologous synapsis. In addition, the prevention of chromatin decondensation in the vicinity of the DSBs, could prevent successful synaptic adjustment. However, when the same heterologous region resides in a much larger chromosome it almost always shows heterologous synapsis, apparently independent of the number of DSBs present at that time. This indicates that the probability for a heterologous region to synapse depends not only on the number of DSBs in that region, but also on the size of the flanking regions. Perhaps the ratio between the synapsed

and unsynapsed regions is critical: once synapsis has proceeded along a certain length, a positive feedback mechanism may enforce heterologous synapsis of the remaining part of the chromosome.

Although heterologous synapsis appears to circumvent MSUC, our recent analyses of XY pairing in dog spermatocytes (Chapter 6) has shown that heterologous synapsis of sex chromosomes does not completely prevent MSCI. This result resembles our observations on the ZW pair in chicken oocytes and provides more evidence for a possible evolutionary link between the mechanisms of meiotic silencing in birds and mammals. In both lineages, the sex chromosomes are the last pair to synapse, partially or complete, in association with persistent DSBs. Heterologous synapsis of autosomal chromatin is likely to occur earlier, when homologous chromosomes also synapse. Hence, we suggest that the timing of synapsis might be an essential factor, to circumvent MSUC. Further investigation of MSUC and MSCI in additional vertebrate species is necessary to precisely define the evolutionary relationship between the meiotic silencing mechanisms in different lineages of animal species.

WHY TRIGGER MEIOTIC SILENCING?
Although multiple mechanisms to silence or even eliminate heterologous chromatin seem to exist in a variety of species, the evolutionary driving force to do so may be similar. From this perspective it is very intriguing that meiotic sex chromosome inactivation can also occur in a situation where two homologous chromosomes are present, as is the case in *C. elegans* hermaphrodite spermatogenesis and oogenesis (reviewed in [3]). In this situation, and also in *Drosophila*, chicken and dog, MSCI appears to be not directly coupled to the final achievement of synapsis. At first sight, there appear to be two obvious possible explanations for the silencing of sex chromosomes in meiotic prophase in such a wide variety of species. First, the whole process may be a side-effect of mechanisms that operate to silence foreign DNA, and that lack a proper pairing partner. Second, the X chromosome is enriched for female beneficial genes that may be harmful during male gametogenesis [50]. Conversely, the Z chromosome in chickens has relatively few female beneficial genes [51]. Thus, sex chromosome silencing during meiosis in the heterochromatic sex could function to silence such possible harmful genes. However, this does not explain why the Y chromosome is turned off during male meiotic prophase in mammals. Moreover, an escape from MSCI in mouse by the Y chromosomes in the case of a XYY chromosomal constitution, leads to an arrest in meiotic progression and cell death [52], indicating the existence of Y encoded genes that are harmful to male meiotic progression. Still, the human Y also harbors genes that are male beneficial and essential for

spermatogenesis [53], and the "toxic" effect of Y expression in case of an XYY constitution during meiotic prophase may be due to aberrant timing of the Y gene expression program.

Neither one of these arguments explains why both X chromosomes are silenced in meiotic prophase in *C. elegans* hermaphrodites. However, this may have evolved as an extreme form of dosage compensation that equalizes gene expression patterns in XO (male) and XX (hermaphrodite) primordial germ cells. Maintenance of X inactivation upon entry into meiotic prophase would also help to equalize gene expression patterns in hermaphrodite spermatocytes (carrying two X chromosomes) and male spermatocytes in which the single X chromosome is silenced by MSUC.

A third possible driving force behind the silencing of single sex chromosomes during meiotic prophase, such as occurs in *C. elegans* and grasshopper XO males [54], could be to help to evade checkpoint activation. This hypothesis is based on recent findings in *C. elegans* that indicate that a single, transcriptionally silenced X can evade checkpoint activation whereas unsynapsed autosomal chromosome pairs elicit a checkpoint response [55].

In *D. melanogaster* and *C. elegans*, chromosome pairing precedes the formation of meiotic DSBs, whereas in yeast and mammals, meiotic DSB formation precedes, and is essential, to achieve chromosome synapsis. This fundamental difference in the mechanisms that achieve synapsis may also lead to differences in factors that act as driving force to trigger the mechanism that detects and silences chromatin that lacks a pairing partner. As discussed in Chapter 2, MSCI and MSUC in mouse share many components with the DNA repair and cell cycle checkpoint machineries that are operative in somatic cells. In Chapter 3, we also found a clear link between the induction of DSBs and the detection of heterologous chromatin [49]. This and other findings point to a possible link between the persistence of meiotic DSBs in unsynapsed regions and the induction of transcriptional silencing. As described above, Shanbhag et al. (2010) have shown that a link between DSB repair and silencing in somatic cells [44]. It appears sensible to silence transcription in the area surrounding a DSB, to allow access of repair factors and prevent the formation of truncated and/or aberrant transcripts. In that context, MSCI and MSUC may have evolved in mammals as an unexpected consequence of DISC.

IS THERE A BIOLOGICALLY RELEVANT TRANSGENERATIONAL EFFECT OF MEIOTIC SEX CHROMOSOME INACTIVATION?

Mammalian MSCI persists into the postmeiotic phase, and the sex chromosomes in spermatids of these species are visible as heterochromatic postmeiotic sex chromatin (PMSC) [56]. Avian MSCI, on the other hand, is reversed for the Z chromosome, which shows re-expression from diplotene onward, indicating that it is possible to quickly reverse the silencing process (Chapter 4, [34]). Why then do the mammalian sex chromosomes remain inactivated? First, it needs to be mentioned that despite a global transcriptional inactivation, the majority of X- and Y-linked multi-copy genes [57] and a significant number of single-copy genes are reactivated during the postmeiotic phase (spermiogenesis) in mouse [57, 58 59], showing that PMSC is not as strict as MSCI. Based on these findings, it might be suggested that PMSC is not mediated by an active process, and that genes which are required can be normally reactivated. It should be noted that the histone-to-protamine transition that accompanies the formation of the compact sperm head, leads to complete genome inactivation, most likely nullifying any differences in chromatin structure between chromosomes or chromosome areas. However, lack of the autosomal *Hr6b/Ube2b* gene ([60], Chapter 7, 8) and knockdown of the Y-linked multi-copy *Sly* gene [61] lead to derepression of X and Y chromosomal genes in spermatids and subsequent sperm defects. Since *Hr6b/Ube2b* seems to play a more general role during the postmeiotic phase (spermiogenesis) in maintaining genome integrity (Chapter 8), and regulation of gene expression, the sperm head defects may not be caused by the reduction of PMSC formation. The effect of *Sly* knockdown, however, was mainly restricted to the upregulated postmeiotic expression of X- and Y-linked genes, arguing against a nonspecific effect. Also, the SLY protein is colocalized with X and Y chromatin, the PMSC chromatin in spermatids. Together, this indicates that an active mechanism to maintain postmeiotic sex chromosome inactivation may exist in mouse. Still, it remains to be established whether postmeiotic sex chromosome inactivation is a general phenomenon among mammals.

Since the X chromosome is largely inactive during meiotic and postmeiotic male germ cell development, and the paternal X chromosome is subjected to imprinted inactivation (XCI) in the early female mammalian embryo, it has been suggested that imprinted XCI is a transgenerational manifestation of MSCI/PMSC [62]. In this context, it is of interest to note that the paternal X in hermaphrodite *C. elegans* worms is silenced during early embryonic development, despite the fact that all histone modifications disappear during the final stages of spermatogenesis, possibly due to a process similar to the histone-to-protamine

transition in mammals. This inactivation is maintained longer when the X is derived from an XO male, compared to an X derived from XX spermatogenesis in a hermaphrodite worm (reviewed in [3]). However, in order for XCI to be induced in female mammalian embryos, active transcription from the X-linked *Xist* gene, generating the noncoding *Xist* RNA is obligatory, indicating that an active configuration of the X chromosome is initiatially required.

An alternative hypothesis states that the transition from a protamine-packaged genome back to a histone-packaged chromatin configuration, in the male pronucleus during fertilization, may actually facilitate transcription from the whole paternal genome. Paternal protamines are exchanged for maternal histones, which are quickly hyperacetylated [63-65], allowing rapid activation of gene transcription, including transcription of the paternal *Xist* gene [66]. Indeed, the paternal genome has a higher transcriptional activity as compared to the maternal genome, in zygotes [64, 67, 68]. Still, at the 2-cell stage the paternal X (Xp) and maternal X (Xm) appear to be equally transcriptionally active [69], making it unlikely that a generally higher transcriptional activity can explain preferential activation of the paternal *Xist* gene. Analyses of gene methylation have revealed some epigenetic differences between the paternal and maternal *Xic* locus [70, 71], pointing to active imprinting of the maternal locus through DNA methylation. It is not known when these imprints are generated.

Taken together, at present there are no indications for a transgenerational effect of MSCI on the behaviour of the paternal X chromosome in the early female embryo. However, it is not excluded that such effects are masked by the dominant role of the *Xic* locus in X chromosome inactivation in female embryos. In marsupials, that lack the *Xist* gene, the Xp is inactivated in all cells of the female embryo. However, at the 2-cell stage, both X chromosomes are initially active [61], similar to what has been observed in mouse embryos. Still, some epigenetic marks, acquired because the X was inactivated by MSCI, may play a functional role in paternal imprinted X-inactivation in marsupials. Recently, Namekawa et al. (2010) [72] provided evidence for *Xist*-independent silencing of repeat element containing regions on the X chromosome at the 2-cell stage, followed by *Xist*-dependent silencing of protein coding genes around the morula-to-blastula transition. The authors suggest the existence of two separate mechanisms that act synergistically to achieve imprinted paternal X-inactivation in female embryos. First, an *Xist*-independent mechanism, that possibly depends on epigenetic imprints placed during MSCI, mediates transcriptional silencing of repeat elements on the paternal X chromosome. Second, independent of MSCI, the paternal *Xist* gene is activated to silence all coding and non-coding genes.

To distinguish between possible roles of MSCI, PMSC, and the histone-to-protamine and protamine-to-histone transitions, in initiation of paternal

X-inactivation it will be interesting to analyse paternal X chromosome activity in embryos derived from mice that show impaired MSCI and/or PMSC, as compared to embryos derived from mice with defects in the protamine-to-histone transition, using either round spermatids (before the histone-to-protamine transition) or mature sperm (protamine-packaged chromatin) to generate zygotes using ROSI and ICSI, respectively.

In summary, sex chromosome silencing in the germ line of a wide variety of animals may have evolved by incorporating aspects of different pathways into the silencing machinery, depending on the differences between the mechanisms of sex determination, dosage compensation, and chromosome pairing. A unifying concept for an evolutionary force to drive sex chromosome inactivation could be, that genes beneficial to one sex and possibly harmful to the other sex tend to localize to the sex chromosomes. In specific species, such as *N. crassa*, and *C. elegans*, RNAi-mediated transcriptional or posttranscriptional silencing of foreign DNA may underlie meiotic silencing. It can not be excluded that RNAi-mediated silencing pathways also cooperate in meiotic silencing in vertebrate species, such as mouse, human and chicken, but in these species, components of the DNA damage response machinery may have co-evolved into a homology-dependent meiotic silencing mechanism, to prevent transcription through damaged DNA, and/or to avoid erroneous recombination in meiotic prophase cells. In addition, MSCI may play a transgenerational role in the very first steps of imprinted X-inactivation in early female embryos, providing benefits of MSCI to both males and females.

REFERENCES

1. Aramayo R, Metzenberg RL. Meiotic transvection in fungi. *Cell*. Jul 12 1996;86(1):103-113.
2. Shiu PK, Raju NB, Zickler D, Metzenberg RL. Meiotic silencing by unpaired DNA. *Cell*. Dec 28 2001;107(7):905-916.
3. Kelly WG, Aramayo R. Meiotic silencing and the epigenetics of sex. *Chromosome Res*. 2007;15(5):633-651.
4. Holmes RJ, Cohen PE. Small RNAs and RNAi pathways in meiotic prophase I. *Chromosome Res*. 2007;15(5):653-665.
5. Matzke MA, Birchler JA. RNAi-mediated pathways in the nucleus. *Nat Rev Genet*. Jan 2005;6(1):24-35.
6. Moazed D. Small RNAs in transcriptional gene silencing and genome defence. *Nature*. Jan 22 2009;457(7228):413-420.
7. Carmell MA, Hannon GJ. RNase III enzymes and the initiation of gene silencing. *Nat Struct Mol Biol*. Mar 2004;11(3):214-218.
8. Xu M, Medvedev S, Yang J, Hecht NB. MIWI-independent small RNAs (MSY-RNAs) bind to the RNA-binding protein, MSY2, in male germ cells. *Proc Natl Acad Sci U S A*. Jul 28 2009;106(30):12371-12376.
9. Mochizuki K, Gorovsky MA. Small RNAs in genome rearrangement in Tetrahymena. *Curr Opin Genet Dev*. Apr 2004;14(2):181-187.
10. Lee Y, Kim M, Han J, et al. MicroRNA genes are transcribed by RNA polymerase II. *Embo J*. Oct 13 2004;23(20):4051-4060.
11. Zaratiegui M, Irvine DV, Martienssen RA. Noncoding RNAs and gene silencing. *Cell*. Feb 23 2007;128(4):763-776.
12. Thomson T, Lin H. The biogenesis and function of PIWI proteins and piRNAs: progress and prospect. *Annu Rev Cell Dev Biol*. 2009;25:355-376.
13. Nguyen DK, Disteche CM. Dosage compensation of the active X chromosome in mammals. *Nat Genet*. Jan 2006;38(1):47-53.
14. Ahmed EA, van der Vaart A, Barten A, et al. Differences in DNA double strand breaks repair in male germ cell types: lessons learned from a differential expression of Mdc1 and 53BP1. *DNA Repair (Amst)*. Sep 1 2007;6(9):1243-1254.
15. Garnier O, Serrano V, Duharcourt S, Meyer E. RNA-mediated programming of developmental genome rearrangements in Paramecium tetraurelia. *Mol Cell Biol*. Sep 2004;24(17):7370-7379.
16. Duncan IW. Transvection effects in Drosophila. *Annu Rev Genet*. 2002;36:521-556.
17. Aravin AA, Naumova NM, Tulin AV, Vagin VV, Rozovsky YM, Gvozdev VA. Double-stranded RNA-mediated silencing of genomic tandem repeats and transposable elements in the D. melanogaster germline. *Curr Biol*. Jul 10 2001;11(13):1017-1027.
18. Josse T, Maurel-Zaffran C, de Vanssay A, et al. Telomeric trans-silencing in Drosophila melanogaster: tissue specificity, development and functional interactions between non-homologous telomeres. *PLoS One*. 2008;3(9):e3249.
19. Vibranovski MD, Lopes HF, Karr TL, Long M. Stage-specific expression profiling of Drosophila spermatogenesis suggests that meiotic sex chromosome inactivation drives genomic relocation of testis-expressed genes. *PLoS Genet*. Nov 2009;5(11):e1000731.
20. Hense W, Baines JF, Parsch J. X chromosome inactivation during Drosophila spermatogenesis. *PLoS Biol*. Oct 2007;5(10):e273.
21. Betran E, Thornton K, Long M. Retroposed new genes out of the X in Drosophila. *Genome Res*. Dec 2002;12(12):1854-1859.
22. Karmakar P, Seki M, Kanamori M, et al. BLM is an early responder to DNA double-strand breaks. *Biochem Biophys Res Commun*. Sep 15 2006;348(1):62-69.

23. Erickson JW, Quintero JJ. Indirect effects of ploidy suggest X chromosome dose, not the X:A ratio, signals sex in Drosophila. *PLoS Biol.* Dec 2007;5(12):e332.

24. Bridges CB. Non-Disjunction as Proof of the Chromosome Theory of Heredity (Concluded). *Genetics.* Mar 1916;1(2):107-163.

25. Bernardo Carvalho A, Koerich LB, Clark AG. Origin and evolution of Y chromosomes: Drosophila tales. *Trends Genet.* Jun 2009;25(6):270-277.

26. Hennig W, Brand RC, Hackstein J, et al. Y chromosomal fertility genes of Drosophila: a new type of eukaryotic genes. *Genome.* 1989;31(2):561-571.

27. Seydoux G, Schedl T. The germline in C. elegans: origins, proliferation, and silencing. *Int Rev Cytol.* 2001;203:139-185.

28. Bean CJ, Schaner CE, Kelly WG. Meiotic pairing and imprinted X chromatin assembly in Caenorhabditis elegans. *Nat Genet.* Jan 2004;36(1):100-105.

29. Baarends WM, Wassenaar E, van der Laan R, et al. Silencing of unpaired chromatin and histone H2A ubiquitination in mammalian meiosis. *Mol Cell Biol.* Feb 2005;25(3):1041-1053.

30. Schimenti J. Synapsis or silence. *Nat Genet.* Jan 2005;37(1):11-13.

31. Turner JM, Mahadevaiah SK, Fernandez-Capetillo O, et al. Silencing of unsynapsed meiotic chromosomes in the mouse. *Nat Genet.* Jan 2005;37(1):41-47.

32. Turner JM. Meiotic sex chromosome inactivation. *Development.* May 2007;134(10):1823-1831.

33. Smith CA, Roeszler KN, Ohnesorg T, et al. The avian Z-linked gene DMRT1 is required for male sex determination in the chicken. *Nature.* Sep 10 2009;461(7261):267-271.

34. Schoenmakers S, Wassenaar E, Hoogerbrugge JW, Laven JS, Grootegoed JA, Baarends WM. Female meiotic sex chromosome inactivation in chicken. *PLoS Genet.* May 2009;5(5):e1000466.

35. Schoenmakers S, Wassenaar E, Laven JS, Grootegoed JA, Baarends WM. Meiotic silencing and fragmentation of the male germline restricted chromosome in zebra finch. *Chromosoma.* 2010;In Press.

36. Song R, Ro S, Michaels JD, Park C, McCarrey JR, Yan W. Many X-linked microRNAs escape meiotic sex chromosome inactivation. *Nat Genet.* Apr 2009;41(4):488-493.

37. Yan W, McCarrey JR. Sex chromosome inactivation in the male. *Epigenetics.* Oct 2009;4(7):452-456.

38. Deng W, Lin H. miwi, a murine homolog of piwi, encodes a cytoplasmic protein essential for spermatogenesis. *Dev Cell.* Jun 2002;2(6):819-830.

39. Kuramochi-Miyagawa S, Kimura T, Ijiri TW, et al. Mili, a mammalian member of piwi family gene, is essential for spermatogenesis. *Development.* Feb 2004;131(4):839-849.

40. Carmell MA, Girard A, van de Kant HJ, et al. MIWI2 is essential for spermatogenesis and repression of transposons in the mouse male germline. *Dev Cell.* Apr 2007;12(4):503-514.

41. Bellani MA, Romanienko PJ, Cairatti DA, Camerini-Otero RD. SPO11 is required for sex-body formation, and Spo11 heterozygosity rescues the prophase arrest of Atm-/- spermatocytes. *J Cell Sci.* Aug 1 2005;118(Pt 15):3233-3245.

42. Keegan KS, Holtzman DA, Plug AW, et al. The Atr and Atm protein kinases associate with different sites along meiotically pairing chromosomes. *Genes Dev.* Oct 1 1996;10(19):2423-2437.

43. Wojtasz L, Daniel K, Roig I, et al. Mouse HORMAD1 and HORMAD2, two conserved meiotic chromosomal proteins, are depleted from synapsed chromosome axes with the help of TRIP13 AAA-ATPase. *PLoS Genet.* Oct 2009;5(10):e1000702.

44. Shanbhag NM, Rafalska-Metcalf IU, Balane-Bolivar C, Janicki SM, Greenberg RA. ATM-dependent chromatin changes silence transcription in cis to DNA double-strand breaks. *Cell.* Jun 11;141(6):970-981.

45. Mahadevaiah SK, Turner JM, Baudat F, et al. Recombinational DNA double-strand breaks in mice precede synapsis. *Nat Genet.* Mar 2001;27(3):271-276.

46. Rogakou EP, Boon C, Redon C, Bonner WM. Megabase chromatin domains involved in DNA double-strand breaks in vivo. *J Cell Biol.* Sep 6 1999;146(5):905-916.

47. O'Hagan HM, Mohammad HP, Baylin SB. Double strand breaks can initiate gene silencing and SIRT1-dependent onset of DNA methylation in an exogenous promoter CpG island. *PLoS Genet.* Aug 2008;4(8):e1000155.

48. Moses MJ, Poorman PA. Synaptosomal complex analysis of mouse chromosomal rearrangements. II. Synaptic adjustment in a tandem duplication. *Chromosoma.* 1981;81(4):519-535.

49. Schoenmakers S, Wassenaar E, van Cappellen WA, et al. Increased frequency of asynapsis and associated meiotic silencing of heterologous chromatin in the presence of irradiation-induced extra DNA double strand breaks. *Dev Biol.* May 1 2008;317(1):270-281.

50. Khil PP, Smirnova NA, Romanienko PJ, Camerini-Otero RD. The mouse X chromosome is enriched for sex-biased genes not subject to selection by meiotic sex chromosome inactivation. *Nat Genet.* Jun 2004;36(6):642-646.

51. Mank JE, Ellegren H. Sex-linkage of sexually antagonistic genes is predicted by female, but not male, effects in birds. *Evolution.* Jun 2009;63(6):1464-1472.

52. Turner JM, Mahadevaiah SK, Ellis PJ, Mitchell MJ, Burgoyne PS. Pachytene asynapsis drives meiotic sex chromosome inactivation and leads to substantial postmeiotic repression in spermatids. *Dev Cell.* Apr 2006;10(4):521-529.

53. Skaletsky H, Kuroda-Kawaguchi T, Minx PJ, et al. The male-specific region of the human Y chromosome is a mosaic of discrete sequence classes. *Nature.* Jun 19 2003;423(6942):825-837.

54. Viera A, Calvente A, Page J, et al. X and B chromosomes display similar meiotic characteristics in male grasshoppers. *Cytogenet Genome Res.* 2004;106(2-4):302-308.

55. Jaramillo-Lambert A, Engebrecht J. A single unpaired and transcriptionally silenced X chromosome locally precludes checkpoint signaling in the Caenorhabditis elegans germ line. *Genetics.* Mar;184(3):613-628.

56. Namekawa SH, Park PJ, Zhang LF, et al. Postmeiotic sex chromatin in the male germline of mice. *Curr Biol.* Apr 4 2006;16(7):660-667.

57. Mueller JL, Mahadevaiah SK, Park PJ, Warburton PE, Page DC, Turner JM. The mouse X chromosome is enriched for multicopy testis genes showing postmeiotic expression. *Nat Genet.* Jun 2008;40(6):794-799.

58. Hendriksen PJM, Hoogerbrugge JW, Themmen APN, et al. Postmeiotic transcription of X and Y chromosomal genes during spermatogenesis in the mouse. *Dev. Biol.* 1995;170:730-733.

59. Mulugeta Achame E, Wassenaar E, Hoogerbrugge JW, et al. The ubiquitin-conjugating enzyme HR6B is required for maintenance of X chromosome silencing in mouse spermatocytes and spermatids. *BMC Genomics.* 2010;11:367.

60. Baarends WM, Wassenaar E, Hoogerbrugge JW, Schoenmakers S, Sun ZW, Grootegoed JA. Increased phosphorylation and dimethylation of XY body histones in the Hr6b-knockout mouse is associated with derepression of the X chromosome. *J Cell Sci.* Jun 1 2007;120(Pt 11):1841-1851.

61. Cocquet J, Ellis PJ, Yamauchi Y, et al. The multicopy gene Sly represses the sex chromosomes in the male mouse germline after meiosis. *PLoS Biol.* Nov 2009;7(11):e1000244.

62. Huynh KD, Lee JT. Inheritance of a pre-inactivated paternal X chromosome in early mouse embryos. *Nature.* Dec 18 2003;426(6968):857-862.

63. Adenot PG, Mercier Y, Renard JP, Thompson EM. Differential H4 acetylation of paternal and maternal chromatin precedes DNA replication and differential transcriptional activity in pronuclei of 1-cell mouse embryos. *Development.* Nov 1997;124(22):4615-4625.

64. van der Heijden GW, Derijck AA, Ramos L, Giele M, van der Vlag J, de Boer P. Transmission of modified nucleosomes from the mouse male germline to the zygote and subsequent remodeling of paternal chromatin. *Dev Biol.* Oct 15 2006;298(2):458-469.

65. van der Heijden GW, Dieker JW, Derijck AA, et al. Asymmetry in histone H3 variants and lysine methylation between paternal and maternal chromatin of the early mouse zygote. *Mech Dev.* Sep 2005;122(9):1008-1022.

66. Heard E, Chaumeil J, Masui O, Okamoto I. Mammalian X-chromosome inactivation: an epigenetics paradigm. *Cold Spring Harb Symp Quant Biol.* 2004;69:89-102.

67. Aoki F, Worrad DM, Schultz RM. Regulation of transcriptional activity during the first and second cell cycles in the preimplantation mouse embryo. *Dev Biol.* Jan 15 1997;181(2):296-307.

68. Wright SJ. Sperm nuclear activation during fertilization. *Curr Top Dev Biol.* 1999;46:133-178.

69. Patrat C, Okamoto I, Diabangouaya P, et al. Dynamic changes in paternal X-chromosome activity during imprinted X-chromosome inactivation in mice. *Proc Natl Acad Sci U S A.* Mar 31 2009;106(13):5198-5203.

70. Ariel M, Cedar H, McCarrey J. Developmental changes in methylation of spermatogenesis-specific genes include reprogramming in the epididymis. *Nat. Gen.* 1994;7:59-63.

71. Boumil RM, Ogawa Y, Sun BK, Huynh KD, Lee JT. Differential methylation of Xite and CTCF sites in Tsix mirrors the pattern of X-inactivation choice in mice. *Mol Cell Biol.* Mar 2006;26(6):2109-2117.

72. Namekawa SH, Payer B, Huynh KD, Jaenisch R, Lee JT. Two-step imprinted X-inactivation: Repeat vs genic silencing in the mouse. *Mol Cell Biol.* Apr 19.

ADDENDUM

SUMMARY

Correct oogenesis and spermatogenesis are necessary to obtain haploid oocytes and sperm, which upon fertilization and fusion can give rise to an euploid zygote. To ensure the formation of proper haploid gametes, accurate repair of meiosis-induced DNA double strand breaks and homologous chromosome pairing during the meiotic prophase are obligatory. Chromosomes which remain unpaired or unsynapsed during this phase are transcriptionally inactivated. In **Chapter 2**, we provide a detailed overview of the processes of transcriptional inactivation of sex chromosomes during meiosis and early embryonic development. In meiotic prophase, endogenous SPO11-induced DNA double strand breaks (DSBs) are essential for the homologous pairing process [1]. Since the repair of these DSBs is mainly mediated via homologous recombination repair, using one of the chromatids of the homologous chromosome as a template for repair, this most likely facilitates associations between homologous chromosomes. In yeast, many transient homologous associations are initially formed, and inappropriate recombination intermediates resulting from incorrect single-stranded DNA invasion are destabilized (reviewed in [2]), indicating the presence of a DSBs-driven mechanism, which checks proper sequence homology between the DNA strands before recombination and pairing is permitted. When chromosomes or chromosomal parts do not find a pairing partner in mammals, DSBs remain unrepaired; these regions do not synapse and are subjected to inactivation by meiotic silencing of unsynapsed chromatin (MSUC) [3-5]. However, escape from MSUC through heterologous synapsis occurs [3, 5, 7]. The largely unpaired heterologous X and Y chromosomes in mammals pair only in the small homologous pseudoautosomal regions and hence are always subjected to meiotic silencing [6]. Following the meiotic divisions, the sex chromosomes remain (partially) inactive, which is visible as the formation of the socalled heterochromatic postmeiotic sex chromatin (PMSC).

After fertilization, both X chromosomes are active in the early female mouse embryo. However, the paternal X chromosome is rapidly being inactivated again to compensate for the difference in X chromosome dosage between males and females. This dosage compensation mechanism ensures that male (XY) and female (XX) embryos have only one active X chromosome in all of their cells. Although it has been suggested that subjection of X to MSCI and PMSC during spermatogenesis is important to mediate the imprinted inactivation of the paternal X in the early female mouse embryo, this hypothesis is not supported by currently available experimental data.

In **Chapter 3**, we investigated if the presence of meiotic DSBs is involved in the recognition of unpaired regions and triggering of MSUC. To answer this question, we used the T(1;13)70H/T(1;13)1WA (T/T') double-heterozygous

mice [8]. These mice are double heterozygote for two very similar translocations. During the male meiotic prophase, two autosomal translocation bivalents, 1^{13} and 13^1, are formed, and both carry the same nonhomologous region. Whereas the larger 13^1 bivalent mostly reaches complete heterologous synapsis during the meiotic prophase (Chapter 3, Figure 1), the small 1^{13} bivalent displays varying degrees of asynapsis [3, 8]. Heterologous 1^{13} synapsis and the associated escape from transcriptional silencing by MSUC occurs in approximately 40% of the nuclei [3]. We hypothesized that if signaling from (unrepaired) DSBs is functionally related to the inhibition of heterologous synapsis and the stimulation of MSUC, the presence of more DSBs within this region would lead to a higher signal level, and this may lead to more frequent induction of asynapsis and transcriptional inactivation. We introduced an additional ~100 irradiation-induced DSBs on top of the endogenous SPO11-induced DSBs throughout the whole genome. First, we found that irradiation-induced DSBs during leptotene can be incorporated in the meiotic recombination process, resulting in more crossovers. Second, we observed an increase of 35% in the frequency of 1^{13} bivalent asynapsis and silencing, indicating more efficient detection of the nonhomologous region in the 1^{13} bivalent. The large 13^1 bivalent, on the other hand, still showed almost 100% heterologous synapsis. Apparently, nonhomologous synapsis can not always be prevented by the presence of DSBs. We propose that the onset and spreading of homologous synapsis by synaptonemal complex formation initiated from regions of homology provides a driving force for heterologous synapsis. The final result of the pairing process, either synapsis or asynapsis, depends on the combination of the level of stimulation of synapsis and the inhibitory action of DSB-repair associated proteins that accumulate in the heterologous region. This may explain the complete heterologous synapsis of the large 13^1 bivalent in the vast majority of nuclei.

In **Chapter 4,** we investigated the behaviour of the heterologous sex chromosomes in another vertebrate class, birds. In contrast to mammalian species where males are the heterogametic sex, females are the heterogametic sex in birds, carrying the heterologous, so-called ZW chromosomes, and males are ZZ. Although the sex specific W chromosome has undergone a comparable evolutionary degeneration as the Y chromosome in mammals, the heterologous Z and W chromosomes undergo complete heterologous synapsis during oogenesis. The meiotic prophase in oocytes lasts months or even years due to its arrest during embryonic development and therefore, it was believed that inactivation of Z and W would be detrimental to the survival of the oocytes [9], because the Z carries many housekeeping genes. Thus, heterologous synapsis of Z and W in chicken oocytes might be a means to escape from Z chromosome silencing. We investigated the behaviour of the Z and W chromosomes during female meiotic

prophase to verify if the heterologous synapsis of Z and W indeed prevented meiotic sex chromosome inactivation. We found that although Z and W show complete synapsis, this does not prevent transcriptional silencing of Z and W. Moreover, we found that the W chromosome is inactivated upon entering the meiotic prophase, and we postulate that the Z is inactivated due to spreading of heterochromatin from W to Z during their synapsed state. These findings indicate that heterologous sex chromosome silencing during meiosis is not spermatogenesis-specific and independent of the final achievement of synapsis.

Since MSCI in mammals is thought to be a special form of the more general inactivation mechanisms of MSUC, we decided to analyse MSUC in birds (**Chapter 5**). We analysed the so-called germline restricted chromosome (GRC) in zebra finch. Among birds, this GRC has only been described in zebra finch, and is present as an univalent during spermatogenesis. This indicates that, during spermatogenesis, the GRC lacks a homolog and has to remain unsynapsed. We confirmed that the GRC indeed remains unsynapsed, and showed that it is immediately inactivated upon entering the meiotic prophase, resembling the behaviour of the W chromosome in female chicken oocytes. However, in contrast to W, the GRC is eliminated around metaphase I, forms a micronucleus in subsequent secondary spermatocytes and spermatids, and is fragmented. Apparently, if a chromosome enters meiosis without a pairing partner it is immediately inactivated and finally eliminated and degraded. In addition, we concluded that the W chromosome might escape from this pathway because it synapses with Z during pachytene. Since the meiotic silencing of W and GRC precedes complete autosomal synapsis and induction of meiotic DSBs we have named this silencing phenomenon meiotic silencing prior to synapsis (MSPS).

To study possible variation in the behaviour of heterologous sex chromosomes among different types of mammals, we decided to investigate the behaviour of the XY pair in the domestic dog (*Canis familiaris*) (**Chapter 6**). We noticed that in contrast to the mouse XY pair, the canine X and Y chromosomes manage to synapse completely, most likely involving self-synapsis of X. We concluded that once mammalian MSCI is trigged, it remains active, even if heterologous synapsis occurs. Also, since the canine XY can accomplish complete synapsis, the processes of avian and mammalian MSCI appear more related than previously assumed.

Following meiosis in mammals, the X and Y chromosomes can be recognized as postmeiotic sex chromosome chromatin (PMSC), adjacent to the DAPI dense chromocenter in round spermatids. The PMSC region carries heterochromatin markers, and publicly available microarray data indicate that the X and Y chromosomes remain largely inactivated during postmeiotic development. In **Chapters 7 and 8** we focussed on the role of the ubiquitin- conjugating

enzyme HR6B/UBE2B in the maintenance of sex chromosome silencing in meiotic and postmeiotic cells, and the role of HR6B/UBE2B in the overall regulation of chromatin structure. HR6B/UBE2B can ubiquitylate histone H2B and proliferating cell nuclear antigen (PCNA) during chromatin remodelling and replicative damage bypass repair, respectively. In addition, HR6B/UBE2B can target protein substrates that carry destabilizing N-termini for degradation. Mutation of *Hr6b/Ube2b* leads to male limited infertility. HR6A/UBE2A is a HR6B/UBE2B-paralogue that shows 91% amino acid identity and performs redundant functions with HR6B/UBE2B in somatic cells. During meiotic prophase, HR6A/UBE2A expression is relatively low, due to the fact that the gene encoding this protein is located on the X chromosome, which is inactivated by MSCI. In **Chapter 7**, we show that both H2AK119 and H2BK120 ubiquitylation in *Hr6b/Ube2b*-knockout mouse spermatocytes are not compromised. However, H2AT120 phosphorylation was enhanced from late pachytene until metaphase I in *Hr6b/Ube2b* knockout spermatocytes. In addition, H3K4 dimethylation was increased on the X and Y chromosomes from diplotene onwards in *Hr6b/Ube2b*-knockout spermatocytes. When we then analysed gene expression levels, X chromosome genes showed derepression in postmeiotic *Hr6b/Ube2b*-knockout spermatids. We concluded that HR6B/UBE2B contributes to the postmeiotic maintenance of X chromosome silencing.

In **Chapter 8**, we analysed the role of UBE2B during spermiogenesis and the consequence of a lack of UBE2B for early embryonic development, using mouse intracytoplasmatic sperm injection (ICSI) and round spermatid injection (ROSI). The results show that UBE2B is instrumental in maintaining genomic integrity during postmeiotic spermatid development. Analyses of *Ube2b^{-/-}* sperm showed that chromatin integrity is compromised and that chromatin of mature sperm is vulnerable and carries many DNA breaks. Comparison between ROSI and ICSI using wild type and *Ube2b* knockout spermatids and sperm revealed that *Ube2b* knockout sperm cells could not generate intact male pronuclei in the zygote, whereas normal male pronuclei were formed after ROSI with *Ube2b* knockout spermatids. When we cultured the *Ube2b* knockout ROSI-resulting zygotes, the majority of developed into hatching blastocysts, and when placed back into pseudopregnant foster mothers they developed normally till term. This indicates, that UBE2B has an essential function during the postmeiotic phase and is necessary for maintenance of genomic integrity. In addition, transgenic spermatocyte- and spermatid-specific expression of hemagglutinin-tagged HR6B partially rescued the postmeiotic disturbances of chromatin structure regulation in *Ube2b* knockout mice. However, ICSI with sperm from this transgenic mouse, in which the endogenous *Ube2b* gene was knocked out, showed that the postmeiotic function of UBE2B is necessary for maintenance of the genomic

integrity during the first embryonic cleavage divisions. Together this reveals a germ-cell specific postmeiotic and paternal-effect function of HR6B.

Finally, in **Chapter 9,** we have explored differences between XX and XY preimplantation embryos and analysed the paternally imprinted inactivation of the X chromosome. The results from these experiments have revealed that male and female embryos both reach the blastocyst stage within a similar time frame, however the number of cells is reduced in XX blastocysts compared to XY blastocysts. An important difference between male and female mouse embryos is the fact that female embryos inactivate the paternal X chromosome to compensate for the difference in X chromosome dosage between males and females. This imprinted X chromosome inactivation (XCI) precedes random XCI. We have studied the dynamics of this imprinted XCI process and asked whether inter-cell and inter-embryo variation in the initiation of XCI could be related to epigenetic differences between blastomeres that result from cell cleavages occurring along the animal-vegetal axis (meridionally) or equatorially. We found that when both second cleavage divisions occur along equatorially, XCI is delayed, whereas XCI is initiated relatively early, and more frequently on both X chromosomes in embryos that have undergone two meridional second cleavage divisions. These data show that paternal imprinted XCI might be modulated by factors that vary in their concentration or activity between blastomeres. In addition, our data indicate that these factors play a role in determining the probability of the maternal X chromosome to become inactivated.

This thesis has focussed on the behaviour of sex chromosomes during gametogenesis and early embryonic development. In **Chapter 10,** we discuss our results again in light of the current knowledge concerning the initiation of MSCI, the evolutionary conservation of meiotic silencing and the possible transgenerational effects of MSCI and MSUC. Our data have provided more insight in processes (DNA repair, synapsis) and proteins (HR6B/UBE2B) that are involved in meiotic sex chromosome inactivation in mammals and birds. Furthermore, our data provide information about possible transgenerational effects of defective sperm chromatin on the developmental potential of early mouse embryos. In addition, it was shown that imprinted X inactivation in female mouse embryos is modulated by factors that are differentially distributed among blastomeres depending on the plane of the cleavage divisions. Finally, this work provides a basis for future experiments directed towards understanding the relation between chromatin structure of the paternal genome and early embryo development, including the regulation of X chromosome silencing.

REFERENCES

1. Mahadevaiah SK, Turner JM, Baudat F, et al. Recombinational DNA double-strand breaks in mice precede synapsis. *Nat Genet*. Mar 2001;27(3):271-276.
2. Bhalla N, Dernburg AF. Prelude to a division. *Annu Rev Cell Dev Biol*. 2008;24:397-424.
3. Baarends WM, Wassenaar E, van der Laan R, et al. Silencing of unpaired chromatin and histone H2A ubiquitination in mammalian meiosis. *Mol Cell Biol*. Feb 2005;25(3):1041-1053.
4. Schimenti J. Synapsis or silence. *Nat Genet*. Jan 2005;37(1):11-13.
5. Turner JM, Mahadevaiah SK, Fernandez-Capetillo O, et al. Silencing of unsynapsed meiotic chromosomes in the mouse. *Nat Genet*. Jan 2005;37(1):41-47.
6. Handel MA, Hunt PA. Sex-chromosome pairing and activity during mammalian meiosis. *Bioessays*. Dec 1992;14(12):817-822.
7. van der Laan R, Uringa EJ, Wassenaar E, et al. Ubiquitin ligase Rad18Sc localizes to the XY body and to other chromosomal regions that are unpaired and transcriptionally silenced during male meiotic prophase. *J Cell Sci*. Oct 1 2004;117(Pt 21):5023-5033.
8. de Boer P, Searle AG, van der Hoeven FA, de Rooij DG, Beechey CV. Male pachytene pairing in single and double translocation heterozygotes and spermatogenic impairment in the mouse. *Chromosoma*. 1986;93(4):326-336.
9. Jablonka E, Lamb MJ. Meiotic pairing constraints and the activity of sex chromosomes. *J Theor Biol*. Jul 8 1988;133(1):23-36.

SAMENVATTING

Correcte oögenese en spermatogenese zijn noodzakelijk om haploïde ei- en zaadcellen te vormen, welke na bevruchting en versmelting een euploïde zygote vormen. Om de vorming van de juiste haploïde gameten te garanderen, is het van essentieel belang dat de homologe chromosomen correct paren tijdens de meiotische profase. Chromosomen die ongepaard blijven tijdens deze fase, worden onderworpen aan transcriptionele inactivatie.

In **Hoofdstuk 2** geven wij een overzicht van de processen van transcriptionele inactivatie van geslachtschromosomen tijdens de meiose en de vroeg embryonale ontwikkeling. Tijdens de meiotische profase zijn de aanwezigheid van endogene SPO11-geïnduceerde DNA dubbel strengs breuken (DSBs) instrumenteel in het homologe paringsproces. Aangezien reparatie van DSBs door het relatief eenvoudige reparatiemechanisme waarbij de gebroken strengen aan elkaar worden geligeerd niet operatief is en homologe recombinatie met de zuster chromatide is geblokkeerd, is reparatie via het homologe chromosoom de enige mogelijkheid tot herstel van het DNA. Dit faciliteert hoogstwaarschijnlijk de associatie tussen de homologe chromosomen. In gist worden vele tijdelijke homologe associaties gevormd en onjuiste recombinaties die het gevolg zijn van incorrecte enkelstrengs DNA invasie worden gedestabiliseerd. Dit wijst op de aanwezigheid van een mechanisme dat gedreven wordt door DSBs, welke controle uitoefent op de juiste homologie tussen de DNA strengen voordat recombinatie en paring is toegestaan. Wanneer in zoogdieren chromosomen of chromosomale gedeeltes geen paringspartner vinden, worden de DSBs niet gerepareerd: deze gebieden synapsen vervolgens niet en worden transcriptioneel geïnactiveerd, een proces genaamd "meiotische silencing van ongesynapst chromatine (MSUC)". Door middel van heterologe synapsis kan heteroloog chromatine soms ontkomen aan deze transcriptionele inactivatie. De grotendeels ongepaarde heterologe X en Y chromosomes paren alleen in het kleine homologe pseudoautosomale gebied en zijn daarom altijd transcriptioneel geïnactiveerd. Deze inactivatie wordt ook na de meiotische delingen grotendeels in stand gehouden, wat zichtbaar is als zogenaamde heterochromatische postmeiotische sex chromatine (PMSC) . Na de bevruchting zijn beide X chromsomen actief in de vroeg vrouwlijke muizenembryo's, echter het paternale X chromosoom wordt weer snel geïnactiveerd, in het kader van dosis compensatie. Het dosis compensatie mechanisme zorgt ervoor dat mannelijke (XY) en vrouwelijke (XX) embryo's in al hun cellen slechts 1 actief X chromosoom bevatten. Momenteel zijn er geen duidelijk aanwijzingen dat de X-inactivatie ten gevolge van MSCI en PMSC tijdens de spermatogenese een effect heeft op de inactivatie van de paternale X in vrouwelijke embryos.

In **Hoofdstuk 3** hebben wij onderzocht of de aanwezigheid van meiotische DSBs betrokken is bij de herkenning van ongepaarde gebieden en bij het activeren van MSUC. Om antwoord te geven op deze vraag hebben wij gebruik gemaakt van de T(1;13)70H/T(1;13)1WA (T/T') dubbel-heterozygote muizen. Deze muizen zijn dubbele heterozygoot voor twee ongeveer dezelfde translocaties. Tijdens de mannelijk meiotische profase worden twee autosomale translocatie bivalenten 1^{13} en 13^1 gevormd en beiden dragen dezelfde nonhomologe regio. Terwijl het langere 13^1 bivalent meestal compleet heteroloog synapst tijdens de meiotische profase, vertoont het kleinere 1^{13} bivalent een variërende mate van asynapsis. Heterologe 1^{13} synapsis en de daaraan gekoppelde ontsnapping aan het transcriptionele inactivatie mechanisme MSUC treedt op in ongeveer 40% van de kernen. Onze hypothese was dat als de signalen van ongerepareerde DSBs functioneel gerelateerd zijn aan de inhibitie van heterologe synapsis en stimulatie van MSUC, de aanwezigheid van meer DSBs in deze gebieden zouden leiden tot een hoger signaleringsniveau, en dat dit vervolgens zou leiden tot een frequentere asynapsis en transcriptionele inactivatie. Wij introduceerden ongeveer 100 extra bestralingsgeïnduceerde DSBs bovenop de endogene SPO11-geinduceerde DBSs in het gehele genoom. Ten eerste vonden wij dat bestralingsgeïnduceerde DBS tijdens het leptoteen geïncorporeerd kunnen worden in het meiotische recombinatie proces, dat uiteindelijke resulteerde in meer crossovers. Ten tweede observeerden wij een stijging van 35% in de frequentie van asynapsis en inactivatie van de kleine 1^{13} bivalent, wat duidt op een meer efficiënte detectie van het nonhomologe gebied in de 1^{13} bivalent. Echter, het grotere 13^1 bivalent, ondergaat nog steeds heterologe synapsis in bijna 100% van de kernen. Blijkbaar kan nonhomologe synapsis niet altijd voorkomen worden door de aanwezigheid van DSBs. Wij stellen dat de initiatie van homologe synapsis vanuit de gebieden van homologe paring, als een voortdrijvende kracht voor heterologe synapsis opereert. Het uiteindelijke resultaat van het paringsproces (synapsis of asynapsis) hangt dan waarschijnlijk af van een combinatie van de mate waarin synapsis gestimuleerd wordt én het remmende effect van DSB reparatie geassocieerde eiwitten die zich verzamelen in het heterologe gebied. Aangezien voor het grotere 13^1 bivalent, een langer synaptonemaal complex tussen homoloog chromatine gevormd kan worden, zou dit kunnen leiden tot een grotere drijvende kracht voor heterologe synapsis en zo een verklaring kunnen geven voor de volledige synapsis die voor dit bivalent werd geobserveerd in de overgrote meerderheid van de kernen.

In **Hoofdstuk 4** hebben wij het gedrag van heterologe geslachtschromosomen in vogels, een ander gewerveld diersoort, onderzocht. In tegenstelling tot zoogdieren waar de man de heterogametische sex is, zijn in vogels de vrouwen de heterogametische sex. Zij dragen de heterologe, zogenaamde ZW chromosomen,

terwijl mannen twee Z chromosomen hebben. Ondanks het feit dat het geslachtsspecifieke W chromosoom een met het Y chromosoom van zoogdieren vergelijkbare evolutionaire degeneratie heeft ondergaan, zijn de heterologe ZW chromosomen wel in staat tot complete heterologe synapsis tijdens de oögenese. De meiotische profase in eicellen duurt maanden tot jaren ten gevolge van hun "arrest" tijdens de embryonale ontwikkeling. Omdat het Z chromosoom veel "huishoud" genen draagt, werd er vanuit gegaan dat inactivatie van Z en W chromosomen schadelijk zou zijn voor de overleving van eicellen. De heterologe synapsis van Z en W zou daarom een ontsnapping bieden aan de transcriptionele inactivatie van Z. We onderzochten het gedrag van Z en W chromosomen tijdens de vrouwelijke meiotische profase om te verifiëren dat heterologe synapsis tussen Z en W inderdaad meiotische geslachtschromosoom inactivatie voorkomt. We constateerden dat ondanks het feit dat Z en W compleet synapsen, transcriptionele inactivatie niet voorkomen wordt. Daarnaast toonden wij aan dat het W chromosoom reeds geïnactiveerd wordt aan het begin van de meiotische profase. Wij stellen dat de inactivatie van Z wordt bewerkstelligd door de spreiding van heterochromatine van W naar Z tijdens de fase waarin de twee chromosomen een volledige synapsis laten zien. Deze bevindingen indiceren dat heterologe geslachtschromosoom inactivatie tijdens de meiose niet spermatogenese specifiek is, en dat in vogels inactivatie niet voorkomen wordt door asynapsis.

Aangezien meiotische geslachtschromosoom inactivatie (MSCI) een geavanceerde vorm van het meer algemene inactivatie-mechanisme van MSUC is, hebben wij besloten om MSUC ook in vogels te bestuderen (**Hoofdstuk 5**). We hebben het zogenaamde, "germline restricted chromosome" (GRC) in zebravinken geanalyseerd. Bij vogels is het GRC alleen aangetoond in de zebravink en het is aanwezig als een enkele kopie tijdens de spermatogenese. Dit impliceert dat tijdens de spermatogenese het GRC een paringspartner mist en per definitie ongepaard blijft. We hebben bevestigd dat het GRC inderdaad niet synapst en daarnaast aangetoond dat het GRC, gelijkend op het W chromosoom, ook reeds geïnactiveerd is als het begint aan de meiotische profase. Echter, in tegenstelling tot het W chromosoom, wordt het GRC geëlimineerd rondom metafase I. Vervolgens vormt het een micronucleus in de daaropvolgende secundaire spermatocyten en spermatiden, waarna het GRC fragmenteert. Blijkbaar wordt een chromosoom zonder paringspartner direct geïnactiveerd als het de meiotische profase start, waarna het fragmentatie en degradatie ondergaat. Deze gegevens suggereren dat het W chromosoom mogelijk aan een dergelijke ondergang ontsnapt omdat het synapst met Z tijdens het pachyteen. Aangezien de inactivatie van W en het GRC voorafgaan aan het proces van synapsis en de inductie van DSBs, hebben wij dit inactivatie-fenomeen meiotische inactivatie voorafgaand aan synapsis (MSPS) genoemd.

Vanwege de verschillen in de inactivatie tijdens de meiose in vogels en muizen, hebben wij besloten om het gedrag van het XY paar in de hond (*Canis familiaris*) te onderzoeken (**Hoofdstuk 6**) om te bepalen hoe representatief de muis is voor andere zoogdieren met betrekking tot de inactivatie van de X en Y chromosomen tijdens de meiose. Wij vonden dat de X en Y chromosomen van de hond in tegenstelling tot die van de muis, compleet synapsen, waarbij het X chromosoom mogelijk een vorm van synapsis met zichzelf vertoont. We concluderen dat zodra de inactivatie van de geslachtschromosomen is geactiveerd, latere heterologe synapsis niet leidt tot reactivatie. Aangezien de X en Y van de hond complete synapsis vertonen, lijkt het erop dat de geslachtschromosoom inactivatie-processen van vogels en zoogdieren meer aan elkaar gerelateerd zouden kunnen zijn dan voorheen werd gedacht.

Na de meiose in zoogdieren kunnen X en Y chromosomen herkend worden als postmeiotisch sex chromatine (PMSC), liggend naast het DAPI-rijke chromocentrum in ronde spermatiden. Het PMSC gebied vertoont de aanwezigheid van heterochromatische markers en openbaar beschikbare micro-array data indiceren dat de X en Y chromosomen grotendeels geïnactiveerd blijven tijdens de postmeiotische ontwikkeling. In **Hoofdstuk 7** en **8** hebben wij ons voornamelijk toegelegd op het identificeren van de rol van het ubiquitine-conjugerende enzym HR6B/UBE2B in het onderhouden van de inactivatie van geslachtschromosomen in meiotische en postmeiotische zaadcellen en de rol van dit eiwit in de algemene regulatie van de chromatine structuur. HR6B/UBE2B kan histon 2B en het eitwit PCNA ubiquitineren tijdens processen waarbij chromatinestructuur moet worden veranderd in respectievelijk de context van genexpressie-regulatie en de zogenaamde "replicative damage bypass pathway". Daarnaast kan HR6B/UBE2B eiwitsubstraten die instabiele N-termini dragen, markeren voor degradatie. Mutatie van *Hr6b/Ube2b* leidt tot mannelijke infertiliteit. HR6A/UBE2A is een HR6B/UBE2B paraloog dat 91% gelijkenis vertoont met de aminozuurvolgorde van HR6B/UBE2B en in somatische cellen qua functie overlapt met die van HR6B/UBE2B. Tijdens de meiotische profase is de expressie van HR6A/UBE2A relatief laag doordat het gen dat codeert voor dit eiwit op het X chromosoom ligt dat geïnactiveerd wordt door MSCI. In **Hoofdstuk 7** laten wij zien dat de ubiquitinatie van H2AK119 en H2BK120 in spermatocyten van *Hr6b/Ube2b*-knockout muizen niet gecompromitteerd wordt. Echter, wij zagen wel een intensere fosforylering van H2AT120 vanaf pachyteen tot metafase I in *Hr6b/Ube2b* knockout spermatocyten. Daarnaast was er een hogere dimethylering van H3K4 op de X en Y chromosomen vanaf het diploteen in *Hr6b/Ube2b* knockout spermatocyten. Toen wij vervolgens de niveaus van gen expressie analyseerden, constateerden wij een derepressie van X chromosoom genen in postmeiotische *Hr6b/Ube2b* knockout spermatiden. We concludeerden

hieruit dat HR6B/UBE2B bijdraagt aan het onderhouden van de inactivatie van het X chromosoom tijdens de postmeiotische fase.

In **Hoofdstuk 8** hebben wij de rol van UBE2B tijdens de spermiogenese en het gevolg van een gebrek aan UBE2B tijdens de vroeg embryonale ontwikkeling geanalyseerd, door gebruik te maken van de intracytoplasmaire sperma injectie (ICSI) en ronde spermatiden injectie (ROSI). De resultaten van deze experimenten tonen aan dat UBE2B onmisbaar is voor het behouden van de integriteit van het genoom tijdens de postmeiotische zaadcel ontwikkeling. Analyse van *Ube2b$^{-/-}$* zaad toonde aan dat de chromatine structuur is aangedaan en dat het chromatine van zaadcellen erg kwetsbaar is en vele DNA breuken vertoont. Een vergelijking tussen ICSI en ROSI met "wilde type" en *Ube2b* knockout spermatiden en zaadcellen liet zien dat *Ube2b* knockout zaadcellen niet in staat zijn tot het vormen van intacte mannelijke pronuclei in de zygote, terwijl wel normale pronuclei worden gevormd na ROSI met *Ube2b$^{-/-}$* spermatiden. Wanneer we de zygotes na ROSI met *Ube2b* knockout spermatiden doorkweekten, groeide de overgrote meerderheid uit tot blastocysten en wanneer deze werden teruggeplaatst in een pseudozwangere draagmoedermuis ontwikkelden ze normaal door. Dit houdt in dat UBE2B een essentiële rol heeft tijdens de postmeiotische fase en noodzakelijk is voor het behoud van de integriteit van het genoom. Daarnaast toonden wij aan dat expressie van een spermatocyt- en spermatide-specifieke hemagglutinine-gelabelde *Ube2b* transgen de postmeiotische verstoring van de regulatie van de chromatine structuur gedeeltelijk voorkomt in *Ube2b* knockout muizen. Echter, ICSI met zaadcellen van deze transgene muis, waarbij het endogene *Ube2b* gen was uitgeschakeld, toonde aan dat de postmeiotische functie van UBE2B van belang is voor het instandhouden van de genomische integriteit tijdens de eerste embryonale klievingsdelingen. Dit alles laat zien dat UBE2B een geslachtscel-specifieke rol speelt tijdens de postmeiotische fase.

In **Hoofdstuk 9** hebben wij de verschillen tussen XX en XY preimplantatie muizenembryo's onderzocht en de ingeprente inactivatie van het paternale X chromosoom geanalyseerd. De resultaten van deze experimenten laten zien dat mannelijke en vrouwelijk muizenembryo's beiden even lang erover doen om het blastocyst stadium bereiken, echter XX embryo's hebben een minder cellen in vergelijk met XY embryo's. Een belangrijk verschil tussen mannelijke en vrouwelijk muizenembryo's is dat vrouwelijke embryo's het paternale X chromosoom inactiveren om te compenseren voor het verschil in de dosis van X chromosomen tussen mannetjes en vrouwtjes. Deze ingeprente X chromosoom inactivatie (XCI) gaat vooraf aan de random X chromosoom inactivatie. Wij hebben de dynamiek van ingeprente X chromosoom inactivatie bestudeerd. We hebben onderzocht of inter-cel en inter-embryo variatie in de initiatie van XCI gerelateerd is aan epigenetische verschillen tussen blastomeren die het resultaat

zijn van celdelingen langs de "animal-vegetal" as (meridionaal) of equatoriaal. Wij toonden aan dat wanneer de 2de klievingsdelingen equatoriaal is, XCI vertraagd is, terwijl XCI relatief vroeger en frequenter geïnitieerd wordt op beide X chromosomen in embryo's die twee meridionale klievingsdelingen hebben ondergaan. Deze data laten zien dat paternale ingeprente XCI gemoduleerd zou kunnen worden door factoren die variëren in hun concentratie of activiteit in verschillende blastomeren. Daarnaast impliceren onze data dat deze factoren een rol spelen in het bepalen van de waarschijnlijkheid dat het maternale X chromosoom geïnactiveerd wordt.

Dit proefschrift heeft zich gericht op het gedrag van geslachtchromosomen tijdens de vorming van de geslachtscellen en de vroeg embryonale ontwikkeling. In **Hoofdstuk 10** worden de gevonden resultaten nogmaals besproken in het licht van de huidige kennis omtrent de initiatie van MSCI, de evolutionaire conservering van meiotische transcriptionele inactivatie, en de mogelijke transgenerationele effecten van MSCI en MSUC. Onze data hebben geleid tot meer inzicht in de processen (DNA herstel, synapsis) en eiwitten (HR6B/UBE2B) die betrokken zijn bij (meiotische) geslachtschromosoom inactivatie in zoogdieren en vogels. Onze resultaten tonen ook mogelijke transgenerationele effecten aan van zaadcellen met beschadigd chromatine op de ontwikkelingspotentie van vroege muizenembryo's. Daarnaast hebben wij aangetoond dat ingeprente X chromosoom inactivatie in vrouwelijke muizenembryo's gemoduleerd wordt door factoren die verschillend verdeeld zijn over de blastomeren, afhankelijk van de richting van de klievingsdelingen. Dit proefschrift voorziet in een basis voor verdere experimenten gericht op het begrijpen van de relatie tussen chromatine structuur van het paternale genoom en de vroeg embryonale ontwikkeling, inclusief de regulatie van de inactivatie van het X chromosoom.

LIST OF ABBREVIATIONS

AE	axial element
AO	acridine orange
ATM	ataxia telangietctasia mutated
ATR	ATM- and RAD3-related
AV-axis	animal-vegetal axis
BrdU	bromodeoxyuridine
C. elegans	*Caenorhabditis elegans*
CBX1	chromobox protein 1
cDNA	complementary DNA
CE	central element
CS	completely synapsed
DAPI	4',6-diamidino-2-phenylindole
DDB	DAPI dense body
DFI	DNA fragmentation index
DIC	differential interference contrast
DISC	DNA double strand break-induced transcriptional silenicng *in cis*
DNA	deoxyribonucleic acid
DSB	double strand break
dsDNA	double stranded DNA
dsRNA	double stranded RNA
E	equatorial
FACS	fluoresence-activated cell sorting
FISH	fluorescence in situ hybridization
FITC	fluorescein isothiocyanate
FSH	follicle stimulation hormone
GRC	germline restricted chromosome
Gy	Gray
H	histone
HA	hemagglutinine
HR	homologous recombination
ICM	inner cell mass
ICSI	intracytoplasmatic sperm injection
IES	internal eliminated element
INCENP	inner centromere protein
IS	incompletely synapsed
IVF	in-vitro fertilization
Kb	kilobase
LAS	long asynaptic segment

LE	lateral element
LH	luteinizing hormone
M	meridonial or mitose
MAS	medium asynaptic segment
Mb	megabase
MESA	microsurgical epidydimal sperm aspiration
miRNA	microRNA
mRNA	messenger RNA
MSCI	meiotic sex chromosome inactivation
MSPS	meiotic silencing prior to synapsis
MSUC	meiotic silencing of unsynapsed chromatin
MSUD	meiotic silencing of unpaired DNA
MSY	male-specific region of Y chromosome
MSY-RNA	MIWI-independent small RNA
MY	million years
N. crassa	*Neurospora crassa*
ncRNA	noncoding RNA
NHEJ	nonhomologous end-joining
NK-1	nucleosomal histone kinase-1
PA	partially synapsed A shape
PAR	pseudoautosomal region
PCNA	proliferating cell nuclear antigen
PESA	percutaneous epidydimal sperm aspiration
PFA	paraformaldehyde
PGC	primordial germ cell
PH	partially horseshoe shape
piRNA	PIWI-interacting RNA
PMSC	postmeiotic sex chromatin
PR	partially synapsed
PTGS	post-transcriptional RNA interference
rasiRNA	repeat-associated RNA
RDB	replicative damage bypass
RdDM	RNA-directed DNA methylation
RING	really interesting new gene
RNA	ribonucleic acid
RNA pol II	RNA polymerase II
RNAi	RNA interference
RNF12	RING finger protein 12
ROSI	round spermatid injection

RPA	replication protein A
S phase	synthesis phase
S. cerevisiae	*Saccharomyces cerevisiae*
S. pombe	*Schizosaccharomyces pombe*
SC	synaptonemal complex
SCSA	sperm chromatin structure assay
SEM	sperm entry point or standard error of the mean
siRNA	short interfering RNA
SRY	sex determining region Y
ssDNA	single stranded DNA
TE	transposable element or transverse element
TESE	testicular sperm extraction
TRITC	tetramethylrhodamine isothiocyanate
TSE	*trans*-silencing effect
Tsix	X inactivative specific transcript, antisense
TUNEL	terminal deoxynucleotidyl transferase dUTP nick end labelling
WT	wild type
XCI	X chromosome inactivation
Xic	X chromosome inactivation center
Xist	X inactive specific transcript
Xite	X inactivation intergenic transcription element
Xm	maternal X chromosome
Xp	paternal X chromosome
γH2AX	phosphorylated H2AX

PHD PORTFOLIO SUMMARY

Summary of PhD training and teaching activities

Name PhD student:	Sam Schoenmakers
Erasmus MC Departments:	Reproduction and Development
	Obstetrics and Gynaecology
Research School:	Medical Genetics Centre South-West
	Netherlands (MCG) Graduate School
PhD Period:	Februari 2006 – July 2010
Promoters:	Prof.dr. J.A. Grootegoed and Prof.dr. J.S.E. Laven
Supervisor:	Dr. W.M. Baarends

General academic skills

2009	Biomedical English Writing & Communication, Erasmus MC Graduate School
2006	Laboratory animal science

Research skills

2007	Principles of Research in Medicine and Epidemiology, NIHES
2007	Introduction to data-analysis, NIHES

In-depth courses

2007	From Development to Disease
2007	Reading and Discussing Literature
2006	Molecular and Cell Biology

Presentations

2010	VSF ESHRE avond 2010, Utrecht, The Netherlands
	26th Annual meeting of ESHRE, Rome, Italy
	VSF Voorjaarsvergadering, Leuven, Belgium
	57th Annual Meeting of the Society for Gynaecologic Investigation, Orlando, USA
	Annual Molmed Day 2010, Rotterdam, The Netherlands
2009	VSF Najaarsvergadering, Tilburg, The Netherlands
	EMBO Conference series on Meiosis, L'Isle sur la Sorgue, Jaarlijkse Onderzoeksmiddag, Rotterdamse Gynaecologen Opleidings Cluster (RGOC), Rotterdam, The Netherlands
	Keystone Symposia Epigenetics, Development and Human Diseases (A1), Breckenridge, Colorado, USA

2008	55th Annual Meeting of the Society for Gynaecologic Investigations, San Diego, USA
	6th Winterschool of the International Graduiertenkolleg GRK767:"Transcriptional Control in Developmental Processes", Kleinwalserthal, Germany
2007	8th European Meiosis Meeting in Japan, Shonan Village, Japan
	5th Winterschool of the International Graduiertenkolleg GRK767: Transcriptional Control in Developmental Processes", Kleinwalserthal, Germany

Awards

2010	Best oral presentation award, 57th Annual Meeting of the Society for Gynaecologic Investigations, Orlando, USA
2009	Short Presenter Invitation Award, Keystone Symposia Epigenetics, Development and Human Diseases (A1), Breckenridge, Colorado, USA
2009	Dagwinnaar VSF-BFS onderzoeksprijs, VSF Najaarsvergadering, Tilburg
	Winnaar Juriy Wladimiroff Onderzoeksprijs 2009, Jaarlijkse Onderzoeksmiddag Rotterdam Rotterdamse Gynaecologen OpleidingsCluster (RGOC)
2007	Recipient of Fellowship for Young Participants, 8th European Meiosis Meeting, Shonan Village, Japan

Grants

2008	Boehringer Ingelheim Travel Grant
	EMBO Short Term Fellowship

International conferences

2010	26th Annual Meeting European Society of Human Reproduction and Embryology, Rome, Italy
	57th Annual Meeting of the Society for Gynaecologic Investigations, Orlando, USA
2009	25th Annual Meeting European Society of Human Reproduction and Embryology, Amsterdam, The Netherlands
	EMBO Conference series on Meiosis, L'Isle sur la Sorgue, France
	56th Annual Meeting of the Society for Gynaecologic, Glasgow, United Kingdom
	Keystone Symposia "Epigenetics, Development and Human Diseases", Breckenridge, USA

2008	55th Annual Meeting of the Society for Gynaecologic Investigations, San Diego, USA
2007	8th European Meiosis Meeting in Japan, Shonan Village, Japan
2006	2nd Conference on X-inactivation, Paris, France

Seminars and workshops

2008	5th and 6th Winterschool of the International Graduiertenkolleg GRK767:
2007	"Transcriptional Control in Developmental Processes", Kleinwalserthal, Germany
2006	Chromatin mediated biological decisions, Marburg, Germany

Fellowships

2008	"Epigenetic differentation of blastomeres in the early mouse embryo", Group of Zernicka-Goetz, the Wellcome Trust / Cancer Research UK Gurdon Institute, University of Cambridge, United Kingdom

Didactic skills, lecturing and teaching activities

2009-2010	Junior Science Program, Erasmus MC, Rotterdam, The Netherlands
2006-2010	Curriculum Erasmus Faculty of Medicine and Health Sciences, Erasmus University Medical Center Rotterdam

- Disorders in gonadal development
- Hypothalamus – pituitary gland – gonads axis
- Fertility disorders
- Diagnostic approach of amenorrhoea
- Non-hormonal anticonception

2008	The Oxbridge Academic Program – The Cambridge Tradition: Major and Minor Course of Molecular Medicine, Cambridge, UK

CURRICULUM VITAE 1.1

Name: Sam Schoenmakers
Date of birth: 25 oktober 1977
Place of birth: Heerlen

Education:

2001 – 2003   Medical Doctor (MD), *cum laude*
               Faculty of Health, Medicine and Life Sciences, University of
               Maastricht, Maastricht, The Netherlands
1996 – 2000   MSc, Medical school
               Faculty of Health, Medicine and Life Sciences, University of
               Maastricht, Maastricht, The Netherlands
1990 – 1996   Lyceum (VWO)
               Sint Janscollege, Hoensbroek, The Netherlands

Research and clinical experience

2010-   AIOS Gynaecology and Obstetrics, Sint Franciscus Gasthuis,
               Rotterdam, The Netherlands

2006-2010   PhD research, Departments of Reproduction & Development
               and Gynaecology & Obstetrics, Erasmus Medical Center
               Rotterdam, The Netherlands

2005 - 2006   ANIOS at Department of Obstetrics & Gynaecology, Albert
               Schweitzer Hospital, Dordrecht, the Netherlands

2004 – 2005   ANIOS at Department of Obstetrics & Gynaecology, Vlietland
               Hospital, Vlaardingen, the Netherlands

2003   Elective internship: Primary Health Care, Obstetrics &
               Gynaecology and Paediatrics, Christian Medical College,
               Vellore, India

2001-2002   Research participation: the Rett-syndrome, Department of
               Clinical Genetics, University of Maastricht, The Netherlands

1999   Elective internship: General Surgery and Medical Genetics,
               Royal Brisbane Hospital, University of Brisbane, Brisbane,
               Australia

1998	Adapted Kinesiology, Hof van Axen, Drenthe, The Netherlands

Other activities

2010	Committee member, De Jonge Orde
2008 – 2009	Course Dutch Deaf Sign Language
2006	Arts-Assistenten Vereniging (AAV), Erasmus MC, Rotterdam, The Netherlands Organising committee Jaarlijkse Wetenschapsdag 2007: "Ruimte voor de Toekomst"
2000 – 2001	World travel

CURRICULUM VITAE 1.2

Sam Schoenmakers is geboren in 1977 te Heerlen. Na het afronden van het VWO op het St Janscollege te Hoensbroek is hij in 1996 gestart met zijn opleiding Geneeskunde aan de Universiteit van Maastricht, waarvoor hij in 2003 *cum laude* afstudeerde. Tijdens zijn studie reisde hij gedurende een jaar letterlijk de wereld rond, en liep hij stages en co-schappen in Australië en India. In de periode van 2004 tot 2006 was hij ANIOS Gynaecologie en Obstetrie in zowel het Vlietland ziekenhuis te Vlaardingen als het Albert Schweitzer Ziekenhuis te Dordrecht. In februari 2006 startte hij aan zijn promotie-onderzoek aan de Erasmus Universiteit te Rotterdam. Van januari 2008 tot augustus 2008 verrichtte hij een deel van zijn onderzoek in de groep van Magdalena Zernicka-Goetz aan de universiteit van Cambridge, waarvoor hij zowel een EMBO Short Term Fellowship als een Boerhinger Ingelheim Travel Grant kreeg toegewezen. In de zomer van 2008 maakte hij deel uit van een internationale summerschool, "The Oxbridge Tradition", alwaar hij gedurende een maand het zelfgeschreven curriculum "Molecular Medicine" onderwees. In augustus 2010 is hij gestart als AIOS Gynaecologie en Obstetrie in het Sint Franciscus Gasthuis te Rotterdam. Vanaf oktober 2010 zal hij zich als bestuurslid van de Jonge Orde gaan inzetten voor de positie van de AIOS in Nederland.

CURRICULUM VITAE 2.0

Sam Schoenmakers, geboren op 25 oktober in het jaar 1977 te Heerlen en opgegroeid te Treebeek en Brunssum. Daarna het VWO, Sint Janscollege in Hoensbroek samen met je vrienden Erik, Bastiaan en Paultje. Als "klein" kind wilde je al 'dokter worden', dus werd het geneeskunde aan de Universiteit in Maastricht.

Al vanaf het VWO en ook tijdens je studietijd was je al bezig met multi-tasking. In 1999 ging je voor een buitenlandse stage naar het Australië. Dat de officiële goedkeuring (en dus de financiële ondersteuning) voor deze stage pas achteraf verkregen werd, nadat de toegevoegde waarde van deze stage door een rapport was aangetoond, kon je niet deren.

Na je doctoraal Geneeskunde ging je samen met Sander een jaar er tussenuit: even de wereld en jezelf verkennen. Je vertrok vanuit Amsterdam naar Azië en daarna naar Australië. Daar heb je gewerkt in het Holland Heineken House, tijdens de Olympische Spelen in 2000 te Sydney. Daarna door naar Nieuw Zeeland, Fiji, en Amerika en toen kwam je weer in het echte leven. Je co-schappen begonnen en je viel er meteen in.

Na het behalen van je bul in 2003, ben je eerst in Utrecht begonnen met chirurgie. Hierna ben je naar Vlaardingen gegaan, om ervaring op te doen bij gynaecologie. Toen Vlaardingen niet meer aan je verwachtingen kon voldoen, vertrok je naar Dordrecht om verder te gaan met gynaecologie in een opleidingsziekenhuis. Plotseling deed zich de kans voor om een promotiestudie te kunnen combineren met de studie gynaecologie aan het Erasmus MC in Rotterdam.

In 2006 ben je in Rotterdam begonnen met je promotie, waar je veel tijd in hebt gestoken. Je bent ook nog een half jaar naar Cambridge geweest en je hebt meerdere congressen gehad o.a. in Japan, USA, Oostenrijk, Frankrijk en Italië waar je je kennis hebt gepresenteerd voor het grote publiek. Echter, nam je overigens ook ruim de tijd om te feesten.

Nu, per 1 augustus 2010, ben je officieel begonnen als AIOS gynaecologie te Rotterdam. Nu begint het echte werk. In oktober 2010 promoveer je. Weet dat ik supertrots op je ben.

Liefs, je moeder Hermine, die heel veel van je houdt. XXXX Hermine *Hartje*

Door Hermine Schoenmakers-Vogels, 18 september 2010

LIST OF PUBLICATIONS

Schoenmakers S, Baarends WM. Meiotic pairing of homologous chromosomes and silencing of heterologous regions. *Accepted* as chapter in Epigenetics and Reproduction, Springer Berlin Heidelberg.

Inagaki A, Schoenmakers S, Baarends WM. Double strand break repair, synapsis and silencing during meiosis. Epigenetics 2010 May 16;5(4).

Schoenmakers S, Wassenaar E, Laven JS, Grootegoed JA, Baarends WM. Meiotic silencing and fragmentation of the male germline restricted chromosome in zebra finch. Chromosoma 2010 Jun;119(3):311-24.

Schoenmakers S, Wassenaar E, Hoogerbrugge JW, Laven JS, Grootegoed JA, Baarends WM. Female meiotic sex chromosome inactivation in chicken. PLoS Genet. 2009 May; 5(5): e1000466.

Schoenmakers S, Wassenaar E, van Cappellen WA, Derijck AA, de Boer P, Laven JS, Grootegoed JA, Baarends WM. Increased frequency of asynapsis and associated meiotic silencing of heterologous chromatin in the presence of irradiation-induced extra DNA double strand breaks. Dev Biol. 2008 May 1;317(1):270-81.

Baarends WM, Wassenaar E, Hoogerbrugge JW, Schoenmakers S, Sun ZW, Grootegoed JA. Increased phosphorylation and dimethylation of XY body histones in the Hr6b-knockout mouse is associated with derepression of the X chromosome. J Cell Sci. 2007 Jun 1;120(Pt 11):1841-51.

Moog U, Smeets EEJ, Roozendaal KEP van, Schoenmakers S, Herbergs J, Schoonbrood-Lenssen AMJ, Schrander-Stumpel CTRM. Neurodevelopmental disorders in males related to the gene causing Rett syndrome in females (MECP2). Eur J Paediatr Neurol 2003;7(1):5-12.

Smeets EJE., Schrander-Stumpel CTRM, Curfs LM, Schrander J, Schoenmakers S, de Nijs Bik H, Het Rett-syndroom, Patient Care, juni 2002, 17-23.

Smeets EEJ, Moog U, Schoenmakers S, Schoonbrood-Lenssen AMJ, Roozendaal KEP van, Herbergs J, Schrander-Stumpel CTRM. MeCP2 related disorders in males. Med Gen 2002;14:289.

DANKWOORD

Zoals wel bekend is het dankwoord praktisch het enige gedeelte dat gelezen wordt, en daarmee ook het meest drukuitoefenende gedeelte van een proefschrift. Wie moet er "bedankt" worden, in welke volgorde en in wat voor een bewoordingen? De eerste conclusie die hieruit volgde was, dat woorden oprecht te kort schieten. Hoe bedank je in en paar woorden vrienden en collega's voor wie ze zijn en wat ze voor je betekenen? Wat ik hier neerpen is per definitie een eufemisme.

Als eerst en meest belangrijke is er Evelyne. Clichématig, maar eigenlijk promoveer jij vandaag ook. Zonder jou lag dit proefschrift er niet. Jij hebt het mogelijk gemaakt dat ik resultaten behaalde die vervolgens tot artikels hebben geleid en mij in staat stelde om (betaald en wel) de wereld rond te vliegen om op tal van congressen (en dus vakanties) een voordracht hierover te geven. Door jouw eeuwige geduld om mij herhaaldelijk hetzelfde protocol uit te leggen, proeven voor mij te herhalen en mijn getier aan te horen, ligt dit proefschrift er nu. Wat ook niet onderschat mag worden, zijn al die dagen die wij samen in het EDC hebben doorgebracht. Voor dag en dauw starten en in eerste instantie maanden zonder succes, maar toch uren verkrapt achter een te lage microscoop zitten, in de weer met semi-joysticks. Uren hebben wij, tussen het gescheld en de frustraties door, zitten praten over van alles nog. Dankjewel, lieve Evelyne.

Willy! 4,5 jaar waren zo om en wat was het leuk (of moet ik zeggen leerzaam en productief?). Co-promotor klinkt zo ondergeschikt, terwijl jij degene bent geweest die mij iedere dag (IEDERE DAG) begeleidde, corrigeerde (op alle gebieden) en meestal het geduld wist op te brengen om mij aan te horen en verder op weg te helpen. Ik prijs mij gelukkig dat jij mijn "sterke-vrouwen" begeleidster bent geweest. Wat ik ontzettend aan je waardeer is dat je naast een positie als professionele bazin ook de tijd neemt en begrip opbrengt voor persoonlijke interesses en sores. Japan (en karaoke), Klein-Walserthal (en een losgeslagen schouder en wijn), Frankrijk (en het eindfeest en presentatie) en het lab (en de verslapen ochtenden en geagiteerde discussies) en en en en.........

Het is dan wel je functie, maar ontzettend bedankt voor je begeleiding, corrigerende overwicht en vooral al het geduld. Ondanks dat het tijd werd voor ons beiden om mijn promotie af te ronden, ben ik nog lang niet uitgeleerd en hoop ik ooit een wetenschappelijk inzicht en denkwijze zoals de jouwe te bereiken.

Dan, geachte promotoren, professor Grootegoed en professor Laven, beste Anton en Joop. Jullie inzet en steun heeft het in eerste instantie überhaupt mogelijk gemaakt dat ik mijn promotietraject mocht en kon voortzetten na een op zijn zachts uitgedrukt turbulente start. Daarnaast hebben jullie mij allebei

gesteund en geholpen bij mijn koppige voornemen om een deel van mijn promotie-onderzoek in het buitenland te verrichten. Toen ik daar vervolgens zat, belde ik jullie met het verzoek of ik nog een maand langer mocht blijven om onderwijs te geven. Gelukkig gingen jullie hiermee (uiteindelijk) ook akkoord. Voor al dit alles, mijn hoogste dank.

Mijn positie als onderzoeker voor jullie beide afdelingen had onder andere als doel de afstand tussen de basale wetenschap en de kliniek te verkleinen. In een tijd waarin de grens tussen deze twee gebieden steeds meer begint te vervagen, denk ik dat jullie toentertijd een wijze, voorzienige stap hebben gemaakt. Ik ben dan ook erg positief gestemd dat deze samenwerking tussen jullie afdelingen wordt voortgezet.

Anton, jij loopt over van wetenschappelijk ideeën en inzichten. De discussies die wij hebben gevoerd, leidden altijd tot vernieuwd of verbeterd inzicht. Ook als jij het niet eens was met mijn ideeën of voorstellen, was jij wel altijd bereid om hierover te discussiëren. Wanneer ik met goede argumenten aankwam, deed jij dan ook niet moeilijk om je mening bij te stellen. Ik wens jou de komende jaren nog heel veel succes, en ik ben benieuwd wat er nog uit jouw koker gaat rollen.

Joop, wellicht is het (ook) onze gedeelde herkomst uit Limburg, maar wij hebben al die jaren behoorlijk op een lijn gezeten. Jij gaf mij het gevoel dat jij mij waardeerde voor zowel mijn wetenschappelijk bijdragen als voor mijn sociale bezigheden. Voor jou als clinicus is mijn werk niet altijd in eerste instantie duidelijk geweest, maar jij wist wel altijd heel snel de spijker op zijn kop te slaan. De afspraken op jouw kantoor om mijn voortzettingen door te nemen waren vooral vaak een podium voor jou om je eigen meningen en ervaringen ten toon te spreiden. Hierdoor heb ik ook jou beter leren kennen, maar heb ik vooral vaak hard moeten lachen. Ik ga er vanuit dat onze wegen zich nog lang mogen blijven kruisen.

Geachte prof. Grosveld, dr. Vermeulen en dr. de Boer, hartelijk dank voor het willen plaatsen nemen in de kleine commissie.

Geachte professor Schrander-Stumpel, beste Connie. Helaas ben jij vandaag verhinderd om plaats te nemen in de grote commissie. Toch wil ik dit moment aangrijpen om je te bedanken voor de mogelijkheid die je mij geboden hebt in 2001 om bij jouw afdeling Klinische Genetica in het AZM mijn co-schap wetenschappelijk onderzoek te volgen. Mijn reeds bestaande interesse in moleculaire celbiologie en genetica is onder jouw begeleiding alleen maar toegenomen, en dat heeft mede bijgedragen aan de totstandkoming van dit proefschrift.

Paranimfjes. In volgorde van onze eerste ontmoetingen.

Sander, Sannnnnnniiiieeee, wie had ooit in 1996 kunnen voorspellen dat wij beste vrienden zou worden. Ik een naïeve limburger, jij een "boer" met houthakkerblouse uit de polder met oorbellen. Samen hebben wij letterlijk de wereld overgevlogen, zijn wij huisgenoten geweest en alles wat ons bezig houdt, is reeds meerdere malen of zelfs tot in den treure besproken. Het enige dat ik mij afvraag is, waar is het Pitt-bier gebleven? Alles is denk ik samen te vatten in een woord: "vangnetje". Maar wat ook niet ongezegd mag blijven is dat ik jou en Judje meer dan al het beste wens.

Evelyne: zie boven.

Paul/Lindy:

Paul, Paul"TJE" wat fijn dat jij er was tijdens die eerste oersaaie cursus. Qua humor zaten wij gelijk op een lijn, tot grote irritatie van menigeen. En nog steeds. De afgelopen jaren is de humor slechts toegenomen, ben jij een goede vriend geworden en dat moet dus nog lang voortgezet worden. Het kan dan ook niet anders dat jij naast mij staat vandaag.

Lindy, LAM, ik leerde jou voor het eerst kennen vlak voor je vader overleed. Tot op de dag van vandaag had ik je graag eerder leren kennen, want dan had ik er toen voor je kunnen zijn. Jij zorgde er in eerste instantie voor dat ik de rest van de gyn-promovendi leerde kennen en het begon met lunchen op vrijdag. Totdat jij, Paul, Ingrid en ik een keer gingen uiteten..........vanaf toen ontspoorde het en begon het grote Promoveren-Festijn. Super dat jij in je rokkostuum mij vandaag bijstaat.

Jullie beiden hebben mijn promotietijd verheven en tot een groot feest gemaakt. Ik ben zelfs Rotterdam enigszins gaan waarderen door jullie. Helaas moe(s)t dit een gecensureerde versie zijn, maar een paar trefwoorden kunnen wel: koffiebar, aap, Skihut, flugel, Che, Schiermonnikoog, noffie, iPhone, starslet, ex'je, "de rode harde schijf", gehandicapten, bouwvakkers decolleté en Cumbridge. Maar los van samen feesten en lol hebben, zijn jullie er altijd wanneer nodig. Voor jullie vriendschap, aandacht, tijd en relativeringsvermogen ben ik jullie (eeuwig?) dankbaar.

A(i)kiko, Iris, Kim en ja, ook jij Joost, de beginkern. Wat was het een genot om met jullie allen tezamen in een hok mijn promotie te starten. Het kamertje, de discussies, de diverse persoonlijkheden, de verschillende muzieksmaken en vooral de uiteenlopende zangkwaliteiten, de borrels, het stappen en de lol in het lab. Het begin was het beste.

Eskeatnaf, Ethiopean-turned-Belgian, jij kwam net wat later, helaas. De manier en rust waarmee jij en Heleen de afgelopen jaren alles hebben doorstaan, vind ik bewonderenswaardig. Nog heel even en dan heb jij wat je toekomt. Nu nog iets minder stug worden ;-).

Sharon & Olivier, jullie waren er vanaf het begin en hebben mij geïntroduceerd en wegwijs gemaakt bij de ferti. Jammer dat jullie zo snel weer vertrokken.

Jos, Esther, Eveline, Marja, Peng, Stephan, Annegien, Ruben, Bas, Christina, Nilhan, Catherina, dank voor jullie geduld, aanwezigheid en hulp in het lab.

Mariekutje, Kleinerwalserthal was het begin. Half-dood werd ik wakker in de trein, en vervolgens heb ik nog nooit heb ik zoveel, zo lang, zo hard en zo irritant (voor anderen) achter elkaar gelachen met iemand die ik net leerde kennen. En toen bleek je ook nog eens ontzettend leuk, aardig, lief en ook ietwat te plannerig te zijn. Dat jij niet mijn paranimf bent, waar ik dat wel voor jou was, zeg niets over hoezeer ik je waardeer.

John en Nicolette, dank voor alle ontspannen uren in de koffiebar het afgelopen jaar. Uren waarin even de promotie- en prive-gerelateerde stress gespuwd kon worden, en daarnaast de voorbijgangers kritisch "besproken" mochten worden. En John, thanks voor het supergezelschap tijdens de fly-drive-fly-congres-drive-fly-fly vakantie. Onwijs veel succes, maar vooral sterkte als enige man onder de gyn-promovendi.

Yvonne, Annelindy, Fatwa, Marijana, Dineke, Annepoes, Robert, Mariëlle, "W", Sarah, Babs, Jashvant & Eveline (en de rest die ik vergeten ben), dank voor de lunches, buiten en binnen.

Marjo, mijn persoonlijke wekker. Zelfs de zwijgzame veevervoer treinreizen in de ochtenden waren leuk en wat ben ik dankbaar dat er een iPhone bestaat (met Whatsapp). En Floris is gewoon onzeker.

Bastiaan en Erik, 20 jaar kennen wij elkaar al. Wij zijn allemaal ons "eigen ding" gaan doen, maar wij zijn elkaar nooit uit het oog verloren. Wat ik het meest toffe en relaxte vind aan jullie is dat ik een topavond kan hebben met jullie zonder wat te zeggen, maar slechts aanwezig hoef te zijn (maar das puur theoretisch natuurlijk). Al die jaren hebben zo'n basis verschaft dat het niet uitmaakt wat er gaat komen: jullie zijn vrienden voor het leven. Als wij nu ook nog eens tijd zouden kunnen maken om dat wat vaker met elkaar te vieren!

Sasje, wij zien elkaar te weinig.

Indraatje, vanaf de eerste dag dat onze studie startte, zat het goed tussen ons. Als ik bedenk wat wij samen allemaal hebben besproken en meegemaakt, is het zo fijn om te weten dat jij nog steeds mijn vriendinnetje bent. Het feit dat ik peetoom ben van Isabelle is de grootste eer die mij welgevallen is, ondanks dat ik dat wellicht niet vaak laat merken.

Nathalie, lieve Parel****, ook jij bent voor mij uniek. Slechts twee korte weken liepen wij samen co-schappen (en ik was beter), maar dat was genoeg. Ook nu zien wij elkaar amper, maar gelukkig zijn wij beiden gemaakt voor het mobiele tijdperk. Hoe jij het allemaal doet, is mij een raadsel. Vandaag mag ik, 10-09-2011 mag jij (nog meer) schitteren.

Philipe, eigenlijk had jij op een andere plaats in dit dankwoord moeten staan. Ik weet oprecht niet wat te zeggen.

Vincent, professioneel eter, drinker, stapper en dan nu ook slaper, maar ook notoire bedil. Ik heb het geluk gehad dat ik jouw humor, gezelschap en ambitie-drang langdurig en (te) vaak dagelijks van dichtbij hebben mogen meemaken. Ik heb hier ten eerste zo ontzettend veel lol door gehad, maar het heeft me ook ervan bewust gemaakt dat als jij maar wil, je heel veel kan bereiken. Ik hoop dat naast Amsterdam, ook jij genoeg slaapt.

Willem, CorPop, Freyke, Jarrik, Meta, Joep, Jasper, Serge en Mischa, met jullie is het nooit saai. Jullie zijn altijd een nieuwe bron van inspiratie en gespreksstof en het is voor mij zo prettig om in gezelschap te verkeren van non-medici met ambitie en humor. Laat K3 voort bestaan.

Arjen, onze wegen moeten elkaar menigmaal hebben gekruist in Maastricht, maar het heeft mogen duren tot Den Haag voor wij elkaar ontmoetten en leerden kennen. Veel blijft ongezegd, maar volgens mij bedoelen wij hetzelfde. Vorig jaar werd dat vooral duidelijk. Dank.

Hans, Hermine/ pap en mam, en Raphke, jullie wonen daar, ik woon hier. Het is voor jullie vaak niet duidelijk of bij te houden wat ik allemaal doe. Het enige dat voor mij belangrijk is, is dat ik weet dat jullie er altijd zijn en dat ik er altijd voor jullie ben. Afgelopen maanden zijn plotsklap erg heftig voor ons allen geweest, maar het heeft mij wel gedwongen tot een pas op de plaats. Soms zijn er intense momenten nodig om bij je prioriteiten stil te staan. Ik ben nooit weg geweest, maar ik ben er weer. Alles wat ik gedaan heb, maar vooral heb kunnen doen, hebben jullie mogelijk gemaakt. Ik hou van jullie.